INVESTIGATION OF MACHINING CHARACTERISTICS OF LBMed Al/Al_2O_3, Al/SiC and Al/ZrO_2 MMCs

A thesis submitted

in fulfilment of the requirements

for the award of the degree

of

DOCTOR OF PHILOSOPHY

by

Vikas Sharma
Reg. No. 951108001

DEPARTMENT OF MECHANICAL ENGINEERING

THAPAR UNIVERSITY

PATIALA– 147004, PUNJAB, INDIA

July, 2016

PREFACE

This research work was carried out by the author under the guidance of **Dr. Vinod Kumar**, Associate Professor, Department of Mechanical Engineering, Thapar University, Patiala. The CO_2 LBM set up (Trumpf 1030, Trucoax 2500, Germany) available at Aman Metal Company Pvt Ltd Greater Noida, U.P was used for the exhaustive experimental work. For analyzing the microstructure of the machined samples, Scanning Electron Microscope (SEM), optical microscope, Energy Dispersive X-ray analysis (EDX) and X-ray Diffraction (XRD) set-ups available at Sophisticated Analytical Instrumentation Laboratory (SAI Labs), Patiala and Indian Institute of Technology (I.I.T), Ropar were used. The other facilities such as disc polishing set-up and optical microscope were used for carrying out the present research work at Chandigarh University, Mohali.

Several research papers were published out of the present research work. **The list of Journals/Conferences in which the papers find place is given below:**

Paper published in journals:

i. Sharma Vikas, Kumar Vinod, Investigating the quality characteristics of Al5052/SiC metal matrix composites machined by CO_2 laser curve cutting. Journals of Materials: Design and Applications, IMechE (L), September 2015, DOI: 10.1177/1464420715608890
   (SCI-Indexed; Thomson Reuters)

ii. Sharma Vikas, Kumar Vinod, Multi-objective optimization of laser curve cutting of aluminium metal matrix composites using desirability function approach, Brazilian Society of Mechanical Sciences and Engineering, Vol. 38, 4, 2016,1221-1238
   (SCI-Indexed; Thomson Reuters)

iii. Sharma Vikas, Kumar Vinod, Application of Box-Behnken design and response surface methodology for multi-optimization of laser cutting of AA5052/ZrO_2 metal matrix composites, Journals of Materials: Design and Applications, IMechE (L), April 2016, DOI: 10.1177/1464420716642619
   (SCI-Indexed; Thomson Reuters)

iv. Sharma Vikas, Kumar Vinod, Theoretical aspects of Laser Processing of Composite Materials, American International Journal of Research in Science, Technology &Engineering, 10(4), March-May, 2015, pp. 355-358
(Non-SCI Indexed)

CONFERENCES (National)

Sharma Vikas, Kumar Vinod, A new industrial era with laser beam machining: Review Proceedings of the 4th National Conference on Recent advancement in manufacturing (RAM-2014), National Institute of Technology, Surat -395007, July 26-28, 2014, 142-146, Gujarat, India.

ACKNOWLEDGEMENT

I am highly grateful to the authorities of Thapar University, Patiala for providing this opportunity to carry out the present research work. I acknowledge with deep sense of gratitude & humility, the inspiring help and guidance rendered by my supervisor, **Dr. Vinod Kumar**, Associate Professor, Department of Mechanical Engineering, Thapar University, Patiala for his interest and encouragement throughout the research work. His deep insight into the problem and ability to provide constructive suggestions have been of immense value in improving the quality of my research work at all stages.

Heartfelt thanks are due to Prof. Prakash Gopalan (Director, Thapar University, Patiala), Dr. O.P Pandey (Dean, Research and Sponsored Projects, Thapar University, Patiala), Dr. S. K. Mohapatra (Senior Prof. & Head, Mechanical Engineering Department, Thapar University, Patiala), Dr. N.K Verma, Dr. J.S Saini, Dr. Tarun Nanda for their encouragement and support during this research work.

I am thankful to Mr. Vineet Sharma (CEO), Mr. Gurmeet Singh (General Manager) and Mr. Anil Kumar (Laser set-up Superintendents) of Aman Metal Company Pvt Ltd, Greater Noida. I am also thankful to the authors whose research has helped me a lot.

I also express my appreciation to the workshop staff, specially Mr Lalit Kumar (Foundry Shop Incharge), Mr. Sandeep Bhatnagar (Lab. Technician) and other attendants for helping in manufacturing of specimens. I am thankful to Mr. Narender Kumar (Lab. Technician, Metrology Lab.), Mr Suresh Kumar (Research scholar), Mr. Gaurav Singla (Research scholar) for providing help in using the Metrology instruments. The author wishes special thanks to Dr. L.D Scintilla, Doctoral research fellow at Polytechnic of Bari, Department of Mechanical Engineering, Mathematics & Management, Bari Area, Italy for providing help in field of laser machining.

A big "Thank you!" also goes out to all my colleagues who imparted some spare time by taking my adjustments during the teaching days and without their supports it was infinite task to complete. I avail the privilege to pour on paper my regards to my parents and my in-laws for their constant unconditional support both emotionally and financially. They had given me unequivocal support throughout, as always, for which my mere expression of thanks likewise does not suffice.

No amount of thanks is enough, finally, for my beloved wife Nitika Sharma who held the key to my success. Her patience and encouragement kept my motivation up. Despite all odds, she single handedly and intelligently managed all family matters as well as my two naughty kids (Pranshi and Pranshu). There were times during the past four years when everything seemed hopeless and I didn't have any hope. I can honestly say that it was only her determination and constant encouragement that ultimately made it possible for me to see this project through to the end.

I thank all the souls who helped me in this herculean task. Finally, I bow my head to the **ALMIGHTY** for all the blessings he has showered on me.

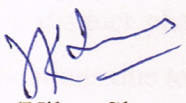

(Vikas Sharma)

CERTIFICATE

Certified that the thesis entitled **"Investigation of Machining Characteristics of LBMed Al/Al_2O_3, Al/SiC and Al/ZrO_2 MMCs"** which is being submitted by Mr. Vikas Sharma, to the Department of Mechanical Engineering, Thapar University, Patiala, in the fulfillment of the requirements for the award of the degree of **DOCTOR OF PHILOSPHY,** is a record of bonafide research work carried out by him under my guidance and supervision. The matter presented in this thesis has not been submitted either in part or full to any other University or Institute for the award of any degree.

07/07/2016

Dr. Vinod Kumar
Associate Professor
Mechanical Engineering Department
Thapar University, Patiala, India

ABSTRACT

In the past time, MMCs materials were famous by the name of steel-wire reinforced copper. This MMC was the material named as continuous-fiber reinforced composites. In 1960s, the aerospace industry was demanding for the high performance material having low weight and high thermal coefficient. The development of MMCs material in the late 1980s provided new revolution to the aviation industry. With the advancement in the properties of these materials, the applications started towards the development of critical space system. Metal matrix composite is a distinct material as it has valuable physical properties as compared to other materials. MMCs gain the properties of two different materials by various fabrication processes. It composed of two or more distinct phases namely matrix phase and reinforcing phase. This material has many applications due to its different properties such as adjustable coefficient of thermal, high strength, high temperature stability expansion, high stiffness, low density, high electrical and thermal conductivity, corrosion resistance, improved wear resistance etc. The fabrication process of MMCs materials depends on the application in particular field. The main focus is provided on the uniform distribution of reinforcement components (reinforced particles) during the manufacturing process of MMCs material. Aluminium alloy (5052) MMCs is made by stir casting method which may replace some of the old industrial applicable materials. The machining of these MMCs materials by the traditional machining methods is a typical process due to some issues related to tool wear and surface roughness. Now days the non-conventional machining process is being used for machining of these metal matrix composites materials. An attempt has been made for machining of these MMCs material by various non-conventional process such as laser beam machining (LBM), electric discharge machining (EDM), abrasive water jet machining (AWJ), ultrasonic machining (USM). These non conventional machining techniques also have some disadvantages such as cutting cost, cutting speed, unable to cut typical geometries, low material removal rate, surface finish, physical constraints with respect to workpiece geometry etc. To overcome these difficulties, the present research work is carried out using laser beam machining (LBM) for machining of MMCs material and for cutting of complicated geometries. This research work investigated the laser beam machining (LBM) characteristics of MMCs consisting of aluminium alloy Al5052 as base material. This study would provide benefits to manufacturing engineers to increase the quality of

edge cutting and decrease the cost of laser machining operations. The emphasis has been devoted on laser curve cutting by using different arc radius and variation of percentage reinforced particles to analyse the effect on different output parameters. The various samples of Al5052/Al_2O_3, Al5052/SiC and Al5052/ZrO_2 metal matrix composite (MMC) material were fabricated using stir casting set-up. The various objectives have been completed using CO_2 laser setup for determining the machining characteristics on MMCs material. The experimental run layout is designed with the help of Box-Behnken design approach. To investigate the effect on output responses, various process parameters were selected such as cutting speed, laser power, nozzle stand-off distance, nozzle diameter, gas pressure, percentage reinforced particles, arc radius, type of gas, laser frequency, and material thickness. The various MMCs such as Al/SiC, Al/Al_2O_3 and Al/ZrO_2 selected as work material. The optimized model has been developed for various output responses such as dross height, kerf taper, edge surface roughness, kerf deviation, striations, heat affected zone width, material removal rate, energy losses using response surface methodology (RSM). These responses have been optimized using multi-response optimization through desirability functional approach. The analysis of variance has been utilized to evaluate the significance of predicted RSM model. The validity and adequacy of predicted model has been confirmed using experimentation work based on response model. The optimized parameter settings have been identified for various output quality characteristics. The finite element method was applied for determining the effect of curved cut geometry for induced stress and temperature analysis. The transient thermal model and static structural model is applied to determine the results of temperature and stress conditions. The value of heat flux has been found using variable temperature conditions. The formation of new compound Al_4C_3 has been examined on laser machined surface using X-ray diffraction technique. The laser cutting speed, percentage reinforced particles and arc radius has been found significant factors for the laser cutting process on various quality characteristics. The morphological and metallurgical changes have been determined using SEM, EDS, optical microscope and XRD technique. The heat affected zone, recast layer, crack formation and dross height is characterized using scanning electron microscope.

LIST OF TABLES

Table No.	Description	Page No.
3.1	ANOVA terms used in multiple regressions	36
3.2	Number of experiments based on various design approach	38
4.1	Specification of CO_2 laser setup	39
4.2	Chemical composition of 5052 aluminium alloy	40
4.3	Mechanical Properties of various MMC work material	41
4.4	Variation of input parameters for pilot experimentation	44
4.5	Design matrix of Box- Behnken design for seven factors at three levels	51
4.6	Laser cutting parameters and their levels for main experimentation	51
4.7	Design matrix for main experimentation	55
4.8	Design matrix and output responses-I for the specimen Al/SiC/0-20% weight	56
4.9	Design matrix and output responses-II for the specimen Al/SiC/0-20% weight	57
4.10	Design matrix and output responses-I for the specimen Al/Al_2O_3/0-20% weight	58
4.11	Design matrix and output responses-II for the specimen Al/Al_2O_3/0-20% weight	59
4.12	Design matrix and output responses-I for the specimen Al/ZrO_2/0-20% weight	61
4.13	Design matrix and output response-II for the specimen Al/ZrO_2/0-20% weight	62
5.1	Adequacy checking of model of dross height	67
5.2	Adequacy checking of model of kerf taper	68
5.3	Adequacy checking of model of surface roughness	69
5.4	Adequacy checking of model of kerf deviation	70
5.5	Adequacy checking of Striation angle	71
5.6	Adequacy checking of model of Heat affected zone width	72
5.7	Adequacy checking of model of material removal rate	73
5.8	Adequacy checking of model of Energy Losses	74
5.9	ANOVA for response surface of reduced quadratic model of dross height	77
5.10	ANOVA for response surface of reduced quadratic model of kerf taper	87

5.11	ANOVA for response surface of reduced quadratic model of R_z	94
5.12	ANOVA for response surface of reduced quadratic model of kerf deviation	104
5.13	ANOVA for response surface of reduced quadratic model of HAZ width	112
5.14	ANOVA for response surface of reduced quadratic model of striation angle	118
5.15	ANOVA for response surface of reduced quadratic model of MRR	124
5.16	ANOVA for response surface of reduced quadratic model of energy losses	132
5.17	Constraints of input parameters and responses	158
5.18	Optimal solutions for dross height, kerf taper, edge surface roughness, kerf deviation	159
5.19	Optimal solutions for striations angle, heat affected zone width, material removal rate, energy losses	160
5.20	Experimental validations of developed models with optimal parameter settings	161
5.21	Parametric conditions for comparison of values	176
5.22	Parametric conditions for literature and experimental data	176
6.1	Physical properties of the Al5052 and laser mode properties	182

LIST OF FIGURES

Fig. No.	Description	Page No.
1.1	Schematic diagram of LBM set-up	5
1.2	Laser material removal mechanism	6
3.1	Design Procedure of Response Surface Methodology	31
3.2	Box–Behnken designs as developed from a cube	38
3.3	BBD represented with Interlocking 2^2 factorial experiments	38
4.1	Stir casting setup for MMCs and line diagram of laser set up	40
4.2	Laser cut profile with different arc radius	44
4.3	Effect of cutting speed on kerf width and surface roughness	46
4.4	Effect of laser power on kerf width and surface roughness	46
4.5	Effect of Stand-off distance on kerf width and surface roughness	48
4.6	Effect of Nozzle Diameter on kerf width and surface roughness	48
4.7	Effect of gas pressure on kerf width and surface roughness	49
4.8	Effect of SiC particles on kerf width and surface roughness	49
4.9	Effect of arc radius on kerf width and surface roughness	50
4.10	Main experimental setup CO_2 laser cutting system	52
4.11	CO_2 Laser cutting head with work material	52
4.12	Laser machined cut profiles of various arc radius	53
5.1	Methodology of statistical analysis of results	65
5.2	Plot of predicted versus actual for dross height	76
5.3	Normal probability plots of residuals for dross height	76
5.4	Effect of cutting speed (a) and laser power (b) on dross height	79
5.5	Effect of nozzle distance (c) and nozzle diameter (d) on dross height	79
5.6	Effect of gas pressure (e) and reinforced particles (f) on dross height	80
5.7	Effect of arc radius on dross height	80
5.8	Percentage contribution effect of parameters on dross height	81
5.9	Interaction plot between cutting speed and gas pressure for dross Height	81
5.10	Interaction plot between nozzle distance and reinforced particles for dross height	82
5.11	Optical micrograph (50 ×) of dross height at X_1: 3000 mm/min, X_2: 2000 watt, X_3: 1.5 mm, X_4: 1.7mm, X_5: 12 bar, X_6: 20%,	

	X_7: 60 mm	83
5.12	Optical micrograph (50 ×) of dross height at X_1: 2000 mm/min, X_2: 2000 watt, X_3: 2 mm, X_4: 1.4 mm, X_5: 12 bar, X_6: 10%, X_7: 20 mm	84
5.13	Optical micrograph (50 ×) of dross height at X_1: 1000 mm/min, X_2: 2500 watt, X_3: 1.5 mm, X_4: 2 mm, X_5: 12 bar, X_6: 10%, X_7: 40 mm	84
5.14	Optical micrograph (50 ×) of dross height at X_1: 1000 mm/min, X_2: 2500 watt, X_3: 1.5 mm, X_4: 1.4 mm, X_5: 12 bar, X_6: 10%, X_7: 40 mm	85
5.15	Plot of actual versus predicted for kerf taper	86
5.16	Normal probability plots of residuals for kerf taper	86
5.17	Effect of cutting speed (a) and laser power (b) on kerf taper	88
5.18	Effect of nozzle distance (a) and nozzle diameter (b) on kerf taper	88
5.19	Effect of gas pressure (a) and reinforced particles (b) on kerf taper	89
5.20	Effect of arc radius on kerf taper	89
5.21	Percentage contribution of input parameters on kerf taper	90
5.22	Interaction plot between gas pressure and arc radius for kerf taper	90
5.23	Interaction plot between laser power and reinforced particles for K_t	91
5.24	Plot of predicted versus actual for surface roughness	93
5.25	Normal probability plots of residuals for surface roughness	93
5.26	Effect of cutting speed (a) and laser power (b) on surface roughness	95
5.27	Effect of nozzle distance (c) and nozzle diameter (d) on surface roughness	95
5.28	Effect of gas pressure (e) and reinforced particles (f) on surface roughness	96
5.29	Effect of arc radius on surface roughness	96
5.30	Interaction plot between arc radius and reinforced particles on surface roughness	97
5.31	Interaction plot between cutting speed and reinforced particles on surface roughness	97
5.32	Percentage contribution of input parameters on surface roughness	98
5.33	Optical microscopic (50 ×) of surface roughness at X_1: 1000 mm/min, X_2: 2000 watt, X_6: 20 %, X_7: 20 mm	100
5.34	Optical microscopic (50 ×) of surface roughness at X_1: 1000 mm/min,	

	X_2: 1500 watt, X_6: 10 %, X_7: 40 mm	100
5.35	Optical microscopic (50 ×) of surface roughness at X_1: 3000 mm/min, X_2: 2000 watt, X_6: 10 %, X_7: 40 mm	101
5.36	Optical microscopic (50 ×) of surface roughness at X_1: 3000 mm/min, X_2: 2000 watt, X_6: 0 %, X_7: 60 mm	101
5.37	Plot of predicted versus actual for kerf deviation	103
5.38	Normal probability plots of residuals for kerf deviation	103
5.39	Effect of cutting speed (a) and laser power (b) on kerf deviation	105
5.40	Effect of nozzle distance (c) and nozzle diameter (d) on kerf deviation	106
5.41	Effect of gas pressure (a) and reinforced particles (b) on kerf deviation	106
5.42	Effect of arc radius on kerf deviation	106
5.43	Interaction plot between gas pressure and reinforced particles for kerf deviation	107
5.44	Interaction plot between laser power and cutting speed for kerf Deviation	108
5.45	Percentage contribution of input parameters on kerf deviation	108
5.46	Optical micrographs (50 ×) for kerf deviation (a), (b)	109
5.47	Optical micrographs (50 ×) for kerf deviation (a), (b)	109
5.48	Plot of predicted versus actual for HAZ width	111
5.49	Normal probability plots of residuals for HAZ width	111
5.50	Effect of cutting speed (a) and laser power (b) on HAZ width	113
5.51	Effect of nozzle distance (a) and nozzle diameter (b) on HAZ width	113
5.52	Effect of gas pressure (a) and reinforced particles (b) on HAZ width	113
5.53	Effect of arc radius on heat affected zone width	114
5.54	Interaction plot between arc radius and laser power for HAZ width	114
5.55	Percentage contribution of input parameters on HAZ width	115
5.56	Plot of predicted versus actual for striation angle	117
5.57	Normal probability plots of residuals for striation angle	117
5.58	Effect of cutting speed (a) and laser power (b) on striation angle	119
5.59	Effect of nozzle distance (a) and nozzle diameter (b) on striation angle	119
5.60	Effect of gas pressure (a) and reinforced particles (b) on striation angle	119
5.61	Effect of arc radius on striation angle	120
5.62	Interaction plot between laser power and arc radius for striation angle	120
5.63	Percentage contributions of various factors on striation angle	121
5.64	Microscopic images (50×), (a) variation in striation angle for cutting	

	speed: 3000 mm/min & arc radius: 20 mm, (b) striation angle for cutting speed: 2000 mm/min & arc radius: 20 mm	122
5.65	Microscopic images (50×), (a) striation angle for cutting speed: 1000 mm/min & arc radius: 40 mm, (b) striation angle for cutting speed: 1000 mm/min & arc radius: 60 mm	122
5.66	Plot of predicted versus actual for material removal rate	125
5.67	Normal probability plots of residuals for material removal rate	125
5.68	Effect of cutting speed (a) and laser power (b) on MRR	127
5.69	Effect of nozzle distance (a) and nozzle diameter (b) on MRR	127
5.70	Effect of gas pressure (a) and reinforced particles (b) on MRR	128
5.71	Effect of arc radius on material removal rate	128
5.72	Interaction plot between gas pressure and reinforced particles on MRR	129
5.73	Percentage contributions of various factors on MRR	129
5.74	Plot of predicted versus actual for energy losses	131
5.75	Normal probability plots of residuals for energy losses	132
5.76	Effect of cutting speed (a) and laser power (b) on energy losses	133
5.77	Effect of nozzle distance (c) and nozzle diameter (d) on energy losses	134
5.78	Effect of gas pressure (e) and reinforced particles (f) on energy losses	134
5.79	Effect of arc radius on energy losses	134
5.80	Interaction plot between laser power and reinforced particles for E.L	135
5.81	Percentage contributions of various factors on energy losses	135
5.82	Perturbation plot of process parameters for dross height	137
5.83	Interaction plot between laser power and reinforced particles for D_t	137
5.84	Perturbation plot of process parameters for kerf taper	139
5.85	Interaction plot between gas pressure and arc radius for kerf taper	139
5.86	Perturbation plot of process parameters for surface roughness	140
5.87	Interaction plot between cutting speed and gas pressure for R_z	141
5.88	Perturbation plot of process parameters for kerf deviation	142
5.89	Interaction plot between cutting speed and gas pressure for kerf deviation	142
5.90	Perturbation plot of process parameters for HAZ width	143
5.91	Interaction plot between cutting speed and gas pressure for HAZ Width	144
5.92	Perturbation plot of process parameters for striation angle	145

5.93	Interaction plot between cutting speed and gas pressure for striation Angle	145
5.94	Perturbation plot of process parameters for MRR	146
5.95	Interaction plot between cutting speed and gas pressure for MRR	147
5.96	Perturbation plot of process parameters for energy losses	148
5.97	Interaction plot between cutting speed and gas pressure for energy Losses	148
5.98	Perturbation plot of process parameters for dross height	149
5.99	Perturbation plot of process parameters for kerf taper	150
5.100	Perturbation plot of process parameters for surface roughness	151
5.101	Perturbation plot of process parameters for kerf deviation	152
5.102	Perturbation plot of process parameters for HAZ width	153
5.103	Perturbation plot of process parameters for striation angle	153
5.104	Perturbation plot of process parameters for MRR	154
5.105	Perturbation plot of process parameters for energy losses	155
5.106	3D surface plot of composite desirability for all responses	161
5.107	Ramp graph of optimal setting for all responses	162
5.108	Bar histogram plot of composite desirability for all responses	162
5.109	SEM micrograph showings striation formation due to restricted flow (a) unburned particles (b)	164
5.110	Crack and recast layer formation	164
5.111	Crack formation and presence of un-burned SiC particles on edge	164
5.112	Accumulation of molten material due to presence of SiC particles (a), formation of recast layer (b)	165
5.113	Dross and striation formation on the Al5052/SiC MMC machined Surface	166
5.114	SEM micrographs: (a) presence of 20 % ZrO_2 particles in specimen, (b) schematic diagram of recast layer and HAZ	167
5.115	Sub-layers of HAZ for machining condition at X_1: 1000 mm/min, X_6: 20 %, X_7: 20 mm	168
5.116	Heat affected zone width and recast layer (a) heat affected zone width for Al/ZrO_2 MMC(b)	168
5.117	SEM micrographs shows presence of Al_2O_3 reinforced particles in Al/Al_2O_3 MMC(a), crack formation on the edge machined surface (b)	170
5.118	Accumulation of Al_2O_3 reinforced particles nearby cut edge (a),	

	presence of un-burned Al_2O_3 reinforced particles (b)	170
5.119	XRD analysis of un-machined AA5052/SiC MMC (a) XRD pattern of machined AA5052/SiC MMC (b)	172
5.120	EDX analysis of laser machined surface of AA5052/SiC MMC (a, b)	173
5.121	SEM micrograph showing presence of 10 % ZrO_2 particles (a), EDS graph depicted the various elements of surface of specimen (b)	174
5.122	Comparison of quality characteristics of various metal matrix composites work material	175
5.123	Variation of dross height (a), striation angle (b) and kerf deviation (c) values w.r.t to various parametric conditions	177
5.124	Variation in heat affected zone width (a), kerf width (b) and surface roughness (c) values by comparing literature and experimental data	178
5.125	Desirability w.r.t predicted experiment number (a), plots between predicted & experimental values (b-d)	179
6.1	Procedure to apply the FEM from initial to post processing phase	181
6.2	Analysis of temperature variation w.r.t time for 20 mm arc radius	184
6.3	Analysis of heat flux variation w.r.t time for 20 mm arc radius	185
6.4	Von-mises stress analysis using transient analysis model for 20 mm arc radius	186
6.5	Temperature analysis for 20 mm arc radius	186
6.6	Variation of heat flux for cutting profile of 20 mm arc radius	187
6.7	Analysis of temperature variation w.r.t time for 40 mm arc radius	188
6.8	Analysis of heat flux variation w.r.t time for 40 mm arc radius	188
6.9	Von-mises stress analysis using transient analysis model for 40 mm arc radius	189
6.10	Temperature analysis for 40 mm arc radius	189
6.11	Variation of heat flux for cutting profile of 40 mm arc radius	190
6.12	Analysis of temperature variation w.r.t time for 60 mm arc radius	191
6.13	Analysis of heat flux variation w.r.t time for 60 mm arc radius	191
6.14	Von-mises stress analysis using transient analysis model for 60 mm arc radius	192
6.15	Temperature analysis for 60 mm arc radius	192
6.16	Variation of heat flux for cutting profile of 60 mm arc radius	193

CONTENTS

S.No.	Description	Page No.
	Abstract	vi-vii
	List of Tables	viii-ix
	List of Figures	x-xv
CHAPTER 1 INTRODUCTION		**1-11**
1.1	Aluminium alloy MMC and its machinability	2
1.2	Problems encountered in machining MMC_S with conventional machining	3
1.3	Laser beam machining	4
1.3.1	Process principle of CO_2 laser beam machining	5
1.3.2	Material removal mechanism in LBM	7
1.3.3	Applications of laser beam machining	7
1.3.3.1	Automobile industries	7
1.3.3.2	Aircraft and aerospace industries	8
1.3.3.3	Medical and surgical industries	8
1.3.3.4	Lasers in electronics industries	8
1.3.4	Advantages of laser beam machining	9
1.3.5	Limitations of laser beam machining	9
1.4	Objective of the study	9
1.5	Scope of work	10
1.6	Phases of research	10
1.6.1	Design of experiment	11
1.6.2	Experimentation work	11
1.6.3	Optimizing the results	11
1.7	Thesis structure	11
CHAPTER 2 LITERATURE REVIEW		**13-26**
2.1	Introduction	13
2.1.1	Laser Machining of metal matrix composite material	13
2.1.2	Effect of laser machining on heat affected zone	14
2.1.3	Striation formations by laser processing	16
2.1.4	Effect of gases on laser machining	16

2.1.5 Change in kerf width with different parameters variations 17
2.1.6 Variations of nozzle design and its effects on machining output 18
2.1.7 Effect of parameters on surface roughness and dross attachment 19
2.1.8 Effects on output variables due to different profiles cutting 21
2.1.9 Energy losses in CO_2 laser machine 22
2.1.10 Application of Finite element method in laser machining 23
2.1.11 Application of artificial neural network and QFN package, fuzzy logic 24
2.1.12 Effect of laser machining process on various quality characteristics 25
2.2 Gaps identified in the literature review 26

CHAPTER 3 DESIGN OF STUDY 28-36

3.1 Introduction 28
3.2 Response Surface Methodology 30
3.2.1 Evaluation of Regression Coefficients 31
3.2.2 Terms used for checking adequacy of model 32
3.3 Analysis of Variance 35
3.4 Box- Behnken Designs 36

CHAPTER 4 EXPERIMENTATION 39-54

4.1 Introduction 39
4.2 Specifications of work piece material 40
4.3 Process parameters of LBM 41
4.3.1 Cutting speed 41
4.3.2 Laser power 42
4.3.3 Nozzle stand-off distance and diameter 42
4.3.4 Gas pressure and type of gas 42
4.3.5 Aluminium alloy metal matrix composite material 43
4.3.6 Cut profiles 43
4.4 Pilot experimentation 43
4.4.1 Procedure for pilot experimentation 44
4.5 Effect of Process Parameters on kerf width and surface roughness 45
4.5.1 Effect of cutting speed on kerf width (K_w) and surface roughness (R_z) 45
4.5.2 Effect of laser power on K_w and R_z 45
4.5.3 Effect of stand-off distance on K_w and R_z 46
4.5.4 Effect of nozzle diameter on K_w and R_z 47

4.5.5 Effect of gas pressure on K_w and R_z 47
4.5.6 Effect of SiC reinforced particles 48
4.5.7 Effect of arc radius 50
4.6 Main experimental plan 50
4.7 Main experimentation 51
4.7.1 Experimental set-up and cut profiles 54
4.7.2 Design layout of main experimentation 54

CHAPTER 5 RESULTS AND DISCUSSION 64-176

5.1 Evaluation of adequacy of predicted model 64
5.2 Analysis of Variance and predicted mathematical models of output responses 66
5.3 Effect of process parameters for work material of AL5052/SiC using ANOVA 75
5.3.1 Effect of process parameters on dross height 75
5.3.2 Effect of process parameters on kerf taper 85
5.3.3 Effect of laser input variables on surface roughness 92
5.3.4 Effect of laser input variables on kerf deviation 102
5.3.5 Effect of laser input variables on HAZ 110
5.3.6 Effect of laser input variables on striation angle 116
5.3.7 Effect of laser input variables on MRR 123
5.3.8 Effect of laser input variables on energy losses 130
5.4 Effect of process parameters on the specimen Al5052/Al_2O_3 using perturbation and interaction plots 136
5.4.1 Effect of various process parameters on dross height 136
5.4.2 Effect of various process parameters on kerf taper 138
5.4.3 Effect of various process parameters on surface roughness 140
5.4.4 Effect of various process parameters on kerf deviation 141
5.4.5 Effect of various process parameters on heat affected zone width 143
5.4.6 Effect of various process parameters on striation angle 144
5.4.7 Effect of various process parameters on material removal rate 146
5.4.8 Effect of various process parameters on energy losses 147
5.5 Effect of process parameters on the specimen Al5052/ZrO_2 using perturbation plots 149
5.5.1 Effect of various process parameters on dross height 149

5.5.2 Effect of various process parameters on kerf taper 150
5.5.3 Effect of various process parameters on surface roughness 151
5.5.4 Effect of various process parameters on kerf deviation 151
5.5.5 Effect of various process parameters on heat affected zone width 152
5.5.6 Effect of various process parameters on striation angle 153
5.5.7 Effect of various process parameters on material removal rate 154
5.5.8 Effect of various process parameters on energy losses 155
5.6 Multi-response optimization using desirability function 156
5.7 Microstructure analysis of machined surfaces 163
5.7.1 XRD and EDX Analysis 170
5.8 Comparison of various output responses for different metal matrix composite work materials 174
5.8.1 Comparison of literature review data with respect to experimental data 176

CHAPTER 6 FINITE ELEMENT METHOD 180-190

6.1 Introduction 180
6.1.1 Assumptions used in the laser source model 181
6.2 Heat transfer model and analysis 182
6.2.1 Thermal stress analysis for laser source model 183
6.2.2 Global equation for heat transfer analysis 183
6.3 Stress, Temperature and Heat Flux Analysis 184
6.3.1 Thermal analysis for 20 mm arc radius 185
6.3.2 Thermal analysis for 40 mm arc radius 187
6.3.3 Thermal analysis for 60 mm arc radius 190

CHAPTER 7 CONCLUSIONS AND SCOPE FOR FUTURE WORK 194-196

7.1 Conclusions 194
7.2 Scope for future work 196

REFERENCES 198-209

APPENDICES 210-212

CHAPTER 01

INTRODUCTION

In the recent decades, the new innovations have been carried out in the field of fabrication of materials and machining. The new materials also challenges to machining technologist for quality and efficient machining methods. The materials such as aluminium alloys, metal matrix composite materials, titanium etc is considered as difficult to machine materials. The traditional machining methods are not feasible for machining of these hard materials due to various issues related to material-tool contact, surface finish, typical cutting profiles, cutting tolerances etc. However, with the new advance non- traditional machining methods such as laser beam machining, electrical discharging machining, electrochemical machining, ultrasonic machining etc, these limitations have been overcome. The current industrial scenario depends on the Non-traditional manufacturing processes which work on the principle of mechanical, electrical, thermal or chemical energy or combinations of these energies.

These machining methods have been categorized according to the source of the energy applied such as:

1. On the basis of mechanical energy source processes:

In this process, the mechanical energy in the form of erosion is used to remove the material from the workpiece. The main energy source is erosion which can be availed by any medium. This process comprises of various machining processes such as Ultrasonic Machining (USM), Abrasive Jet Machining (AJM),Water Jet Machining (WJM) and Abrasive Water jet Machining (AWJM).

2. Electrical energy based processes:

Here, the electrical energy performs the machining operation. During the machining operations thousands of sparks developed and raises the temperature of material to be cut and remove the molten material with the help of vaporization. There are two processes such as Electrical Discharge Machining (EDM) and Wire Cut Electrical Discharge Machining (WEDM).

3. On the basis of electro-thermal energy source processes:

The un-conventional machining process uses the electrical and heat energy to remove the unwanted material. In this process, the heat generated with the help of electrical energy and hence with the process of vaporization the material is removed. These processes comprises of Electron Beam machining (EBM), Plasma Arc Machining (PAM), Laser Beam Machining (LBM) and Ion Beam Machining (IBM).

4. Electrochemical energy based processes:

In this process, the material is removed with the help of electrochemical principle. The workpiece is to be machined remain in contact with electrolyte which initiate the process by ion dissolution process. The processes which follow this principle are Electro-Chemical Machining (ECM) and Electro Chemical Grinding (ECG).

1.1 ALUMINIUM ALLOY MMC AND ITS MACHINABILITY

Aluminum alloys is considered as engineering material used widely in the technical world. In aluminum alloys the aluminum is considered as important metal. The elements of aluminum alloys are zinc silicon, copper, magnesium, manganese and tin. The aluminium alloys are further divided into two categories of casting alloys and wrought alloys. The cast aluminum alloys have low melting point and tensile strength than wrought aluminum alloys.

The metal matrix composite (MMC) materials are considered in category of advanced materials due to its light weight, high specific modulus, thermal stability and advanced properties. Among various metal matrix composites, Al-alloy-based composites are always on the top of research ethics. Accompanying the industrial developments these metal matrix composites materials are high in demand in various industries such as aeronautics, automobiles and defense services. The challenges in the manufacturing of composites material is the equal distribution and proper mixing of reinforced particles. Due to non-uniform distribution of reinforced particles in the specimen, the hardness and strength properties may deviate to some levels. The strength to weight and weight to stiffness ratios can be easily achieved with the aluminium metal matrix composites reinforced with various reinforced particulates. To obtain the proper distribution of reinforced particles and due to its unique properties stir casting method is used in the industries for the fabrication of aluminium MMCs. In most of the MMCs the reinforced particulates are mainly the oxides, borides and carbides such as TiC, B_4C, Al_2O_3, TiB_2, TiO_2, SiC and ZrO_2. The machinability properties of MMCs mainly depend upon the

machining conditions, chemical affinity, shape and size of reinforced particles. The major applications of aluminium metal matrix composites materials are as follows:

1. MMCs are extensively used in manufacturing of aircraft brakes due to good thermal conductivity high and specific strength properties.
2. For the fabrication of airframe and aircraft engine parts.
3. The properties like the specific strength and elastic modulus enables it use in sports industries like bicycle frames and rackets.
4. In manufacturing of turbine and combustion engine components, disc brakes and brake parts and drive shaft components.
5. To provide cladding in the nuclear reactor.
6. It can be used in power electronic modules due to high thermal conductivity.

1.2 PROBLEMS ENCOUNTERED IN MACHINING MMCs WITH CONVENTIONAL MACHINING

The metal matrix composites materials are categorized for hard to cut materials due to its unique physical properties. Previously, the major problems encountered during the traditional machining of MMCs are summarized as follows:

1. The hardness of MMCs materials proved a significant challenge for traditional machining processes. As reinforcement of ceramic particles provides more hardness which becomes difficult to machined using commonly used high-speed steel (HSS) and carbide tools (Miracle et al., 2005).
2. The distribution of reinforced particles also plays a major role in deciding the surface defects on the machined surface. It has been examined that distribution of reinforced particles are associated with high localized stresses, abrasion, voids, pull-out of ceramic particles, particle fracture and significant micro-hardness alterations (Chan et al.,2001; Basavarajappa et al., 2007).
3. The surface roughness of the machined surfaces becomes lesser with the increase in the particle size and the volume percentage fraction. With the increase in particle volume fraction, the tools wear rate increases as well as increase the surface roughness of the machined specimen. (Dabade U. et al., 2009)
4. The thin chip segments produced when machining MMCs and highly strained region near the cut edge leads to the decrease in the strength of workpiece (Ciftci I. et al, 2004).
5. The stress and strain development in the MMCs is based on the interaction of reinforced particles with the cutting tool. The particle fracture and debonding of particles

are the main reason for the increase in stress concentration of specimen. The production of large cavities on the machined surface may be due to the pull out of reinforced particles (Davim J., 2010).

6. In conventional machining process, the mechanical forces are higher in nature which causes prominent domains of work hardening. Moreover, non-traditional machining process also works on the micro levels in comparison of traditional machining.

The above discussed problems usually faced by the technical industries for the machining of MMCs using conventional machining processes. To avoid all such types of problems non-conventional machining processes can be used such as laser beam machining, ultrasonic machining, abrasive jet machining processes etc. can be used. It has been examined that some processes have low material removal rate with lower ability to machine complex shapes. However, due to higher cutting speed, material removal rate, lower surface roughness and ability to cut complex shapes makes it suitable for machining of MMCs materials. Consequently, the investigations have been performed for the use of laser beam machining for machining of various metal matrix composites materials.

1.3 LASER BEAM MACHINING

Laser beam machining uses the source of laser to cut the materials. It has been reported in literature survey that the applications of CO_2 gas lasers contribute to over 40% to the industrial sector. Laser is an acronym of light amplification by the stimulated emission of radiation. The concept of production of laser was first introduced by the Albert Einstein in 1916. Laser machining is a non- contact, reacting-force free and localized machining process. Laser cutting process removes the material with the help of melting and vaporization of the molten material. The ability of this process is that it can cut typical shapes with the high cutting speed and low cost. However, the other advantage is that it can cut hard to cut materials with higher surface finish. The current industrial era changing towards the laser source oriented applications. It has been analysed that percentage of laser source used by various industries are laser drilling (4%), laser micromachining (8%), laser cutting (39%), laser welding (20%) and laser labeling (16%)[point 55]. The first industry ready CO_2 laser cutting system was introduced in 1975. The application of laser beam machining depends on the various industries. For the heavy production industry laser welding, drilling and cladding is performed whereas for

small manufacturing units laser engraving type work usually executed. Now a day the major application of laser is more pronounced in the electronics and medical industry.

1.3.1 Process principle of CO_2 laser beam machining

LBM is capable of machining any material which can absorb the irradiation laser. CO_2 lasers emit the infrared laser radiation with a wavelength of 10.6 μm. The laser-active medium in a CO_2 laser is a mixture of CO_2, N_2 and He gases, where CO_2 is the laser-active molecule. The stimulation of the laser-active medium is accomplished by electrical discharge in the gas. During the stimulation process, the nitrogen molecules transfer energy from electron impact to the CO_2 molecules. The transition from energetically excited CO_2 molecules (upper vibrational level) to a lower energy level (lower vibrational level) is accompanied by photon release leading to emission of a laser beam. The CO_2 molecules return to the ground state by colliding with the helium atoms, which comprise the major share of the gas mixture, and the CO_2 molecules in the ground state are then available for another cycle. It has been analysed that helium gas has high thermal diffusivity whereas thermal diffusivity of CO_2 is low. Due to having this property the combination of helium and CO_2 produce high lasing efficiency. The stimulation of the electrical gas discharge in the gas mixture is accomplished by either direct current or radio frequency stimulation.

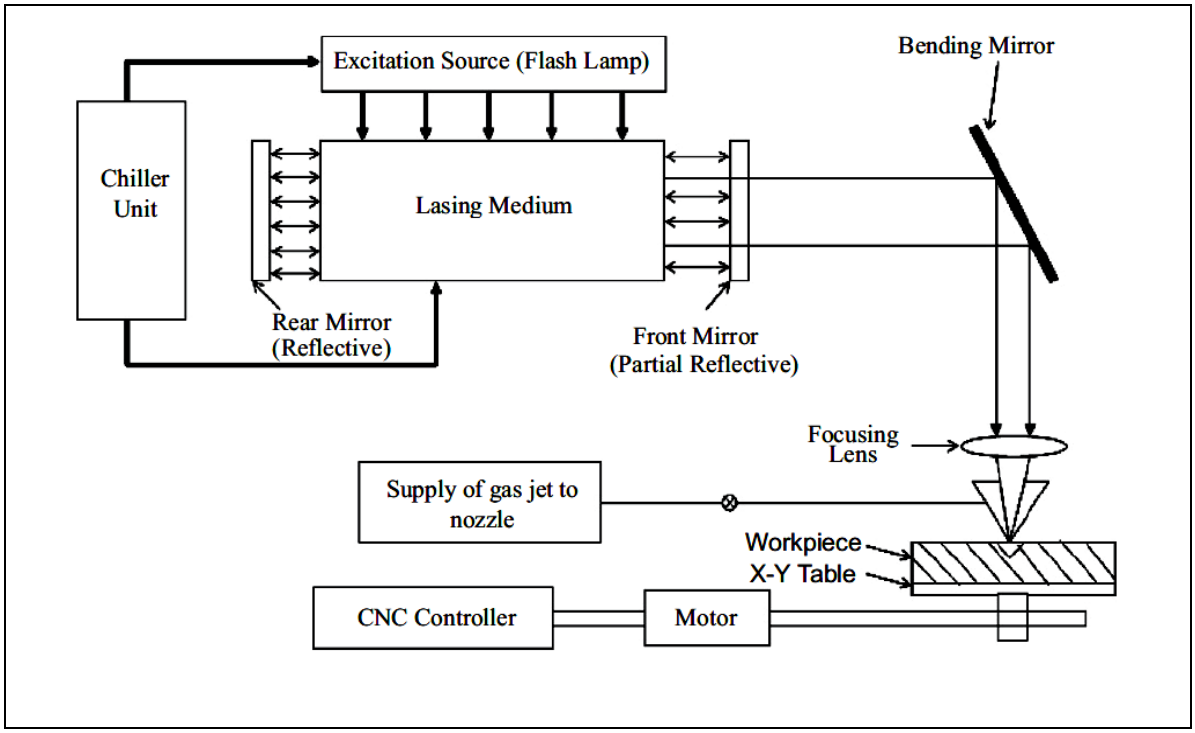

Figure 1.1 Schematic diagram of LBM set-up (Sharma A. et al., 2010)

In direct current stimulated lasers, gas discharge between electrodes allows the electrical energy to be directly coupled into the laser gas while the radio frequency stimulated lasers are characterized by capacitive in coupling of the electrical energy needed for gas discharge.

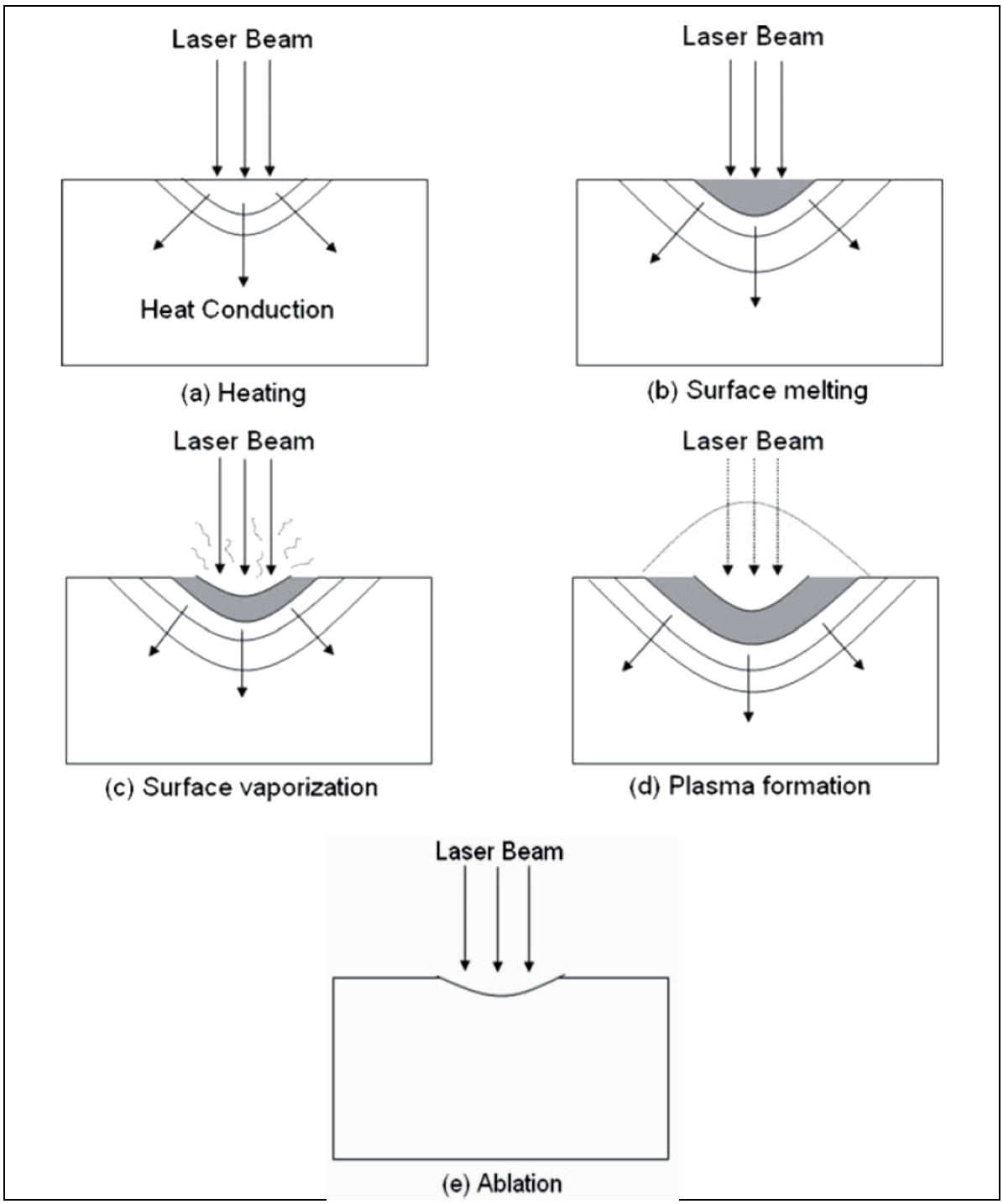

Figure 1.2 Laser material removal mechanism (Dahotre N. et al, 2008)

The figure 1.1 shows the schematic diagram of CO_2 LBM set-up where CO_2 gas is used with mixture of all gases to produce the lasing action. After production of laser, the laser beam is facilitated to pass through the nozzle where assist gas also flows to provide the exothermic reaction during the cutting process.

1.3.2 Material Removal Mechanism in LBM

Material removal rate of laser machining is considered higher as compared to other non-conventional machining process. On the basis of intensity levels of laser beam, the specimen to be machined experiences various steps for the removal process. The surface undergoes five basic process such as heating, surface melting, vaporization, plasma formation and ablation process. The figure 1.2 shows the basic steps for the metal removal process. The laser beam energy transfers the heat via conduction process on the target area as shown in figure 1.2 (a). The material starts to melt when proper oxidation process takes place with the sufficient melting temperature. The melting process of material surface is shown in figure 1.2 (b). After the heating and melting process, higher laser intensity target the surface to induce the required temperature to vaporize the material as shown in figure 1.2 (c). Before the molten metal removal process or ablation process, plasma formation takes place which is due to ionization of particles. The formation of plasma is shown in figure 1.2 (d) in pink shaded area. In last, the ablation of molten material takes place as shown in figure 1.2 (e) which gets enhanced with application of assist gas which produces exothermic reaction.

1.3.3 Applications of Laser Beam Machining

LBM a non-contact process comes under the category of non-traditional machining processes. Due to its fast cutting speed and good surface finish, this process is replacing traditional processes for drilling, cutting, engraving and other non-mechanical processes. Followings are some of the best applications in various industrial and medical fields.

1.3.3.1 Automobile industries

The demand of LBM in automotive industries increasing rapidly to enhance the performance of high speed and efficient engines. Many of the products manufactured by LBM process in automotive industry are:

1. Engine mountings and chassis
2. Car engine prototypes
3. Hydro-formed structures

4. Headliners
5. Dashboards & Consoles
6. Door Moldings
7. Gears and rear housing support
8. Car Frames
9. Bearings bushing

1.3.3.2 Aircraft and aerospace industries

The use of laser source in the manufacturing of various parts of Aircraft and Aerospace Industries has emerged on large scale in previous years. Some of the parts manufactures for both industries are listed below:

1. Duct subassemblies
2. Engine Strut
3. Rocket guidance setup
4. Airframes for the aerospace industry
5. Satellite structural component
6. Fin actuator housing for a missile
7. Turbine blades
8. Jet engine blade sets
9. Turbine diffusers

1.3.3.3 Medical and surgical industries

Due to higher accuracy of laser cutting, the use of this process in manufacturing of medical devices is increasing rapidly. Few applications of laser is listed below:

1. Surgical screws, bolts and hardware.
2. Manufacturing of heart stent and valves
3. Fabrication of syringe components.
4. Dental implants parts.
5. Go Gauges for medical inventory quality control.
6. Manufacturing of regulator valves for oxygen masks.

1.3.3.4 Lasers in electronics industries

In the world of electronics micromachining plays a vital role in deciding the performance of electronics systems. To fulfill the requirement, the current laser set-up is capable to perform the micromachining process.

There are few applications which are listed below:

1. Cutting of thick-film chip resistors and low resistance metal resistors.

2. Laser patterning of thin-film amorphous silicon solar cells.

3. The most important function is laser welding of electronic components such as hard-disk head suspensions, optical modules, miniature relays and lithium ion batteries.

1.3.4 Advantages of Laser Beam Machining

The commercialization of LBM mainly depends on its capabilities for quality cut with lower cost. Followings are various advantages listed:

1. LBM is known for its non contact process. The clamping of the materials need not to be accurate as compared to traditional machining.

2. LBM can perform cutting of typical profiles of hard to cut materials.

3. The surface roughness of edge remains lower for the entire laser cut.

4. This process is also known for its high cutting speed.

5. A better quality of cut can be obtained in terms of lower developed stresses and heat affected zone width.

6. Higher aspect ratios and precise cut dimension can be accomplished with LBM.

7. LBM is also a flexible process as it can cut various materials from ferrous to non-metallic materials

8. The wastages of raw material can be avoided if initial planning and checking of the program is executed on time.

1.3.5 Limitations of Laser Beam Machining

There are some disadvantages of LBM process as compared to other non-traditional processes as given below:

1. The capital and maintenance cost of set-up is high due to various components.

2. The set-up requires high skilled operator to work.

3. This process consumes lots of electrical energy.

4. LBM process can not cut materials with higher thickness.

5. The energy losses are higher which also depends on the type of material to be cut.

6. The heat affected zone can be high if optimized machining conditions are not used.

1.4 OBJECTIVE OF THE STUDY

The present study was presented to investigate the machining characteristics of MMCs under the various parametric conditions in laser beam machining process. The various regression models reported for the application in the manufacturing industry of LBMs and

MMCs. Following are the listed objectives accomplished successfully according to the presented plan.

1. Identification and characterizing of cut quality in laser cutting of different metal matrix composite materials.
2. To analyze the energy losses for MMCs with different reinforced particles using CO_2 laser machine.
3. To relate temperature and stress field variation for laser cutting by varying different input variables using FEM.
4. To examine the effect of process variables for CO_2 laser machine (like gas pressure, type of gas, cutting speed, nozzle stand-off distance, laser frequency, laser power, material thickness, nozzle diameter, arc radius, % reinforced particles, Al/Al_2O_3, Al/SiC and Al/ZrO_2 as work material)on various output characteristics like striations, heat affected zone width, edge surface roughness, dross height, material removal rate, kerf taper, kerf deviation, energy losses, temperature and stress fields using FEM, morphological and metallurgical changes using SEM and XRD technique.
5. To obtain the optimal parametric combinations of laser beam machining.

1.5 SCOPE OF WORK

The work has been limited to laser beam machining of aluminium metal matrix composite as work material under the different experimental conditions by varying the process parameters (gas pressure, type of gas, cutting speed, nozzle stand-off distance, laser frequency, laser power, material thickness, nozzle diameter, arc radius, % reinforced particles, Al/Al_2O_3, Al/SiC and Al/ZrO_2) using suitable optimization technique. The results obtained have been modeled for their application in manufacturing industry.

1.6 PHASES OF RESEARCH

- Literature review
- Design of experiment
- Experimentation work
- Optimizing the results
- Confirmation of the results
- Finite element analysis

1.6.1 Design of Experiment

The primary work of Design of Experiment has been carried out using Response surface methodology (RSM) via Box-Behnken design. Before carrying out the main experimentation, the pilot experimentation was conducted to identify the range of various process parameters. The pilot experimentation was conducted using OFTA approach to decide the number of levels for each factor. However, the final experimentation was performed with the help of RSM technique which eliminate the non-significant factors by using backward elimination technique.

1.6.2 Experimentation work

The experimentation work has been carried out using CO_2 laser beam machining setup on aluminium metal matrix composite as work material. The various process parameters varied according to proposed design plan, so as to find out the impact on following output quality characteristics.

1. Striations angle
2. Heat affected zone width
3. Edge surface roughness
4. Dross height
5. Material removal rate
6. Kerf taper
7. Kerf deviation
8. Energy losses
9. Temperature and stress field analysis using FEM

1.6.3 Optimizing the Results

The results obtained have been optimized using desirability approach via desirability bar and graph. Various optimal settings obtained using this approach and further analysed for the confirmatory tests. The adequacy of the predicted model was tested by calculating the prediction error between the experimental and predicted values.

1.7 THESIS STRUCTURE

This thesis covers a number of scientific and experimental aspects associated with laser cutting of aluminium metal matrix composites. It consists of seven chapters. Brief description of the contents of each chapter has been given as following:

Chapter: 1 contains introduction to non-conventional machining methods, metal matrix composite materials and its applications, LBM process, the process capabilities, applications and advantages of LBM process. Problems that occur during machining of MMCs with traditional machining processes have also been discussed. Various aspects of LBM process, including the basic principle, material removal mechanism and its limitations have also been included. Objectives, scope and overall methodology of the work have also been described.

Chapter: 2 presents a detailed literature review on the research work reported with respect to various laser beam machining conditions and MMCs materials. Literature review also presents a discussion on various optimization techniques used by different researchers. Gaps in the literature have also been identified.

Chapter: 3 reported about the pilot experimentation performed using one factor at a time approach (OFTA). This approach used to identify the significant process parameters for LBM process and to fix the range of these process parameters. Finally, main experimentation plan and the experimental observations are presented.

Chapter: 4 reported with an introduction of the various methods of experimental design. The response surface methodology, desirability functional approach and Box-Behnken design used in the present study are then presented in detail. The theoretical concepts of model adequacy and regression analysis are also presented.

Chapter: 5 explored the results of parametric optimization with the help of response surface and perturbation plots. The desirability functional approach combined with multi response optimization is then presented for various process parameters and quality responses. Moreover, results of confirmatory experiments are presented. The morphological and metallurgical variations in the specimen are presented using energy dispersive X-rays, scanning electron microscope and X-ray diffraction techniques.

Chapter: 6 reported the results of finite element method analysis for temperature and stress analysis using transient thermal analysis model.

Chapter: 7 presents the conclusions of present research work and reported with scope for future work in the field of LBM and MMCs. This chapter is followed by references.

CHAPTER 02
LITERATURE REVIEW

2.1 INTRODUCTION

In new era of industrial world, the application of non-conventional machining increasing rapidly due to its quality performance and low processing time. Laser beam machining is widely used in various fields such as machining operations of cutting, drilling, cladding, bending etc. For better understanding of laser machining process, process parameters and quality characteristics a detailed literature survey has been presented in this chapter. Various researchers have reported the work to reduce the kerf deviation, surface roughness, kerf taper, heat affected zone width, recast layer etc.

The application of experimental methodologies for planning and analyzing the experiments is described in detail. Various techniques for optimization of input parameters are also discussed including response surface methodology and Box-benhken method. A significant amount of work has been explored in optimization of various input parameters like gas pressure, type of gas, cutting speed, nozzle stand-off distance, laser frequency, laser power, material thickness, nozzle diameter, arc radius, % reinforced particles, Al/SiC MMC, Al/Al_2O_3 MMC and Al/ZrO_2 MMC as work material. The morphological and metallurgical changes of specimen machined surface have been reported to explore the crack propagation and recast layer formation.

2.1.1 Laser Machining of metal matrix composite material

Ghosal A. et al. (2012) investigated results on machining of Al/Al_2O_3-MMC by ytterbium fiber laser. The wait time and modulation frequency was investigated the most significant parameter for material removal rate. The various optimized parameters for MRR and taper were found as 473.12 W laser power, 604.54 Hz modulation frequency, 0.18s wait time, 19.82 bar assist gas pressure and 93.47% of duty cycle pulse width. Moreover, the confirmation tests were conducted for the validation of the models. Muller F. et al. (2001) investigated the machinability of silicon carbide particle reinforced aluminium alloy matrix composites using non-conventional processes such as laser and electric discharge cutting. The comparison has been studied for different removal mechanisms of various machining processes. The morphological changes for the machined surfaces using various

machining processes have been examined on microlevels. Grabowski A. et al. (2008) prepared theoretical models and analysis was carried out for the interaction between a focused laser beam and the individual components of an AlSi alloy/SiCp composite material the reinforcement particles, SiC and the AlSi-alloy metal matrix by laser machine. The various input parameters were identified on the basis of basic principles for unit thickness of the composite materials.

Nowak M. et al. (2005) measured the optical properties like reflectivity, real part of the refractive index, absorption coefficient as well as the thermal and electrical conductivity of AlSi-alloy/SiC_p composite. It was found that both conductivities and optical parameters shown lower values with the increase of SiCp particles volume in AlSi-alloy matrix. These lower values were almost linear for the volume fraction of SiCp/10vol%p. On the other hand, the linearity of the curve departed due to the presence of additional phases in AlSi-alloy/SiC_p composite materials. Sleziona J. et al. (2007) presented a physical model characterizing the geometry of gas-assisted laser cutting of the AlSi-alloy/SiCp composite. To develop the efficient model the various parameters were used having inhomogeneous optical and thermophysical properties of AlSi-alloy/SiC_p. The developed model has shown the numerical solutions with double slope formation mechanism during laser cutting of the AlSi-alloy/SiC_p. It was also demonstrated that increasing laser beam cutting speed also depicted with higher values of slope of cutting front.

2.1.2 Effect of laser machining on heat affected zone

Sheng Paul et al. (1995) studied a numerical methodology for the development of the heat-affected zone during the laser cutting of 304 stainless steel. The heat-affected zone (HAZ) has been analyzed with the help of the time-temperature response of the workpiece material. The numerical estimations and experimental investigations have shown comparable results of HAZ with respect to the grain refinement, impurities and possible carbide precipitation in stainless steel 304. Araujo D. et al. (2003) studied a heat affected zone (HAZ) extension lower than 5 mm. It was revealed that the micro structural analysis demonstrated the HAZ having melting temperature of 548 and 596.8 ˚C where a-liquid phases are present. The high Nitrogen gas pressure of the laser cutting process depicted with three types of roughness on this viscous material during the laser processing.

Davim J. et al. (2008) evaluated the effect of the processing parameters (laser power and cutting velocity) on edge quality for various polymeric materials. A plan of experiments was established considering CO_2 laser cutting with prefixed processing parameters in several polymeric materials with different thickness. Rao B. et al. (2005) studied the dynamic behavior of melt ejection in laser cutting of 1mm thick titanium sheet and to obtain dross-free cuts with minimum heat affected zone (HAZ). CO_2 laser cutting of titanium sheet was carried out with continuous wave (CW) and pulsed mode laser operation with different shear gases namely argon, helium and nitrogen. Laser cutting with high frequency and low-duty cycle pulse mode operation produced dross free cuts with no noticeable HAZ. Herzog D. et al. (2008) investigated the influence of laser cutting on the static strength of a CFRP laminate. The work material was machined using three different high-power laser sources: a pulsed Nd: YAG laser, a disk laser and a CO_2 laser. The various workpiece have been examined using static tensile and bending conditions. Moreover, the results have been compared to conventional milling as well as abrasive water-jet cut samples.

Stournaras A. et al. (2009) investigated experimentally the quality of laser cutting for the aluminum alloy AA5083 using pulsed CO_2 1.8 kW laser set up. The various output responses were measured such as the edge roughness, kerf width, and the size of the heat affected zone (HAZ). Pfeifer R. et al. (2010) studied Nd:YAG laser machining of shape memory alloys (SMAs) of 1mm thick NiTi shape memory alloys for medical applications. The major factor for research of these shape memory alloys due to their outstanding properties such as the shape memory effect (SME) and high biocompatibility. It was revealed that due to the local energy input the lower values of heat-affected zones (HAZ) attained whereas the shape memory properties remained with the same values. Salem G. et al. (2008) evaluated the continuous wave ND:YAG laser cutting of 1.2 mm thick ultra-low carbon steel sheets. The effect of the cutting parameters such as gas pressure, laser power, and scanning speed was revealed with investigation of hardness, oxide layer width and microstructural changes.

Rajaram N. et al. (2003) studied samples of 4130 steel with the help of CO_2 laser cutting system. It was investigated that combinations of laser power and feed rate on kerf width, surface roughness, striation frequency and the size of heat affected zone (HAZ) have been studied. The regression models developed which explored the effect of the independent process parameters on laser cut quality.

2.1.3 Striation formations by laser processing

Yan Yinzhou et al. (2012) studied the effects of gas type, gas pressure, nozzle standoff distance, average laser power, cutting speed, and pulse repetition rate on striation characteristics. The various optimized operating conditions for striation-free cutting were demostrated. Karatas Cihan et al. (2006) examined the striation formation for steel as work material machined using CO_2 laser cutting system. It was analyzed that the beam waist position and the specimen thickness have effect on the striation formation. A lump parameter analysis has been applied to develop the model of kerf width. The effect of experimental conditions on the machined surfaces was measured using SEM and optical microscopy. Hirano Koji et al. (2011) investigated striation generation mechanism for the steel as work material. It was explored that kerf front was effected by the hydrodynamics of melt layer. The various velocities ranges of melt flows determine the kerf side and kerf front instability.

Li Lin et al. (2007) investigated different parameters for investigating the striation formation of machined EN43 mild steel having thickness of 2 mm using 1 kW single mode fiber laser. The various optimized parametric conditions have been investigated to achieve the striation-free laser cutting. A theoretical model was developed to analyze the cutting speed for striation-free cutting. Powell J. et al. (2011) presented the results of an experimental and theoretical investigation into the phenomenon of striation free cutting. The investigations revealed for low surface roughness and are related to an optimization of cut front geometry. This condition achieved when the cut front is inclined at angles close to the Brewster angle for the laser specimen combination. Hu Jun et al. (2011) developed a three-dimensional axial symmetrical model of laser cutting. It was explored that by adopting N–S equation and RNG k–e on flow model and numerical simulation explored the flow field of shield gas in cutting slot. This study explored the results of variation of nozzle stand-off distance on the dynamic characteristic of gas jet during the cutting process. It was examined that distribution of pressure and velocity of gas jet always has effect on the various output responses.

2.1.4 Effect of gases on laser machining

Kovalev B. et al. (2009) described the results of mathematical modeling using the three-dimensional full Navier- Stokes equations. It was revealed that gas flow structure originating for a sonic (conical) or supersonic nozzle. The visualization of gas jet flows in

channels geometrically shown similar results for the laser cut. Chen S. et al. (1998) examined the effects of gas composition on the CO_2 laser cutting of mild steel. It was investigated that there are various non-linear interacting factors responsible for laser cutting process performance. Riveiroa A.et al. (2011) studied the main variables controlling the laser cutting process. This work presented a study on the influence of different assist gases (argon, nitrogen, oxygen and air) on the edge quality and its surface chemistry during laser cutting of a typical Al-Cu alloy. Chen Shang (1999) investigated CO_2 laser cutting performance on 3 mm thick mild steel plate with assistant-gas pressures of up to 10 bar. A co-axial cutting nozzle able to withstand pressures of up to 12 bar was designed and set up. Experiments were performed with this high-pressure coaxial nozzle. For inert-gas cutting, dross under the cut kerf was formed with most of the cutting parameters.

Golnabi H. et al. (2009) investigated power level and cutting gas pressure in order to obtain an optimum kerf width. The results of kerf width was investigated for the various laser power range such as 50–170 W with the gas pressure of 1–6 bar steel materials. The various parametric conditions has been investigated for finding out the average kerf width of 0.2 mm such as cutting rate of 7.1 mm/s, laser power of 67W and oxygen pressure of 4 bar.

2.1.5 Change in kerf width with different parameters variations

Eltawahni A. H et al. (2010) related the cutting edge quality parameters (responses) namely: upper kerf, lower kerf, ratio of the upper kerf to lower kerf and cut edge roughness. They developed the mathematical models to determine the optimal cutting conditions for various process parameters. With the help of developed model the relationship was established between the process parameters and the edge quality parameters. Yilbas B. et al. (2008) studied kerf width variation by analyzing the effect of various process parameters on thick mild steel sheets. They examined the effect of control factors on the output responses by denoting the percentage effect of each process parameters. The formulation was attained using the thermal efficiency of cutting and liquid layer thickness. To determine the machined defects and kerf width size the application of optical microscopy and scanning electron microscopy (SEM) was performed. The kerf width variation attained higher values with the effect of oxygen gas pressure and laser output power.

Eltawahni A. et al. (2012) investigated laser cutting of stainless steel of medical grade AISI316L. The experimental layout was designed using Box–Behnken design and also with the help of Design of experiment (DOE). The investigation was done to identify the various process parameters which have significant effect on the output responses such as kerf ratio, surface roughness and operating cost. The various regression models were formulated to identify the effect of process parameters on various output responses. Salman N.et al. (2010) developed the finite element model for the laser cutting process using the transient model for the moving laser source. It was identified that effect of glass thickness, laser power and the cutting speed has significant effect on the cut path deviation. With the help of finite model the thermal stress and temperature variations has been studied.

Dubey A.et al. (2008) presented a hybrid Taguchi method and response surface method (TMRSM) for the multi-response optimization of a laser beam cutting process. The approach first uses the Taguchi quality loss function to find the optimum level of input cutting parameters such as assist gas pressure, pulse width, pulse frequency and cutting speed. The simultaneous optimization has been performed for two output responses viz. material removal rate (MRR) and Kerf width (K_W). Pandey A. et al. (2012) performed simultaneously optimization of various input and output parameters such as kerf taper and surface roughness in the laser cutting of Titanium alloy sheet. The objective functions for the genetic algorithm were selected on the basis of developed regression models for kerf taper and surface roughness using multi-objective optimization. Dubey A.et al. (2008) found that the kerf width variation was higher in case of pulse laser cutting. It was examined that kerf unevenness and kerf width has shown maximum variation along the length of cut during the laser cutting process. Dubey A. et al. (2008) applied hybrid approach of Taguchi method (TM) for multi-objective optimization of pulsed Nd: YAG laser beam cutting (LBC) process. The nickel-based super alloy (SUPERNI 718) has been selected to perform the laser beam cutting process and to identify the significant parameters for this process. The principal component analysis (PCA) has been performed to determine the optimized laser process parameters. The simultaneous optimization has been performed on output responses such as kerf deviation, kerf width and kerf taper.

2.1.6 Variations of nozzle design and its effects on machining output

Kovalev B. et al. (2009) developed the mathematical model for the supersonic flows of a viscous compressible gas by using the three-dimensional full Navier-Stokes equations. It

was revealed that mathematical model results confirmed with the experimental results. Man C. et al. (1998) studied laser cutting of stainless steels, titanium and aluminum alloys. The high pressure inert gas and coaxial nozzle jet has been applied to achieve the cut edge quality. They used the two dimensional steady state gas dynamic theory, computer simulation and shadow graphic techniques, the gas jet patterns to analyze the newly designed supersonic nozzles.

Quintero F. et al. (2006) designed the different gas injection systems by using the interactions of the gas jet with the work piece. The objective of the research work was achieved by reducing the disadvantages of the conventional cutting heads. They successfully reduced the recast layer thickness and increased metal removal rate by optimizing the various gas injection systems. Melhem A. et al. (2011) studied the conical convergent nozzle for the kerf width investigations. They used conical convergent nozzle with respect to surface distance variation. They explored the heat transfer rates from the kerf wall, flow field in the kerf and the skin friction along the kerf surface. The above mentioned parameters are calculated by taking average of four jet velocities at the nozzle exit and two kerf wall wedge angles. Riveiro A. et al. (2006) presented work on quantitative experimental study to determine the influence of processing parameters on the laser cutting speed. They explored the quality characteristics by applying the off-axial supersonic nozzles. The various cutting experiments were conducted using pulsed mode. The various output responses were explained using the molten material removal phenomenon. Jacksona M.J. et al. (2005) fabricated the axi-symmetric, straight, sonic-line, minimum length micro nozzles that are suitable for laser micromachining. For this process they used the computational techniques. They developed the process using gas jets to protect the interaction zone between laser and specimen material for the laser micro-machining processing. They developed the methods to examine the machining efficiency of laser micromachining process.

2.1.7 Effect of parameters on surface roughness and dross attachment

Olsen Flemming et al. (2001) studied the effects of cutting speed, assist gas pressure, average laser power and pulse energy on medium strength steel GA 260 with a thickness of 1.8 mm. The various quality characteristics viz. the squareness, roughness and dross attachment of laser cut blanks were measured using different techniques. For quality assessment, were measured. Yilbas B.S. et al. (2008) studied CO_2 laser cutting of the wedge surfaces as well as normal surfaces (normal to laser beam axis). The quality

characteristics were considered and determined by using the international standards for thermal cutting. The various optical micrographs were analyzed for various geometrical output responses such as out of flatness and dross height.

Riveiro A. et al. (2010) determined the effect of processing parameters on laser cutting of an aluminium–copper alloy (2024-T3). They determined the various optimal conditions for different output responses by using CO_2 laser cutting setup. It was analyzed that better results were attained with the help of laser continuous mode as compared to laser pulse mode. Cicala E.et al. (2008) examined the operating parameters for laser cutting process of an aluminium alloy, stainless steel and a titanium alloy. They determined the various significant input parameters to increase the productivity of the process and quality of the machined surfaces. The disadvantages of laser machining of metals have been identified in this research work. The quality characteristics were determined for various input laser parameters. It was analyzed that laser pulse frequency and laser cutting speed has some significant effect on surface roughness.

Gyu-Dong et al. (2009) investigated the influence of laser cutting parameters on surface characteristics of Inconel 718 super-alloy as work material. To carry out this process Nd:YAG laser set up has been used by considering continuous wave processing mode. The various cutting experiments were executed using a laser cutting system with six-axis controlled automatic robot and auto-tracking system of the focal distance. Gilbert Tod et al. (2007) conducted parametric study on the surface of aluminium nitride (AlN) ceramic with an ultra-violet (UV) and near-infrared (NIR) laser. The lines and single-layer pockets was used as laser cut profiles for this process. The effect of pulse overlap and pulse frequency were studied on various quality characteristics. It was analyzed that the maximum material removal rate (MRR) was 0.011 mm^3/s with the UV laser and 0.094 mm^3/s with the NIR laser. Ghany K. et al. (2005) evaluated the optimum laser cutting parameters for 1.2 mm austenitic stainless steel sheets. They performed experimentation by using both processing modes such as laser pulse and laser continuous mode. The effect of various gases such as nitrogen or oxygen as assistant gases on the output responses has been analysed. It was explored that by increasing the frequency and cutting speed the effect on the kerf width and the roughness of cut surface decreased by large extent. On the other hand, increasing the laser power and gas pressure has shown increased kerf width and roughness values.

Thawari G. et al. (2005) studied the typical cutting regime for pulsed Nd:YAG laser cutting of 1mm thick Hastelloy-X sheet. The various cut quality characteristics such as kerf width, cut edge kerf profile and surface roughness were examined for various laser process parameters. Sharma A. et al. (2012) examined average kerf taper (Ta) and average surface roughness (Ra) for Nd:YAG laser cutting of thin Al-alloy sheet for straight profile. The various regression models were presented and optimization of cut quality characteristics has been performed using pulse mode. For both quality characteristics various input significant parameters were identified such as oxygen pressure, pulse width, pulse frequency and cutting speed.

2.1.8 Effects on output variables due to different cutting profiles

Sharma A. et al. (2012) presented the modeling and optimization of cut quality characteristics for an aluminum alloy thin sheet as work material. To perform this process, Nd: YAG laser cutting set up has been used to cut the along the curved profile. The hybrid approach of Taguchi methodology (TM) and response surface methodology (RSM) has been applied to develop the regression model for kerf deviation and average kerf taper. Lum P. et al. (2000) investigated the laser processing of medium-density fiberboard (MDF). They expressed the optimal parameter settings for various output responses. The various experiments has been performed by using both processing modes such as pulse and continuous mode. The methodology to carry out the effective cutting has been developed by correlating the input and output parameters.

Sharma A. et al. (2010) presented parameter optimization of the kerf quality characteristics using pulsed Nd: YAG laser cutting of nickel based super alloy thin sheet. The various output responses were analyzed in the form of kerf quality characteristics such as kerf width, kerf taper and kerf deviation. The variation in kerf quality characteristics measured with the help of tool makers microscope. Muhammada N. et al. (2010) studied fiber lasers for stent cutting for profiling thin (<4mm diameter) stainless steel tubes. The investigations on comparison of wet and dry pulsed fiber laser were presented for a profile cutting of 316L stainless steel tubes. It was examined that heat affected zone (HAZ), kerf width, surface roughness and dross deposition improved as compared with the dry cutting. Bandyopadhyay S. et al. (2002) studied Nd: YAG laser drilling for 4 and 8 mm thick sections of IN718 and Ti–6Al–4V materials. It was determined that laser drilling process has shown variation in the results when used with various type of material and its thickness. The parametric effect of input parameters has

been analyzed for pulse frequency and pulse energy. The effect on the geometrical features of work material has been estimated for various drilled holes such as hole diameter and taper angle.

2.1.9 Analysis of energy losses during laser machining

Scintilla L.D. (2011) investigated experimentally primary energy losses with two operating systems such as CO_2 and disk laser system. The primary energy losses were accumulated with the help of polymethylmethacrylate (PMMA) blocks. These blocks were kept under the work material sheets to collect the spark and to collect the print caused by the sparks. To carry out the investigations on primary energy losses the specimen of various thicknesses have been used.

Scintilla L.D. (2012) developed a three-dimensional, semi stationary, simplified thermal numerical model. To determine the cutting front temperature difference the conductive power losses has been examined during laser cutting process via disk and CO_2 laser beam cutting system. With the help of inverse methodology approach and heat affected zone width the unknown thermal load on the cutting front during laser cutting was determined.

Ng S.L. et al. (2000) developed experimentally-based method for laser cutting of MDF sheets using continuous and pulse processing mode of laser cutting systems to examine the power distribution. The examinations has been predicted for variations in power distribution by using various input parameters such as cutting speeds, material thickness and pulse ratios. The various input parameters were identified to determine the cutting efficiency and absorptivity index. Jebbari N. et al. (2008) proposed the model which was determined using the energy balance equations. The amount of energy inducing the thermal affected zone was calculated by considering the interaction time, laser energy and impact diameter of the laser beam. Scintilla L.D. (2012) studied the influence of processing parameters and laser source type on quality characteristics of AZ31 magnesium alloy sheets. The cutting efficiency of two cutting systems has been analyzed such as fiber and CO_2 lasers. The various experiments have been performed a fiber and CO_2 laser source for cutting of 1 mm thick sheets using argon as a assist gas and continuous wave mode of cutting systems. Karim K. et al. (2012) used the Fresnel absorption model to control the absorption of the incident wave by the surface of the liquid metal. The enthalpy-porosity technique has been applied to determine the latent

heat during melting and solidification of the molten material. the shape of the kerf has been analyzed using the VOF method.

2.1.10 Application of Finite element method in laser machining

Kim Jung et al. (2000) developed a computational model for the transient laser-cutting process using boundary element method (BEM). To formulate this model the unsteady heat transfer has been considered with the help of time dependent history of continuous Gaussian laser beam. The developed model applied for the material-cutting process using material removal process. Kim Jung et al. (2005) developed the computational model of evaporative laser-cutting process using a finite element method. For this model steady heat transfer equation was modeled for laser-cutting process with a moving laser source. The developed model used temperature distributions to determine the numerical results for groove shapes. These numerical results were compared with respect to semi-analytical methods.

Arif A.et al. (2009) considered the laser cutting of tailored blanks for a thick mild steel sheet. The finite element method has been used to develop the formulation between temperature and stress field in the cutting sections. With the help of X-ray diffraction (XRD) the residual stress were predicted for the machined sections of the work materials. The residual stress results were validated with the help of predicted results. Sowdari D. et al. (2010) examined the laser heating and melting of metals with the help of an enthalpy-based computational model. The finite element method was applied to derive the solutions of the laser cutting process and the results were validated by comparing with analytical solutions.

Yilbas B.S et al. (2010) examined the thermal stress development due to laser cutting of sharp edge of the cutting section. The temperature and stress fields were analyzed using finite element method whereas the residual stress was investigated using X-ray diffraction (XRD) technique. Yu L. M. et al. (1997) presented a FEM model using ANSYS software to determine the numerical studies of laser cutting. They used the 3-D finite element modeling to understand the mechanism of changing boundary, loading conditions and phase changes during the cutting process. Choudhury A. et al. (2010) investigated the CO_2 laser cutting of three polymeric materials namely polypropylene (PP), polycarbonate (PC) and polymethylmethacrylate (PMMA). It was evaluated that the effect of laser

power, cutting speed and compressed air pressure was considered as most significant parameters for the various output responses.

Al-Sulaiman A. et al. (2006) studied the significance of laser power on the kerf size by comparing the experimental and analytical results. The kerf width size was predicted with the help of scale law analysis. It was analyzed kerf width size increases with increasing laser power intensity whereas striation formation was explored with the help of scanning electron micrographs. Quinteroa F. et al. (2011) assessed CO_2 laser cutting process of phenolic resin boards using a design of experiments (DOE) based methodology. It was investigated by experimental results that CO_2 laser system easily cut the phenolic resin boards by using laser power of 3 KW at a 3.5 m/min cutting speed.

2.1.11 Application of artificial neural network and QFN package, fuzzy logic

Sangwan K.S et al. (2015) presented an approach for examining the optimized parametric conditions to achieve the minimum surface roughness using Artificial Neural Network (ANN) and Genetic Algorithm (GA). To identify the capability of the ANN-GA approach for optimization of surface roughness, the experimentation work has been conducted.

Li Chen-Hao et al. (2007) studied optimal laser parameters for cutting QFN (Quad Flat No-lead) packages with the help of diode pumped solid-state laser system (DPSSL). The optimal parametric combinations have been determined using Taguchi's method for the cutting of two work materials namely encapsulated epoxy and a copper lead frame substrate. Pandey A. et al. (2012) investigated the laser cutting of Duralumin sheet to minimize the kerf deviation and kerf width. The simultaneous optimization has been performed on various output responses for top and bottom side of the machined specimen.

Tsai J. et al. (2008) studied a multiple regression analysis (MRA) and an artificial neural network (ANN) to develop the predicting model for cutting Quad Flat Non-lead (QFN) packages by using a Diode Pumped Solid State Laser (DPSSL) System. The predicting model explored the results by using the input variables of the current, the frequency and the cutting speed. By using this predicting model various output responses were analyzed such as depths of the cutting line, widths of heat affected zone (HAZ) and cutting line for epoxy and for copper-compounded epoxy.

Syn Chong et al.. (2011) investigated laser cutting parameters for 1mm thickness of Incoloy alloy 800. They developed an expert system using fuzzy logic model and implemented on Fuzzy Logic Toolbox of MATLAB using Mamdani technique. The

effect of various parameters analyzed such as laser power, assist gas pressure and cutting speed for two output parameters viz. surface roughness and dross inclusion.

2.1.12 Effect of process parameters on various laser quality characteristics

The research work presented in the literature reviews shows the parametric combinations for efficient cutting of MMCs material. Stournaras et al. (2009) investigated the cutting of aluminium alloy using CO_2 laser cutting system. It was analysed that the cutting speed and laser power are the most influencing factors for heat affected zone and kerf width size. Singh et al. (2008) analysed that heat affected zone width decreases with the increase in cutting speed at constant laser power. They developed transient finite element model to predict the temperature distribution and induced stress in the specimen.

Pfeifer et al. (2010) performed the laser cutting process for 1 mm thick NiTi shape memory alloys. It was reported that variables like pulse energy, pulse width and spot overlap are the significant parameters for heat affected zone width. Yang et al. (2010) performed the parametric analysis for depth and width of heat affected zone width. They examined that heat affected zone width decreased with an increase of the laser spot size and the laser scan speed. Rajaram et al. (2003) investigated the cutting process of 4130 steel using CO_2 laser cutting system. It was stated that laser power has higher effect on heat affected zone width in comparison of cutting speed. The higher striation patterns are caused by high laser power and oxygen pressure.

Nyon et al. (2012) developed finite element model to predict the thermal stress and kerf width using element death methodology. It was analyzed that stress values increased with the increase in temperature gradient values. Arif et al. (2008) developed the simulated model by varying various parameters like cutting speed, laser power and specimen materials. It was analyzed that Inconel 625 had higher stress and temperature values in comparison to Ti-6Al-4V alloy and steel. Ozden et al. (2007) reported the effect of the accumulation of reinforced particles in composite material. Due to unequal distribution and accumulation of particles resulted into reduction of toughness properties of the material. Yan B. et al. (2005) investigated laser cutting of aluminium alloy reinforced with Al_2O_3 ceramic particles. They examined that higher quantity of reinforced particles shown higher surface roughness as compared to lower quantity.

Shabani et al. (2013) used spray atomization and co-deposition process to fabricate the MMC material having uniform distribution of reinforced particles. Pramanik A. et al.

(2015) explored the study to improve machining efficiency of titanium alloy Ti-6Al-4V. It was analyzed that the machining of titanium alloys is typical due to the deformation mechanism which causes difficulties like sawtooth chips, high temperature, high stress on cutting tool, high tool wear and undercut parts.

Venkata et al. (2013) analyzed the machinability of various composite materials. They recommended the aluminum metal-matrix composite material by considering various parameters like radial force, cutting force and surface roughness. Das Saradindu et al. (2010) examined the cathode erosion rate for a single- and multi-spark in micro-WEDM. They developed mathematical model to identify the relationship between plasma features, moving heat source characteristics, multi-spark phenomenon and wire vibrational effect. Lau et al. (1995) examined two processes laser cutting and wire electrical discharge machining for composite material. The results revealed that laser machining has higher cutting speed and heat affected zone as compared to other process. Mazahery et al. (2013) examined that higher quantity of SiC particles improved the various properties of MMC material like hardness, elongation and ultimate tensile strength.

Banea M. D. et al. (2012) studied the effect of temperature on adhesively-bonded joints. It was explored that adhesive strength and strain has strong relation with rise in temperature especially near the glass transition temperature (Tg) of the adhesive. Tofigh A. et al. (2013) analysed that addition of large sized B_4C reinforced particles decreases the wear rate of metal matrix composite material. Yilbas et al. (2010) analysed that aluminium alloy reinforced with 20% Al_2O_3 has higher kerf width values as compared to 20% B_4C composite material. Araujo et al. (2007) explored the study to analyze the microstructure and heat affected zone of aluminium alloy via laser cutting system. It was investigated that heat affected zone width is more pronounced due to thermal energy of laser beam. Sharma A. et al. (2015) developed the mathematical models of reinforcement and penetration profile in welding process. To analyze the shape and size of weld bead a physical approach was used by introducing the parametric equations and depicted as functions of process parameters such as welding current, speed, and voltage.

2.2 GAPS IDENTIFIED IN THE LITERATURE REVIEW

On the basis of literature review, following gaps in the literature are identified:

1. A thorough study of the literature observed that a few work is reported on LBM of Al/Al_2O_3, Al/SiC and Al/ZrO_2 metal matrix composite material and most of the LBM

studies on aluminium alloys are centered. These metal matrix composite material are used in manufacturing of aircraft components, space systems, automobiles and in defence weapons etc.

2. The effect of different quantity of reinforced particles on output characteristics like material removal rate, kerf deviation, kerf taper, striations, heat affected zone, surface roughness, dross height, energy losses is not mentioned in the literature review.

3. There is least work reported in the literature about the cut profiles of metal matrix composite materials. The various curve cut profiles have been selected to analyze the effect on various output characteristics.

4. Less work is reported about predictive modeling for the effects of machining variables in LBM of aluminium metal matrix composite materials. So, experimental investigations regarding LBM of MMCs, leading to predictive models using regression analysis for different responses has been carried out.

5. For analysis of stress and temperature distribution, a least work is done on curved cut profiles using finite element method.

CHAPTER 03

DESIGN OF STUDY

3.1 INTRODUCTION

LBM is complicated process if the large number of process parameters is not controlled with a optimized method. The change in value of any parameter in higher or limits may produce lack of cut quality, increase in cost and wastage of time. Thus, it is very necessary to gain optimized machining conditions with selection of appropriate cutting materials. To attain optimized parametric conditions, the detailed experimentation of the process is essential with respect to selected material for the machining operation. The detailed experimentation plan layout can be designed using some statically technique which reduces the number of experiments. The results of experimentation work may be analyzed further to determine the optimized process parameters. The various process parameters also called as control factors and their values may vary during the experimentation. This change in control factors values also known as levels. The level of any particular parameter or control factor may vary from one to multiple levels. These variables levels always have some effect on the output quality characteristics.

There are many a scientific approach to plan the run layout and levels of the control factors to validate the process. After applications of such type of approaches, the number of experimentation reduce to large numbers which saves the time, investments, increase the productivity and quality indirectly. The one factor at a time (OFTA) approach is used to design the experimental layout. This approach designs the run layout by varying one factor at a time and other parameters at fixed values. This approach is known for the screening of insignificant parameters when the control factors are large in number [Montgomery, 2002]. However, this approach has some disadvantages as follows:

i. This approach consider only one control factor at a time and the effect of all other parameters is not considered during the application of this approach. Therefore, the optimal setting of process parameters cannot be attained.
ii. OFTA approach involves large number of runs to determine the effect of parameters as compared to other scientific approaches.

iii. OFTA approach shows the effect of one parameter and effect of interactions of two or more parameters is not accounted for this approach.

To overcome above mentioned disadvantages of OFTA approach, an important approach called by name of design of experiments (DOE) was developed. Design of experiments (DOE) is defined as a tool for modeling and analysis of various problems dependent on the various control parameters using mathematical and statistical technique. [Antony, 2003] defined as designing, planning and analyzing the experimental data to attain the optimized results in efficient way.

The DOE approach has number of positive facts as listed below due to which it is commonly used in many problems [Ferreira et al.., 2007]:

i. One of the basic applications of the process is to reduce the large number of experiments which increase the efficiency of the process by eliminating the insignificant factors
ii. Using this approach the mathematical model can be developed which includes input and output responses variables.
iii. This approach identifies the experimental error during the experimentation stage.
iv. The approach is very famous due to its technique to find the optimal solutions or parametric conditions.

The approach is very famous due to its technique to find the optimal solutions or parametric conditions. With due time, there were number of scientific approaches developed which used the basic theory of design of experiments (DOE). Various methodologies such as Response Surface methodology (RSM), full factorial designs, Taguchi methodology etc have some of advantages over the basic DOE approach. These approaches are one of the most useful and significant in current industrial era to carrying out the various optimized process. However, all these approaches have some disadvantages as follows:

i. The location (mean) and dispersion (variance) effects provide typical data using Taguchi's methodology. However, this approach also uses the signal to noise ratios (S/N ratios) data to carry out the detailed analyses work.
ii. With the help of Taguchi's methodology, the information about the interaction effects cannot not be attained and considered as negligible. Due to this effect optimum design of the whole process cannot be attained efficiently.

iii. Using Taguchi's methodology, the optimized solutions cannot be obtained and also it does not pursue the sequential experimentation.

iv. This approach also not able to develop the mathematical models which have many applications for analyzing the process

v. The multi or simultaneous optimization of various parameters cannot be attained till other technique is applied.

Due to consideration of all these disadvantages the present research work is based on response surface methodology for conducting the experimentation work on LBM process. The detailed introduction of response surface methodology is given below:

3.2 Response Surface Methodology

The RSM is one of the most applicable technique in various fields such as industrial engineering, chemical engineering, structural work, aerospace engineering, manufacturing etc. This methodology uses mathematical and statistical techniques to attain the optimal solutions for any process. This technique was developed by Box and Wilson in 1951 during chemical related research work. After this successful year, this theory is still famous and applicable in various fields of technical as well general industries to achieve the optimized conditions. The RSM approach uses the response surface as a multivariate function whereas it also determines the polynomial coefficients. This approach also measures the relationship between the controllable input parameters and obtained response surfaces [Kwak, 2005]. The basic procedure to apply the response surface methodology approach is shown in figure 3.1.

If all control factors are assumed to be measurable, the response surface can be expressed as follows:

$$y = f(x_1, x_2, x_3, \ldots, x_n) \qquad \ldots\ldots\ldots\ldots (3.1)$$

y = output response

x_i = i^{th} independent variable (process parameter)

The main objective is to obtain the optimized value of the response parameter y. It is assumed that to attain the approximation of the model the existence of relationship between response surface and independent variables is necessary.

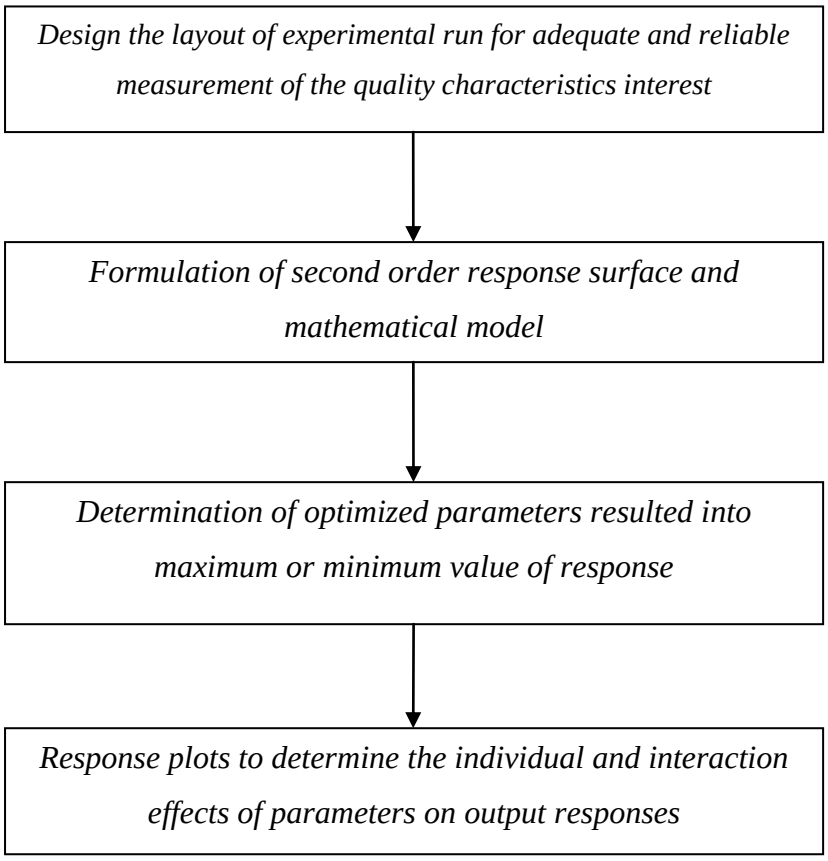

Figure 3.1 Design Procedure of Response Surface Methodology (Gunaraj et al.. 1999)

In the RSM for the interaction of two control variables, a second order surface is applied and is given by the equation as shown below:

$$y = \beta_0 + \sum_{i=1}^{k} \beta_i x_i + \sum_{i=1}^{k} \beta_{ii} x_i^2 + \sum_{i<j} \beta_{ij} x_i x_j + \varepsilon \qquad \ldots\ldots\ldots\ldots (3.2)$$

ε = random error

β = regression coefficient

y = output response

x_i = i^{th} control factor

3.2.1 Evaluation of Regression Coefficients

The method of least squares is usually to evaluation the regression coefficients in a multiple linear or quadratic regression model [Gunaraj et al.., 1999]. In general Equation (3.2) can be written in matrix form.

$$y = X \beta + \varepsilon \qquad \ldots\ldots\ldots\ldots (3.3)$$

Where y is used for showing the matrix of measured values, X to be a matrix of independent variables. The matrixes β and ε consist of coefficients and errors, respectively.

$$y = \begin{bmatrix} y_1 \\ y_2 \\ . \\ . \\ y_n \end{bmatrix} \quad X = \begin{bmatrix} 1 & X_{11} & X_{21} & . & X_{1k} \\ 1 & X_{21} & X_{22} & . & X_{2k} \\ . & . & . & . & . \\ . & . & . & . & . \\ 1 & X_{n1} & X_{n2} & . & X_{nk} \end{bmatrix} \quad \beta = \begin{bmatrix} \beta_0 \\ \beta_1 \\ . \\ . \\ \beta_k \end{bmatrix} \quad \varepsilon = \begin{bmatrix} \varepsilon_0 \\ \varepsilon_1 \\ . \\ . \\ \varepsilon_n \end{bmatrix}$$

In general, y is an n×1 vector of observations, X is an n×k matrix of levels of independent variables, β is a k×1 vector of regression coefficients and ε is an n×1 vector of random errors. The objective is to find the vector of least square estimators, b that minimizes L that is as follows:

$$L = \sum_{i=1}^{n} \varepsilon_i^2 = \varepsilon'\varepsilon = (y - X\beta)'(y - X\beta)$$
$$= y'y - \beta'X'y - y'X\beta + \beta'X'X\beta$$
$$= y'y - 2\beta'X'y + \beta'X'X \qquad \ldots\ldots\ldots\ldots (3.4)$$

Since $\beta'X'y$ is a 1×1 matrix, or scalar, and its transpose $(\beta'X'y)' = y'X\beta$ is the same scalar. The least square estimators must satisfy the following condition.

$$\left.\frac{\partial L}{\partial \beta}\right|_b = -2X'y + 2X'Xb = 0$$
$$X'Xb = X'y \qquad \ldots\ldots\ldots\ldots (3.5)$$

Equation 3.6 is set of normal equations in matrix form. Multiply both sides of this by inverse of $X'X$. Thus, least square estimator of β is (Kwak, 2005; Gunaraj and Murugan 1999):

$$b = (X'X)^{-1}X'y \qquad \ldots\ldots\ldots\ldots (3.6)$$

The fitted regression model is

$$\hat{y} = Xb \qquad \ldots\ldots\ldots\ldots (3.7)$$

Where $\hat{y}$ = estimate of y

3.2.2 Terms used for checking adequacy of model

The requirement of model adequacy checking is to (a) Identify the fitted model to check that it provides an adequate approximation to the true system and (b) to affirm that none

of the least square assumptions are violated. The various methods used for it are described below [Myers, 2002].

The deviation between observation y_i and fitted value $\hat{y}$ is called residual (e). The n×1 vector of residuals is denoted by

$$e = y - \hat{y} \quad \text{..... (3.8)}$$

The least square method produces an unbiased estimator of the parameter β in the multiple regression models. The important parameter is the sum of squares of the residuals (SS_E)

$$SS_E = \sum_{i=1}^{n} (y_i - \hat{y})^2 = \sum_{i=1}^{n} (e_i)^2 = e'e \quad \text{... ... . (3.9)}$$

From (3.7 and 3.8) substituting $e = y - \hat{y} = y - Xb$,

$$ss_E = (y - Xb)'(y - Xb)$$
$$= y'y - b'X'y \quad \text{..... (3.10)}$$

The above equation is called error or residual sum of squares with n-k-1 degrees of freedom.

Total sum of squares (SS_T) is given by following equation with n-1 degrees of freedom

$$SS_T = y'y - \left(\sum_{i=1}^{n} y_i\right)^2 / n \quad \text{..... (3.11)}$$

It is necessary to test for significance of the model. This method involves partitioning the total sum of squares into sum of squares due to model (regression) and sum of squares due to error [Myers, 2002].

$$SS_T = SS_R + SS_E \quad \text{..... (3.12)}$$

$$SS_R = b'X'y - \left(\sum_{i=1}^{n} y_i\right)^2 / n \text{ with k degrees of freedom} \quad \text{..... (3.13)}$$

F Statistics is a test for comparing model variance with residual (error) variance. It is the ratio of mean square of regression (MS_R) to the mean square of error (MS_E).

Where

$$MS_R = \frac{SS_R}{k} \quad \text{..... (3.14)}$$

$$MS_E = \frac{SS_E}{n-k-1} \quad \text{..... (3.15)}$$

If model F value is greater than $F_{\alpha,k,n-k-1}$, then the model is considered valid. Alternatively, p-value approach to hypothesis testing can be utilized, according to which if p-value of the F statistics of the model is lower than the confidence interval (α), the model is considered valid.

R^2 is a measure of amount of reduction in the variability of y obtained by using the regressor variables x_1, x_2,..,x_n in the model and can be determined by ratio of sum of squares due to regression to the total sum of squares ($\frac{SS_R}{SS_T}$) . The domain for R^2 = 0 to 1. A larger value of R^2 does not fulfill the condition of good regression model. It has been analysed that by addition a variable to the model will always increase R^2, regardless of whether the additional variable is statistically significant or not. Thus, it is always selected to use an adjusted R^2 statistics that is defined as follows:

$$R^2_{adj} = 1 - \frac{SS_E/(n-k)}{SS_T/(n-1)} \qquad \text{..... (3.16)}$$

Adjusted R^2 evaluate the amount of variation around the mean given by the model, adjusted for the number of terms in the model. The adjusted R-square values show lower variation as the number of terms in the model increases, if additional terms do not include value to the model. Adequate Precision is a term that identify signal to noise ratios. It equated the range of the predicted values at the design points to the average prediction error. The ratios greater than 4 indicate adequate model discrimination.

It is frequently useful to obtain two or more observations (replicates) on the response at the same settings of independent variables. As replicates of the central point are made, it is possible to estimate pure error associated with repetitions. Thus, sum of the square for residuals can be dismembered into two more parcels: the sum of the square due to pure error (SS_{PE}) and the sum of the square due the lack of fit (SS_{LOF}), as shown below:

$$SS_{RES} = SS_{PE} + SS_{LOF} \qquad \text{..... (3.17)}$$

$$SS_{PE} = \sum_{i=1}^{m}\sum_{j=1}^{n_i}(y_{ij} - \bar{y}_i)^2 \qquad \text{..... (3.18)}$$

$$SS_{LOF} = \sum_{i=1}^{m} n_i\ (\bar{y}_i - \hat{y}_i)^2 \qquad \text{..... (3.19)}$$

$$MS_{PE} = \frac{SS_{PE}}{n_i - 1} \qquad \text{..... (3.20)}$$

$$MS_{LOF} = \frac{SS_{LOF}}{m-k} \quad \text{..... (3.21)}$$

where

y_{ij} = j^{th} observation on the response at y_i

n_i = number of observations at i^{th} level

m = levels of x_i

$n_i - 1$ = degrees of freedom associated with SS_{PE}

$m - k$ = degrees of freedom associated with SS_{LOF}

Another way to evaluate the model is the lack of fit test. If the mathematical model is well fitted to the experimental data, MS_{LOF} will reflect only the random errors inherent to the system. Additionally, MS_{PE} is also an estimate of these random errors and it is assumed that these two values are not statistically different. This is the key idea of the lack of fit test. It is possible to use the *F* distribution to evaluate if there is some statistical difference between these two media, in the same way that the significance of regression was verified:

$$\frac{MS_{LOF}}{MS_{PE}} \approx F_{(dlof\ ,dpe)} \quad \text{..... (3.22)}$$

where, *dlof* and *dpe* are the degree of freedom associated with the lack of fit and the pure error respectively. If this ratio is higher than tabulated value of *F*, it is concluded that there is evidence of a lack of fit and that the model needs to be improved. However, if the value is lower than tabulated value, the model fitness can be considered satisfactory. To apply a lack of fit test, the experimental design must be performed with authentic repetitions at least at its central points.

3.3 Analysis of Variance

Analysis of variance (ANOVA) is a technique for analyzing experimental data in which one or more response (or dependent) variables are measured under various conditions identified by one or more classification variables. In ANOVA, variation in the response is separated into variation attributable to differences between the classification variables and variation attributable to random error. To accomplish this, Sum of squares due to error (SS_E), Sum of squares due to regression (SS_R) and Total Sum of squares (SS_T) are utilized. The (SS_T) is divided into following four parts to measure the deviations of the

response from the fitted surface and estimation of the experimental error from center runs (Pecas and Henriques, 2003). Table 3.1 shows the various terms related the Analysis of variance of input functions.

Table 3.1: ANOVA terms used in multiple regressions (Marcos et al.., 2008)

Variation Source	Sum of Squares (SS)	Degrees of Freedom	Mean Square (MS)
Regression	$SS_R = \sum_{i=1}^{m}\sum_{j=1}^{n_i}(\hat{y}_i - \bar{y})^2$	$p-1$	$MS_R = \frac{SS_R}{p-1}$
Residuals	$SS_{residual} = \sum_{i=1}^{m}\sum_{j=1}^{n_i}(y_{ij} - \hat{y}_i)^2$	$n-p$	$MS_{residual} = \frac{SS_{residual}}{n-p}$
Lack of fit	$SS_{LOF} = \sum_{i=1}^{m}\sum_{j=1}^{n_i}(\hat{y}_i - \bar{y}_i)^2$	$m-p$	$MS_{LOF} = \frac{SS_{LOF}}{m-p}$
Pure error	$SS_{PE} = \sum_{i=1}^{m}\sum_{j=1}^{n_i}(y_{ij} - \bar{y}_i)^2$	$n-m$	$MS_{PE} = \frac{SS_{PE}}{n-m}$
Total	$SS_T = \sum_{i=1}^{m}\sum_{j=1}^{n_i}(y_{ij} - \bar{y})^2$	$n-1$	

n = number of observations

m = total number of levels in the design

p = number of parameters of model

$\bar{y}$ = overall mean

$\hat{y}_i$ = estimated value by the model for the level *i*;

y_{ij} = replicates performed in each individual levels;

$\bar{y}_i$ = mean of replicates performed in the same set of experimental conditions.

Based upon results obtained from ANOVA, mathematical models consisting of significant terms of individual and interaction effects are built for responses of interest.

3.4 Box- Behnken Designs

Box–Behnken designs (BBD) are one class of the experimental designs for response surface methodology. They are rotatable or nearly rotatable based on three-level incomplete factorial designs (Box and Behnken, 1960). Rotatable means that the model

would possess a reasonably stable distribution of scaled prediction variance throughout the experimental design region (Montgomery, 2002).

The special arrangement of the BBD levels allows the number of design points to increase at the same rate as the number of polynomial coefficients. For example, for three factors, the design can be constructed as three blocks of four experiments consisting of a full two-factor factorial design with the level of the third factor set at zero (Souza et al.., 2005).

BBD allows calculations of the response function at intermediate levels and enables estimation of the system performance at any experimental point within the range studied through careful design and analysis of experiments. Another advantage of the BBD is that it does not contain combinations for which all factors are simultaneously at their highest or lowest levels. Thus, these designs are useful in avoiding experiments performed under extreme conditions, for which unsatisfactory results might occur (Ferreira et al.., 2007; Myers and Montgomery, 2002).

Therefore, for three factors BBD, its graphical representation can be seen as a cube that consists of the central point and the middle points of the edges as shown in figure 3.2. However, it can also be viewed as consisting of three interlocking 2^2 factorial designs and a central point (figure. 3.3). BBD requires three levels of each factor instead of five as in the case of Central Composite Designs (CCD), which results in fewer experimental trials to evaluate multiple variables and their interactions and is more convenient and less expensive to run than CCD with the same number of factors (Ragonese et al.., 2002) as indicated in Table 3.2. From the previous literature it has been analysed that Box - Behnken Design develop good run layout as compared to other techniques such as central composite design and full factorial design. From the table, it can be analyzed that only box-behnken technique has potential to develop the design with lower run layout. Box - Behnken Design uses the backward elimination process to eliminate the non-significant parameters after the application of ANOVA.

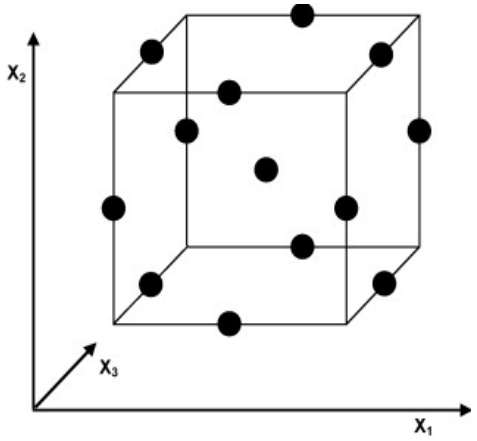

Figure 3.2 Box–Behnken designs as developed from a cube [Souza et al.., 2005]

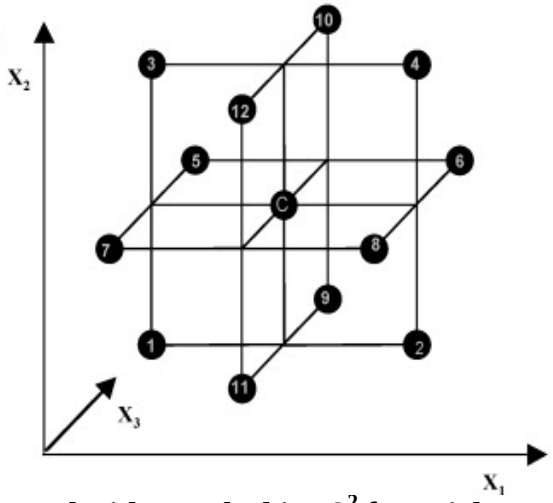

Figure 3.3 BBD represented with Interlocking 2^2 factorial experiments (Souza et al.., 2005)

Table 3.2 Number of experiments based on various design approach (Source: www. It1.nist.gov, 2011)

No. of Factors	Number of Experiments		
	Central Composite Design	Full Factorial Design	Box -Behnken Design
2	13	9	11
3	20	27	15
4	30	81	27
5	50	243	46
6	86	729	54
7	152	2187	62

CHAPTER 04
EXPERIMENTATION

4.1 INTRODUCTION

In LBM process the main role of optimized input parameters is to achieve best quality characteristics. To acquire the optimized parameters, it is necessary to accomplish the experimentation work followed by statistical analysis and validation experimentation. Thus, set of various experiments have been performed in order to analyze the effect of different process parameters on various output responses such as striations, heat affected zone width, edge surface roughness, dross height, material removal rate, kerf taper, kerf deviation, energy losses, analysis of temperature and stress fields, morphological and metallurgical variation on the machined surface. In the present research work an attempt has been made to perform exhaustive experimentation work to analyze the optimized parameters. All the experimentation work has been performed on CO_2 laser setup (manufactured by Trumpf 2500, Tru-laser 1030, Germany). The specifications of the setup are tabulated in table 4.1.

Table 4.1 Specification of CO_2 laser setup

S.NO.	Parameter	Units	CO_2 laser
1	Power	watt	2500
2	Mode of operation	--	Continuous or pulse
3	Wavelength	µm	10.6
4	Focus length	mm	Variable (-2 to + 2)
5	Frequency	kHz	20
6	Cutting Speed	mm/min	4000
7	Mode Quality	--	TEM_{00}
8	Nozzle Type	--	Co-axial Nozzle
9	Focal Length of lens	mm	120
10	Bed Dimension	mm	3000×1500
11	Gas Type	--	Nitrogen gas
12	Gas Pressure	bar	6-16
13	Duty Cycle	%	1-100
14	Power Requirement	volt	230

4.2 SPECIFICATIONS OF WORK PIECE MATERIAL

The specimen material Aluminium alloy 5052 series required for experimentation was procured from M/s Virat Aluminium, Mumbai, India. To fabricate the aluminium metal matrix composites the ceramic powders SiC, Al_2O_3 and ZrO_2 was used in variable quantity. To manufacture the various Al5052/SiC, Al5052/Al_2O_3 and Al5052/ZrO_2 MMCs work material the stir casting set up has been used. The schematic diagram of stir casting setup and line diagram of laser set up is shown in figure 4.1 (a, b). The chemical composition of Aluminium alloy 5052 series is shown in table 4.2. The mechanical properties of various metal matrix composites material is shown in table 4.3.

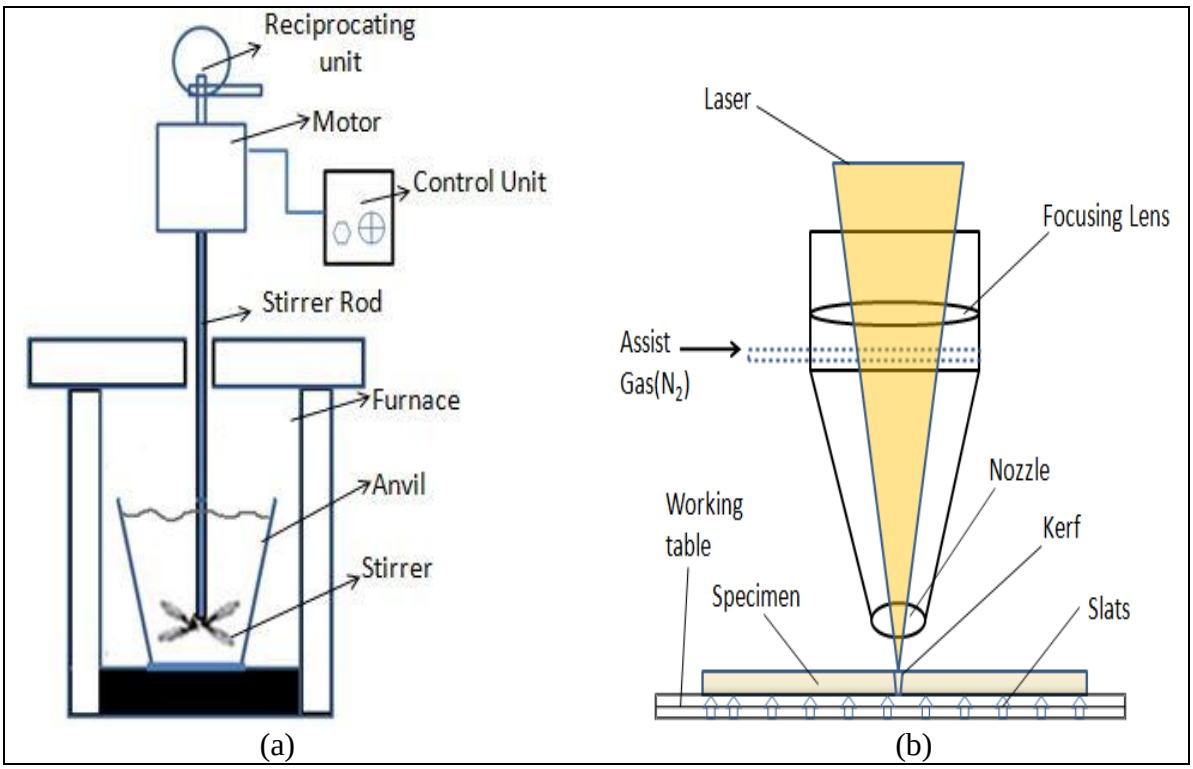

Figure 4.1 Stir Casting setup for MMCs and line diagram of laser set up (a, b)

Table 4.2 Chemical composition of 5052 aluminium alloy

S.No.	Element	Si	Fe	Cu	Mg	Ti	Mn	Cr	Al
1	Wt %	0.12	0.28	0.02	2.29	0.01	0.06	0.18	97.04

Table 4.3 Mechanical Properties of MMC work material

Reinforced Particles wt %	Brinell Hardness (HB)	Tensile Strength (MPa)
Al 5052	60	207
10 % SiC	73	251
20 % SiC	80	276
10 % Al_2O_3	72	248
20 % Al_2O_3	76	258
10 % ZrO_2	76	262
20 % ZrO_2	85	293

4.3 PROCESS PARAMETERS OF LBM

Laser beam cutting is basically controlled by optical parameters like optical lens, focal length etc. There are many parameters which cannot be controlled by operators such as beam quality, wavelength and maximum output laser power. Other parameters like gas pressure, type of gas, cutting speed, nozzle stand-off distance, laser frequency, laser power, material thickness, nozzle diameter, focal length and focal point position can be controlled by the operator. Thus, laser process parameters can be divided into three categories such as:

(i) Optical parameters: focal length, lens diameter and focal point position.

(ii) Electrical parameters: laser frequency, laser power etc.

(iii) Non-electrical parameters: gas pressure, type of gas, nozzle diameter, stand-off distance, material type and thickness.

The selection of input parameters and their range mainly effects the quality of the cut in terms of surface roughness, heat affected zone, kerf taper etc. Thus, the selection of controllable process parameters and their ranges becomes important factor. These controllable machining parameters are discussed as follows:

4.3.1 Cutting Speed

During the laser cutting operation the laser energy travels in two way path, energy supplied to produce the required cut and secondly is energy losses from the kerf zone. With increase in cutting speed the energy losses decreases to lower levels resulting into increase in cutting efficiency of laser setup. The laser cutting speed also depends on the cutting profile, for straight cut profile the cutting speed remains higher whereas for curve

or complex profiles the cutting speed decreases rapidly. The cutting speed must be maintained gas pressure and laser power. It has been observed that with low cutting speed and high power, the side burning occurs in terms of heat affected zone width and dross height.

4.3.2 Laser Power

Laser power and cutting speed are interrelated to each other as when the laser power increases, laser cutting speed also increases. Laser power can be defined as the total energy emitted in the form of laser beam or light per second. It is very necessary to have optimum power range for cutting of various materials. Due to non-optimum incident laser power may produce higher heat affected zone, kerf width, kerf taper, recast layer, dross height etc. Whenever, the average laser power is high the vaporized material contains heats transferred to kerf front and may decline the cut quality. During the cutting of complex or curved profiles with high laser power the overheating of kerf edges take place resulting in lack of cut quality. Moreover, the insufficient incident power may not provide the required amount of energy for initiating the cutting process.

4.3.3 Nozzle stand-off distance and diameter

Nozzle stand-off distance is distance between the specimen and the nozzle. Nozzle stand-off distance influences the turbulence factor and pressure variation of assist gas. It has been explored that nozzle diameter should be greater than standoff distances to avoid the turbulence of the assist gas. Nozzle diameter is small orifice in the nozzle to perform a job to supply the laser beam and assist gas simultaneously. The main function of nozzle and nozzle diameter is to minimize the turbulence in the molten zone of material to be cut. The quality of cut also depends on variation in the nozzle diameter. Nozzle diameter varies from 0.8 mm and 3 mm which depends upon the thickness of the material to be cut and type of the material.

4.3.4 Gas pressure and type of gas

The selection of assist gas and gas pressure also decides the quality of cut. The assist gas pressure exits the molten material without solidification resulting into less formation of dross height. The selection of particular gas depends on the material type and thickness of the material. The assist gases such as oxygen and nitrogen are commonly used gas in the industries. However the oxygen gas is known as assist gas used to cut steels and some of its alloys. The nitrogen gas categorized in the inert gases used to cut materials such as stainless

steel, aluminium and nickel alloys etc. The gas pressure may vary from 1 bar to 20 bar depending upon the cutting conditions, material thickness and type.

4.3.5 Aluminium alloy metal matrix composite material

A metal matrix composite (MMC) is material which is having excellent properties such as strength, light weight, toughness etc. MMCs material is a combination of two constituent parts, one is metal and other may be ceramics material, metal and organic compound. The ceramic material may be in the powder form such as boron nitride, Silicon carbide, aluminium oxides etc. In the present study, aluminium alloy 5052 is used as base metal whereas SiC, Al_2O_3, ZrO_2 powders used as reinforced material. The various types of specimens fabricated by stir casting setup with the variation of ceramic powders of 0, 10 and 20 %. Before pouring into molten aluminium metal, the particulate was preheated to 500-600 ˚C to remove the moisture content. The particle size of all the ceramic or reinforced particles was of 37 µm.

4.3.6 Cut Profile

The cut profile also plays an important role in deciding the quality of the cut in terms of heat affected zone, kerf width, kerf taper etc. The cut profiles are basically categorized in three parts such as straight, zig-zag and circular cut. The straight cut is assumed to be simplest profile to perform machining operation on it. The zig-zag cut may have corners in which stress concentration factor also involves a important point to be considered. One of the most typical cut profiles is contour or circular cut which consists of various arc of different radius. In the present study, the contour profiles have been selected for the analysis work. These contours profiles selected in the form of arc of different radius like 2, 4 and 6 cm.

4.4 PILOT EXPERIMENTATION

The pilot experimentation is performed using one-factor-at–a–time approach (OFTA) which differs from other design approaches like Taguchi, Box-Behnken etc. One-factor-at–a–time approach follows the fixed parameters values by incrementing the value of one parameter. According to literature survey, various researchers have applied this approach to analyse the effect of single parameter on output response. (Rao Paramsewar et al.., 2010; Tarang et al.., 1995). The selected cut profile for pilot experimentation is shown in figure 4.2 having various arc of different radius such as 2, 4 and 6 cm. The variation of input parameters for pilot experimentation is tabulated in the table 4.4.

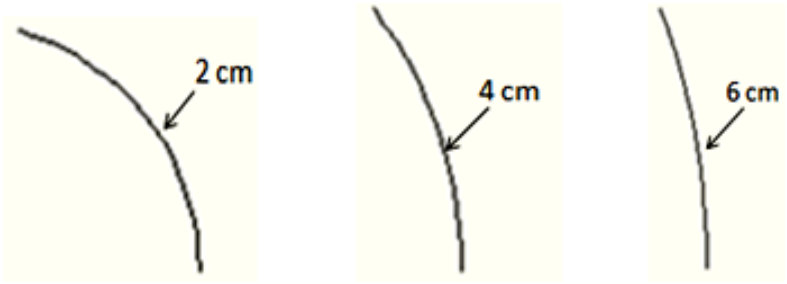

Figure 4.2 Laser cut profile with different arc radius

Table 4.4 Variation of input parameters for pilot experimentation

Parameters	**Range (machine units)**	**Units**
Cutting Speed	500-3000	mm/min
Laser Power	100-2500	watt
Standoff Distance	0.5-3	mm
Nozzle Diameter	0.8-2.3	mm
Gas Pressure	6-16	bar
R. SiC Particles	0-25	% wt
Arc Radius	10-60	mm

4.4.1 Procedure for Pilot Experimentation

In this research work, the pilot experimentation was carried out on Al/SiC/10-25% composite material by following various steps as reported in followings explanation.

(i) The specimen of 18×18 cm was clamped on the machine bed by checking the correction of x and y –axis.

(ii) Within the laser head assembly, the production of laser takes place via CO2 and combination of other gases in a gain medium.

(iii) With the help of working coordinate system (WCS), a reference point is set on the corner of the workpiece.

(iv) The produced laser output is then travelled to collimated unit to increase the quality of beam and waist diameter.

(v) The laser head then shifted where the initial cutting has to start and set a zero point at the starting location.

(vi) The various process parameters are set on the Technology software via manual operation. After all the process, the circular cut of arc radius of 6 cm is executed.

(vii) The whole process is repeated for the next cut to be made on the specimen material.

4.5 Effect of Process Parameters on kerf width and surface roughness

The variation of input parameter (incremental) and its effect on the output responses such as kerf width and surface roughness are discussed below by keeping other parameters at fixed middle level.

4.5.1 Effect of cutting speed on kerf width (K_w) and surface roughness (R_z)

The cutting speed increased from 500 mm/min to 3000 mm/min keeping all other parameters at their mid values (X_2: 2000 watt, X_3: 1.5 mm, X_4: 1.7 mm, X_5: 12 bar, X_6: 10 %, X_7: 4 cm). Figure 4.3 (a, b) shows the scatter plots of cutting speed versus response characteristics. From the graph it can be predicted that as the cutting speed increased the kerf width decreased to lower levels. When the cutting speed was kept at 3000 mm/min the kerf width was reduced to 0.492 mm. Moreover, the lower cutting speed of 500 mm/min raised the kerf width more than 0.502 mm which is the highest value. This is attributed to the fact that with higher cutting speed the interaction time is less between specimen and laser beam which decreases the energy losses. The similar evolutions have been investigated in case of surface roughness with the increase in cutting speed. From figure 4.3 (a) it can be examine that when the cutting speed kept at 500 mm/min the value of surface roughness was raised to highest value of 0.368 µm. Moreover, with the increased cutting speed value of 3000 mm/min the surface roughness value was noted as lowest of 0.290 µm. It may be due to less heat diffusion process which leads to lower side burning process with higher cutting speed.

4.5.2 Effect of laser power on K_w and R_z

Figure 4.4 (a), (b) shows the effect of laser power on the kerf width. It has been investigated that with increase in laser power the kerf width increased to higher values. From the plot it can be examine that when the laser power increased from 1500 watt to

2500 watt, the value of kerf width increased from 0.480 to 0.497 mm as shown in figure 4.4 (a).

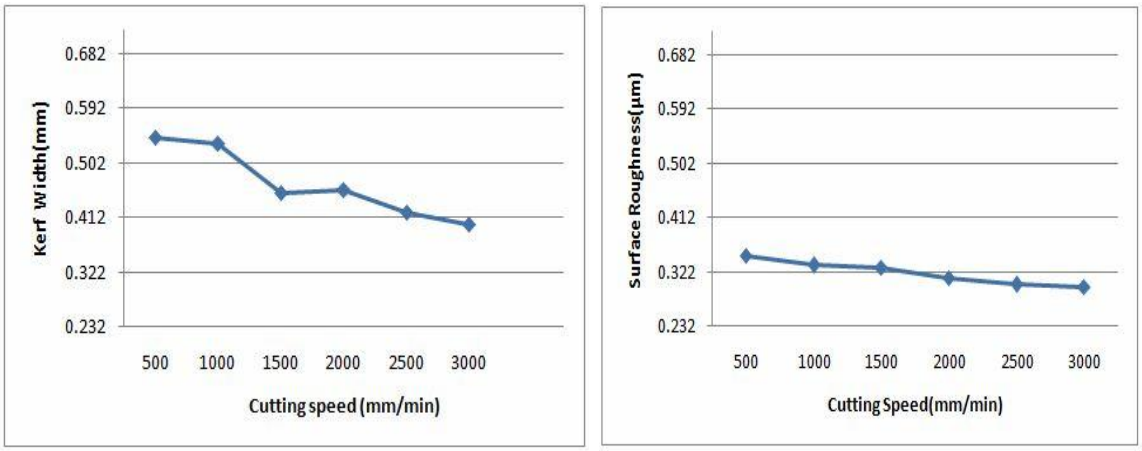

(a) (b)

Figure 4.3 Effect of cutting speed on kerf width (a) **and surface roughness** (b)

With the increment in laser power, the energy in the kerf zone increases resulted into higher kerf width size. On the other hand, higher laser power decreases the surface roughness of machined surface. It has been noticed that when laser power kept constant at 2500 watt, the surface roughness decreased to lower levels of 0.352 µm. On the other hand vice-versa results have been examined for least value of laser power as shown in figure 4.4 (b). With the increment in laser power from 1500 W to 2500 W the surface roughness decreased significantly as sufficient energy is deported to cutting zone for clear cut.

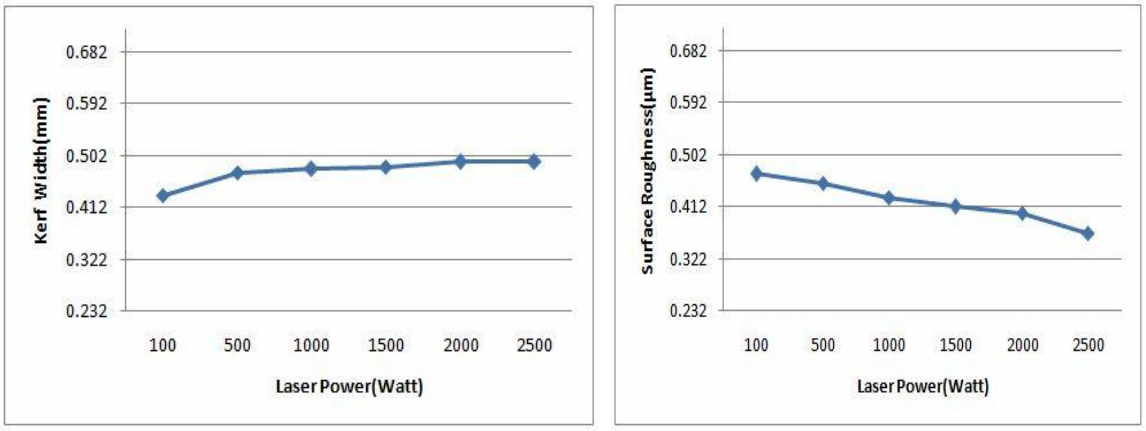

(a) (b)

Figure 4.4 Effect of laser power on kerf width (a) **and surface roughness** (b)

4.5.3 Effect of stand-off distance on K_w and R_z

The nozzle stand-off distance decides variation of the turbulence and pressure of assist gas flowing from the nozzle. It can be explored from the figure 4.5 (a) that when the

stand-off distance set at 0.5 mm, the kerf width value raised to 0.464 mm. It can be investigated that with the increase in stand-off distance from 2 mm to 3 mm, the change in kerf width value shown large variation. With the increase in stand-off distance from 0.5 mm to 3 mm, the kerf width value increased to 0.502 mm which is the highest value of kerf width. It may be due to large distance between specimen and nozzle developed the large turbulence of assist gas resulted into high exothermic reaction which increased the kerf width value to higher level. From the figure 4.5 (b) it can be examine that when the stand-off distance increased from 0.5 mm to 1.5 mm, a small variation in surface roughness is noticed. Moreover, when the distance increased 2 mm to 3 mm a higher variation is noticed. As a result, the R_z value increased from 0.421 mm to 0.471 µm and may be attributed to turbulence factor.

4.5.4 Effect of nozzle diameter on K_w and R_z

The nozzle diameter used according to thickness of material to be cut and material type. The other machining conditions also decide the diameter of nozzle to be used. From the figure 4.6 (a) it can be explored that when the nozzle diameter set at 0.8 mm the kerf value reported as 0.423 mm. When the diameter increased to 1.1 mm the kerf value also raised to highest value of 0.489 mm. The kerf value attained lower value when the diameter set at 1.4 mm. When the nozzle diameter value raised to 2.3 mm the kerf value also increased to 0.402 mm. Due to this type of variation, the selection of values of diameter was set from 1.4 mm to 2 mm for the main experimentation. Similarly, the unpredictable variation trend has been reported in case of surface roughness. The lower variation of surface roughness has been noticed when the diameter was varied between 1.4 µm to 2 µm as shown in figure 4.6 (b). It may be due to the fact that higher turbulence of assist gas able to exit the molten metal from the cut zone.

4.5.5 Effect of gas pressure on K_w and R_z

The gas pressure also decides the velocity of flow of the molten material in the kerf zone. It is evident that on increasing gas pressure the melt flow velocity of molten material in the kerf zone also increased. This, in turns, lower thickness of melt film resulted into lower kerf width.

From the figure 4.7 (a) it can be analyzed that when the gas pressure kept at 6 bar the kerf width value raised higher than 0.412 mm. With the increase in gas pressure from 10 to 14 bar, the kerf width value also decreased to 0.346 mm.

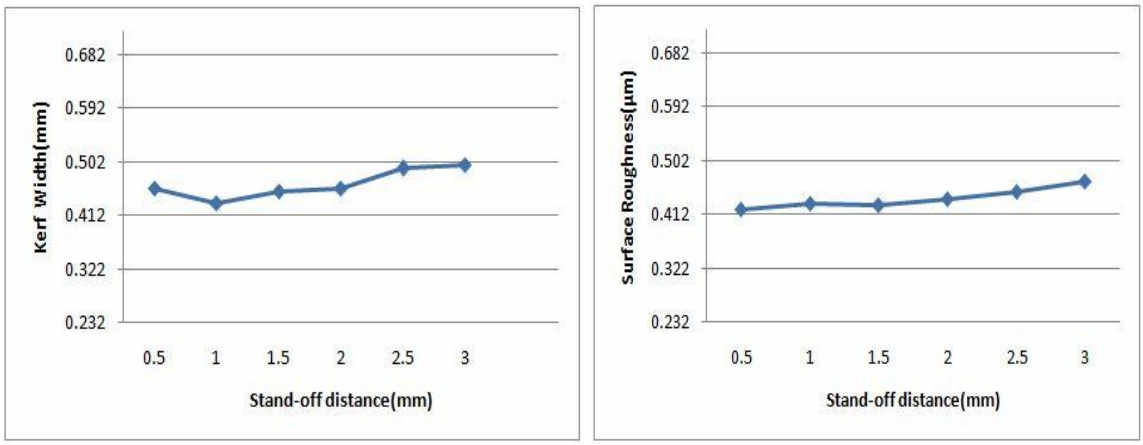

(a) (b)

Figure 4.5 Effect of stand-off distance on kerf width (a) and surface roughness (b)

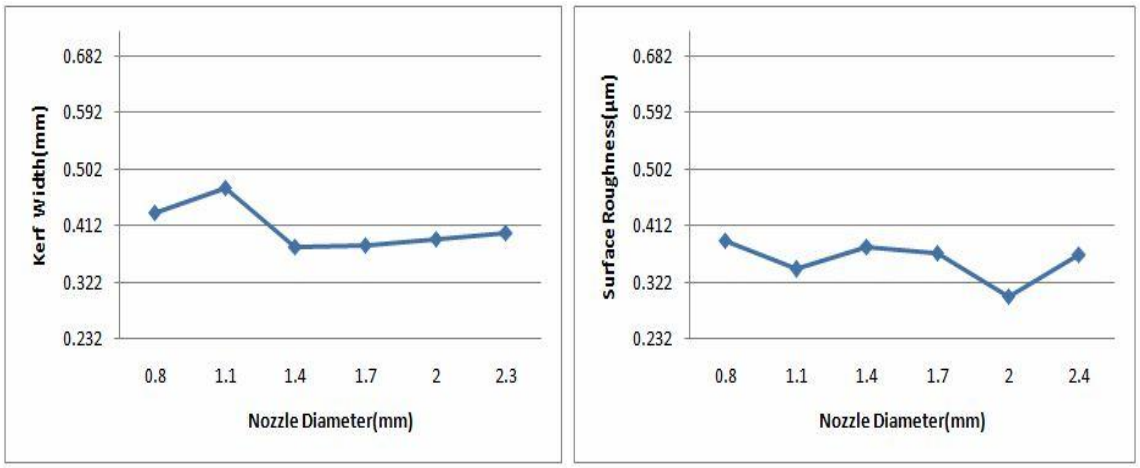

(a) (b)

Figure 4.6 Effect of Nozzle Diameter on kerf width (a) and surface roughness (b)

It may be attributed to lower melt film thickness which is due to developed by the high turbulence of gas pressure in the kerf zone. For the lower surface roughness, the higher gas pressure plays an important role as can be examined from the figure 4.7 (b). It can be observed from the graph that when gas pressure increased from 10 bar to 14 bar, R_z value decreased from 0.418 to 0.387 µm.

4.5.6 Effect of SiC reinforced particles

The percentage reinforced particles also decide the performance and efficiency of the machining process. The interaction of laser with reinforced particles is typical mechanism due to variation of melting temperature of base metal and matrix material.

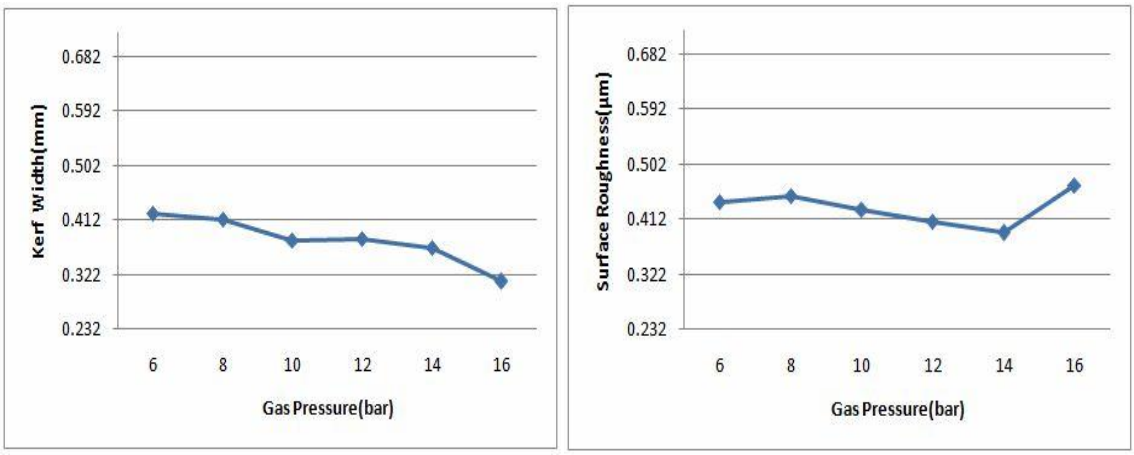

(a) (b)

Figure 4.7 Effect of gas pressure on kerf width (a) and surface roughness (b)

From the figure 4.8 (a) it can be examine that with the increment in the quantity of SiC reinforced particles from 0 to 10 % in the specimen, the kerf width also increased with higher levels of 0.264 mm to 0.322 mm. The kerf width value increased to higher levels when the reinforced particles quantity increased further from 10 to 25 %. The higher quantity of SiC reinforced particles in specimen increases the roughness of the surface as depicted in the figure 4.8 (b). Because presence of high quantity of ceramic particles modifies the cutting front dynamics (Lamikiz et al.., 2005) and raise the viscosity levels. The values of surface roughness were lower for 0 to 10 % reinforced particles quantity in the specimen. Moreover, the surface roughness value shown increment from 0.324 to 0.413 µm when the quantity of SiC reinforced particles increased from 15 to 25 %.

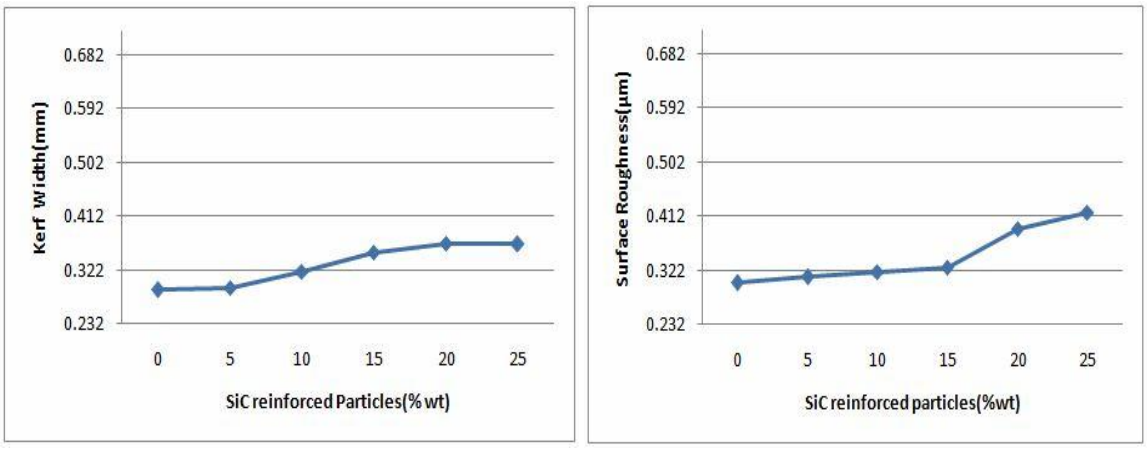

(a) (b)

Figure 4.8 Effect of SiC particles on kerf width and surface roughness

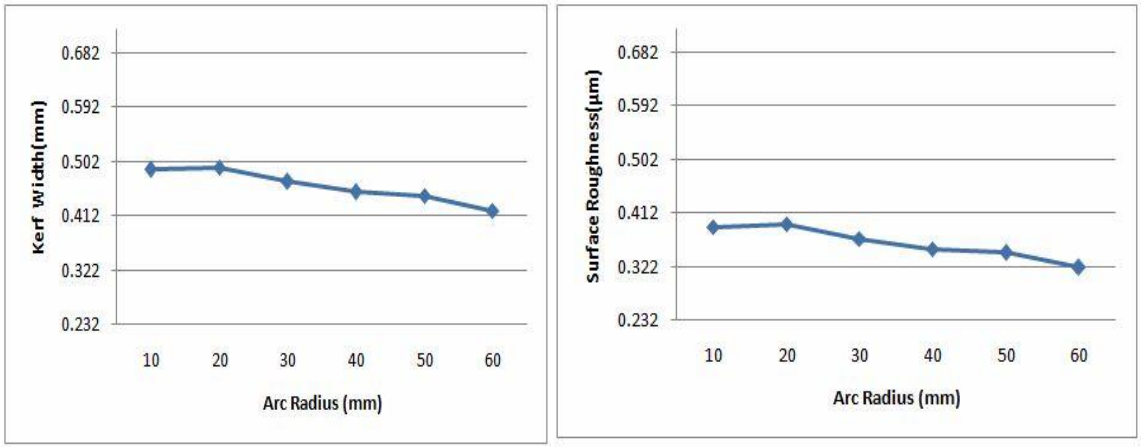

(a) (b)

Figure 4.9 Effect of arc radius on kerf width (a) and surface roughness (b)

4.5.7 Effect of arc radius

The cut profile also a deciding factor for the quality characteristics. The results for straight and curve cut profiles always differ due to energy levels in the cutting zone. From the figure 4.9 (a) it can be analysed that when the arc radius set at 10 mm the kerf width shown highest value of 0.490 mm. The arc of radius 10 mm means it has more curvature than the 60 mm arc. Due to this factor the kerf width has shown higher value. This may be attributed to the fact that ejection of molten material becomes difficult in more complex cut profile (i.e. arc radius 20 mm) than the less curvature cut profile (Sharma A et al.., 2013). From the figure 4.9 (b) it can be analyzed that for the arc radius of 60 mm the surface roughness value decreased to lower levels of 0.322 µm whereas it is higher for 20 mm arc radius.

4.6 MAIN EXPERIMENTAL PLAN

The main experimentation plan for the present research work is designed using response surface methodology (RSM). The Box-Behnken design (BBD) approach is used to design the run layout for the experimentation. The BBD construction for seven process parameters basically depends on partially balanced incomplete block designs. A box-bhenken method is considered as excellent statistical tool and having significance in finding multi-optimization model which further helps to make the design for experimental run. This method also useful to find the interaction effects between various input variables for a particular process. Total seven laser input process parameters were varied, with 3 levels of each parameter. In Table 4.5 the design matrix of BBD is shown for seven process parameters at three levels. A total 62 design points are developed using design expert software 6.0. All process parameters such as X_1, X_2, X_3, X_4, X_5, X_6 and X_7

varied by three levels and are depicted as +1, -1 and 0 depict high, low and zero level respectively. The range of all process parameters is based on pilot experimentation. Table 4.5 shows the parameter range and their levels for the main experimentation.

Table 4.5 Design matrix of Box- Behnken design for seven factors at three levels

$$D(X)=\begin{bmatrix} X1 & X2 & X3 & X4 & X5 & X6 & X7 \\ \pm1 & \pm1 & 0 & \pm1 & 0 & 0 & 0 \\ 0 & \pm1 & \pm1 & 0 & \pm1 & 0 & 0 \\ 0 & 0 & \pm1 & \pm1 & 0 & \pm1 & 0 \\ \pm1 & 0 & 0 & \pm1 & \pm1 & 0 & \pm1 \\ 0 & \pm1 & 0 & 0 & \pm1 & \pm1 & 0 \\ \pm1 & 0 & \pm1 & 0 & 0 & \pm1 & \pm1 \\ 0 & 0 & 0 & 0 & 0 & 0 & 0 \end{bmatrix}$$

Legend: X_1, X_2 , X_3, X_4, X_5, X_6 & X_7 = Control Factors,+1= high level, -1= low level, 0= zero level

Table 4.6 Laser cutting parameters and their levels for main experimentation

S.No.	Input factors	Level			Units
		I	II	III	
1.	Cutting Speed	1000	2000	3000	mm/min
2.	Laser Power	1500	2000	2500	watt
3.	Standoff Distance	1	1.5	2	mm
4.	Nozzle Diameter	1.4	1.7	2.0	mm
5.	Gas Pressure	10	12	14	bar
6.	R. SiC Particles	0	10	20	wt%
7	Arc Radius	20	40	60	mm

4.7 MAIN EXPERIMENTATION

The experimental work performed on 2.5 KW CO_2 laser cutting set-up (Model: Trucoax 2500, Trulaser 1030) using continuous wave model. Nitrogen gas is used as assisted gas for efficient cutting of aluminium alloy 5052 reinforced with SiC, Al_2O_3 and ZrO_2 particles. Different process variables like cutting speed, laser power, stand-off distance, nozzle diameter, nitrogen gas pressure, percentage reinforced particles and arc radius

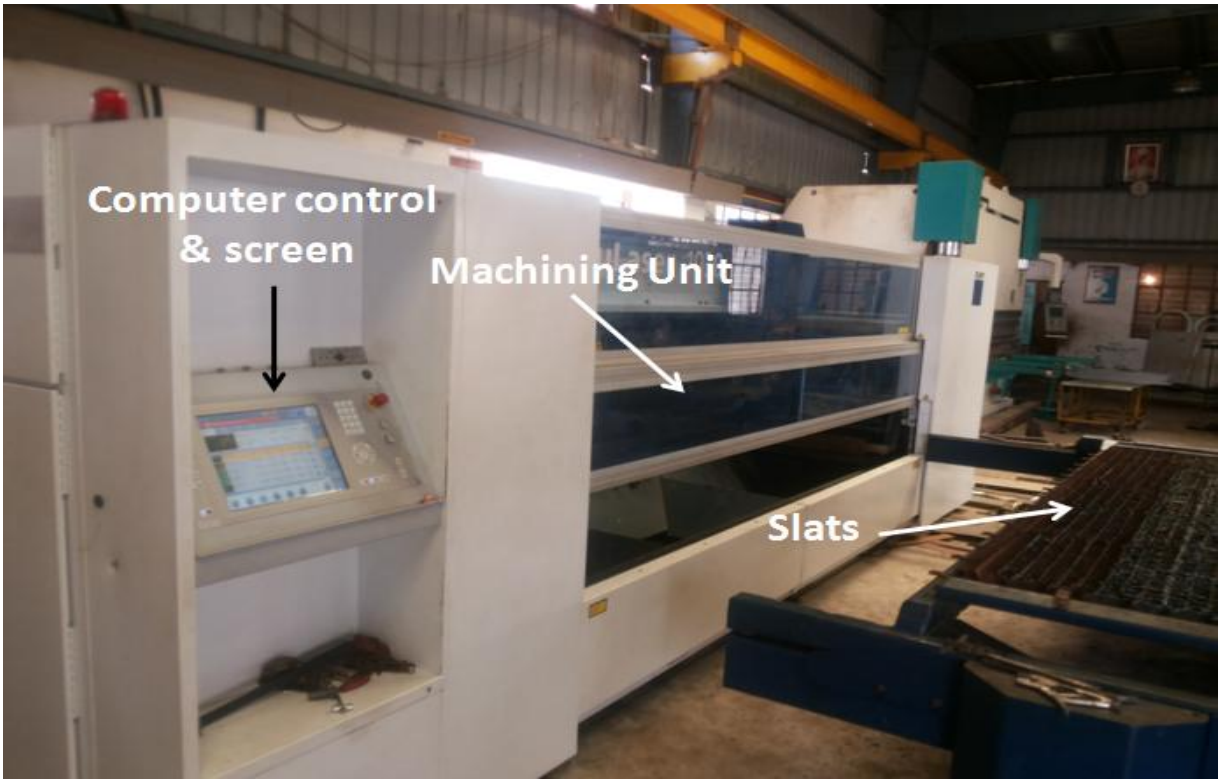

Figure 4.10 Main experimental setup CO_2 laser cutting system (Source: Aman Metal Pvt. Ltd.)

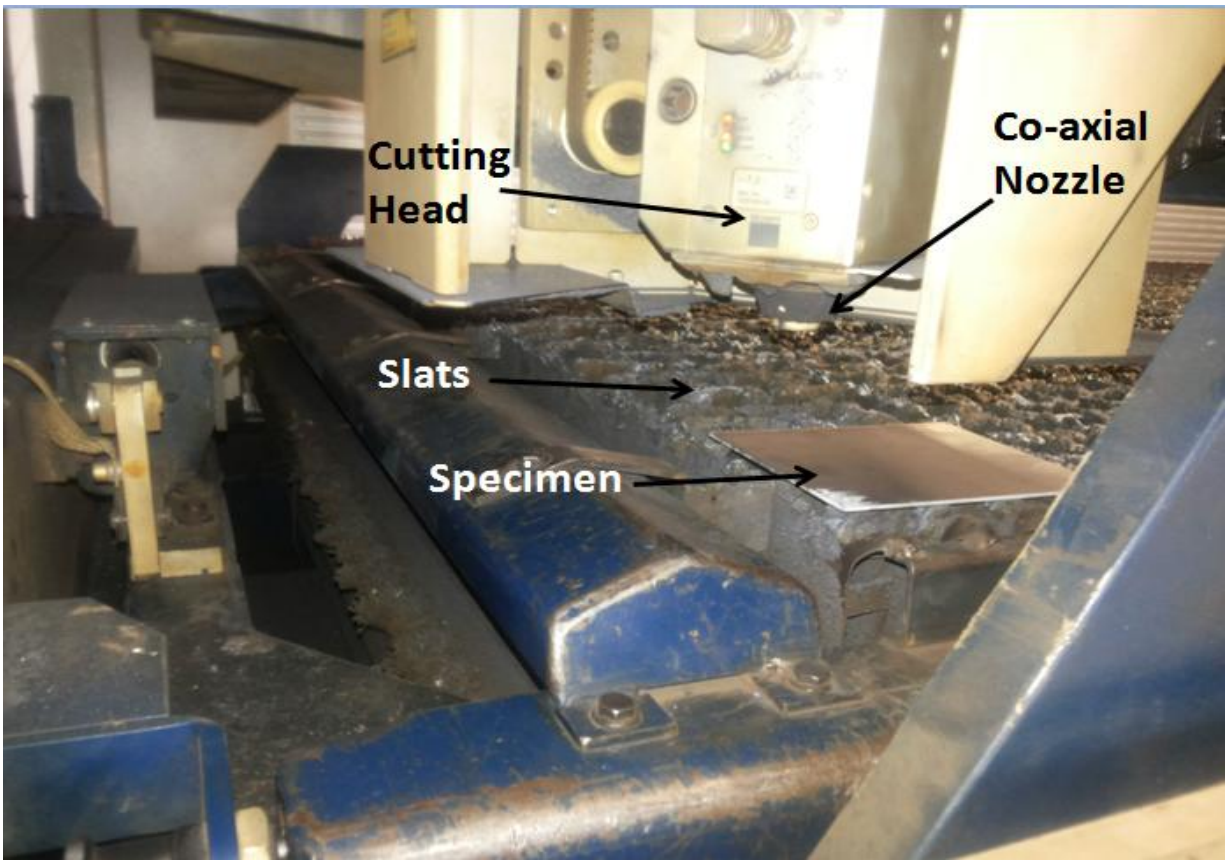

Figure 4.11 CO_2 Laser cutting head with work material

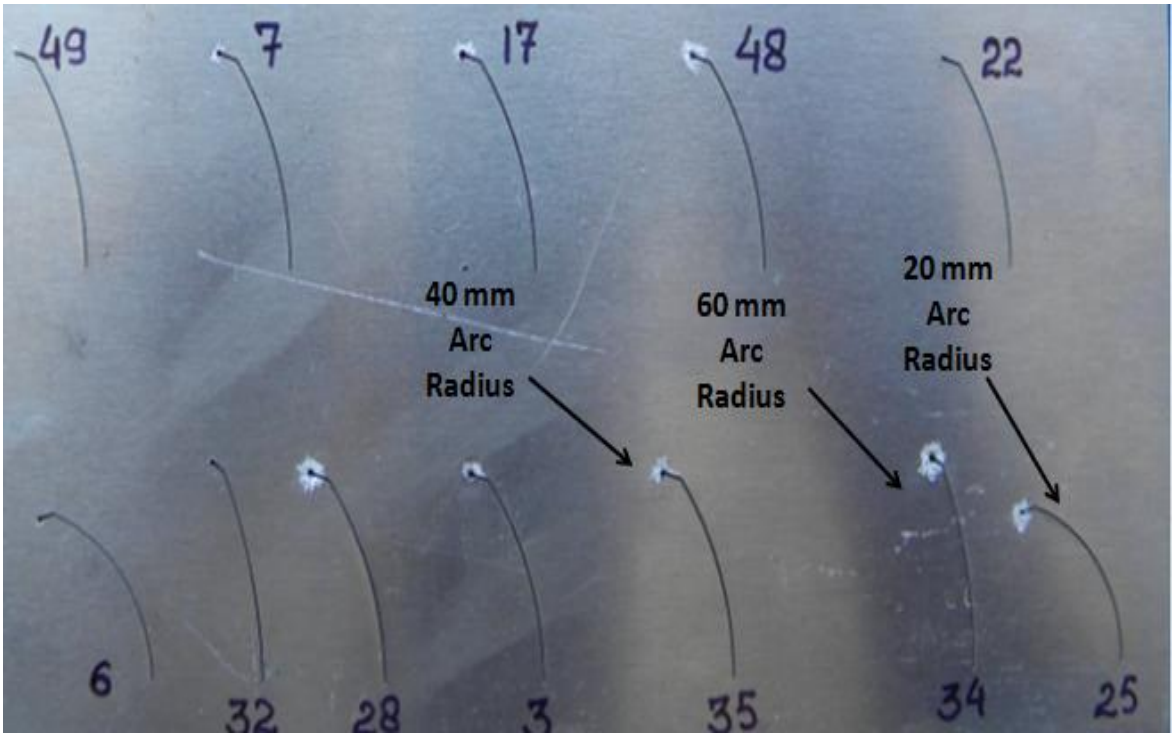

Figure 4.12 Laser machined cut profiles of various arc radius

The kerf width and kerf deviation were measured with the help of optical microscope (Olympus, range 1500x) whereas surface roughness was evaluated by using surface tester, Mitutoyo, SJ400 (Japan). The surface roughness was analysed at three locations for particular experiment run and was considered by taking mathematical average of three values. For analyzing surface structure of various specimens the scanning electron microscope (Jeol : 6510LV) has been used. Before testing through SEM, all specimens were polished whereas kellers agent used on the specimen surfaces for optical analysis. The work samples were prepared by polishing the surfaces using silicon emery paper having grit size of 800, 1000 and 1500, for the EDS and XRD analysis. were selected according to pilot experimentation based on one factor approach. The parameters and their levels is shown in table 4.6. The range of all input parameters were selected on the basis of variations in output results. According to design, total 62 experiments were planned to perform for individual work material viz. Al5052/ SiC, Al5052/Al_2O_3 and Al5052/ZrO_2 MMCs. The laser cut profile has been selected as curve profile by taking circular arc of different radius of 2, 4 and 6 cm.

The polishing process was done using disc polisher via valvet cloth. To examine the compounds and elements the XRD pattern was determined with the help of X-Ray diffractometer (Panalytical XPRT Pro). All microscopic results were measured with the

help of image software. The nozzle stand-off distance was taken from the surface of workpiece. The final outcome of the laser has to deliver through the nozzle of various diameters. The cut profile for laser is considered as circular in curvature. The arc radius was varied 20 mm, 40 mm and 60 mm.

4.7.1 Experimental set-up and Cut profiles

The main experimental setup CO_2 laser cutting system is shown in figure 4.10 which consists of three main components viz. computer control unit, machining unit and specimen bed. Figure 4.11 illustrates the CO_2 Laser cutting head with work material in the form of square sheet having dimension 18 cm × 18 cm with thickness of 3 mm. The cut profiles have been shown in figure 4.12 with the help of laser machined specimen of various arc radius of 20 mm, 40 mm and 60 mm. The cut profiles dimensions are decided in such a way so that arc length is kept equal for all the three cut profiles of various arc radius.

4.7.2 DESIGN LAYOUT OF MAIN EXPERIMENTATION

The main experimentation has been carried out using design layout attained by Box-Bhenken Design. The BBD approach developed the 62 experimental run for individual work materials. The design matrix for main experimentation is tabulated in table 4.7. The various process variables such as cutting speed, laser power, nozzle distance, nozzle diameter, gas pressure, percentage reinforced particles and arc radius have been varied upto three levels. These three levels are varied from minimum to maximum value of -1, 0 and +1. The lower level of variable is depicted by -1 whereas middle levels shown by 0 and highest level is denoted by +1 as shown in the table. The various process parameters were varied according to the experimental layout which designed sixty two experiments for the laser cutting process. The details of standard run number, process parameters, their levels and output responses values are tabulated in table 1 and table 2 for individual work material. Table 4.8 (I) shows details of experimentation for the work material Al5052/SiC with four output responses such as dross height, kerf taper, surface roughness, kerf deviation. Table 4.9 (II) shows the results for striation angle, heat affected zone width, material removal rate and energy losses. Table 4.10 (I) and table 4.11 (II) illustrates the results for the Al5052/Al_2O_3 as a work material. Table 4.12 (I) and table 4.13 (II) shows the results for the Al5052/ZrO_2 as a work material.

Table 4.7 Design matrix for main experimentation

Run Order	Standard Order	Control Factors						
		Cutting Speed	Laser Power	Nozzle Distance	Nozzle Diameter	Gas Pressure	Percentage Reinforced particles	Arc Radius
1	45	0	-1	0	-1	+1	-1	-1
2	33	-1	+1	-1	-1	0	-1	+1
3	51	-1	0	+1	-1	-1	0	-1
4	8	-1	-1	-1	+1	+1	+1	-1
5	11	0	-1	-1	-1	-1	+1	0
6	10	+1	-1	-1	-1	-1	0	0
7	3	-1	-1	-1	0	+1	0	-1
8	27	0	+1	-1	0	-1	-1	-1
9	35	-1	-1	0	+1	-1	-1	0
10	59	-1	-1	-1	-1	-1	-1	-1
11	53	-1	0	0	-1	-1	+1	-1
12	16	+1	-1	-1	-1	-1	0	+1
13	47	0	-1	+1	-1	+1	-1	-1
14	34	-1	-1	+1	0	-1	-1	0
15	32	+1	+1	-1	+1	-1	-1	-1
16	55	-1	0	+1	-1	-1	+1	-1
17	1	-1	-1	-1	0	0	0	-1
18	12	+1	-1	-1	-1	-1	+1	0
19	19	-1	0	-1	-1	+1	-1	0
20	31	0	+1	-1	+1	-1	-1	-1
21	33	-1	-1	0	0	-1	-1	0
22	4	-1	-1	-1	+1	+1	0	-1
23	28	+1	+1	-1	0	-1	-1	-1
24	26	+1	0	-1	0	-1	0	+1
25	9	0	-1	-1	-1	-1	0	0
26	46	+1	-1	0	-1	+1	-1	-1
27	25	0	0	-1	0	-1	-1	-1
28	52	-1	+1	+1	-1	-1	0	-1
29	18	-1	+1	-1	-1	0	-1	0
30	17	-1	0	-1	-1	0	-1	0
31	58	-1	-1	-1	-1	-1	-1	-1
32	14	+1	-1	-1	-1	-1	0	+1
33	44	+1	-1	+1	-1	0	-1	-1
34	13	0	-1	-1	-1	-1	0	+1
35	49	-1	0	0	-1	-1	0	-1
36	7	-1	-1	-1	0	+1	+1	-1
37	37	-1	-1	0	0	-1	-1	+1
38	36	-1	-1	+1	+1	-1	-1	0
39	56	-1	+1	+1	-1	-1	+1	-1
40	61	-1	-1	-1	-1	-1	-1	-1
41	48	+1	-1	+1	-1	+1	-1	-1
42	62	-1	-1	-1	-1	-1	-1	-1
43	15	0	-1	-1	-1	-1	+1	+1
44	29	0	0	-1	+1	-1	-1	-1
45	54	-1	+1	0	-1	-1	+1	-1
46	24	-1	+1	-1	-1	+1	-1	+1
47	40	-1	-1	+1	+1	-1	-1	+1
48	2	-1	-1	-1	+1	0	0	-1
49	50	-1	+1	0	-1	-1	0	-1
50	38	-1	-1	+1	0	-1	-1	+1
51	41	0	-1	0	-1	0	-1	-1
52	42	+1	-1	0	-1	0	-1	-1
53	21	-1	0	-1	-1	0	-1	+1

Run Order	Standard Order	Cutting Speed	Laser Power	Nozzle Distance	Nozzle Diameter	Gas Pressure	Percentage Reinforced particles	Arc Radius
54	6	-1	-1	-1	+1	0	+1	-1
55	30	+1	0	-1	+1	-1	-1	-1
56	43	0	-1	-1	-1	0	-1	-1
57	20	-1	+1	-1	-1	+1	-1	0
58	60	-1	-1	-1	-1	-1	-1	-1
59	23	-1	0	-1	-1	+1	-1	+1
60	57	-1	-1	-1	-1	-1	-1	-1
61	5	-1	-1	-1	0	0	+1	-1
62	39	-1	-1	0	+1	-1	-1	+1

Table 4.8 Design matrix and output responses-I for the specimen Al/SiC/0-20% weight

Run no.	Cutting speed mm/min	Laser power watt	Standoff distance mm	Nozzle diameter mm	Gas pressure bar	Reinf. SiC particles %	Arc radius mm	Dross Height mm	Kerf Taper deg.	Surface Roughness µm	Kerf Deviation mm
1	1000	2000	1.0	1.7	14	10	40	1.30	0.299	3.11	0.115
2	2000	2500	1.5	1.7	10	10	60	0.50	0.290	1.81	0.065
3	2000	1500	2.0	1.7	12	0	40	1.10	0.284	2.33	0.031
4	2000	2000	1.5	2.0	14	20	40	0.48	0.348	2.09	0.095
5	1000	2000	1.5	1.7	12	20	20	1.20	0.455	3.56	0.135
6	3000	2000	1.5	1.7	12	0	20	0.60	0.324	2.52	0.098
7	2000	2000	1.5	1.4	14	0	40	0.39	0.257	1.24	0.097
8	1000	2500	1.5	1.4	12	10	40	0.91	0.379	3.11	0.140
9	2000	2000	1.0	2.0	12	10	20	0.50	0.357	2.48	0.091
10	2000	2000	1.5	1.7	12	10	40	0.59	0.332	2.08	0.042
11	2000	1500	1.0	1.7	12	20	40	0.21	0.330	2.85	0.095
12	3000	2000	1.5	1.7	12	20	60	0.37	0.309	2.88	0.025
13	1000	2000	2.0	1.7	14	10	40	0.65	0.280	2.84	0.099
14	2000	2000	2.0	1.4	12	10	20	0.82	0.384	3.44	0.092
15	3000	2500	1.5	2.0	12	10	40	0.56	0.367	1.97	0.098
16	2000	1500	2.0	1.7	12	20	40	0.42	0.312	2.67	0.031
17	2000	2000	1.5	1.4	10	0	40	0.69	0.317	1.99	0.017
18	3000	2000	1.5	1.7	12	20	20	0.57	0.399	2.65	0.095
19	2000	1500	1.5	1.7	14	10	20	0.95	0.319	3.01	0.097
20	1000	2500	1.5	2.0	12	10	40	0.88	0.398	2.55	0.141
21	2000	2000	1.0	1.4	12	10	20	0.91	0.478	3.13	0.121
22	2000	2000	1.5	2.0	14	0	40	0.55	0.323	1.88	0.089
23	3000	2500	1.5	1.4	12	10	40	0.22	0.297	1.33	0.139
24	3000	1500	1.5	1.4	12	10	40	0.58	0.299	2.34	0.016
25	1000	2000	1.5	1.7	12	0	20	1.33	0.498	3.99	0.136
26	3000	2000	1.0	1.7	14	10	40	0.48	0.278	1.45	0.088
27	1000	1500	1.5	1.4	12	10	40	1.10	0.379	3.15	0.260
28	2000	2500	2.0	1.7	12	0	40	0.86	0.312	1.86	0.056
29	2000	2500	1.5	1.7	10	10	20	1.0	0.407	3.01	0.095
30	2000	1500	1.5	1.7	10	10	20	1.08	0.478	3.24	0.076
31	2000	2000	1.5	1.7	12	10	40	0.62	0.332	1.87	0.035
32	3000	2000	1.5	1.7	12	0	60	0.48	0.276	1.34	0.018
33	3000	2000	2.0	1.7	10	10	40	0.79	0.356	2.67	0.022
34	1000	2000	1.5	1.7	12	0	60	0.89	0.298	2.47	0.117
35	2000	1500	1.0	1.7	12	0	40	0.61	0.276	1.87	0.095
36	2000	2000	1.5	1.4	14	20	40	0.14	0.297	1.56	0.096
37	2000	2000	1.0	1.4	12	10	60	0.47	0.289	1.41	0.058
38	2000	2000	2.0	2.0	12	10	20	1.30	0.419	3.11	0.128

Run no.	Cutting speed mm/min	Laser power watt	Standoff distance mm	Nozzle diameter mm	Gas pressure bar	Reinf. SiC particles %	Arc radius mm	Dross Height mm	Kerf Taper deg.	Surface Roughness µm	Kerf Deviation mm
39	2000	2500	2.0	1.7	12	20	40	0.34	0.455	1.92	0.099
40	2000	2000	1.5	1.7	12	10	40	0.63	0.323	1.89	0.045
41	3000	2000	2.0	1.7	14	10	40	0.40	0.284	1.21	0.035
42	2000	2000	1.5	1.7	12	10	40	0.66	0.322	1.98	0.025
43	1000	2000	1.5	1.7	12	20	60	0.43	0.321	2.51	0.191
44	1000	1500	1.5	2.0	12	10	40	1.10	0.368	2.78	0.116
45	2000	2500	1.0	1.7	12	20	40	0.56	0.398	2.22	0.139
46	2000	2500	1.5	1.7	14	10	60	0.41	0.308	1.48	0.095
47	2000	2000	2.0	2.0	12	10	60	0.79	0.397	1.86	0.075
48	2000	2000	1.5	2.0	10	0	40	0.76	0.309	2.11	0.031
49	2000	2500	1.0	1.7	12	0	40	0.51	0.286	1.67	0.095
50	2000	2000	2.0	1.4	12	10	60	0.40	0.311	1.67	0.036
51	1000	2000	1.0	1.7	10	10	40	0.74	0.387	2.23	0.091
52	3000	2000	1.0	1.7	10	10	40	0.70	0.348	2.11	0.033
53	2000	1500	1.5	1.7	10	10	60	0.66	0.310	1.99	0.045
54	2000	2000	1.5	2.0	10	20	40	0.68	0.409	2.46	0.098
55	3000	1500	1.5	2.0	12	10	40	0.70	0.274	1.98	0.036
56	1000	2000	1.5	1.7	10	10	40	0.85	0.402	2.77	0.056
57	2000	2500	1.5	1.7	14	10	20	0.65	0.337	2.11	0.136
58	2000	2000	1.5	1.7	12	10	40	0.52	0.332	1.96	0.042
59	2000	1500	1.5	1.7	14	10	60	0.50	0.264	2.01	0.057
60	2000	2000	1.5	1.7	12	10	40	0.66	0.322	1.98	0.031
61	2000	2000	1.5	1.4	10	20	40	0.53	0.394	2.44	0.096
62	2000	2000	1.0	2.0	12	10	60	0.50	0.333	1.24	0.097

Table 4.9 Design matrix and output responses-II for the specimen Al/SiC/0-20% weight

Run no.	Cutting speed mm/min	Laser power watt	Standoff distance mm	Nozzle diameter mm	Gas pressure bar	Reinf. SiC particles %	Arc radius mm	S.A deg.	HAZ µm	MRR mg/min	Energy Losses watt
1	1000	2000	1.0	1.7	14	10	40	8.32	290.96	72.90	1371.56
2	2000	2500	1.5	1.7	10	10	60	3.23	459.37	51.12	1474.77
3	2000	1500	2.0	1.7	12	0	40	7.43	189.92	69.45	1304.13
4	2000	2000	1.5	2.0	14	20	40	9.91	311.24	64.27	1599.54
5	1000	2000	1.5	1.7	12	20	20	8.18	369.55	60.68	2099.99
6	3000	2000	1.5	1.7	12	0	20	8.14	188.99	107.34	1487.61
7	2000	2000	1.5	1.4	14	0	40	5.23	104.13	67.97	1182.11
8	1000	2500	1.5	1.4	12	10	40	5.72	409.92	73.01	1842.66
9	2000	2000	1.0	2.0	12	10	20	5.49	264.30	46.12	1640.83
10	2000	2000	1.5	1.7	12	10	40	6.48	211.11	54.42	1525.23
11	2000	1500	1.0	1.7	12	20	40	8.26	266.64	19.37	1524.31
12	3000	2000	1.5	1.7	12	20	60	8.98	260.09	119.51	1621.10
13	1000	2000	2.0	1.7	14	10	40	6.66	265.70	68.95	1287.61
14	2000	2000	2.0	1.4	12	10	20	9.33	349.90	88.40	1763.76
15	3000	2500	1.5	2.0	12	10	40	12.10	186.18	121.65	1686.70
16	2000	1500	2.0	1.7	12	20	40	9.25	156.24	30.74	1432.57
17	2000	2000	1.5	1.4	10	0	40	3.29	223.60	52.64	1457.80
18	3000	2000	1.5	1.7	12	20	20	15.54	332.13	112.57	1831.19
19	2000	1500	1.5	1.7	14	10	20	15.55	281.61	117.62	1464.68
20	1000	2500	1.5	2.0	12	10	40	4.57	285.35	45.40	1829.36
21	2000	2000	1.0	1.4	12	10	20	9.99	292.83	83.93	2196.33
22	2000	2000	1.5	2.0	14	0	40	7.11	201.21	90.73	1482.57
23	3000	2500	1.5	1.4	12	10	40	10.99	283.48	132.29	1365.14

Run no.	Cutting speed mm/min	Laser power watt	Standoff distance mm	Nozzle diameter mm	Gas pressure bar	Reinf. SiC particles %	Arc radius mm	S.A deg.	HAZ µm	MRR mg/min	Energy Losses watt
24	3000	1500	1.5	1.4	12	10	40	8.75	190.86	53.49	1371.56
25	1000	2000	1.5	1.7	12	0	20	4.60	307.80	55.67	2287.61
26	3000	2000	1.0	1.7	14	10	40	10.07	98.24	74.58	1278.90
27	1000	1500	1.5	1.4	12	10	40	9.46	333.06	39.45	1742.20
28	2000	2500	2.0	1.7	12	0	40	7.54	314.35	103.32	1432.57
29	2000	2500	1.5	1.7	10	10	20	7.33	281.61	75.54	1870.18
30	2000	1500	1.5	1.7	10	10	20	11.86	303.13	84.61	2196.79
31	2000	2000	1.5	1.7	12	10	40	6.84	268.51	57.49	1523.85
32	3000	2000	1.5	1.7	12	0	60	7.18	97.30	93.27	1268.81
33	3000	2000	2.0	1.7	10	10	40	9.63	287.22	82.86	1636.24
34	1000	2000	1.5	1.7	12	0	60	6.24	203.02	78.08	1370.64
35	2000	1500	1.0	1.7	12	0	40	8.48	128.17	65.26	1269.72
36	2000	2000	1.5	1.4	14	20	40	8.68	145.95	42.91	1366.51
37	2000	2000	1.0	1.4	12	10	60	3.37	225.47	38.35	1329.82
38	2000	2000	2.0	2.0	12	10	20	8.11	281.61	125.90	1925.69
39	2000	2500	2.0	1.7	12	20	40	5.88	273.19	29.36	2091.28
40	2000	2000	1.5	1.7	12	10	40	6.92	270.38	58.10	1482.57
41	3000	2000	2.0	1.7	14	10	40	8.36	113.20	67.20	1305.05
42	2000	2000	1.5	1.7	12	10	40	7.25	185.24	60.87	1477.98
43	1000	2000	1.5	1.7	12	20	60	6.03	234.83	25.66	1478.90
44	1000	1500	1.5	2.0	12	10	40	14.34	260.09	101.45	1691.74
45	2000	2500	1.0	1.7	12	20	40	6.62	301.25	50.65	1829.36
46	2000	2500	1.5	1.7	14	10	60	9.62	325.58	90.81	1413.30
47	2000	2000	2.0	2.0	12	10	60	7.13	174.02	62.86	1824.77
48	2000	2000	1.5	2.0	10	0	40	5.01	197.41	59.09	1421.10
49	2000	2500	1.0	1.7	12	0	40	3.34	156.24	62.04	1314.68
50	2000	2000	2.0	1.4	12	10	60	3.44	156.24	31.89	1430.73
51	1000	2000	1.0	1.7	10	10	40	4.59	208.63	38.56	1777.98
52	3000	2000	1.0	1.7	10	10	40	8.91	197.41	74.87	1599.54
53	2000	1500	1.5	1.7	10	10	60	6.45	186.18	37.18	1425.69
54	2000	2000	1.5	2.0	10	20	40	6.87	192.73	37.72	1879.82
55	3000	1500	1.5	2.0	12	10	40	11.97	129.11	90.56	1258.26
56	1000	2000	1.5	1.7	10	10	40	2.79	259.15	23.40	1844.95
57	2000	2500	1.5	1.7	14	10	20	6.42	197.41	83.95	1549.54
58	2000	2000	1.5	1.7	12	10	40	5.71	183.37	47.96	1523.85
59	2000	1500	1.5	1.7	14	10	60	5.01	188.05	45.12	1213.76
60	2000	2000	1.5	1.7	12	10	40	7.25	185.24	60.87	1478.44
61	2000	2000	1.5	1.4	10	20	40	6.30	228.28	32.88	1809.17
62	2000	2000	1.0	2.0	12	10	60	4.66	97.30	41.12	1528.90

Table 4.10 Design matrix and output responses-I for the specimen Al/Al_2O_3/0-20% weight

Run no.	Cutting speed mm/min	Laser power watt	Standoff distance mm	Nozzle diameter mm	Gas pressure bar	Reinf. Al_2O_3 particles %	Arc radius mm	Dross Height mm	Kerf Taper deg.	Surface Roughness µm	Kerf Deviation mm
1	1000	2000	1.0	1.7	14	10	40	1.26	0.308	2.89	0.1
2	2000	2500	1.5	1.7	10	10	60	0.49	0.309	1.76	0.057
3	2000	1500	2.0	1.7	12	0	40	1.07	0.293	2.26	0.027
4	2000	2000	1.5	2.0	14	20	40	0.47	0.359	2.03	0.083
5	1000	2000	1.5	1.7	12	20	20	1.17	0.469	3.06	0.118
6	3000	2000	1.5	1.7	12	0	20	0.58	0.334	2.45	0.086
7	2000	2000	1.5	1.4	14	0	40	0.38	0.265	1.2	0.085
8	1000	2500	1.5	1.4	12	10	40	0.87	0.391	3.02	0.122

Run no.	Cutting speed mm/min	Laser power watt	Standoff distance mm	Nozzle diameter mm	Gas pressure bar	Reinf. Al_2O_3 particles %	Arc radius mm	Dross Height mm	Kerf Taper degree	Surface Roughness µm	Kerf Deviation mm
9	2000	2000	1.0	2.0	12	10	20	0.49	0.368	2.41	0.08
10	2000	2000	1.5	1.7	12	10	40	0.57	0.342	2.02	0.037
11	2000	1500	1.0	1.7	12	20	40	0.2	0.342	2.77	0.083
12	3000	2000	1.5	1.7	12	20	60	0.31	0.319	2.8	0.019
13	1000	2000	2.0	1.7	14	10	40	0.63	0.289	2.76	0.087
14	2000	2000	2.0	1.4	12	10	20	0.83	0.396	3.34	0.08
15	3000	2500	1.5	2.0	12	10	40	0.54	0.379	1.91	0.086
16	2000	1500	2.0	1.7	12	20	40	0.41	0.322	2.59	0.027
17	2000	2000	1.5	1.4	10	0	40	0.6	0.327	1.93	0.015
18	3000	2000	1.5	1.7	12	20	20	0.55	0.411	2.57	0.083
19	2000	1500	1.5	1.7	14	10	20	0.92	0.329	2.92	0.085
20	1000	2500	1.5	2.0	12	10	40	0.83	0.411	2.48	0.123
21	2000	2000	1.0	1.4	12	10	20	0.88	0.493	3.04	0.106
22	2000	2000	1.5	2.0	14	0	40	0.53	0.333	1.83	0.078
23	3000	2500	1.5	1.4	12	10	40	0.21	0.307	1.29	0.121
24	3000	1500	1.5	1.4	12	10	40	0.56	0.308	2.27	0.01
25	1000	2000	1.5	1.7	12	0	20	1.29	0.514	3.87	0.119
26	3000	2000	1.0	1.7	14	10	40	0.47	0.287	1.41	0.077
27	1000	1500	1.5	1.4	12	10	40	1.15	0.391	3.46	0.227
28	2000	2500	2.0	1.7	12	0	40	0.83	0.322	1.81	0.049
29	2000	2500	1.5	1.7	10	10	20	0.97	0.42	2.92	0.083
30	2000	1500	1.5	1.7	10	10	20	1.05	0.493	3.15	0.066
31	2000	2000	1.5	1.7	12	10	40	0.61	0.342	1.82	0.031
32	3000	2000	1.5	1.7	12	0	60	0.47	0.285	1.3	0.016
33	3000	2000	2.0	1.7	10	10	40	0.77	0.367	2.59	0.019
34	1000	2000	1.5	1.7	12	0	60	0.86	0.308	2.4	0.102
35	2000	1500	1.0	1.7	12	0	40	0.59	0.285	1.82	0.083
36	2000	2000	1.5	1.4	14	20	40	0.14	0.307	1.51	0.084
37	2000	2000	1.0	1.4	12	10	60	0.46	0.299	1.37	0.051
38	2000	2000	2.0	2.0	12	10	20	1.26	0.432	3.02	0.112
39	2000	2500	2.0	1.7	12	20	40	0.33	0.47	1.86	0.087
40	2000	2000	1.5	1.7	12	10	40	0.61	0.333	1.83	0.039
41	3000	2000	2.0	1.7	14	10	40	0.39	0.293	1.17	0.031
42	2000	2000	1.5	1.7	12	10	40	0.64	0.332	1.92	0.022
43	1000	2000	1.5	1.7	12	20	60	0.42	0.332	2.44	0.167
44	1000	1500	1.5	2.0	12	10	40	1.07	0.38	2.7	0.101
45	2000	2500	1.0	1.7	12	20	40	0.54	0.411	2.16	0.121
46	2000	2500	1.5	1.7	14	10	60	0.4	0.317	1.44	0.083
47	2000	2000	2.0	2.0	12	10	60	0.77	0.41	1.81	0.066
48	2000	2000	1.5	2.0	10	0	40	0.74	0.319	2.05	0.027
49	2000	2500	1.0	1.7	12	0	40	0.5	0.295	1.62	0.083
50	2000	2000	2.0	1.4	12	10	60	0.39	0.321	1.62	0.031
51	1000	2000	1.0	1.7	10	10	40	0.72	0.399	2.17	0.08
52	3000	2000	1.0	1.7	10	10	40	0.68	0.359	2.05	0.029
53	2000	1500	1.5	1.7	10	10	60	0.64	0.32	1.93	0.039
54	2000	2000	1.5	2.0	10	20	40	0.66	0.422	2.39	0.086
55	3000	1500	1.5	2.0	12	10	40	0.68	0.283	1.92	0.031
56	1000	2000	1.5	1.7	10	10	40	0.83	0.414	2.69	0.049
57	2000	2500	1.5	1.7	14	10	20	0.63	0.348	2.05	0.119
58	2000	2000	1.5	1.7	12	10	40	0.5	0.342	1.9	0.037
59	2000	1500	1.5	1.7	14	10	60	0.49	0.273	1.95	0.05
60	2000	2000	1.5	1.7	12	10	40	0.64	0.332	1.92	0.027
61	2000	2000	1.5	1.4	10	20	40	0.51	0.406	2.37	0.084
62	2000	2000	1.0	2.0	12	10	60	0.49	0.343	1.2	0.085

Table 4.11 Design matrix and output responses-II for Al/Al_2O_3/0-20% weight

Run no.	Cutting speed mm/min	Laser power watt	Standoff distance mm	Nozzle diameter mm	Gas pressure bar	Reinf. Al_2O_3 particles %	Arc radius mm	S.A degree	HAZ μm	MRR mg/min	Energy Losses watt
1	1000	2000	1.0	1.7	14	10	40	7.92	296.78	69.43	1288.33
2	2000	2500	1.5	1.7	10	10	60	4.11	468.55	48.68	1402.21
3	2000	1500	2.0	1.7	12	0	40	7.08	193.72	62.34	1291.22
4	2000	2000	1.5	2.0	14	20	40	7.41	301.12	61.21	1583.7
5	1000	2000	1.5	1.7	12	20	20	7.79	376.94	57.79	1903.11
6	3000	2000	1.5	1.7	12	0	20	7.75	192.77	102.23	1472.89
7	2000	2000	1.5	1.4	14	0	40	6.42	99.25	64.73	1170.41
8	1000	2500	1.5	1.4	12	10	40	5.44	418.12	69.53	1725.41
9	2000	2000	1.0	2.0	12	10	20	5.23	255.75	43.92	1624.58
10	2000	2000	1.5	1.7	12	10	40	6.17	198.49	51.82	1510.13
11	2000	1500	1.0	1.7	12	20	40	7.86	271.97	18.45	1509.22
12	3000	2000	1.5	1.7	12	20	60	8.55	265.29	113.82	1407.03
13	1000	2000	2.0	1.7	14	10	40	6.34	271.02	62.81	1274.87
14	2000	2000	2.0	1.4	12	10	20	8.89	356.9	74.66	1746.3
15	3000	2500	1.5	2.0	12	10	40	11.52	189.9	115.86	1670
16	2000	1500	2.0	1.7	12	20	40	8.81	159.37	29.27	1418.38
17	2000	2000	1.5	1.4	10	0	40	3.13	228.07	50.13	1443.36
18	3000	2000	1.5	1.7	12	20	20	14.8	338.77	107.21	1788.22
19	2000	1500	1.5	1.7	14	10	20	14.81	287.24	112.02	1450.18
20	1000	2500	1.5	2.0	12	10	40	4.35	291.06	43.23	1811.25
21	2000	2000	1.0	1.4	12	10	20	9.52	298.69	79.93	2174.58
22	2000	2000	1.5	2.0	14	0	40	6.77	103.06	86.41	1467.89
23	3000	2500	1.5	1.4	12	10	40	10.46	289.15	125.99	1351.62
24	3000	1500	1.5	1.4	12	10	40	8.33	194.67	50.95	1357.98
25	1000	2000	1.5	1.7	12	0	20	4.38	313.96	53.02	2264.97
26	3000	2000	1.0	1.7	14	10	40	9.59	100.2	71.03	1266.24
27	1000	1500	1.5	1.4	12	10	40	9.01	339.73	37.57	1724.95
28	2000	2500	2.0	1.7	12	0	40	7.18	320.64	98.4	1418.38
29	2000	2500	1.5	1.7	10	10	20	6.98	287.24	71.94	1851.67
30	2000	1500	1.5	1.7	10	10	20	11.29	309.19	80.58	2175.04
31	2000	2000	1.5	1.7	12	10	40	6.52	273.88	54.75	1508.77
32	3000	2000	1.5	1.7	12	0	60	6.83	99.25	88.83	1256.24
33	3000	2000	2.0	1.7	10	10	40	9.17	292.97	78.92	1620.04
34	1000	2000	1.5	1.7	12	0	60	5.94	207.08	74.37	1357.07
35	2000	1500	1.0	1.7	12	0	40	8.08	130.74	62.15	1257.15
36	2000	2000	1.5	1.4	14	20	40	8.27	148.87	40.87	1352.98
37	2000	2000	1.0	1.4	12	10	60	3.21	229.98	36.52	1316.65
38	2000	2000	2.0	2.0	12	10	20	7.72	287.24	119.9	1906.62
39	2000	2500	2.0	1.7	12	20	40	5.6	278.65	27.96	2070.58
40	2000	2000	1.5	1.7	12	10	40	6.59	275.79	55.34	1467.89
41	3000	2000	2.0	1.7	14	10	40	7.96	115.47	64	1292.12
42	2000	2000	1.5	1.7	12	10	40	6.9	188.95	57.97	1463.35
43	1000	2000	1.5	1.7	12	20	60	5.74	239.53	24.44	1464.26
44	1000	1500	1.5	2.0	12	10	40	13.66	265.29	96.62	1674.99
45	2000	2500	1.0	1.7	12	20	40	6.31	307.28	48.24	1811.25
46	2000	2500	1.5	1.7	14	10	60	9.16	332.09	86.49	1399.31
47	2000	2000	2.0	2.0	12	10	60	6.79	177.5	59.87	1806.7
48	2000	2000	1.5	2.0	10	0	40	4.77	201.35	56.28	1407.03
49	2000	2500	1.0	1.7	12	0	40	3.18	159.37	59.08	1301.66
50	2000	2000	2.0	1.4	12	10	60	3.28	159.37	30.37	1416.57
51	1000	2000	1.0	1.7	10	10	40	4.37	212.81	36.72	1760.38
52	3000	2000	1.0	1.7	10	10	40	8.49	201.35	71.3	1583.7

Run no.	Cutting speed mm/min	Laser power watt	Standoff distance mm	Nozzle diameter mm	Gas pressure bar	Reinf. Al_2O_3 particles %	Arc radius mm	S.A deg.	HAZ µm	MRR mg/min	Energy Losses watt
53	2000	1500	1.5	1.7	10	10	60	6.14	189.9	35.41	1411.57
54	2000	2000	1.5	2.0	10	20	40	6.54	196.58	35.92	1861.2
55	3000	1500	1.5	2.0	12	10	40	11.4	131.69	86.25	1245.8
56	1000	2000	1.5	1.7	10	10	40	2.65	264.34	22.28	1826.69
57	2000	2500	1.5	1.7	14	10	20	6.12	201.35	79.95	1534.2
58	2000	2000	1.5	1.7	12	10	40	5.44	187.04	45.68	1508.77
59	2000	1500	1.5	1.7	14	10	60	4.77	191.81	42.97	1201.74
60	2000	2000	1.5	1.7	12	10	40	6.9	188.95	57.97	1463.8
61	2000	2000	1.5	1.4	10	20	40	6.0	232.85	31.32	1791.26
62	2000	2000	1.0	2.0	12	10	60	4.43	99.25	39.16	1513.76

Table 4.12 Design matrix and output responses-I for the specimen Al/ZrO_2/0-20% weight

Run no.	Cutting speed mm/min	Laser power watt	Standoff distance mm	Nozzle diameter mm	Gas pressure bar	Reinf. ZrO_2 particles %	Arc radius mm	Dross Height mm	Kerf Taper deg.	Surface Roughness µm	Kerf Deviation mm
1	1000	2000	1.0	1.7	14	10	40	1.16	0.317	3.36	0.106
2	2000	2500	1.5	1.7	10	10	60	0.45	0.318	1.95	0.046
3	2000	1500	2.0	1.7	12	0	40	0.98	0.302	2.52	0.022
4	2000	2000	1.5	2.0	14	20	40	0.43	0.37	2.26	0.086
5	1000	2000	1.5	1.7	12	20	20	1.07	0.483	3.4	0.126
6	3000	2000	1.5	1.7	12	0	20	0.53	0.344	2.72	0.089
7	2000	2000	1.5	1.4	14	0	40	0.35	0.273	1.34	0.088
8	1000	2500	1.5	1.4	12	10	40	0.8	0.403	3.36	0.131
9	2000	2000	1.0	2.0	12	10	20	0.45	0.379	2.68	0.082
10	2000	2000	1.5	1.7	12	10	40	0.53	0.353	2.25	0.033
11	2000	1500	1.0	1.7	12	20	40	0.19	0.353	3.08	0.086
12	3000	2000	1.5	1.7	12	20	60	0.29	0.329	3.11	0.011
13	1000	2000	2.0	1.7	14	10	40	0.58	0.298	3.07	0.09
14	2000	2000	2.0	1.4	12	10	20	0.76	0.408	3.72	0.083
15	3000	2500	1.5	2.0	12	10	40	0.5	0.39	2.13	0.089
16	2000	1500	2.0	1.7	12	20	40	0.37	0.331	2.88	0.022
17	2000	2000	1.5	1.4	10	0	40	0.55	0.337	2.15	0.008
18	3000	2000	1.5	1.7	12	20	20	0.51	0.424	2.86	0.086
19	2000	1500	1.5	1.7	14	10	20	0.85	0.339	3.25	0.088
20	1000	2500	1.5	2.0	12	10	40	0.76	0.423	2.75	0.132
21	2000	2000	1.0	1.4	12	10	20	0.81	0.508	3.38	0.112
22	2000	2000	1.5	2.0	14	0	40	0.49	0.343	2.03	0.08
23	3000	2500	1.5	1.4	12	10	40	0.2	0.316	1.44	0.13
24	3000	1500	1.5	1.4	12	10	40	0.52	0.317	2.53	0.002
25	1000	2000	1.5	1.7	12	0	20	1.18	0.529	4.31	0.127
26	3000	2000	1.0	1.7	14	10	40	0.43	0.296	1.57	0.079
27	1000	1500	1.5	1.4	12	10	40	1.06	0.403	3.84	0.251
28	2000	2500	2.0	1.7	12	0	40	0.77	0.331	2.01	0.047
29	2000	2500	1.5	1.7	10	10	20	0.89	0.433	3.25	0.086
30	2000	1500	1.5	1.7	10	10	20	0.96	0.508	3.5	0.067
31	2000	2000	1.5	1.7	12	10	40	0.56	0.352	2.02	0.026
32	3000	2000	1.5	1.7	12	0	60	0.43	0.293	1.45	0.009
33	3000	2000	2.0	1.7	10	10	40	0.7	0.378	2.88	0.013
34	1000	2000	1.5	1.7	12	0	60	0.79	0.317	2.67	0.098
35	2000	1500	1.0	1.7	12	0	40	0.54	0.294	2.02	0.086
36	2000	2000	1.5	1.4	14	20	40	0.12	0.316	1.68	0.087

Run no.	Cutting speed mm/min	Laser power watt	Standoff distance mm	Nozzle diameter mm	Gas pressure bar	Reinf. ZrO_2 particles %	Arc radius mm	Dross Height mm	Kerf Taper deg.	Surface Roughness µm	Kerf Deviation mm
37	2000	2000	1.0	1.4	12	10	60	0.42	0.308	1.52	0.049
38	2000	2000	2.0	2.0	12	10	20	1.16	0.445	3.36	0.119
39	2000	2500	2.0	1.7	12	20	40	0.3	0.484	2.07	0.09
40	2000	2000	1.5	1.7	12	10	40	0.56	0.343	2.04	0.036
41	3000	2000	2.0	1.7	14	10	40	0.36	0.302	1.31	0.026
42	2000	2000	1.5	1.7	12	10	40	0.59	0.342	2.14	0.016
43	1000	2000	1.5	1.7	12	20	60	0.38	0.342	2.71	0.182
44	1000	1500	1.5	2.0	12	10	40	0.98	0.391	3	0.107
45	2000	2500	1.0	1.7	12	20	40	0.5	0.423	2.4	0.13
46	2000	2500	1.5	1.7	14	10	60	0.37	0.327	1.6	0.086
47	2000	2000	2.0	2.0	12	10	60	0.7	0.422	2.01	0.066
48	2000	2000	1.5	2.0	10	0	40	0.68	0.329	2.28	0.022
49	2000	2500	1.0	1.7	12	0	40	0.45	0.304	1.8	0.086
50	2000	2000	2.0	1.4	12	10	60	0.36	0.331	1.8	0.027
51	1000	2000	1.0	1.7	10	10	40	0.66	0.411	2.41	0.082
52	3000	2000	1.0	1.7	10	10	40	0.63	0.37	2.28	0.024
53	2000	1500	1.5	1.7	10	10	60	0.59	0.33	2.15	0.036
54	2000	2000	1.5	2.0	10	20	40	0.61	0.435	2.66	0.089
55	3000	1500	1.5	2.0	12	10	40	0.62	0.291	2.14	0.027
56	1000	2000	1.5	1.7	10	10	40	0.76	0.427	2.99	0.047
57	2000	2500	1.5	1.7	14	10	20	0.58	0.358	2.28	0.127
58	2000	2000	1.5	1.7	12	10	40	0.46	0.352	2.12	0.033
59	2000	1500	1.5	1.7	14	10	60	0.45	0.281	2.17	0.048
60	2000	2000	1.5	1.7	12	10	40	0.59	0.342	2.14	0.022
61	2000	2000	1.5	1.4	10	20	40	0.47	0.418	2.64	0.087
62	2000	2000	1.0	2.0	12	10	60	0.45	0.354	1.34	0.088

Table 4.13 Design matrix and output response-II for Al5052/ZrO_2/0-20% weight

Run no.	Cutting speed mm/min	Laser power watt	Standoff distance mm	Nozzle diameter mm	Gas pressure bar	Reinf. ZrO_2 particles %	Arc radius mm	S.A deg.	HAZ µm	MRR mg/min	Energy Losses watt
1	1000	2000	1.0	1.7	14	10	40	9.14	311.62	77.08	1495
2	2000	2500	1.5	1.7	10	10	60	3.87	491.98	47.26	1498.5
3	2000	1500	2.0	1.7	12	0	40	8.92	203.41	59.82	1421.5
4	2000	2000	1.5	2.0	14	20	40	11.9	291.58	59.43	1743.5
5	1000	2000	1.5	1.7	12	20	20	12.61	395.79	56.1	2277
6	3000	2000	1.5	1.7	12	0	20	9.76	202.4	99.25	1621.5
7	2000	2000	1.5	1.4	14	0	40	6.28	104.21	62.85	1288.5
8	1000	2500	1.5	1.4	12	10	40	6.86	411.82	71.83	1899.5
9	2000	2000	1.0	2.0	12	10	20	6.59	268.54	42.64	1788.5
10	2000	2000	1.5	1.7	12	10	40	7.77	208.42	50.32	1662.5
11	2000	1500	1.0	1.7	12	20	40	9.91	285.57	21.09	1661.5
12	3000	2000	1.5	1.7	12	20	60	18.36	278.56	110.51	1549
13	1000	2000	2.0	1.7	14	10	40	7.99	284.57	60.98	1403.5
14	2000	2000	2.0	1.4	12	10	20	11.2	374.75	72.49	1922.5
15	3000	2500	1.5	2.0	12	10	40	14.52	199.4	112.48	1838.5
16	2000	1500	2.0	1.7	12	20	40	11.11	167.33	31.22	1561.5
17	2000	2000	1.5	1.4	10	0	40	3.95	239.48	61.08	1589
18	3000	2000	1.5	1.7	12	20	20	19.36	355.71	104.09	1996
19	2000	1500	1.5	1.7	14	10	20	18.66	301.6	108.76	1596.5
20	1000	2500	1.5	2.0	12	10	40	5.49	305.61	41.97	1994

Run no.	Cutting speed mm/min	Laser power watt	Standoff distance mm	Nozzle diameter mm	Gas pressure bar	Reinf. ZrO_2 particles %	Arc radius mm	S.A deg.	HAZ µm	MRR mg/min	Energy Losses watt
21	2000	2000	1.0	1.4	12	10	20	11.99	313.63	77.6	2394
22	2000	2000	1.5	2.0	14	0	40	8.53	108.22	83.89	1616
23	3000	2500	1.5	1.4	12	10	40	13.18	303.61	122.32	1488
24	3000	1500	1.5	1.4	12	10	40	10.5	204.41	49.46	1495
25	1000	2000	1.5	1.7	12	0	20	5.52	329.66	51.47	2493.5
26	3000	2000	1.0	1.7	14	10	40	12.08	105.21	68.96	1394
27	1000	1500	1.5	1.4	12	10	40	11.43	356.71	36.47	1899
28	2000	2500	2.0	1.7	12	0	40	9.05	336.67	95.53	1561.5
29	2000	2500	1.5	1.7	10	10	20	8.79	301.6	69.85	2038.5
30	2000	1500	1.5	1.7	10	10	20	16.23	324.65	78.23	2394.5
31	2000	2000	1.5	1.7	12	10	40	8.21	287.57	53.16	1661
32	3000	2000	1.5	1.7	12	0	60	7.42	104.21	86.24	1383
33	3000	2000	2.0	1.7	10	10	40	11.43	307.61	76.62	1783.5
34	1000	2000	1.5	1.7	12	0	60	5.73	217.43	72.2	1494
35	2000	1500	1.0	1.7	12	0	40	10.18	137.27	60.34	1384
36	2000	2000	1.5	1.4	14	20	40	10.42	156.31	39.68	1489.5
37	2000	2000	1.0	1.4	12	10	60	4.05	241.48	41.21	1449.5
38	2000	2000	2.0	2.0	12	10	20	17.13	301.6	116.41	2099
39	2000	2500	2.0	1.7	12	20	40	7.05	292.58	27.15	2279.5
40	2000	2000	1.5	1.7	12	10	40	8.3	289.58	60.12	1616
41	3000	2000	2.0	1.7	14	10	40	10.03	121.24	62.14	1422.5
42	2000	2000	1.5	1.7	12	10	40	8.7	198.4	56.28	1611
43	1000	2000	1.5	1.7	12	20	60	8.42	251.5	23.73	1612
44	1000	1500	1.5	2.0	12	10	40	16.21	278.56	93.81	1844
45	2000	2500	1.0	1.7	12	20	40	7.95	322.64	46.83	1994
46	2000	2500	1.5	1.7	14	10	60	11.54	348.7	83.97	1540.5
47	2000	2000	2.0	2.0	12	10	60	8.55	186.37	58.12	1989
48	2000	2000	1.5	2.0	10	0	40	6.01	211.42	54.64	1549
49	2000	2500	1.0	1.7	12	0	40	4.01	167.33	57.36	1433
50	2000	2000	2.0	1.4	12	10	60	4.13	167.33	29.49	1559.5
51	1000	2000	1.0	1.7	10	10	40	4.37	212.81	36.72	1760.38
52	3000	2000	1.0	1.7	10	10	40	8.49	201.35	71.3	1583.7
53	2000	1500	1.5	1.7	10	10	60	7.74	199.4	34.38	1554
54	2000	2000	1.5	2.0	10	20	40	8.25	206.41	34.87	2049
55	3000	1500	1.5	2.0	12	10	40	14.37	138.28	83.74	1371.5
56	1000	2000	1.5	1.7	10	10	40	3.34	277.55	21.63	2011
57	2000	2500	1.5	1.7	14	10	20	7.71	211.42	77.62	1689
58	2000	2000	1.5	1.7	12	10	40	6.85	196.39	44.35	1661
59	2000	1500	1.5	1.7	14	10	60	6.02	201.4	41.72	1323
60	2000	2000	1.5	1.7	12	10	40	8.7	198.4	56.28	1611.5
61	2000	2000	1.5	1.4	10	20	40	7.55	244.49	30.4	1972
62	2000	2000	1.0	2.0	12	10	60	5.59	104.21	38.02	1666.5

CHAPTER 5
RESULTS AND DISCUSSION

In the previous chapters, the results are reported for the preliminary experimentation of various laser input parameters to examine the effect on output quality characteristics. These reported results are then identified to select the range or levels of various input parameters. The selected parameters levels then utilized in the designing the run layout for the experimentation work. This chapter focuses on the results and discussion of main experimentation of various input parameters.

The flow chart has been shown in figure 5.1 from the starting of the main experimentation to validation process. Each part of the chart is discussed in the following sections in detail. The response plots have been depicted to identify the results of individual parameter as well as various parameters via interaction effects. The results are plotted for the various output responses such as dross height, kerf taper, edge surface roughness, kerf deviation, striations, heat affected zone width, material removal rate, energy losses, and temperature and stress fields. The regression models of various output responses developed using response surface methodology via Design Expert 6.0 software. The analysis of variance has been performed to verify the adequacy of analytical and fitted model. The fitted model has been developed using quadratic model and backward elimination test of input parameters. The desirability functional approach has been applied to perform the multi-optimization of input parameters. The validation of predicted model has been done by conducting the various experiments.

5.1 Evaluation of Adequacy of Predicted Model

The adequacy of the predicted model has been identified with the help of various tests namely are model summary statistics, sequential model sum of squares and lack of fit test. The model summary statistics emphasis on the predicted model for maximizing the Predicted R-Squared and Adjusted R-Squared values. This model also summarizes about standard deviation and Prediction error sum of squares.

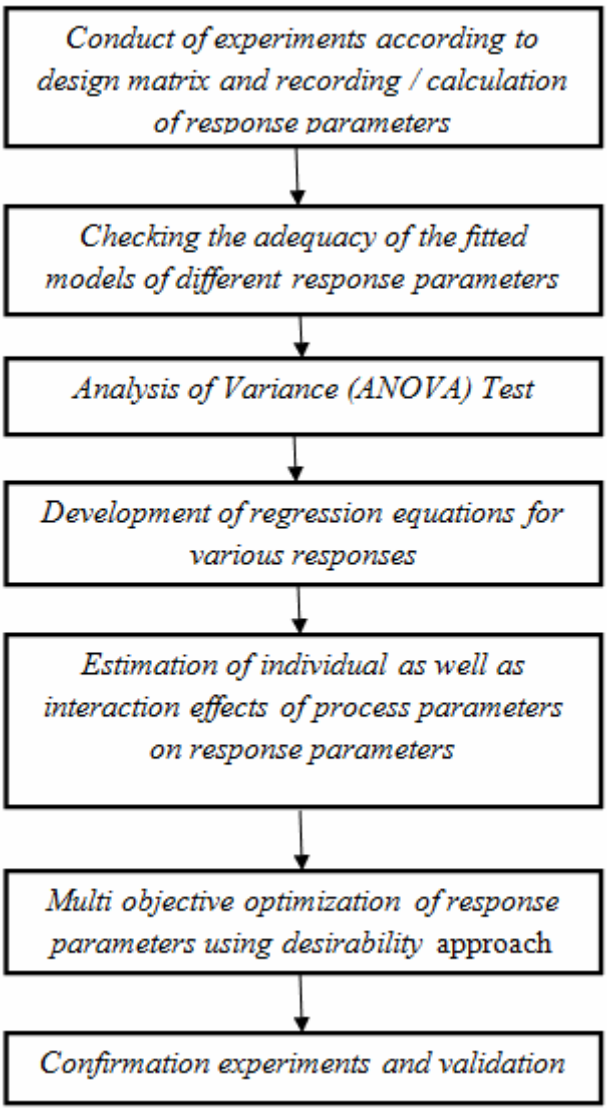

Figure 5.1 Methodology of the statistical analysis of results (Myers H et al.., 2009)

The sequential sum of squares identifies the highest order polynomial for the significant additional terms and non-aliased model terms. The lack of fit test is used to evaluate the inadequacy of the model by verifying the insignificant lack of fit. This test also depicts the data in the experimental area for which points are not admitted in the regression model [Montgomery, 2002]. These all test has been performed for various output responses and input parameters viz. cutting speed, laser power, nozzle stand-off distance, nozzle diameter, gas pressure, percentage reinforced particles, arc radius, type of gas, laser frequency, material thickness, Al/SiC, Al/Al_2O_3 and Al/ZrO_2 as work material. Figure 5.1 shows the methodology to conduct the statistical analysis from conduct of experiment to confirmation of experimentation for analyzing the adequacy of the model.

5.2 Analysis of Variance and Predicted Mathematical Models of Output Responses

To analyse the experimental data statistically analysis of variance is performed for various output responses. From the anova results the average variance of simultaneous conditions with respect to error variance can be analysed. With the help of this approach adequate precision of data can be done which further evaluate the signal to noise ratios. The significant terms can be distinguish if any parameters having p-value < 0.05. The fitted quadratic model is developed with the implementation of backward elimination process. A regression model is considered as approximation model for a defined objective. This model represents the link between the design input variables and the output response functions. In the present work, response surface methodology has been implemented to formulate the mathematical models. All the mathematical models are shown using multiple regression equations for the quality characteristic of LBM process. To develop the regression equations of various output responses of LBM process, the second order response surface has been applied.

Following are the results discussed for various output responses with the help of three tests such as model summary statistics, sequential model sum of squares and lack of fit test. The result of these tests is based on the analysis of variance approach. Tables 5.1-5.8 shows the statistical data related to sequential model sum of squares, lack of fit test and model summary statistics for dross height, kerf taper, surface roughness, kerf deviation, striation angle, heat affected zone width, edge, material removal rate and energy losses. Among the various model such as cubic, mean, linear and 2FI, the Quadratic models are recommended for the various output quality characteristics.

The backward elimination method has been applied in this research work. The f-test and p-test is applied to determine the significant and non-significant parameters on the output responses. The lack of fit test is used to evaluate the inadequacy of the model by verifying the insignificant lack of fit. The insignificant lack of fit is recommended for the perfect predicted model. It has been analyzed that value of p-test < 0.0001 shows the condition for the significance of the process. The quadratic model has been selected among all the models such as cubic, 2FI and linear model for which the p-value suggested by the design expert of < 0.0001. For the lack of fit tests, model summary statistics and sequential model sum of squares the quadratic model has been selected.

Table 5.1 Adequacy checking of model of dross height

Sequential Model Sum of Squares						
Source	**Sum of Squares**	**Degrees of Freedom**	**Mean Square**	**F-Value**	**Prob.> F (p-value)**	**Remarks**
Mean	28.221	1	28.221			
Linear	0.420	7	0.060	2.959	0.0202	
2FI	0.893	21	0.042	1.482	0.151	
Quadratic	2.742	7	0.391	11.492	< 0.0001	Suggested
Cubic	0.513	21	0.024	8.736	0.012	
Residual	0.013	5	0.002			
Total	32.805	62	0.529			
Lack of Fit Tests						
Source	**Sum of Squares**	**Degrees of Freedom**	**Mean Square**	**F-Value**	**Prob.> F (p-value)**	**Remarks**
Linear	1.827	49	0.037	13.328	0.0043	
2FI	0.933	28	0.033	11.916	0.0058	
Quadratic	0.513	21	0.024	8.736	0.0122	Suggested
Cubic	0.132	3	0.043		0.0214	
Model Summary Statistics						
Source	**Standard Deviation**	**R-Squared**	**Adjusted R-Squared**	**Predicted R-Squared**	**PRESS**	**Remarks**
Linear	0.184	0.598	0.546	0.458	2.484	
2FI	0.169	0.793	0.617	0.142	3.929	
Quadratic	0.142	0.884	0.730	0.199	3.669	Suggested
Cubic	0.052	0.996	0.962			

Table 5.2 Adequacy checking of model of kerf taper

Sequential Model Sum of Squares						
Source	**Sum of Squares**	**Degrees of Freedom**	**Mean Square**	**F-Value**	**Prob.> F (p-value)**	**Remarks**
Mean	7.299	1	7.299			
Linear	0.126	7	0.018	13.546	< 0.0001	
2FI	0.038	21	0.001	1.822	0.0596	
Quadratic	0.013	7	0.001	2.622	0.0344	Suggested
Cubic	0.019	21	0.0009	32.425	0.0005	
Residual	0.0001	5	0.00002			
Total	7.498	62	0.120			
Lack of Fit Tests						
Source	**Sum of Squares**	**Degrees of Freedom**	**Mean Square**	**F-Value**	**Prob.> F (p-value)**	**Remarks**
Linear	0.072	49	0.001	51.476	0.0002	
2FI	0.033	28	0.001	41.616	0.0003	
Quadratic	0.019	21	0.0009	32.425	0.0005	Suggested
Cubic	0.009	2	0.002			
Model Summary Statistics						
Source	**Standard Deviation**	**R-Squared**	**Adjusted R-Squared**	**Predicted R-Squared**	**PRESS**	**Remarks**
Linear	0.036	0.637	0.590	0.510	0.097	
2FI	0.031	0.831	0.689	0.308	0.137	
Quadratic	0.027	0.901	0.768	0.3036	0.138	Suggested
Cubic	0.005	0.999	0.991			

Table 5.3 Adequacy checking of model of surface roughness

Sequential Model Sum of Squares						
Source	**Sum of Squares**	**Degrees of Freedom**	**Mean Square**	**F-Value**	**Prob.> F (p-value)**	**Remarks**
Mean	322.66	1	322.665			
Linear	15.213	7	2.173	12.820	< 0.0001	
2FI	4.440	21	0.211	1.480	0.1527	
Quadratic	3.067	7	0.438	6.924	0.0001	Suggested
Cubic	1.617	21	0.077	13.655	0.0044	
Residual	0.028	5	0.005			
Total	347.033	62	5.597			
Lack of Fit Tests						
Source	**Sum of Squares**	**Degrees of Freedom**	**Mean Square**	**F-Value**	**Prob.> F (p-value)**	**Remarks**
Linear	9.12578	49	0.18624	33.02135	0.0005	
2FI	4.68538	28	0.167335	29.66933	0.0007	
Quadratic	1.617383	21	0.077018	13.65572	0.0044	Suggested
Cubic	0.9124	3	0.178342			
Model Summary Statistics						
Source	**Standard Deviation**	**R-Squared**	**Adjusted R-Squared**	**Predicted R-Squared**	**PRESS**	**Remarks**
Linear	0.412	0.624	0.576	0.499	12.201	
2FI	0.378	0.807	0.642	0.260	18.035	
Quadratic	0.252	0.932	0.842	0.526	11.542	Suggested
Cubic	0.075	0.999	0.986			

Table 5.4 Adequacy checking of model of kerf deviation

Sequential Model Sum of Squares						
Source	**Sum of Squares**	**Degrees of Freedom**	**Mean Square**	**F-Value**	**Prob.> F (p-value)**	**Remarks**
Mean	0.4255	1.0000	0.4255			
Linear	0.0619	7.0000	0.0088	6.0322	<0.0004	
2FI	0.0246	21.0000	0.0012	0.8746	0.6198	
Quadratic	0.0276	7.0000	0.0039	6.1830	0.0003	Suggested
Cubic	0.0163	21.0000	0.0008	13.0511	0.0048	
Residual	0.0003	5.0000	0.0001			
Total	0.5561	62.0000	0.0090			
Lack of Fit Tests						
Source	**Sum of Squares**	**Degrees of Freedom**	**Mean Square**	**F-Value**	**Prob.> F (p-value)**	**Remarks**
Linear	0.069	49	0.001	23.520	0.001	
2FI	0.044	28	0.002	26.380	0.001	
Quadratic	0.016	21	0.001	13.051	0.005	Suggested
Cubic	0.009	3	0.001		0.005	
Model Summary Statistics						
Source	**Standard Deviation**	**R-Squared**	**Adjusted R-Squared**	**Predicted R-Squared**	**PRESS**	**Remarks**
Linear	0.036	0.473	0.405	0.318	0.089	
2FI	0.037	0.662	0.375	0.121	0.146	
Quadratic	0.025	0.873	0.702	0.110	0.116	Suggested
Cubic	0.008	0.998	0.972			

Table 5.5 Adequacy checking of striation angle

Sequential Model Sum of Squares						
Source	**Sum of Squares**	**Degrees of Freedom**	**Mean Square**	**F-Value**	**Prob.> F (p-value)**	**Remarks**
Mean	3543.893	1	3543.893			
Linear	237.329	7	33.904	7.469	< 0.0001	
2FI	122.007	21	5.810	1.557	0.124	
Quadratic	67.500	7	9.643	4.507	0.002	Suggested
Cubic	53.935	21	2.568	7.616	0.017	
Residual	1.686	5	0.337			
Total	4026.350	62	64.941			
Lack of Fit Tests						
Source	**Sum of Squares**	**Degrees of Freedom**	**Mean Square**	**F-Value**	**Prob.> F (p-value)**	**Remarks**
Linear	243.442	49.000	4.968	14.732	0.003	
2FI	121.435	28.000	4.337	12.860	0.005	
Quadratic	53.935	21.000	2.568	7.616	0.017	Suggested
Cubic	98.012	3.000	3.438		0.022	
Model Summary Statistics						
Source	**Standard Deviation**	**R-Squared**	**Adjusted R-Squared**	**Predicted R-Squared**	**PRESS**	**Remarks**
Linear	2.131	0.492	0.426	0.315	330.459	
2FI	1.932	0.745	0.528	0.052	507.340	
Quadratic	1.463	0.885	0.730	0.200	385.968	Suggested
Cubic	0.581	0.997	0.957			

Table 5.6 Adequacy checking of model of heat affected zone width

Sequential Model Sum of Squares						
Source	**Sum of Squares**	**Degrees of Freedom**	**Mean Square**	**F-Value**	**Prob.> F (p-value)**	**Remarks**
Mean	3415167.00	1.00	3415167.00			
Linear	37042.13	7.00	5291.73	1.86	0.12	
2FI	104621.20	21.00	4981.96	1.48	0.15	
Quadratic	151301.80	7.00	21614.54	5.41	< 0.0001	Suggested
Cubic	65249.80	21.00	3107.13	1.79	0.27	
Residual	8684.63	5.00	1736.93			
Total	3782067.00	62.00	61001.07			
Lack of Fit Tests						
Source	**Sum of Squares**	**Degrees of Freedom**	**Mean Square**	**F-Value**	**Prob.> F (p-value)**	**Remarks**
Linear	65249.8	21	3107.133	1.788	0.269	
2FI	102291.9	28	3653.283	2.103	0.208	
Quadratic	206913.1	49	4222.716	2.431	0.161	Suggested
Cubic	34213.23	3	2136.128		0.298	
Model Summary Statistics						
Source	**Standard Deviation**	**R-Squared**	**Adjusted R-Squared**	**Predicted R-Squared**	**PRESS**	**Remarks**
Linear	63.187	0.412	0.336	0.213	288886.000	Suggested
2FI	57.991	0.698	0.441	0.199	439997.700	
Quadratic	53.326	0.798	0.527	0.299	476504.500	
Cubic	41.676	0.976	0.711			

Table 5.7 Adequacy checking of model of material removal rate

Sequential Model Sum of Squares						
Source	**Sum of Squares**	**Degrees of Freedom**	**Mean Square**	**F-Value**	**Prob.> F (p-value)**	**Remarks**
Mean	275908.8	1	275908.8			
Linear	20985.98	7	2997.997	6.384	< 0.0001	
2FI	10638.32	21	506.586	1.135	0.3630	
Quadratic	7031.559	7	1004.508	3.398	0.0103	Suggested
Cubic	7566.675	21	360.317	15.142	0.0034	
Residual	118.979	5	23.795			
Total	322250.3	62	5197.586			
Lack of Fit Tests						
Source	**Sum of Squares**	**Degrees of Freedom**	**Mean Square**	**F-Value**	**Prob.> F (p-value)**	**Remarks**
Linear	25236.55	49	515.031	21.643	0.0013	
2FI	14598.23	28	521.365	21.909	0.0014	
Quadratic	7566.675	21	360.317	15.142	0.0034	Suggested
Cubic	6246.75	3	412.553		0.0037	
Model Summary Statistics						
Source	**Standard Deviation**	**R-Squared**	**Adjusted R-Squared**	**Predicted R-Squared**	**PRESS**	**Remarks**
Linear	21.669	0.453	0.382	0.263	34137.510	
2FI	21.118	0.682	0.413	0.305	60495.470	
Quadratic	17.193	0.834	0.611	0.165	53978.800	Suggested
Cubic	4.878	0.997	0.969			

Table 5.8 Adequacy checking of model of energy losses

Sequential Model Sum of Squares						
Source	**Sum of Squares**	**Degrees of Freedom**	**Mean Square**	**F-Value**	**Prob.> F (p-value)**	**Remarks**
Mean	150080.12	1	150080.12			
Linear	2666567	7	380938.2	13.546	< 0.0001	
2FI	815403.5	21	38828.74	1.822	0.0596	
Quadratic	291006.3	7	41572.33	2.622	0.0344	Suggested
Cubic	409136.2	21	19482.67	32.425	0.0005	
Residual	3004.236	5	600.847			
Total	1.58E+08	62	2544725			
Lack of Fit Tests						
Source	**Sum of Squares**	**Degrees of Freedom**	**Mean Square**	**F-Value**	**Prob.> F (p-value)**	**Remarks**
Linear	1515546	49	30929.51	51.47649	0.0002	
2FI	700142.5	28	25005.09	41.616	0.0003	
Quadratic	409136.2	21	19482.67	32.425	0.0005	Suggested
Cubic	323346.1	3	17885.14		.00007	
Model Summary Statistics						
Source	**Standard Deviation**	**R-Squared**	**Adjusted R-Squared**	**Predicted R-Squared**	**PRESS**	**Remarks**
Linear	167.694	0.637	0.590	0.510	2047623	
2FI	145.970	0.831	0.689	0.308	2892964	
Quadratic	125.903	0.901	0.768	0.303	2913739	Suggested
Cubic	24.512	0.999	0.991			

5.3 EFFECT OF PROCESS PARAMETERS FOR WORK MATERIAL OF Al5052/SiC USING ANOVA AND MATHEMATICAL MODEL

5.3.1 Effect of process parameters on dross height

Dross height is considered as one of the important factor to reduce so that quality of the cut edge can be improved. The formation of large dross height occurs due to high viscosity of molten material and higher surface tension. This, in turn, makes necessary to examine the significant and non-significant parameters affecting the dross formation.

The normal probability plot of residuals for dross height is shown in figure 5.2. From the linearity of the graph, the adequacy of the model can be predicted. From the graph, it can be predicted that residuals are normally distributed and scattered nearby the straight line resulted into less errors as shown in plot. It can also be observed that predicted values resembles with observed response values which shows the adequacy of the model and process parameters. The normal plots of residual values are shown in figure 5.3 which also shows the linearity of the model.

The regression equation is modeled in form of various combinations of input parameters as depicted in equation 1. The regression model shows combinations of main parameters and interaction of parameters for the dross height.

$$\textit{Dross Height (mm)} = 1.692 - 1.407E{-}004 \times X_1 - 1.447E{-}004 \times X_2 - 0.026 \times X_3 - 1.316 \times X_4 + 0.250 \times X_5 + 0.037 \times X_6 - 0.035 \times X_7 + 1.110E{-}007 \times (X_1)^2 + 8.834E - 004 \times (X_6)^2 + 1.926E{-}004 \times (X_7)^2 - 6.020E\text{-}005 \times X_1 \times X_5 + 5.250E\text{-}006 \times X_1 \times X_7 + 1.016 \times X_3 \times X_4 - 0.115 \times X_3 \times X_5 - 0.021 \times X_3 \times X_6 \quad \text{.....(5.1)}$$

To verify the satisfactory results, the analysis of variance has been performed for D_t. For ANOVA the quadratic model for the dross height is necessary and contributes feasible results. The ANOVA table for the dross height is shown in table 5.9 which shows that quadratic model lies at 95% confidence level. The model F-value for dross height is 13.48 which show that only a 0.01% chance is there for higher value of F- value which may occur due to noise and corresponding p-value is less than 0.001.

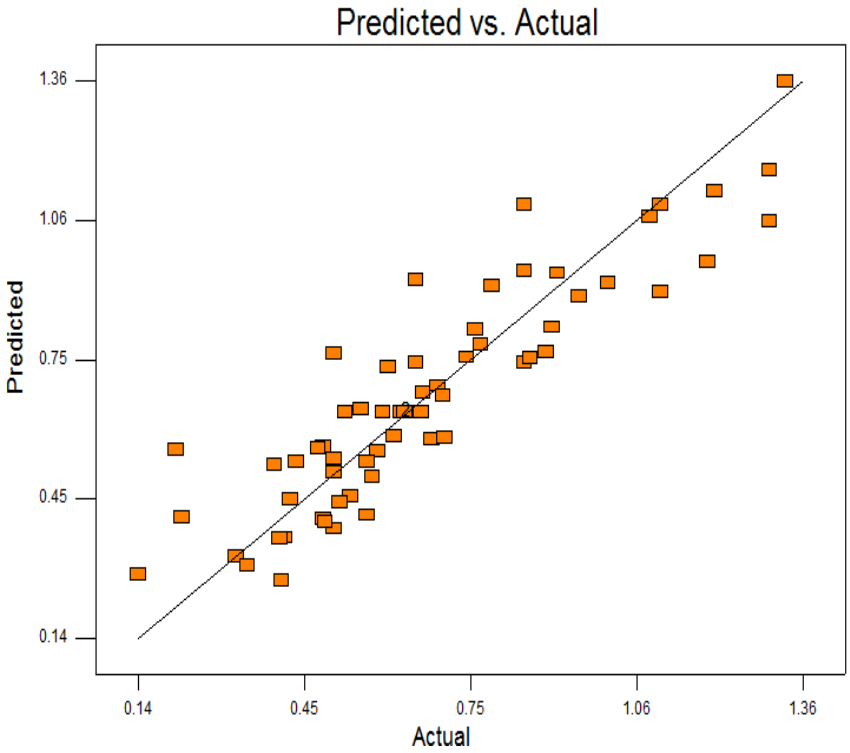

Figure 5.2 Plot of predicted versus actual for dross height

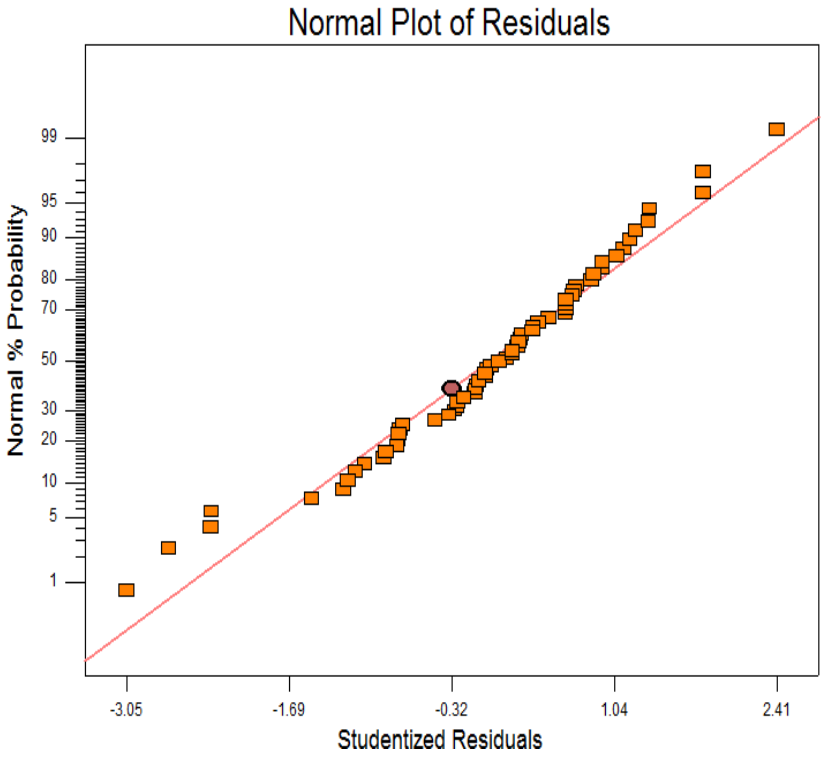

Figure 5.3 Normal probability plots of residuals for dross height

Table 5.9 ANOVA for response surface of reduced quadratic model of dross height

Source	Sum of Squares	Degrees of Freedom	Mean Square	F-Value	Prob. > F (p-value)	Remarks
Model	3.73	15	0.25	13.48	< 0.0001	Significant
X_1	1.05	1	1.05	56.85	< 0.0001	Significant
X_2	0.13	1	0.13	6.80	0.012	Significant
X_3	0.065	1	0.065	3.54	0.066	Not-significant
X_4	0.094	1	0.094	5.10	0.028	Significant
X_5	0.18	1	0.18	9.82	0.003	Significant
X_6	0.35	1	0.35	18.84	< 0.0001	Significant
X_7	0.88	1	0.088	47.53	< 0.0001	Significant
X_1^2	0.18	1	0.18	9.65	0.003	Significant
X_6^2	0.11	1	0.11	6.11	0.017	Significant
X_7^2	0.086	1	0.086	4.65	0.036	Significant
X_1X_5	0.12	1	0.12	6.28	0.015	Significant
X_1X_7	0.088	1	0.088	4.78	0.034	Significant
X_3X_4	0.19	1	0.19	10.07	0.002	Significant
X_3X_6	.090	1	0.090	4.89	0.032	Significant
Predicted R^2 0.914						

***Legend: X_1: Cutting speed, X_2:* Laser power , *X_3:* Nozzle stand-off distance , *X_4:* Nozzle diameter , *X_5:* Gas pressure , *X_6:* Percentage reinforced particles, *X_7:* Arc radius**

Moreover, lack of fit of 0.450 implies that it is not significant relative to pure error. Thus, quadratic model is significant at 95% confidence level. It indicates that F-value of model is 115.61. It implies that there is only a 0.01% chance that such large F- value of model can occur due to noise. The other important coefficient R^2, which is called determination coefficient, is defined as the ratio of the explained variation to the total variation and is a

measure of the degree of fit. When R^2 approaches to unity, the response model fits better to the actual data and shows less difference between the predicted and actual values. It was found that the "Pred R-Squared" value of 0.914 is closely matched with the "Adj R-Squared" value of 0.891.The probability 'p' value of nozzle distance is predicted as 0.0661 which is highest value of the model resulted into insignificant parameter.

On the basis of experimental results, the main plots have been explored for determining the effect of individual factor on output response. The effect of cutting speed on dross height is shown in figure 5.4 (a). It was analyzed from the main plots that dross height is significantly affected by cutting speed, gas pressure, reinforced particles and arc radius. Based on main effect plot, with the increase in cutting speed from 1000 to 3000 mm/min the dross height decreased by 0.956 mm to 0.537 mm. This is due to the fact that higher cutting speed decreases the beam and workpiece interaction resulted into decrease in the backward flow of the molten material. The effect of laser power on the dross height also has considerable effect as shown in the main effect plot in figure 5.4 (b).

It was reported that as laser power increased from 1500 to 2500 watt the decrease in dross height noted to decrease by 0.708 to 0.563 mm. It caused mainly due to the expelling of molten material by large amount of energy attained in the kerf zone. The lower values of nozzle distance and nozzle diameter found suitable for decreased values of D_t. However, with the increase in nozzle stand-off distance from 1.0 to 2.0 mm, the D_t value increased by 0.583 mm to 0.688 mm as shown in figure 5.5 (d). The overall effect of nozzle distance was not significant due to having low variation in the dross height value. With the increment in nitrogen gas pressure the D_t value decreased to higher extent. From the figure 5.6 (e) , the main plot shows that when the gas pressure was kept at 10 bar the dross height analysed with value of 0.723 mm, whereas with increase in gas pressure to 14 bar the Dt value decreased to 0.549 mm. The higher nitrogen gas pressure increases the effect of exothermic reaction and exit the molten material easily with higher expel force from the kerf zone resulting into less dross height. The higher arc radius proved to be significant for lower values of D_t as with increase in arc radius from 20 mm to 60 mm the Dt value shown decrement from 0.928 mm 0.527 mm as shown in figure 5.7. This fact may be attributed to the arc of lower radius having more circular in nature which caused the variation in dross height.

Also with increase in percentage volume of reinforced particles the pattern of dross height reduces to lower rate as shown in figure 5.6 (e). Because the presence of 20 % SiC particles and unburned SiC develops more viscosity level resulted into restricted metal flow in downward direction.

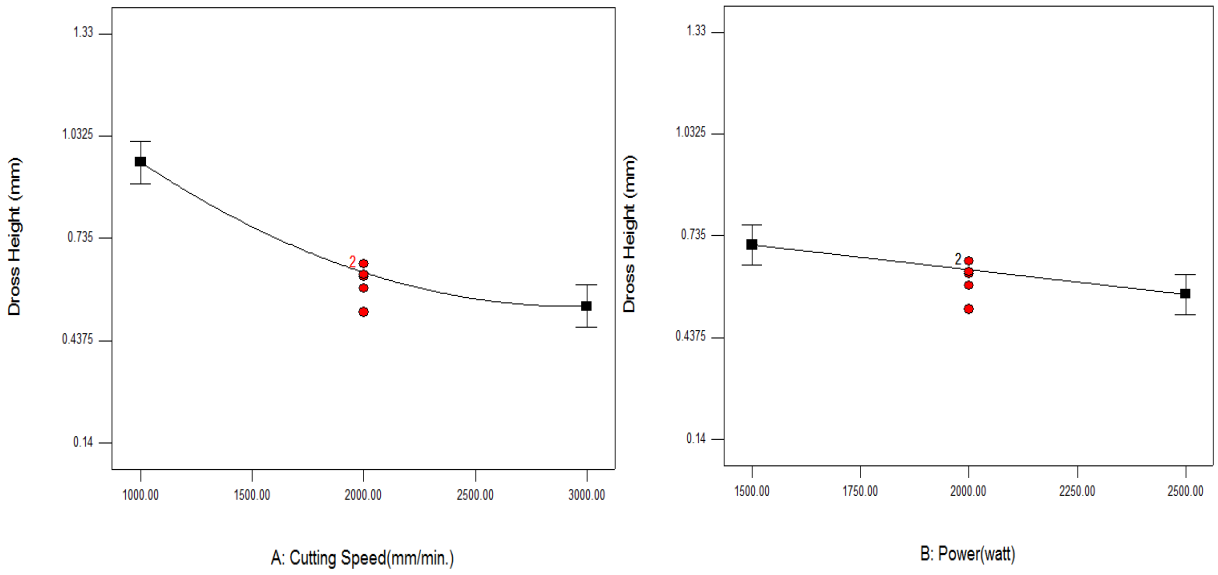

(a) **(b)**

Figure 5.4 Effect of cutting speed (a) and laser power (b) on dross height

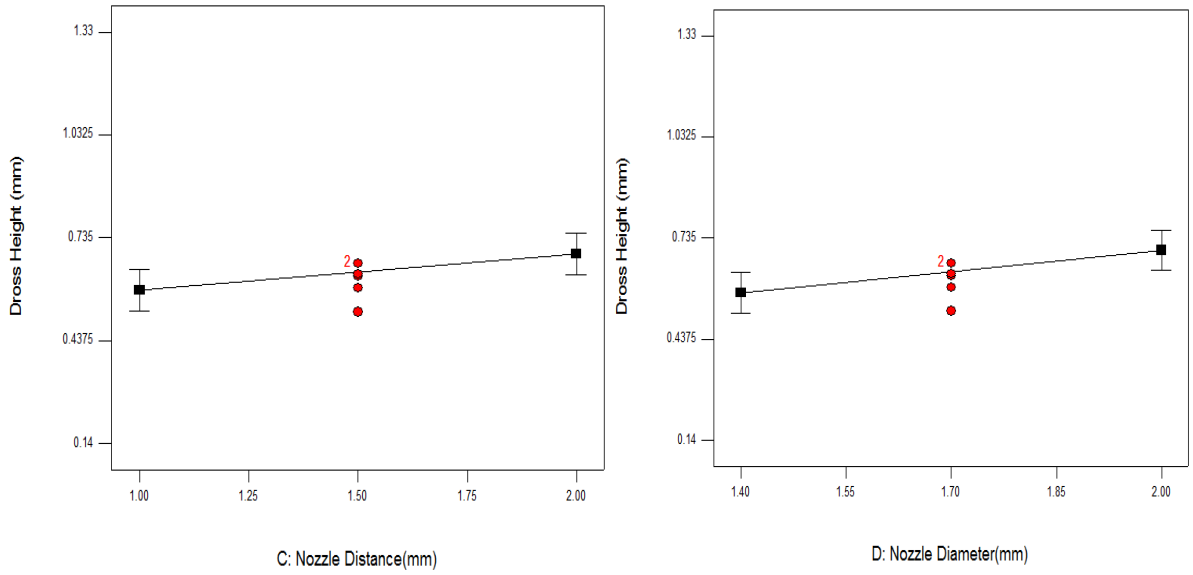

(c) **(d)**

Figure 5.5 Effect of nozzle distance (c) and nozzle diameter (d) on dross height

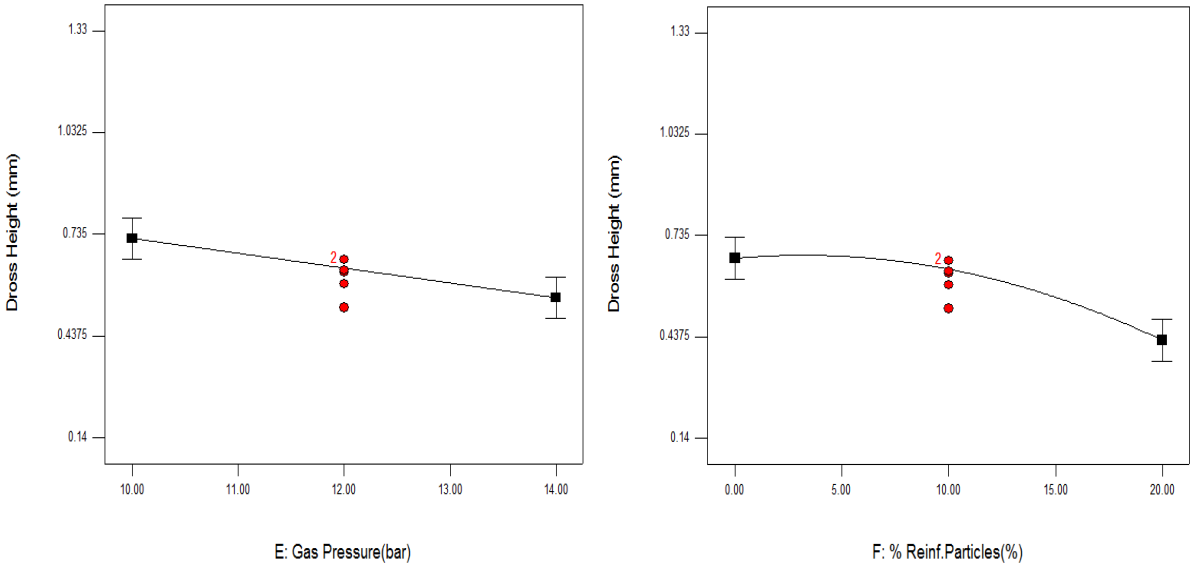

(e) **(f)**

Figure 5.6 Effect of gas pressure (e) and reinforced particles (f) on dross height

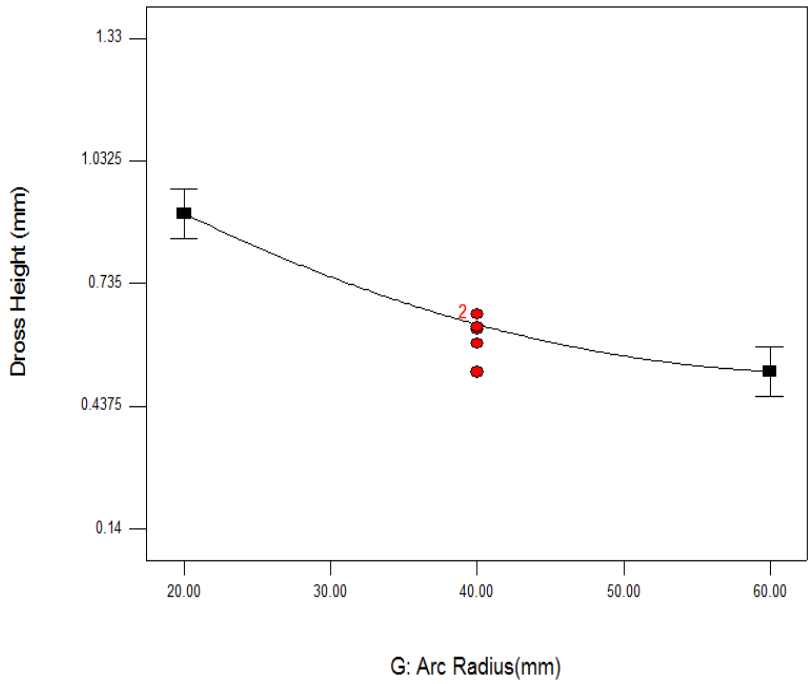

Figure 5.7 Effect of arc radius on dross height

The effect of cutting speed and gas pressure on D_t have been depicted simultaneously in figure 5.9 for constant values of X_2, X_3, X_4, X_6 and X_7 at 2000 watt,1.5mm,1.7 mm,12 bar and 40 mm respectively. From the response plot it can be examined that combination of higher value of cutting speed and gas pressure is suitable for low D_t value.

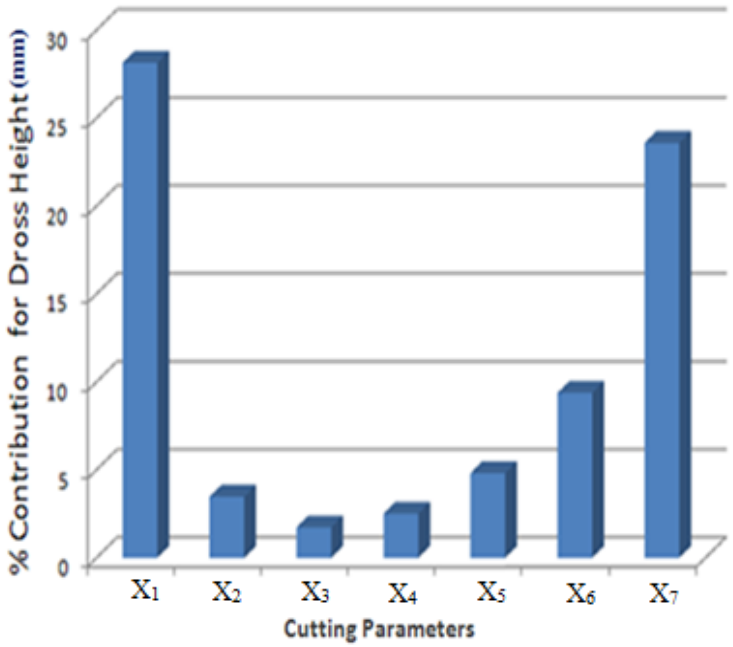

Figure 5.8 Percentage contribution effect of parameters on dross height

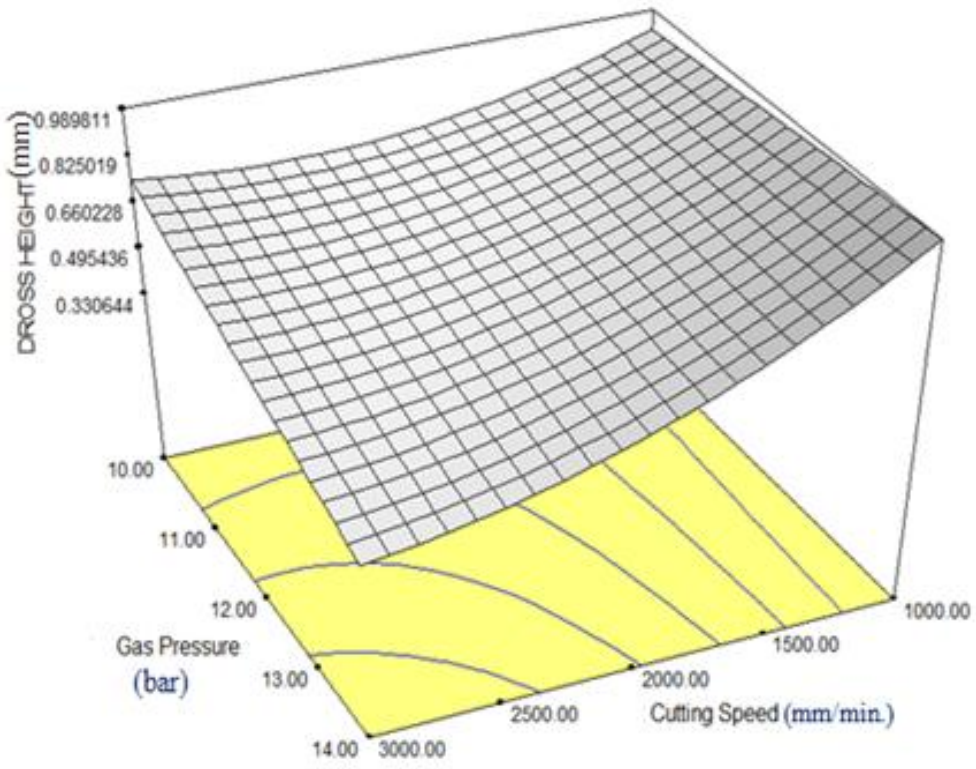

Figure 5.9 Interaction plot between cutting speed and gas pressure for dross height

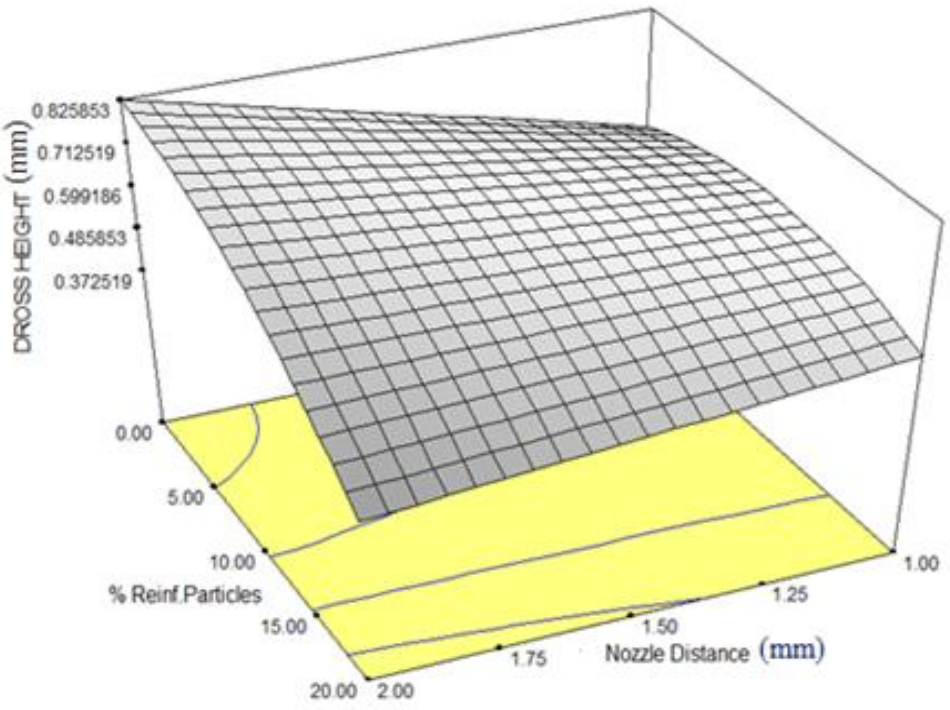

Figure 5.10 Interaction plot between nozzle distance and reinforced particles for dross height

When gas pressure set at 14 bar for lower values of cutting speed, the slope of D_t curve increased dramatically. Further, it can be concluded that with increase in cutting speed from 1000 mm/min to 3000 mm/min and gas pressure from 10 bar to 14 bar, dross height reduced to large extent. The probable reason for it is that high gas pressure enhances the momentum of molten metal by overcoming the values of tension forces resulted into large expulsion of molten material. Additionally, higher cutting speed decreases the backward flow of molten material by expelling the molten material from the bottom part of kerf. Moreover, lower cutting speed increases the backward flow of melt material resulted into collection of molten material in form of clinging dross near the bottom kerf (Arata Y. et al.., 1981).

The effect of thermal behavior of ceramic particles on the variation of dross height is important to examine. Figure 5.10 exhibits the combined effects of silicon carbide particles and nozzle stand-off distance, where other parameters are kept constant. From the response plot, it is seen that when the reinforced SiC particles quantity was fixed at 20 % and nozzle stand-off distance decreased from the 2 mm to 1 mm the dross height increased from 0.373mm to 0.481 mm. It may be due to large stand-off distance impel the gas to expand and causes high momentum of molten material to exit.

The nature of variation of D_t decreases with the increase in % volume of reinforced SiC particles. It has been observed that reinforced specimen with 20 % volume SiC particles has lower D_t value as compared to non-reinforced specimen of 0 % volume. Because the unburned SiC particles mixes with molten material in the cutting zone resulted into high viscosity. This, in turn, restricts the molten material to downward motion which resulted into less dross height. The percentage contribution of different factors on dross height is shown in figure 5.8. It has been observed that cutting speed has maximum significant contribution of 29 % whereas arc radius shown 24 % of contribution.

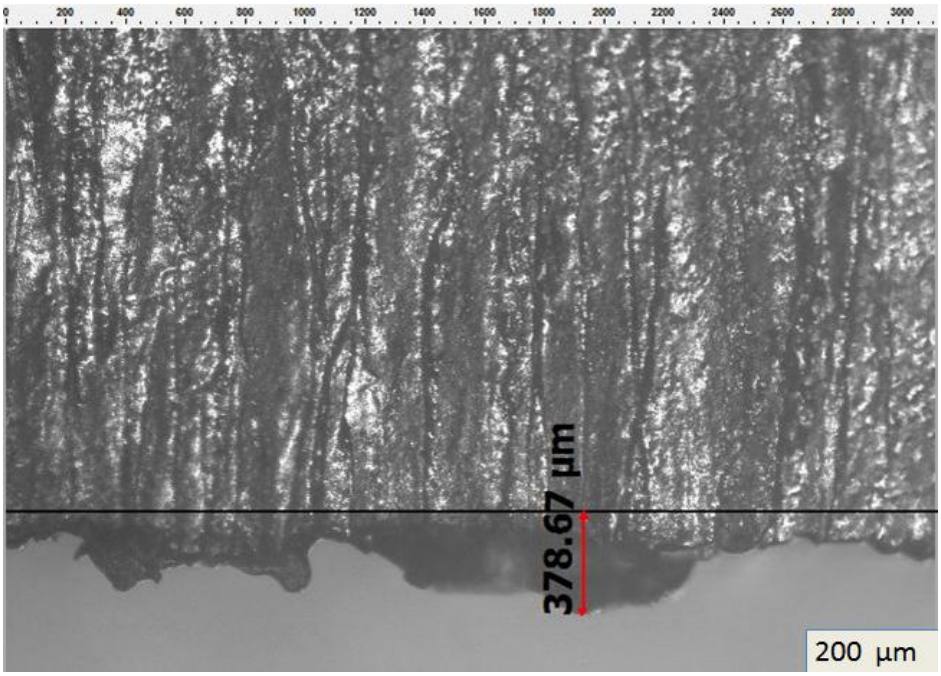

Figure 5.11 Optical micrograph (50 ×) of dross height at X_1: 3000 mm/min, X_2: 2000 watt, X_3: 1.5 mm, X_4: 1.7mm, X_5: 12 bar, X_6: 20%, X_7: 60 mm

From the microscopic observations as shown in figure 5.11, it can be easily predicted that dross height has significant effect with variation in the values of cutting speed, % SiC particles and arc radius. From the figure, it is examined that when cutting speed set at 3000 mm/min, 20 % volume SiC particles and arc radius at 60 mm, the dross height reduces to low value of 0.378 mm. The lower dross height 0.378 mm indicated the higher viscosity which restricts the molten material flow into the downward direction. It has been examined that due to decrease in the quantity of reinforced particles the dross height is increased as compared to the work materials having higher quantity.

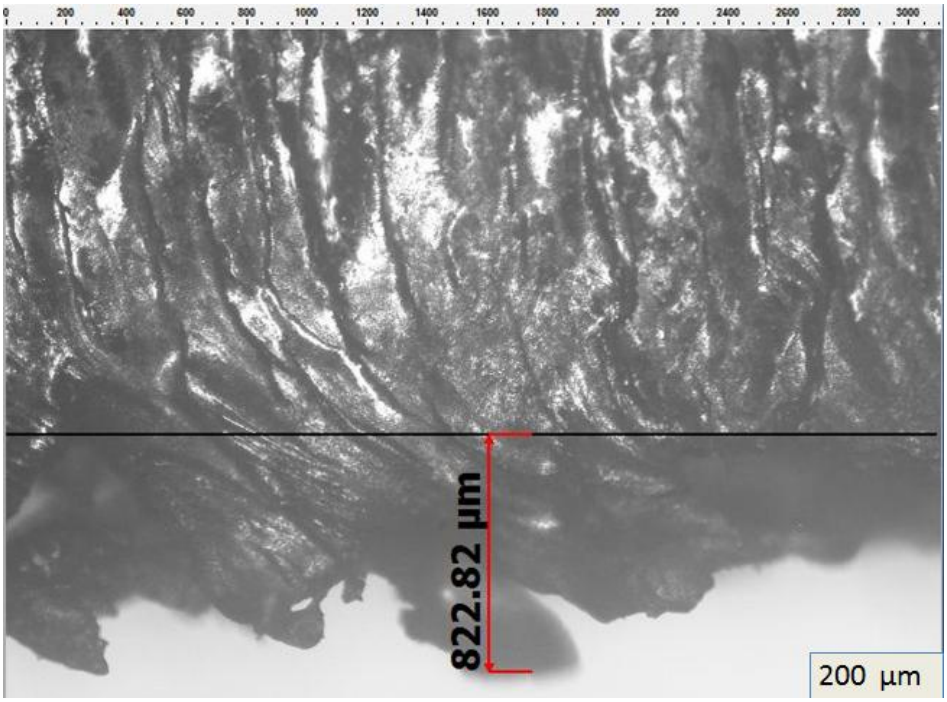

Figure 5.12 Optical micrograph (50 ×) of dross height at X_1: 2000 mm/min, X_2: 2000 watt, X_3: 2 mm, X_4: 1.4 mm, X_5: 12 bar, X_6: 10%, X_7: 20 mm

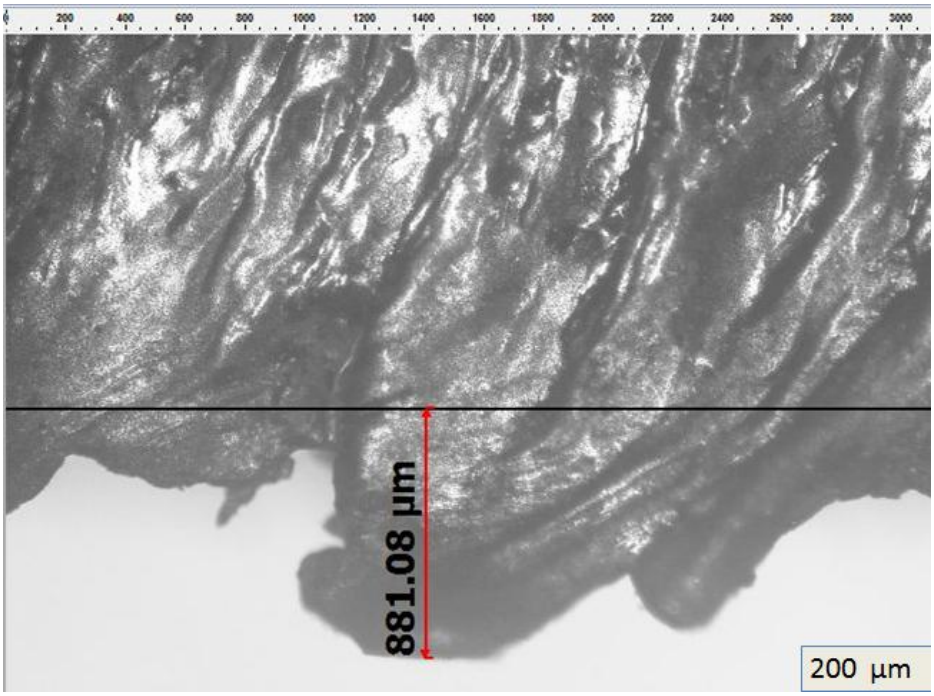

Figure 5.13 Optical micrograph (50 ×) of dross height at X_1: 1000 mm/ min, X_2: 2500 watt, X_3: 1.5 mm, X_4: 2 mm, X_5: 12 bar, X_6: 10%, X_7: 40 mm

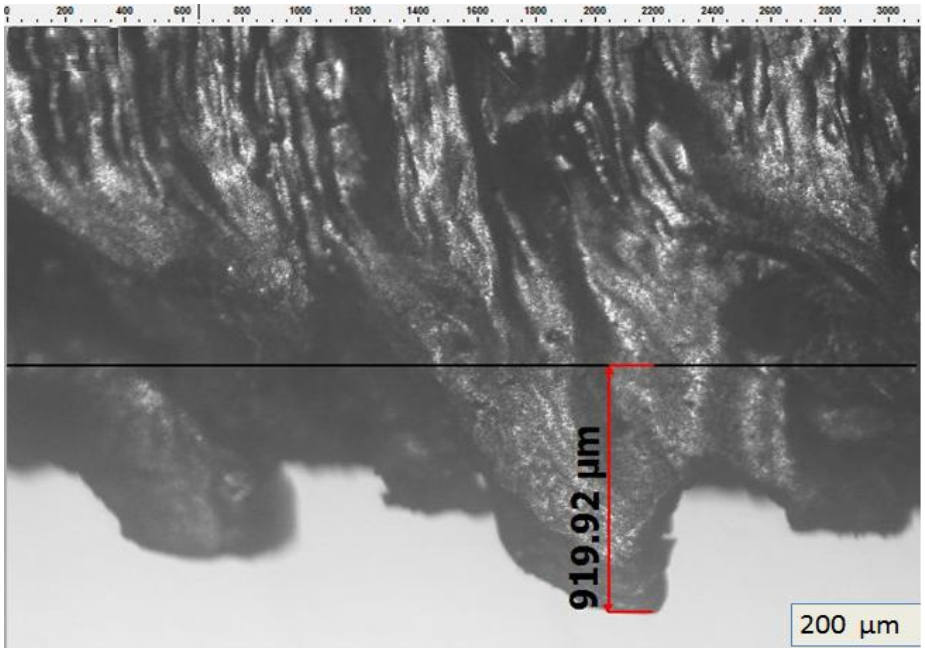

Figure 5.14 Optical micrograph (50 ×) of dross height at X_1: 1000 mm/min, X_2: 2500 watt, X_3: 1.5 mm, X_4: 1.4 mm, X_5: 12 bar, X_6: 10 %, X_7: 40 mm

Figure 5.12 reflects that when the machining condition set as cutting speed: 2000mm/min., 10 % volume SiC particles and arc radius at 20 mm, the value of D_t increased to 0.822 mm. Additionally, the dross height increased to 0.919 mm when the cutting speed decreased to 1000 mm/min. with increasing % volume of SiC particles as depicted in figure 5.14. It can be concluded that D_t value had higher impact with higher cutting speed, % volume SiC particles and lower arc radius. Moreover, D_t value has been observed with lower impact with the variation of other factors like laser power, nozzle diameter, nozzle stand-off distance.

5.3.2 Effect of process parameters on kerf taper

Kerf taper mainly develops when the work specimen is reflective in nature and combination of various input parameters are not in optimized range. It may also occurs when the laser cut profile is complex in nature having curved trajectory. In this work, efforts are made to determine the effect of different parameters on kerf taper. The kerf taper is basically develop when the top and bottom kerf have difference in the kerf width value. There are various process parameters which effects the kerf taper significantly.

The normal probability plot of residuals for kerf taper is shown in figure 5.15. From the linearity of the graph, the adequacy of the model can be predicted. From the graph, it can be predicted that residuals are normally distributed and scattered nearby the straight line

resulted into less errors as shown in plot. It can also be observed that predicted values resembles with observed response values which shows the adequacy of the model and process parameters. The normal plots of residual values are shown in figure 5.16 which also shows the linearity of the model.

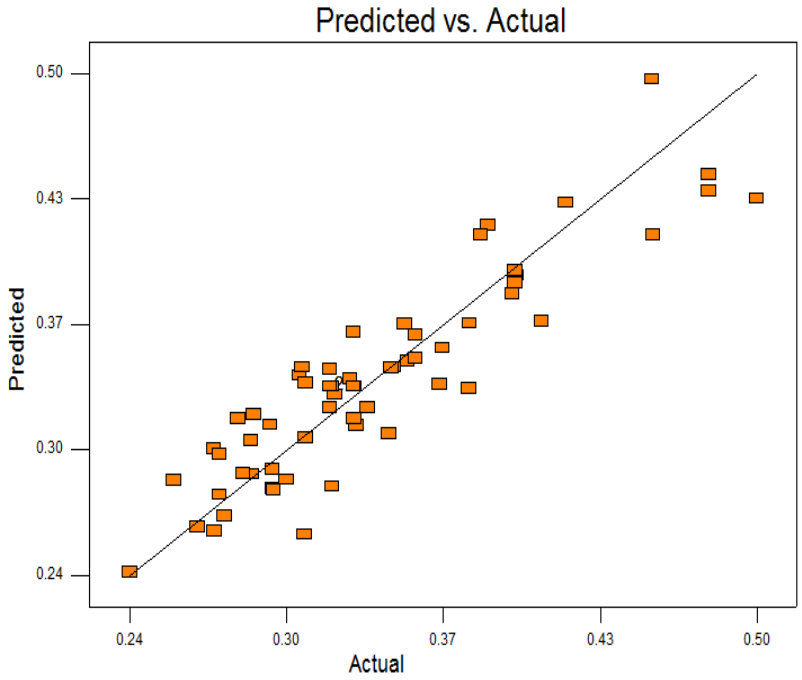

Figure 5.15 Plot of actual versus predicted for kerf taper

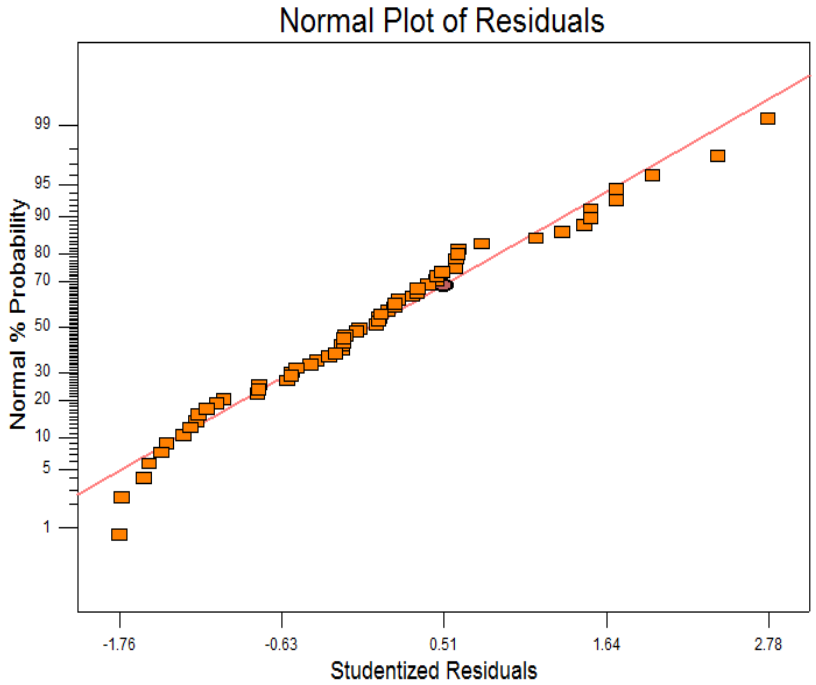

Figure 5.16 Normal probability plots of residuals for kerf taper

Table 5.10 ANOVA for response surface of reduced quadratic model of kerf taper

Source	Sum of Squares	Degrees of Freedom	Mean Square	F-Value	Prob. > F (p-value)	Remarks
Model	0.1589	13	0.0122	14.68	< 0.0001	Significant
X_1	0.0178	1	0.0178	21.46	< 0.0001	Significant
X_2	0.0050	1	0.0050	6.119	0.017	Not-Significant
X_3	0.0007	1	0.0007	0.906	0.345	Not-Significant
X_4	0.0020	1	0.0020	2.433	0.125	Significant
X_5	0.0282	1	0.0282	33.96	< 0.0001	Significant
X_6	0.0187	1	0.0187	22.46	< 0.0001	Significant
X_7	0.0539	1	0.0539	64.85	< 0.0001	Significant
X_7^2	0.0083	1	0.0083	10.06	0.002	Significant
X_1X_7	0.0047	1	0.0047	5.755	0.020	Significant
X_2X_6	0.0037	1	0.0037	4.457	0.040	Significant
X_3X_4	0.0049	1	0.0049	5.939	0.018	Significant
X_4X_7	0.0057	1	0.0057	6.946	0.011	Significant
X_5X_7	0.0045	1	0.0045	5.517	0.023	Significant
Predicted R^2 0.884						

***Legend: X_1: Cutting speed, X_2:* Laser power , *X_3:* Nozzle stand-off distance , *X_4:* Nozzle diameter , *X_5:* Gas pressure , *X_6:* Percentage reinforced particles, *X_7:* Arc radius**

The Model F-value of 14.68 implies the model is significant. There is only a 0.01% chance that a "Model F-Value" is higher in nature which may be due to noise. The Values of "Prob > F" less than 0.050 indicate model terms are significant. In this case X_1, X_2, X_5, X_6, X_7, X_7^2, X_1X_7, X_2X_6, X_3X_4, X_4X_7, X_5X_7 are significant model terms. The "Pred R-Squared" value of 0.8848 is closely matched with the "Adj R-Squared" value of 0.8611. A backward elimination method is applied to eliminate the non-significant parameters. The Anova results for the kerf taper are shown in table 5.10.

Kerf taper can be found from the following relation :

$$K_t = \{(K_{wt} - K_{wb}) \times 180\} / 2\pi t \quad \text{..... (5.2)}$$

K_{wt} is kerf width on top surface, K_{wb} is kerf width of bottom surface and t denotes the thickness of workpeice material. The developed model for kerf taper based on RSM approach is given below in equation 3.

$$Kerf\ Taper = 1.828 - 7.623E-005 \times X_1 - 1.393E-005 \times X_2 - 0.270 \times X_3 - 0.397 \times X_4 - 0.041 \times X_5 - 5.823E-003 \times X_6 - 0.024 \times X_7 + 5.966E-005 \times (X_7)^2 + 1.223E-006 \times X_1 \times X_7 + 4.307E-006 \times X_2 \times X_5 + 0.165 \times X_3 \times X_4 + 4.481E-003 \times X_4 \times X_7 + 5.990E-004 \times X_5 \times X_7 \quad \text{..... (5.3)}$$

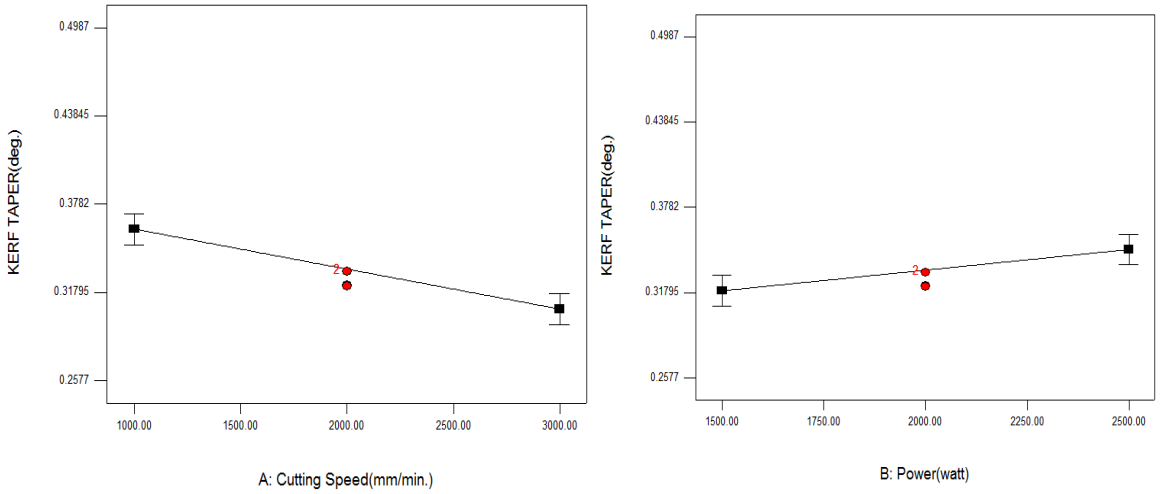

(a) **(b)**

Figure 5.17 Effect of cutting speed (a) and laser power (b) on kerf taper

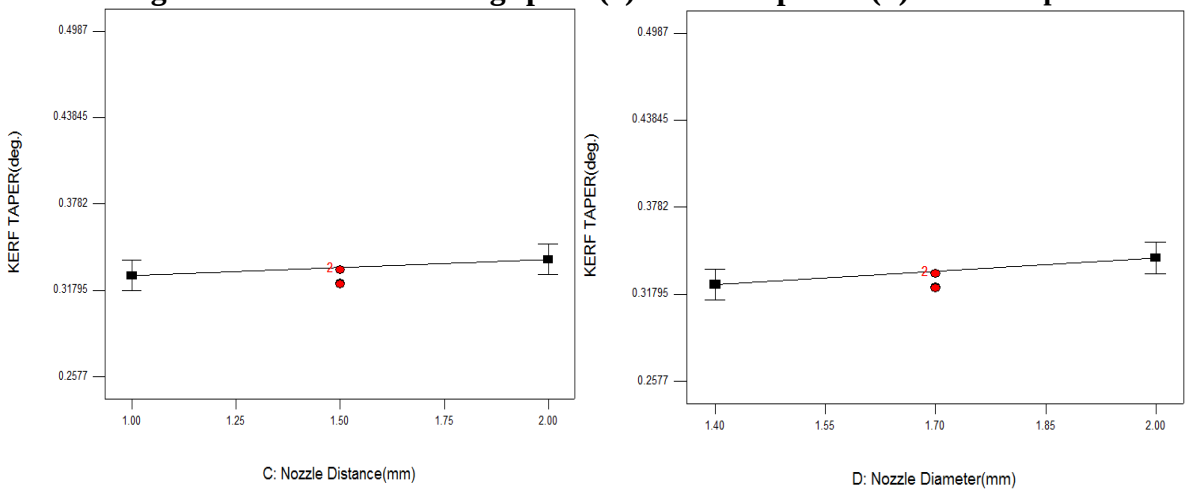

(a) **(b)**

Figure 5.18 Effect of nozzle distance (a) and nozzle diameter (b) on kerf taper

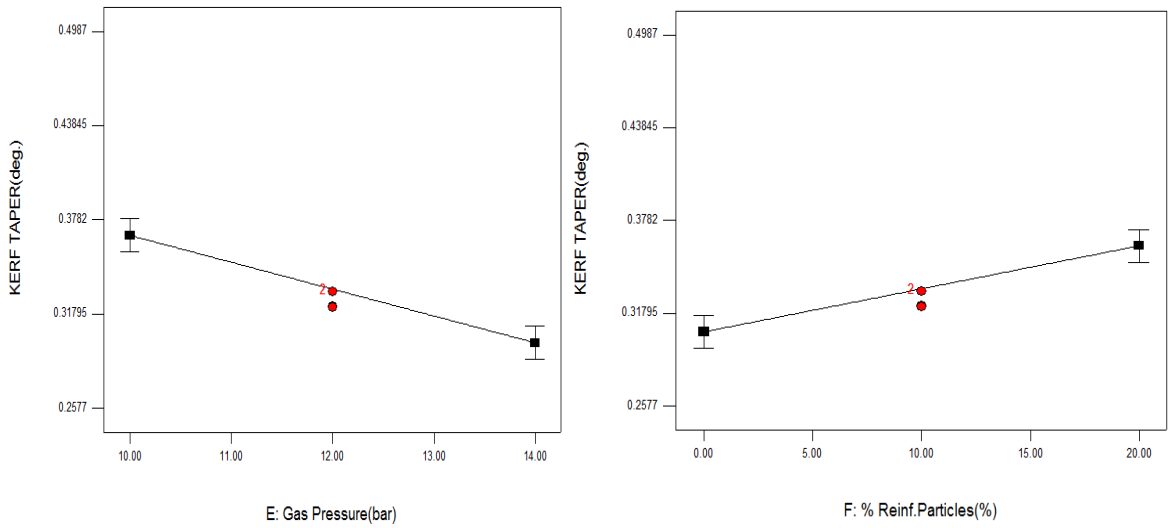

(a) **(b)**

Figure 5.19 Effect of gas pressure (a) and reinforced particles (b) on kerf taper

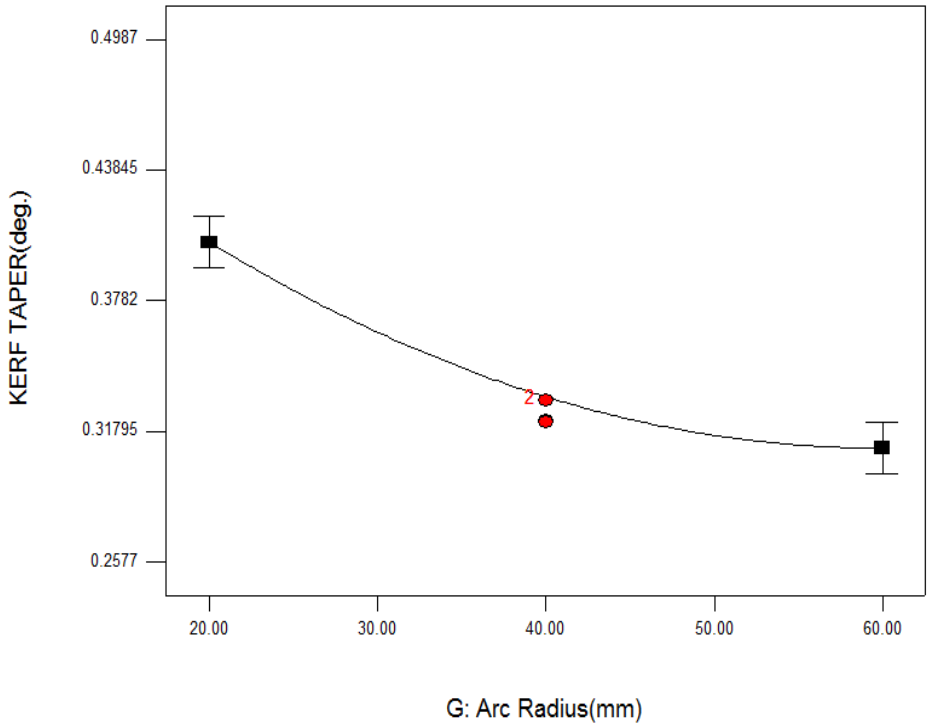

Figure 5.20 Effect of arc radius on kerf taper

From the figure 5.17, the effects of main process parameters have shown which predict the levels of control variables affecting the taper. The laser cutting speed has significant effect on kerf taper as shown in figure 5.17(a). When the cutting speed increased from 1000 to 3000 mm/min the kerf taper predicted with decreased value by 0.361 to 0.306

degree. The increase in cutting speed prevents the backward flow of molten material due to which the molten material does not make cluster in kerf zone.

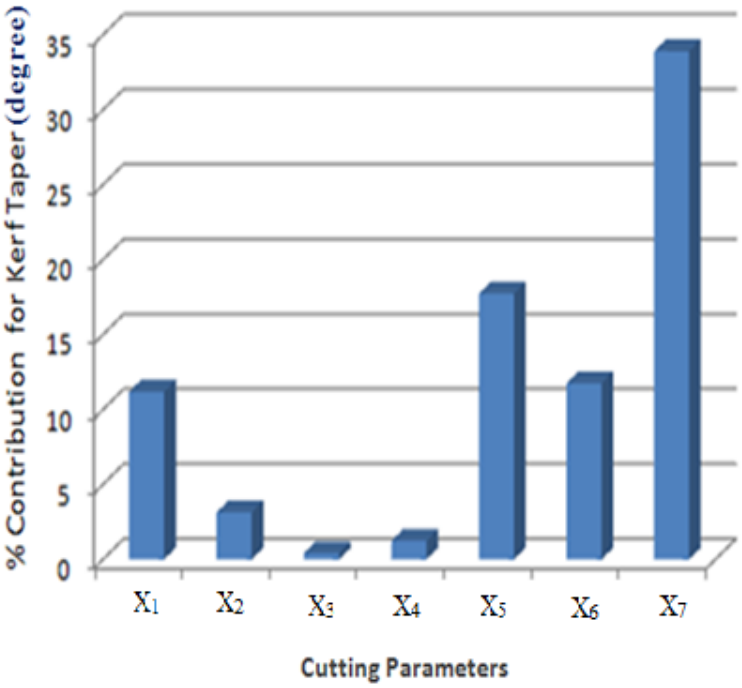

Figure 5.21 Percentage contributions of input parameters on kerf taper

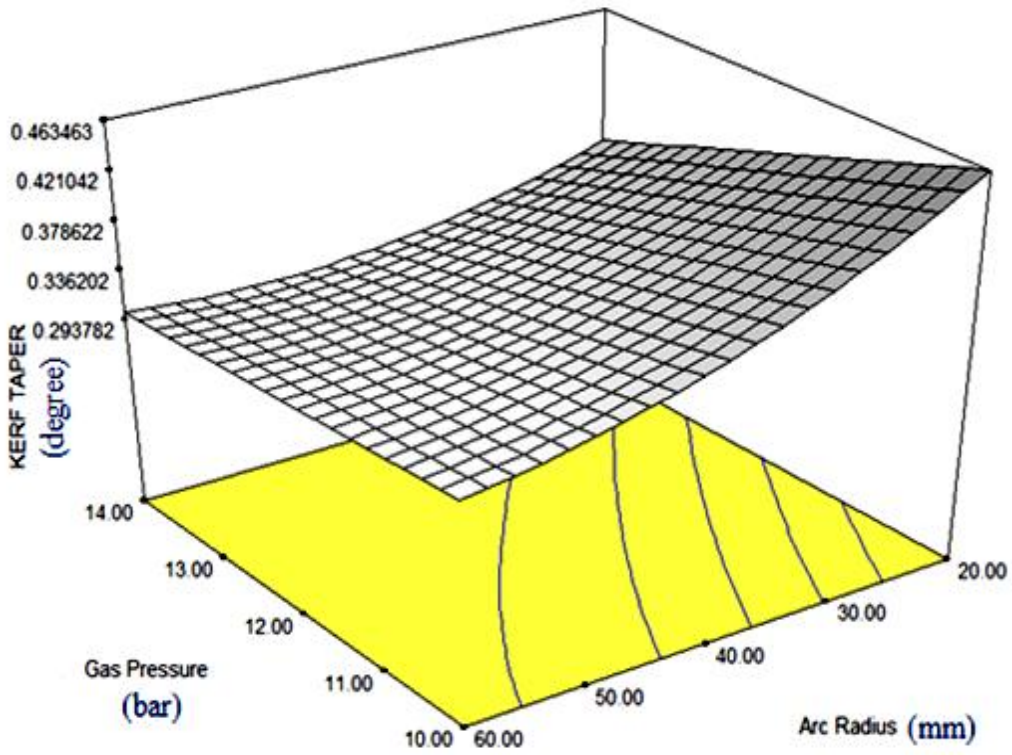

Figure 5.22 Interaction plot between gas pressure and arc radius for kerf taper

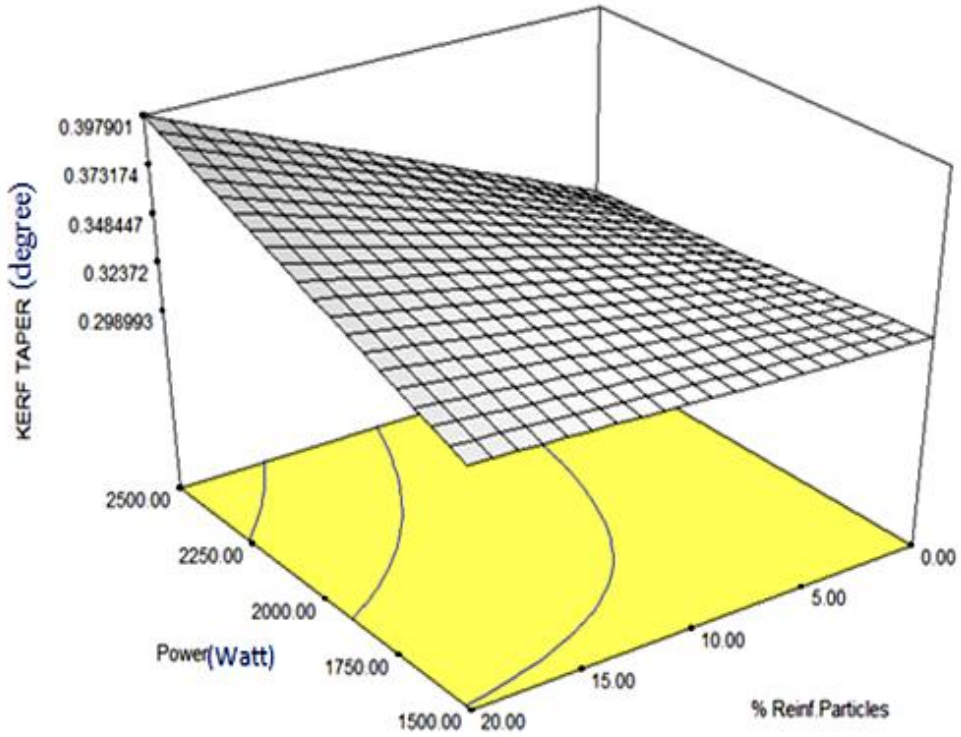

Figure 5.23 Interaction plot between laser power and reinforced particles for kerf taper

The laser power also had shown significant effect on kerf taper as shown in figure 5.17(b). For the lower laser power of 1500 watt the kerf taper predicted with less values whereas with the increase in laser power to 2500 watt the kerf taper increased to 0.348 degree. The nozzle stand-off distance and nozzle diameter have not shown significant values as shown in figure 5.18 (a). The linearity of the plots predicted that middle levels of both parameters can be selected for the kerf taper appropriate value. The nitrogen gas pressure has significant effect on kerf taper. It has been predicted that with the increase in gas pressure from 10 bar to 14 bar the kerf taper decreased from 0.368 to 0.299 degree as depicted in figure 5.19 (a). This may be attributed to the fact that low gas pressure remove the molten material from the upper surface easily but in lower surface oxidation process occurs which develop the oxide layer resulted into the higher kerf taper. The most significant parameter for the kerf taper is predicted as percentage SiC particles which shown decreased values of Kt from 0.361 to 0.305 degree. From figure 5.19 (b) it can be examined that with increase in percentage of SiC reinforced particles the kerf taper also increased to higher levels which may be caused due to temperature differences developed in between kerf zones resulted into large K_t value. The cut profile also had shown significant result for the kerf taper values as shown in figure 5.20. It was analysed that with the straight cut profiles has lower kerf taper values due to less accumulation of

molten material in the lower portion of kerf zone. From the plot it was explored that when the arc radius kept at 20 mm the kerf values increased to 0.405 degree which is reported as highest value of the process.

Figure 5.22 reflects the simultaneous effects of arc radius and gas pressure on kerf taper. From the plot it has been observed that kerf taper recorded as 0.320 deg. when the arc radius and gas pressure set at 60 mm and 10 bar respectively. Further it can be observed that when arc radius set at 60mm and gas pressure set to increase from 10 bar to 14 bar, kerf taper decreased from 0.320 deg. to 0.299 deg. respectively. Because molten material gets removed by the high gas pressure resulted into low difference between top and bottom kerf. The low gas pressure results in removing the molten material from top surface but lower surface is covered by oxide layer. The cut profile also decides the kerf taper value as in circular profile the expulsion of molten material becomes difficult (Sharma A et al.., 2013). Due to this, variation in top and bottom the kerf taper increases at various locations of cutting section. From figure 5.23, combined effects of SiC particles and laser power has been observed. It was found that kerf taper increased from 0.325 to 0.397 deg. with higher volume percentage of SiC particles and laser power. When the power is set at 1500 watt and reinforced particles quantity increased from 0 to 20 %, K_t values shows a significant rise. The high temperature in the middle kerf zone develop the liquid layer and hence reduces the size from the bottom edge resulted into large kerf taper (Yilbas B.S, 2008). The percentage contribution of different parameters is shown in figure 5.24 where arc radius, gas pressure, SiC reinforced particles and cutting speed are found to be prominent factors for the kerf taper.

5.3.3 Effect of laser input variables on surface roughness

Surface finish is considered as important quality parameter for laser machined specimens. Surface finish, striation formation and crack propagation are related to each other which define the surface roughness of machined surface. The higher inclinations of striation formation resulted into surface roughness of the machined surface. The normal probability plot of residuals for dross height is shown in figure 5.24. From the linearity of the graph, the adequacy of the model can be predicted. From the graph, it can be predicted that residuals are normally distributed and scattered nearby the straight line resulted into less errors as shown in plot. It can also be observed that predicted values resembles with observed response values which shows the adequacy of the model and

process parameters. The normal plot of residual values is shown in figure 5.24 which also shows the linearity of the model. The regression model shows combinations of main parameters and interaction of parameters for the Surface roughness. The regression equation is modeled in form of various combinations of input parameters as depicted in equation 5.4.

$$\textit{Surface roughness} = 9.935E-004 \times X_1 - 4.658E-004 \times X_2 + 2.630 \times X_3 - 1.448 \times X_4 + 0.584 \times X_5 - 0.101 \times X_6 - 0.098 \times X_7 + 3.493E\text{-}007 \times (X_1)^2 + 7.154E-004 \times (X_6)^2 - 6.750E\text{-}004 \times X_1 \times X_3 + 1.918E-004 \times X_1 \times X_5 + 3.087E\text{-}005 \times X_1 \times X_6 + 0.201 \times X_3 \times X_5 + 1.431E\text{-}003 \times X_6 \times X_7 \quad \ldots\ldots\ldots\ldots\ldots\ldots (5.4)$$

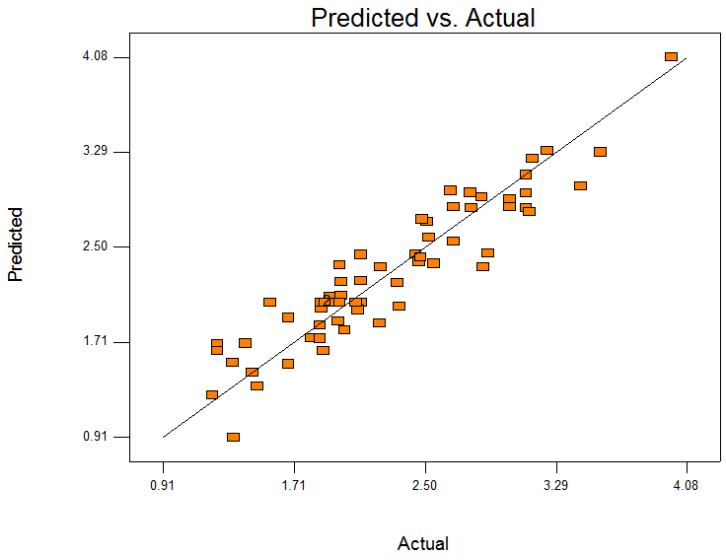

Figure 5.24 Plot of predicted versus actual for surface roughness

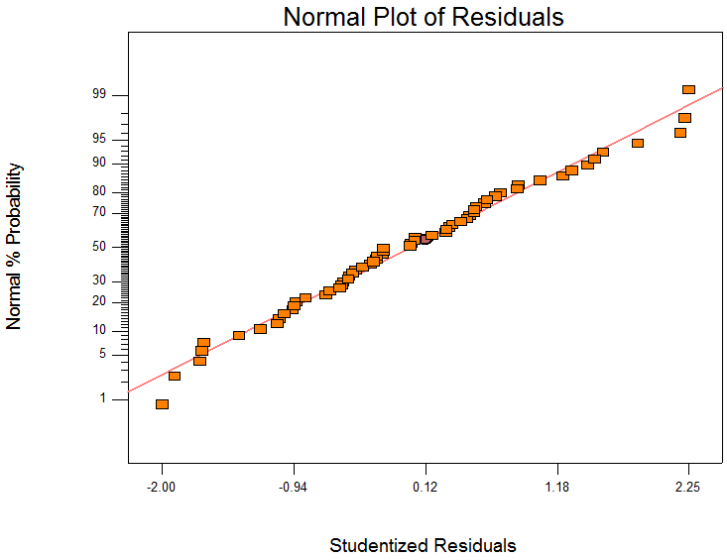

Figure 5.25 Normal probability plots of residuals for surface roughness

Table 5.11 ANOVA for response surface of reduced quadratic model of surface roughness

Source	Sum of Squares	Degrees of Freedom	Mean Square	F-Value	Prob. > F (p-value)	Remarks
Model	22.26	15	1.48	23.88	< 0.0001	Significant
X_1	5.02	1	5.02	80.81	< 0.0001	Significant
X_2	1.29	1	1.29	20.87	< 0.0001	Significant
X_3	0.27	1	0.27	4.46	0.040	Significant
X_4	0.02	1	0.02	0.33	0.563	Not-Significant
X_5	0.98	1	0.98	15.76	0.0002	Significant
X_6	0.84	1	0.84	13.51	0.0006	Significant
X_7	7.63	1	7.63	122.89	< 0.0001	Significant
X_1^2	1.95	1	1.95	31.45	< 0.0001	Significant
X_7^2	1.33	1	1.33	21.45	< 0.0001	Significant
X_1X_4	0.32	1	0.32	5.277	0.026	Significant
X_1X_5	1.17	1	1.17	18.95	< 0.0001	Significant
X_1X_6	0.55	1	0.55	8.95	0.004	Significant
X_1X_7	0.30	1	0.30	4.95	0.030	Significant
X_3X_5	0.32	1	0.32	5.21	0.027	Significant
X_6 X_7	0.46	1	0.46	7.49	0.008	Significant
Predicted R^2 0.886						

***Legend: X_1: Cutting speed, X_2:* Laser power , *X_3:* Nozzle stand-off distance , *X_4:* Nozzle diameter , *X_5:* Gas pressure , *X_6:* Percentage reinforced particles, *X_7:* Arc radius**

The analysis of variance has been performed to find the adequacy of the results as shown in table 5.11. From the ANOVA results the average variance of simultaneous conditions with respect to error variance can be analysed. The response surface methodology helps to determine the multiple response optimization with the help of Box-Behnken Design

method. The R-Squared value 0.886 is in well agreement with Adj R-Squared 0.849 whereas as lack of fit resulted into non- significant value of 0.564 which shows that the model is well defined. The F-value for arc radius and cutting speed is determined as 122.89 and 80.81 respectively. The highest F-values signify the most significant parameter. The low variation in arc radius and cutting speed deflects the large variation in the result. The lower F-value of stand-off distance and nozzle diameter signify about least significant parameters.

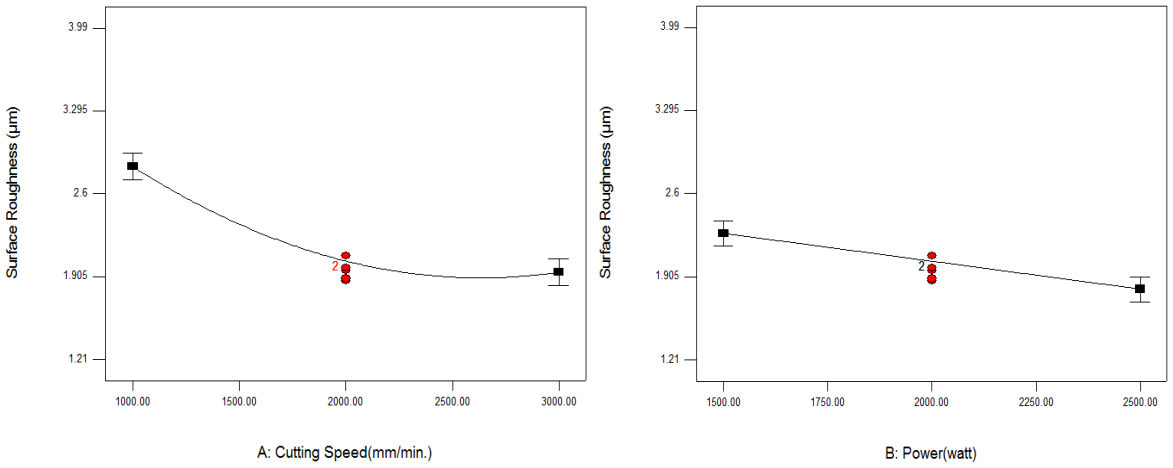

(a) **(b)**

Figure 5.26 Effect of cutting speed (a) and laser power (b) on surface roughness

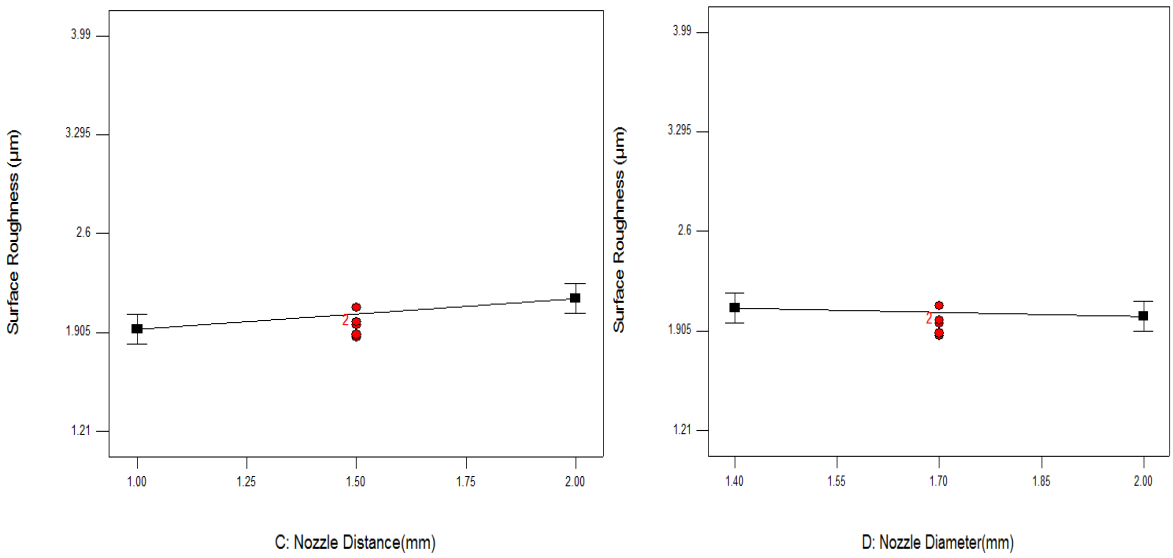

(a) **(b)**

Figure 5.27 Effect of nozzle distance (a) and nozzle diameter (b) on surface roughness

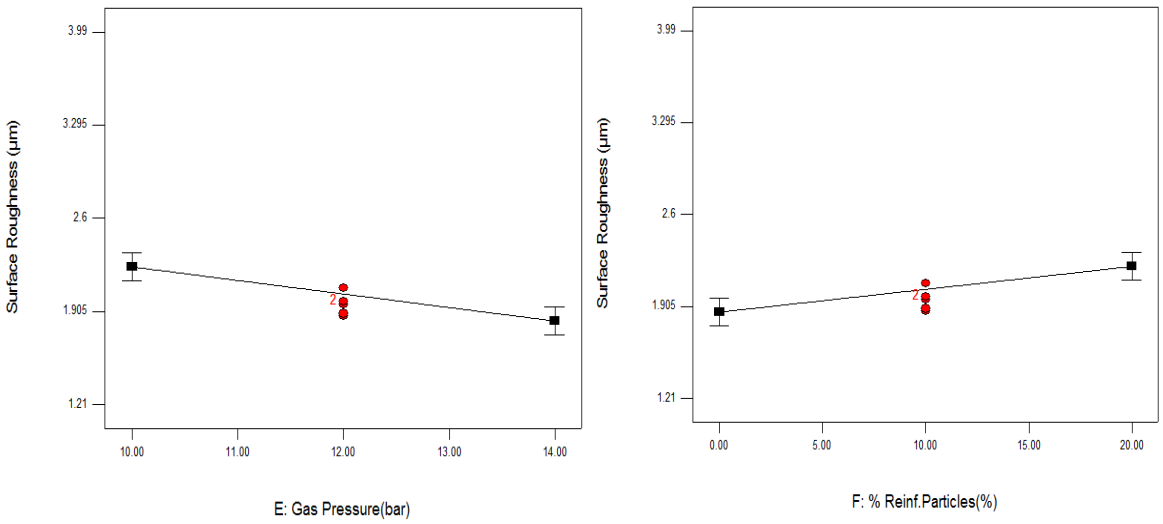

(a) **(b)**

Figure 5.28 Effect of gas pressure (a) and reinforced particles (b) on surface roughness

It was analyzed from the main plots that surface roughness is significantly affected by cutting speed, reinforced particles and arc radius. It has been observed that with increment in cutting speed from 1000 mm/min. to 3000 mm/min. the R_z value reduced to significant levels as shown in figure 5.26 (a). This mechanism of low roughness with increasing cutting speed also agreed with Dong et al.., 2009.

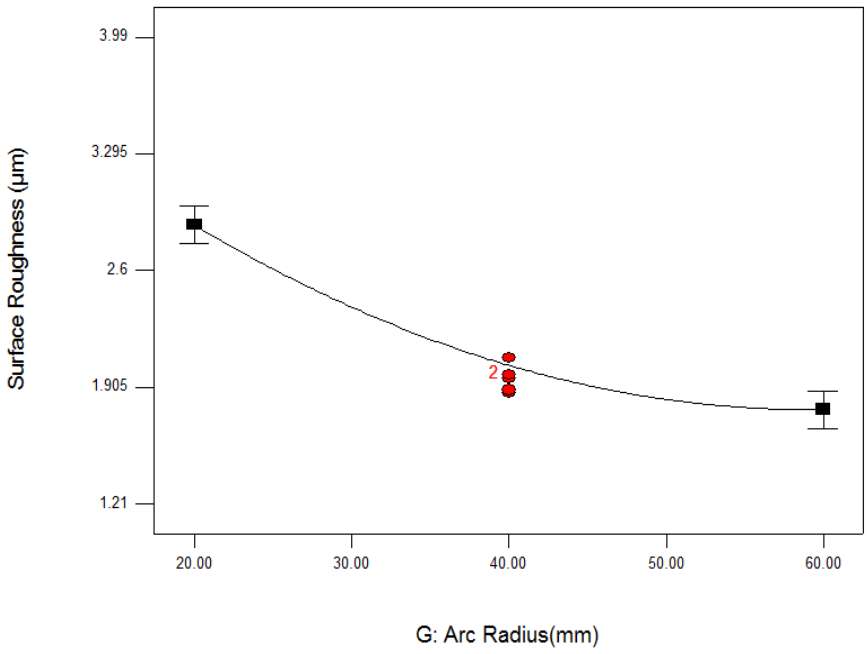

Figure 5.29 Effect of arc radius on surface roughness

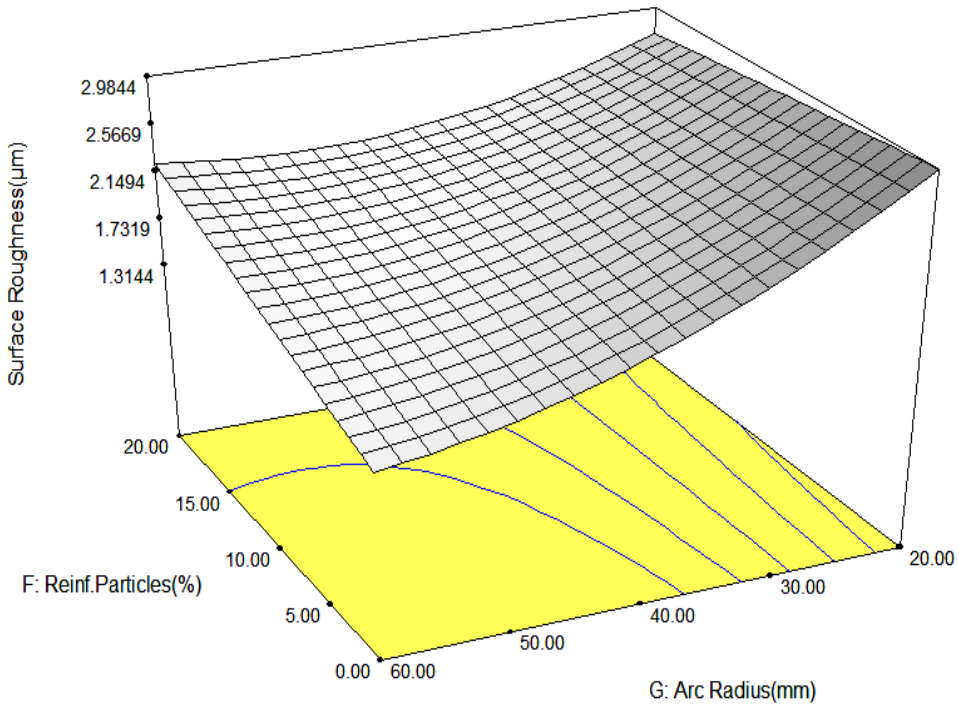

Figure 5.30 Interaction plot between arc radius and reinforced particles for surface roughness

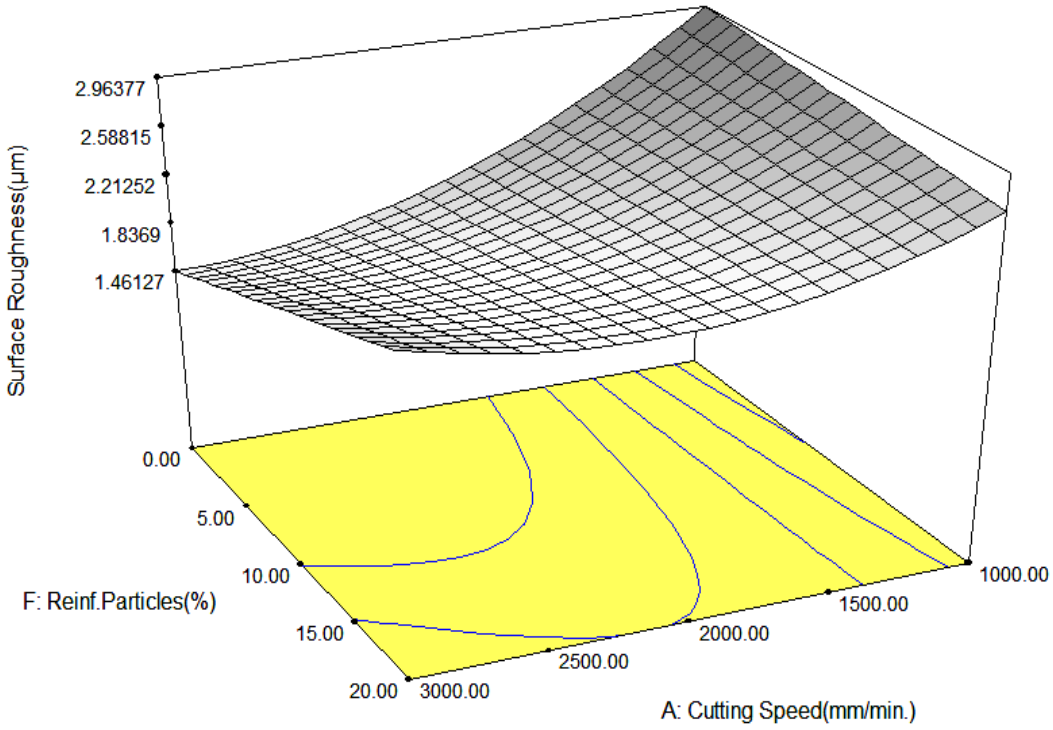

Figure 5.31 Interaction plot between cutting speed and reinforced particles for surface roughness

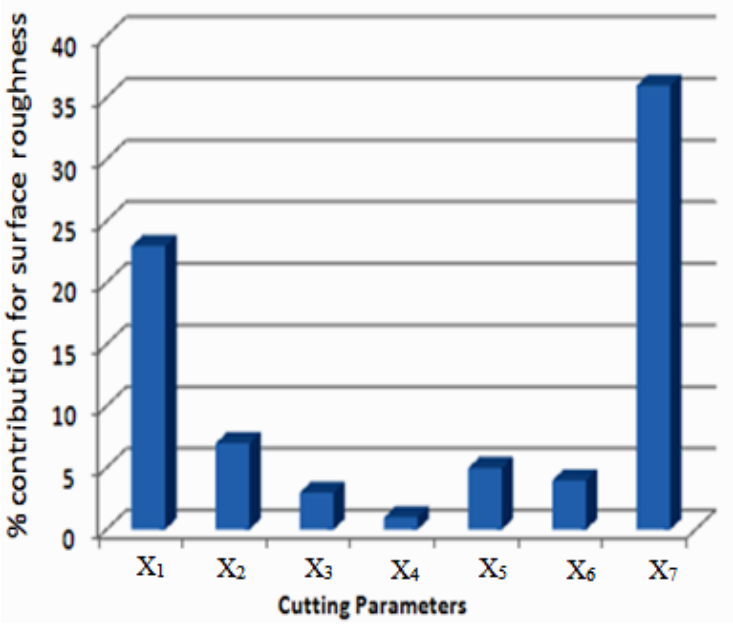

Figure 5.32 Percentage contribution of input parameters on surface roughness

Based on main effect plot, it was reported that as laser power increased from 1500 to 2500 watt the decrease in surface roughness noted to decrease by 2.26 to 1.80 µm. The probable reason for decrease in R_z value is that as sufficient energy is deported to cutting zone for clear cut with the increase in the laser power. The nozzle distance shown less effect on the increase in R_z value as shown in figure 5.27 (a). It has been predicted that higher nozzle distance develop more turbulence of the assist gas which scatters the molten material resulted into higher values of surface roughness.

The linearity of nozzle diameter plot predict about less effect on R_z values. The middle value of nozzle diameter can be selected for the process as lower and higher values have nearby same effects as shown in figure 5.27 (b). From the figure 5.28 (a) the effect of nitrogen gas pressure can be predicted where the plot having downward slope which shows that pressure has significant result on R_z values. With the increase in gas pressure from 10 to 14 bar the R_z value decreased from 2.23 to 1.83 µm. The mechanism of exothermic reactions play an important role in this process as higher gas pressure produces sufficient drag to molten material to expel from the kerf zone resulting into surface finish cut. The higher quantity of SiC reinforced particles (X_6) in specimen increases the roughness of the surface as depicted in the plot. Because presence of large quantity of ceramic particles modified the cutting front dynamics. The most significant factor for R_z value is cut profile arc radius. With decrease in arc radius upto20 mm the roughness of the surface increases dramatically as compare to 60 mm arc radius.

The interaction effect of arc radius and reinforced particles on surface roughness has been depicted in response plot figure 5.30. It has been examined that R_z value increases with higher quantity of reinforced particles. On the other hand the lower value of arc radius increased the R_z value. When the arc radius fixed at 60 mm and percentage reinforced particles increased from 0% to 20 %, the R_z also shown prominent rise in values. Moreover, when the reinforced particles quantity set at 0 % and arc radius reduced from 60 mm to 20 mm, the R_z value increased from 1.31 to 2.96 μm. Because ejection of molten material becomes difficult in more complex cut profile (i.e. arc radius 20 mm) than the less curvature cut profile. Due to this large number of striations develop on the surface which is responsible factor for high R_z values. Moreover, with increment in presence of unburned SiC particles raises the viscosity levels in the vicinity of the kerf zone. The combined effect of cutting speed and reinforced particles on R_z is shown in figure 5.31 where the input parameters X_2, X_3, X_4, X_5 and X_7 are kept at 2000 watt, 1.5 mm, 1.7 mm, 10 % and 40 mm respectively. From the response plot it can be examined that combination of lower cutting speed and higher reinforced particles exhibits higher values of surface roughness. With the decrement in cutting speed from 3000 mm/min. to 1000 mm/min. the R_z values observed with high variations from 1.4 μm to 2.56 μm. The change in percentage of reinforced particles from 0 to 20 % presents increment in R_z value. The non-reinforced specimen exhibits lower value of surface roughness. Because when the reinforced particles are small in quantity, it does not provide much obstacles to the flow of molten metal resulted into less striations pattern. A fewer striations ensued into controlled R_z value.

The percentage contribution bar graph shows that arc radius has maximum impact, whereas nozzle diameter and nozzle distance has least effect on surface roughness as displayed in figure 5.32. It has been analyzed that arc radius and laser cutting speed has highest significant contribution on surface roughness. The least significant parameters for the surface roughness has been examined as nozzle diameter and nozzle stand- off distance. It has been analyzed previously that arc radius and cutting speed is one of the most influencing factors for all output responses.

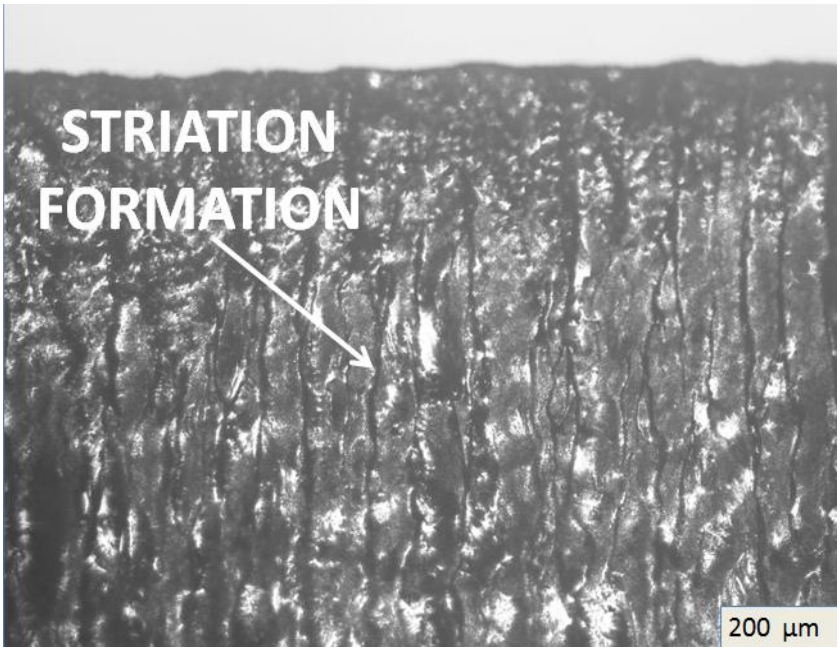

Figure 5.33 Optical microscopic (50 ×) of surface roughness at X_1: 1000 mm/min, X_2 : 2000 watt, X_6: 20%, X_7: 20 mm

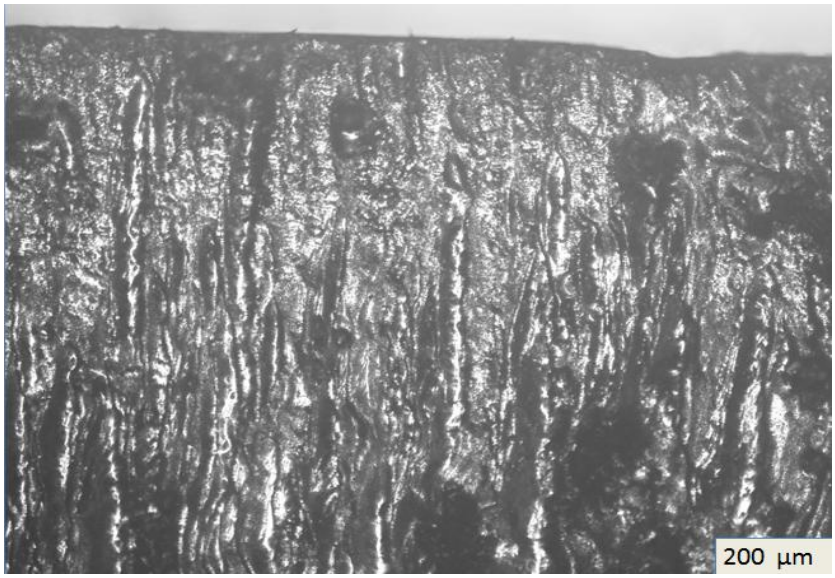

Figure 5.34 Optical microscopic (50 ×) of surface roughness X_1: 1000 mm/min, X_2: 1500 watt, X_6: 10%, X_7: 40 mm

Figure 5.33-5.36 exhibits the surface roughness of various selected specimens. It has been observed previously in detail that surface roughness and striation formation are related to each other. Whenever striation formation is higher in nature, the surface roughness also increases in that proportion. The surface roughness increased when the lower values of cutting speed and arc radius were maintained. Furthermore, the increment in the values of laser power and gas pressure reduced the R_z values.

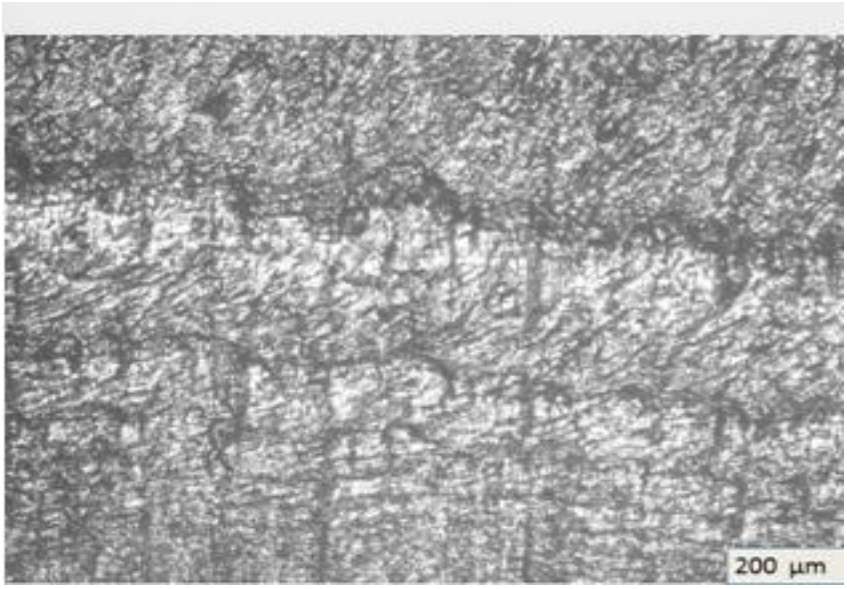

Figure 5.35 Optical microscopic (50 ×) of surface roughness at X_1: 3000 mm/min, X_2: 2000 watt, X_6: 10%, X_7: 40 mm

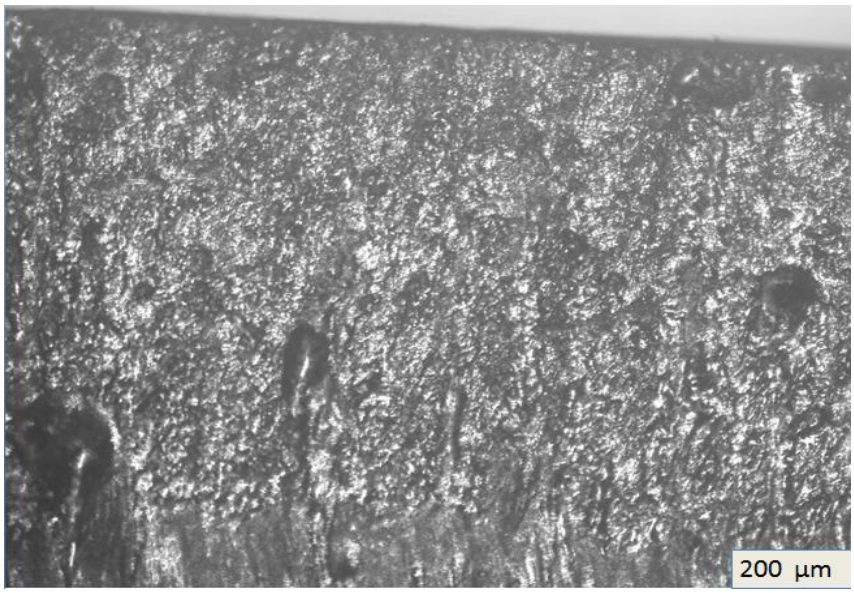

Figure 5.36 Optical microscopic (50 ×) of surface roughness at X_1: 3000 mm/min, X_2: 2000 watt, X_6: 0%, X_7: 60 mm

The higher quantity and unburned behavior of SiC reinforced particles influenced the roughness of the surface. From figure 5.33, it can be explored that value of R_z: 3.56 µm reached when cutting speed, arc radius and reinforced particles were maintained at 1000 mm/min, 20 mm and 20 % respectively. The reduced R_z value upto 3.16 µm were observed when the machining conditions were changed with arc radius and reinforced particles at 40 mm and 10 % respectively as shown in 5.34. The surface roughness tests of the surfaces as shown in figure 5.35-5.36 depicted large variation in result as compared to surface shown in figure 5.33. There was dramatically change in R_z value (1.34 µm) when

the cutting speed, arc radius and reinforced particles were set at 3000 mm/min, 60 mm and 0 %. From the above roughness test results it is clear that higher value of cutting speed and arc radius whereas lower values of reinforced particles influenced surface roughness to large extent.

5.3.4 Effect of laser input variables on kerf deviation

Kerf deviation occurs due to variation of various input laser cutting parameters. For achieving consistent kerf width it is very important to have proper selection of laser operating parameters. In case of laser cutting the possibilities of unevenness in kerf width may also increase due to thermal process. It has been observed previously that chances of kerf deviation may be due to the material properties like reflectivity which as in case of aluminium and its alloys. In this study, it was interested to examine about the kerf deviation for the laser curve cutting of aluminum alloy metal matrix composite. The normal probability plot of residuals for kerf deviation is shown in figure 5.37. From the linearity of the graph, the adequacy of the model can be predicted. From the graph, it can be predicted that residuals are normally distributed and scattered nearby the straight line resulted into less errors as shown in plot. It can also be observed that predicted values resembles with observed response values which shows the adequacy of the model and process parameters. The normal plots of residual values are shown in figure 5.38 which also shows the linearity of the model. The regression equation for the kerf deviation is formulated using RSM by using various values of input parameters as shown in equation 5.4.

$$\textit{Kerf Deviation (mm)} = 1.771 - 3.35E-004 \times X_1 - 5.227E-004 \times X_2 - 0.029 \times X_3 - 1.105 \times X_4 + 0.0166 \times X_5 - 8.959E\text{-}003 \times X_6 - 2.723E\text{-}003 \times X_7 + 2.832E\text{-}008 \times (X_1)^2 + 1.023E\text{-}007 \times (X_2)^2 + 0.2916 \times (X_4)^2 + 1.457E\text{-}004 \times (X_6)^2 + 5.269E\text{-}005 \times (X_7)^2 + 7.125E-008 \times X_1 \times X_2 + 5.291E\text{-}005 \times X_1 \times X_4 - 1.187E\text{-}006 \times X_1 \times X_7 - 8.812E\text{-}004 \times X_5 \times X_6 \quad \text{.....(5.5)}$$

The analysis of variance has been performed to analyze the R-square and approximate R-square value which signify the adequacy of the model. All the values related to significant and non-significant parameter are tabulated in table 5.12. The R-square value for K_d is 0.901 which is in good agreement with approximate R-square value of 0.891. The F-value of 82.006 is recorded as highest value of cutting speed within all parameters. The nozzle diameter is considered as non-significant parameters on the basis of lowest F-value of

0.007. The higher cutting speed of 3000 mm/min. is considered to develop lower values of quality characteristics in terms of kerf width and surface roughness values.

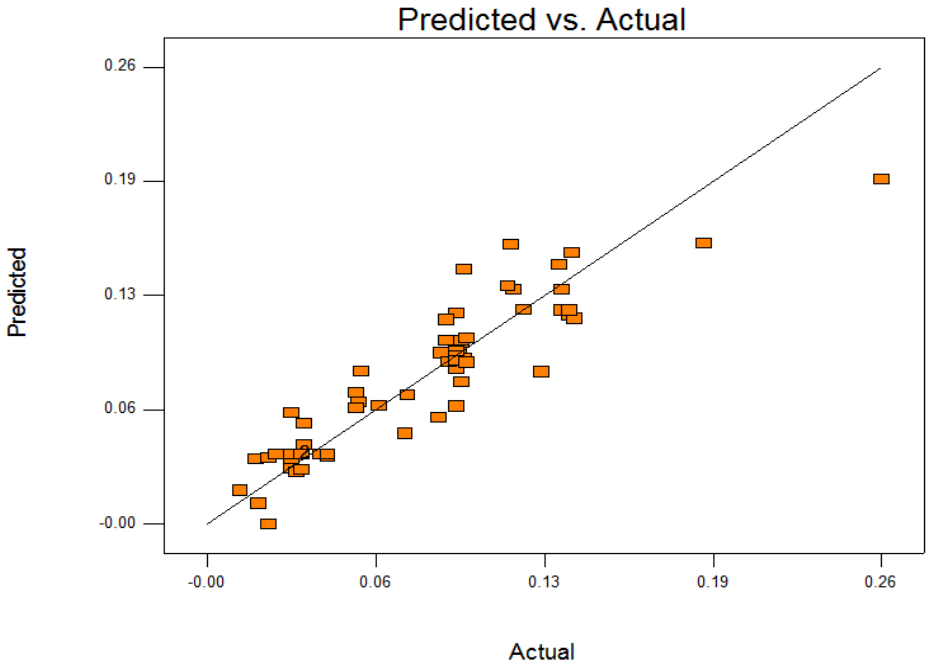

Figure 5.37 Plot of predicted versus actual for kerf deviation

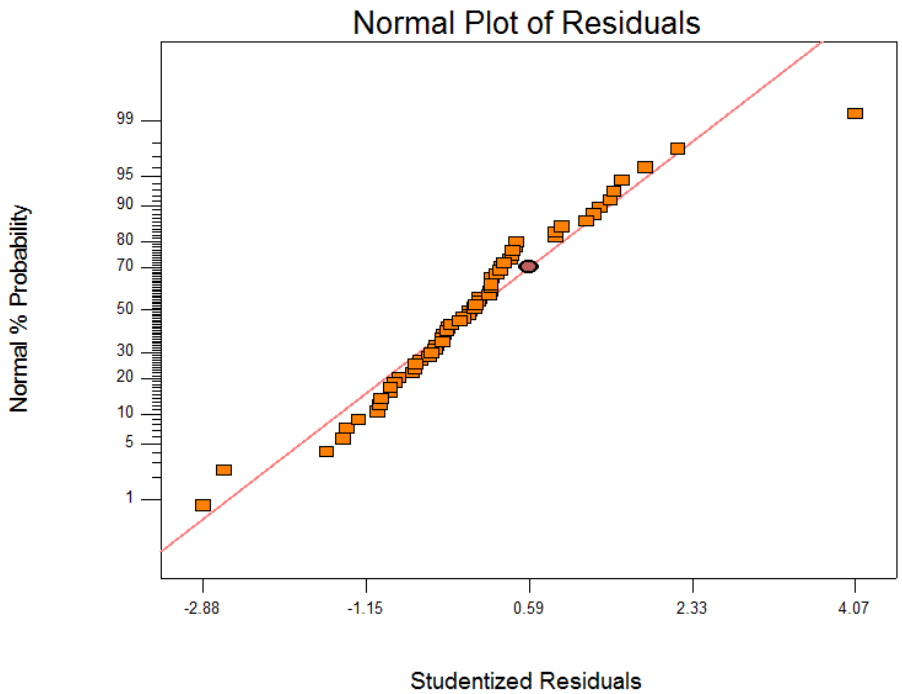

Figure 5.38 Normal probability plots of residuals for kerf deviation

Table 5.12 ANOVA for response surface of reduced quadratic model of kerf deviation

Source	Sum of Squares	Degrees of Freedom	Mean Square	F-Value	Prob. > F (p-value)	Remarks
Model	0.0976	15	0.0065	17.486	< 0.0001	Significant
X_1	0.0305	1	0.0305	82.006	< 0.0001	Significant
X_2	0.0069	1	0.0069	18.630	< 0.0001	Significant
X_3	0.0054	1	0.0054	14.585	0.0004	Significant
X_4	0.0002	1	0.0002	0.0071	0.9329	Not-Significant
X_5	0.0059	1	0.0059	15.906	0.0002	Significant
X_6	0.0037	1	0.0037	10.005	0.0028	Significant
X_7	0.0078	1	0.0078	21.177	< 0.0001	Significant
X_1^2	0.0087	1	0.0087	23.433	< 0.0001	Significant
X_3^2	0.0074	1	0.0074	20.034	< 0.0001	Significant
X_4^2	0.0078	1	0.0078	21.137	< 0.0001	Significant
X_6^2	0.0065	1	0.0065	17.608	0.0001	Significant
X_1X_3	0.0063	1	0.0063	16.997	0.0002	Significant
X_1X_6	0.0050	1	0.0050	13.564	0.0006	Significant
X_5X_6	0.0025	1	0.0025	6.865	0.0119	Significant
Predicted R^2 0.901						

***Legend: X_1: Cutting speed, X_2:* Laser power , *X_3:* Nozzle stand-off distance , *X_4:* Nozzle diameter , *X_5:* Gas pressure , *X_6:* Percentage reinforced particles, *X_7:* Arc radius**

It was analyzed from the main plots that kerf deviation is significantly affected by laser cutting speed, nozzle distance and arc radius. The laser cutting speed proved to be most significant process parameter as analyzed by the plot values. From the figure 5.39 (a) the slope of the curve can be analysed which shows that with the increase in cutting speed from 1000 to 3000 mm/min, K_d value decreased by by 0.103 to 0.028 mm. The effect of laser power on K_d also has considerable effect as shown in the main effect plot in figure 5.39 (b). It was analysed that as laser power increased from 1500 to 2500 watt the decrease in K_d value noted to decreased by 0.0781 to 0.0481 mm. The reason for this phenomenon may be the sufficient amount of energy in kerf zone which resulted into

constant kerf width zone during the cut. The lower values of nozzle distance raised the kerf deviation value to higher levels. From the figure 5.40 (a) it can be explored that with the increase in nozzle stand-off distance from 1.0 to 2.0 mm the Kd value decreased by 0.0529 to 0.0231 mm. The probable reason for this may be the lower focussing of laser beam on the target zone. Due to which it deviates the laser beam to cut for the particular profile and thus resulted into higher kerf deviation value. Figure 5.40 (b) shows that middle values of nozzle diameter proved to significant for the lower values of kerf deviation. From the figure 5.41 (a, b) the plot curve shows the same trend. It has been analysed that with increase in gas pressure and percentage SiC reinforced particles, the kerf deviation predicted with higher values. With the arc radius of 20 mm, the kerf deviated with higher values due to curved nature of cut profile the molten material trap in the kerf zone.

The Kerf deviation can be evaluated by having a difference between maximum and minimum kerf width values. The following equation has been used to find out the various values.

$$K_d = K_w\,(\text{maximum}) - K_w\,(\text{minimum}) \qquad \ldots\ldots\ldots\ldots\ldots\ldots (5.6)$$

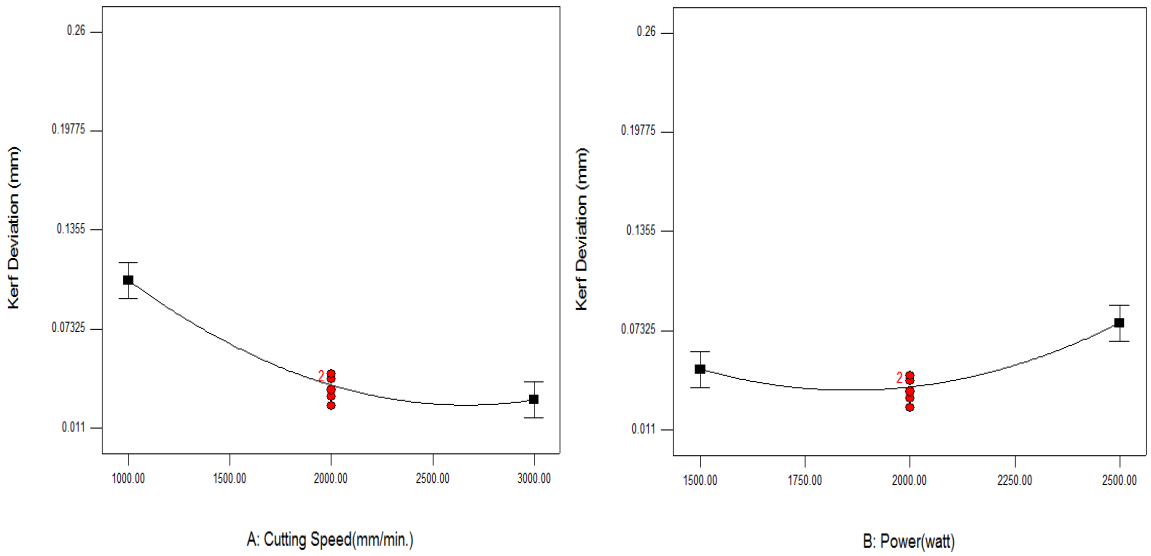

(a) **(b)**

Figure 5.39 Effect of cutting speed (a) and laser power (b) on kerf deviation

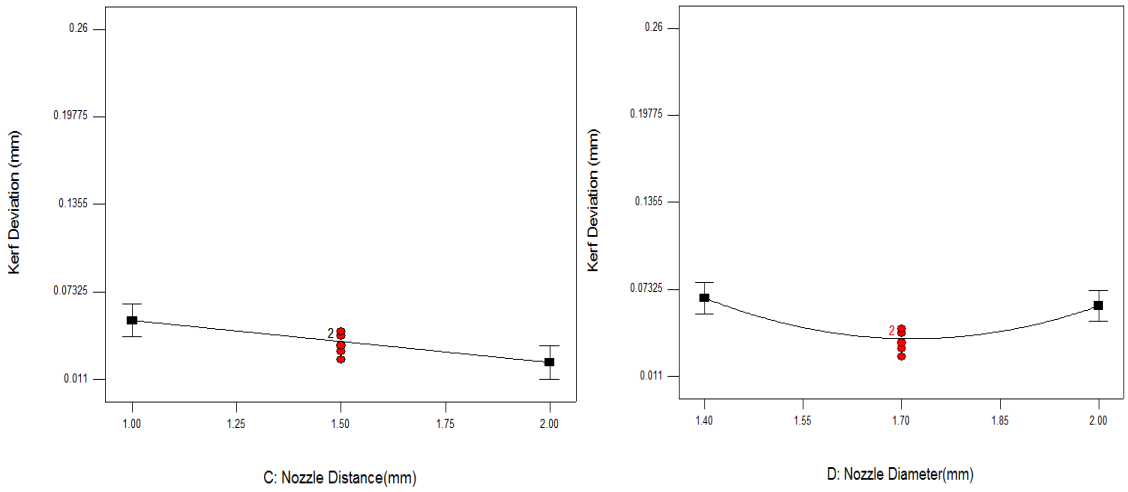

(a) **(b)**

Figure 5.40 Effect of nozzle distance (c) and nozzle diameter (d) on kerf deviation

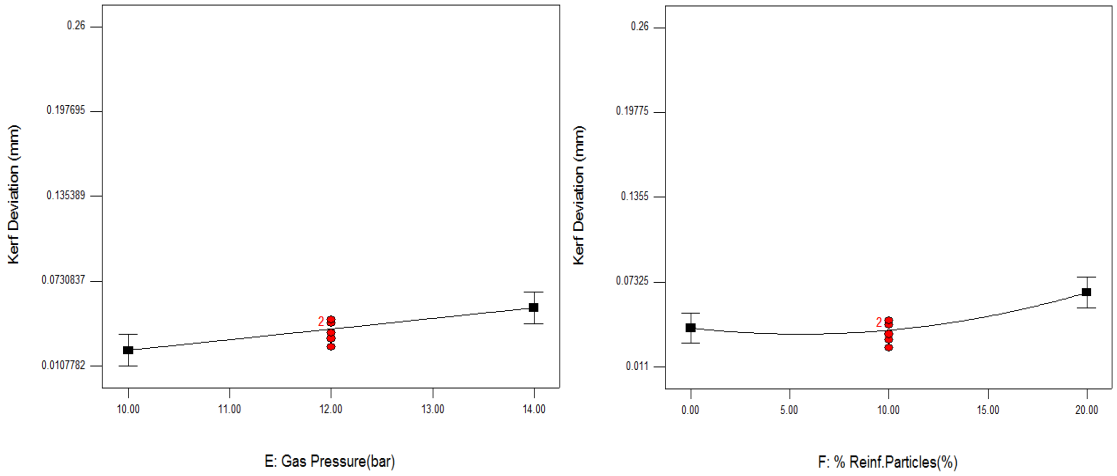

(a) **(b)**

Figure 5.41 Effect of gas pressure (a) and reinforced particles (b) on kerf deviation

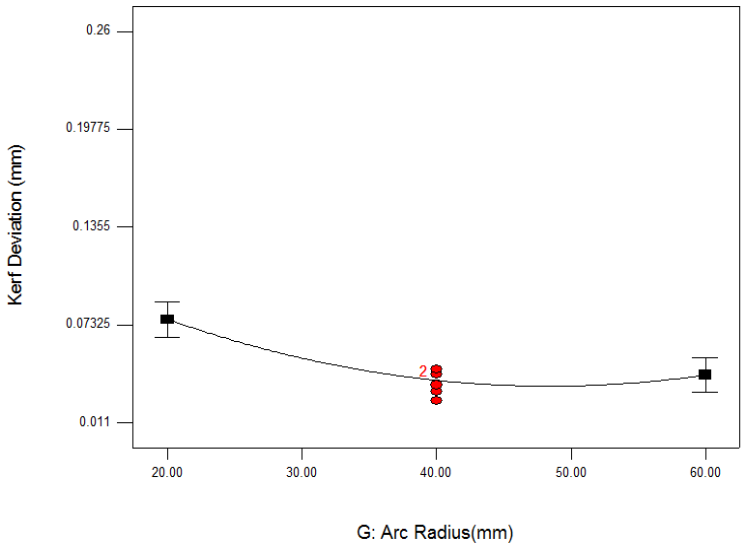

Figure 5.42 Effect of arc radius on kerf deviation

The effect of reinforced particles and gas pressure on K_d have been depicted simultaneously in figure 5.43 for constant values of X_1, X_2, X_3, X_4, and at 2000 mm/min., 2000 watt, 1.5mm,1.7 mm and 40 mm respectively. From the response plot it has been examined that combination of lower value of reinforced particles and gas pressure is suitable for low K_d value. When the gas pressure set at 10 bar for higher values of reinforced particles quantity, the slope of K_d curve increased dramatically. Because the reinforced particles had high melting temperature which remain in unburned stage during laser cutting process. On the other hand, the higher quantity of reinforced particles reduces the penetration of laser beam and heats the top surface area. Due to high pressure large portion of the molten material move out but remaining molten material resolidified resulting into unevenness. Figure 5.44 exhibits the combined effect of cutting speed and laser power on kerf deviation. It has been observed that when the laser power set at 1500 watt and cutting speed decreased from 3000 mm/min to 1500 mm/min, K_d value examined with high deviation of 0.15 mm. This may be attributed to high interaction time between specimen and laser beam. Moreover, the circular or complex cut profile also responsible for large K_d value as ejection of molten material becomes difficult in the random location of kerf zone. The laser power determines the energy input levels inside the kerf zone.

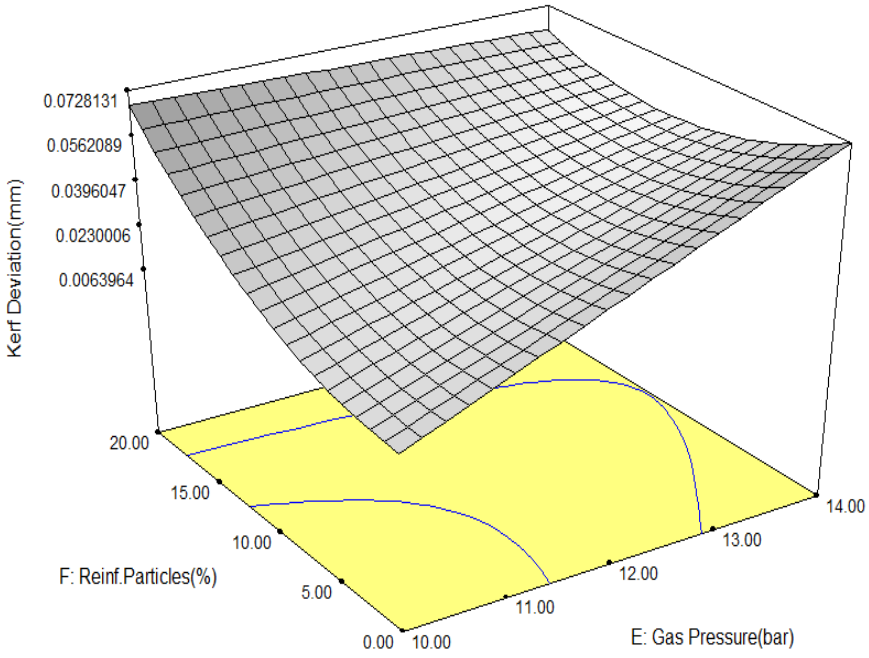

Figure 5.43 Interaction plot between gas pressure and reinforced particles for kerf deviation

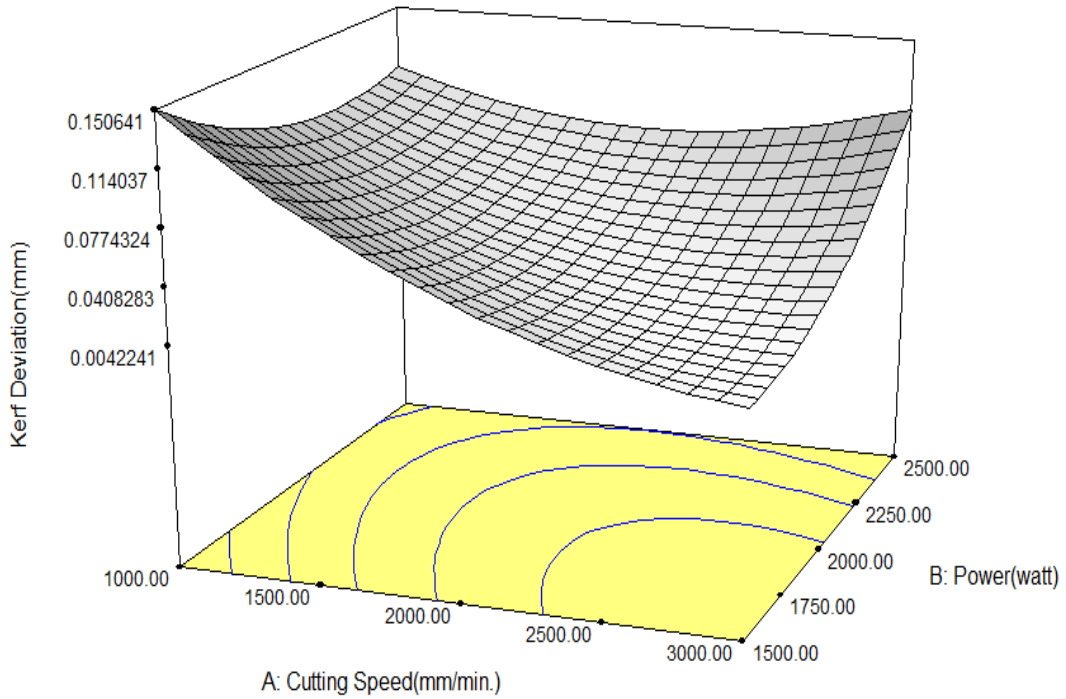

Figure 5.44 Interaction plot between laser power and cutting speed for kerf deviation

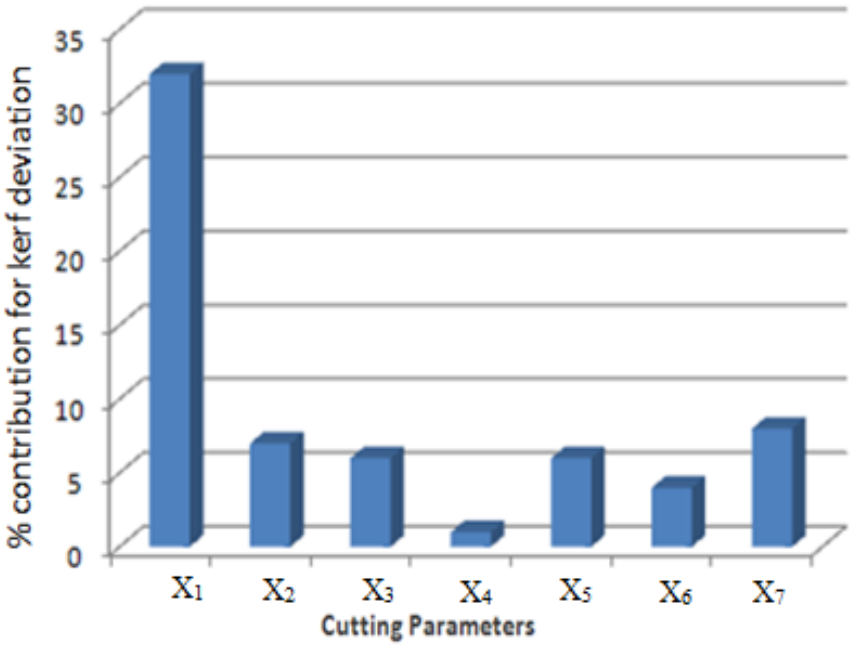

Figure 5.45 Percentage contribution of input parameters on kerf deviation

However, the intensity of absorption of the surface may also depends upon many factors mainly are laser pulse energy, material thickness, laser absorptivity and laser spot diameter etc. The variation of all these factors may vary the process results in large extent. The focal diameter of laser beam was kept on surface of the specimen. The

attainable value of focused diameter was 0.32 mm by using a lens of focal length of 120 mm. Figure 5.45 shows the bar graph of percentage contribution of input parameters on kerf deviation where the most significant effect has been examined for cutting speed.

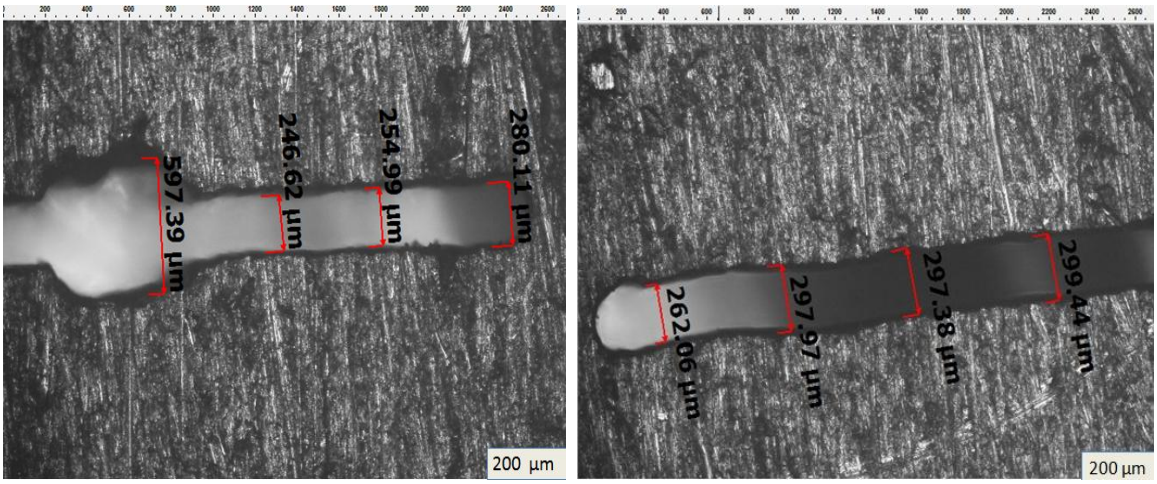

(a) **(b)**

Figure 5.46 Optical micrographs (50 ×) for kerf deviation: (a) at X_1: 1000mm/min., X_2: 1500 watt, X_3: 1.5 mm, X_4: 1.4 mm, X_5: 12 bar, X_6: 10%, X_7: 40 mm; (b) at X_1: 3000 mm/min, X_2: 2000 watt, X_3: 2.0 mm, X_4: 1.7 mm, X_5: 10 bar, X_6: 10%, X_7: 40 mm

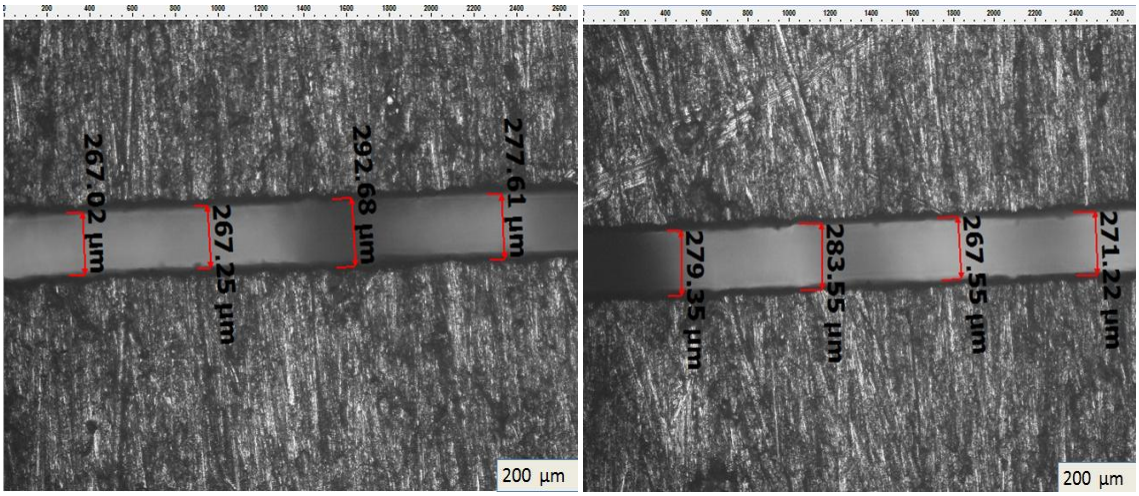

(a) **(b)**

Figure 5.47 Optical micrographs (50 ×) for kerf deviation: (a) at X_1: 3000 mm/min., X_2: 2000 watt, X_3: 1.5 mm, X_4: 1.7mm, X_5: 12 bar, X_6: 0%, X_7: 60 mm; (b) at X_1: 3000 mm/min., X_2: 1500 watt, X_3: 1.5 mm, X_4: 1.4 mm, X_5: 12 bar, X_6: 0%, X_7: 60 mm

Figure 5.46 exhibits the microscopic images of unevenness in kerf. The kerf deviation was calculated according to variation in K_w values. From figure 5.46 (a-b), it has been observed that value of K_d attained at 0.351 µm when the input parameters were set at cutting speed: 1000mm/min., power: 1500 watt, stand-off distance: 1.5 mm, nozzle diameter: 1.4mm, gas pressure: 12 bar, reinforced particles: 10%, arc radius: 40 mm. The value of K_d changed dramatically with a value of 0.037 mm when the input conditions changed at cutting speed: 3000 mm/min., power: 2000 watt, stand-off distance: 2.0 mm, nozzle diameter: 1.7 mm, gas pressure: 10 bar, reinforced particles: 10%, arc radius: 40 mm. The kerf unevenness was observed with less value (K_d: 0.025 mm) when the cutting conditions were set at cutting speed: 3000 mm/min., power: 1500 watt, reinforced particles: 0 %, arc radius: 60 mm. Moreover, the unevenness in kerf decreased upto 0.016 mm when machining conditions changed at cutting speed: 3000 mm/min, power: 1500 watt reinforced particles: 0 %, arc radius: 60 mm as shown in figure 5.47. From above results it can be easily predicted that when the cutting speed raised from higher to lower level the kerf deviation exhibits reverse values. When the laser cutting speed of 1000 mm/min was attained, the interaction time between specimen and laser beam increases due to this high exothermic reaction takes place. With increment in reinforced particles from 0 to 20 % and decrease in arc radius from 60 mm to 20 mm, the unevenness in kerf increased which resulted into large kerf deviation.

5.3.5 Effect of laser input variables on heat affected zone width

Laser cutting is considered as thermal process due to which microstructure of machined surface develop the variation in physical properties. The heat affected zone is one of the most undesirable factors when the process is thermal in nature. Due to the occurrence of oxidation process, the oxide layer solidifies around the cut edge. The width of the oxide layer depends upon various input laser parameters.

The normal probability plot of residuals for dross height is shown in figure 5.48. From the linearity of the graph, the adequacy of the model can be predicted. From the graph, it can be predicted that residuals are normally distributed and scattered nearby the straight line resulted into less errors as shown in plot. It can also be observed that predicted values resembles with observed response values which shows the adequacy of the model and process parameters. The normal plots of residual values are shown in figure 5.49 which

also shows the linearity of the model. The regression model for heat affected zone width is shown in equation 5.7.

$$HAZ\ Width\ (\mu m) = 2250.39 + 0.227\times X_1 - 0.725 \times X_2 + 114.023\times X_3 - 860.740\times X_4 - 79.979\times X_5 - 16.603 \times X_6 - 21.044\times X_7 + 1.347E-004\times (X_1)^2 + 1.023E-007\times (X_2)^2 + 0.0797\times (X_7)^2 + 0.0226\times (X_6)^2 + 6.455E-003\times X_2 \times X_7 - 8.958\times X_3 \times X_6 + 67.524 \times X_3 \times X_5 \quad \text{.....(5.7)}$$

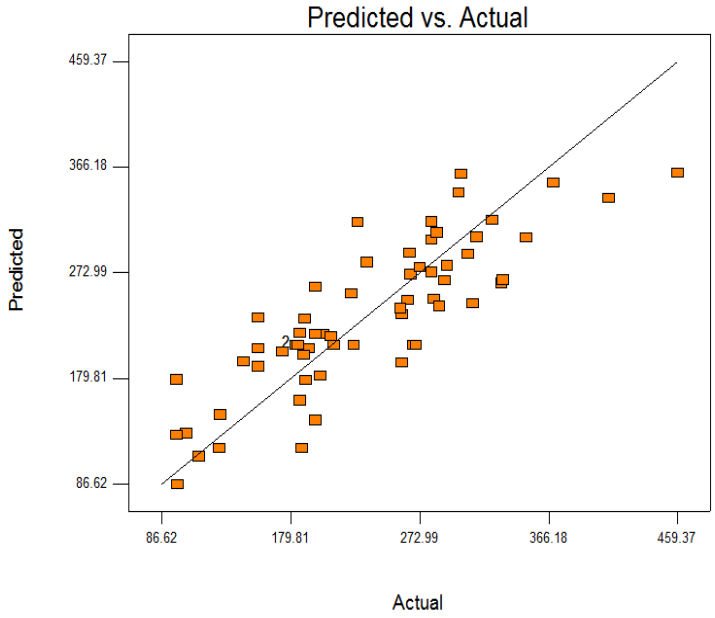

Figure 5.48 Plot of predicted versus actual for heat affected zone width

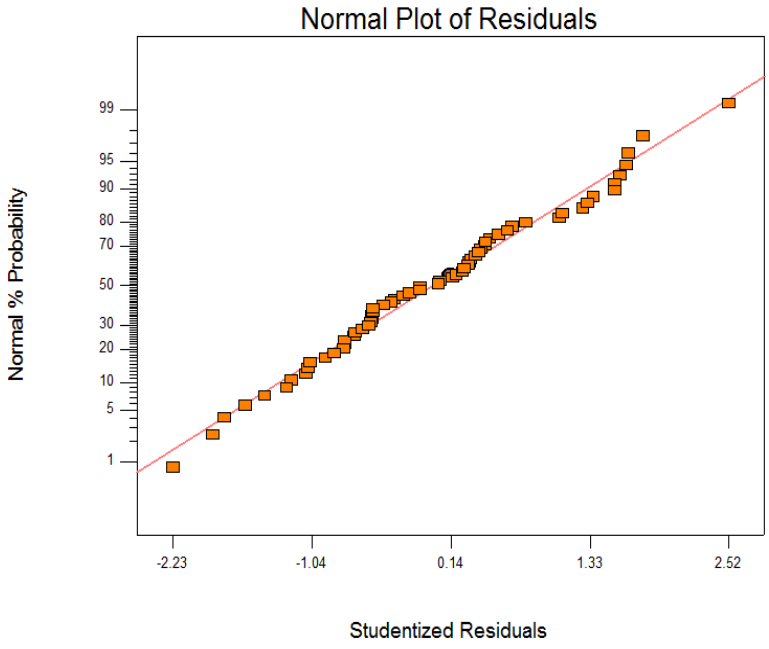

Figure 5.49 Normal probability plots of residuals for heat affected zone width

Table 5.13 ANOVA for response surface of reduced quadratic model of HAZ width

Source	Sum of Squares	Degrees of Freedom	Mean Square	F-Value	Prob. > F (p-value)	Remarks
Model	259072.7	13	19928.67	8.871	< 0.0001	Significant
X_1	47160.73	1	47160.73	20.993	< 0.0001	Significant
X_2	30878.93	1	30878.93	13.746	0.0005	Significant
X_3	3584.425	1	3584.425	1.595	0.1226	Significant
X_4	5496.449	1	5496.449	2.446	0.1243	Significant
X_5	10476.39	1	10476.39	4.663	0.0358	Significant
X_6	24064.95	1	24064.95	10.712	0.0020	Significant
X_7	29639.92	1	29639.92	13.194	0.0007	Significant
X_2^2	16553.61	1	16553.61	7.368	0.0092	Significant
X_7^2	14838.59	1	14838.59	6.605	0.0133	Significant
X_1X_5	16386.58	1	16386.58	7.294	0.0095	Significant
X_2X_7	33338.39	1	33338.39	14.840	0.0003	Significant
X_3X_6	16049.59	1	16049.59	7.144	0.0102	Significant
X_4X_5	13131.59	1	13131.59	5.845	0.0195	Significant
Predicted R^2 0.911						

***Legend: X_1: Cutting speed, X_2:* Laser power , *X_3:* Nozzle stand-off distance , *X_4:* Nozzle diameter , *X_5:* Gas pressure , *X_6:* Percentage reinforced particles, *X_7:* Arc radius**

The analysis of variance performed on various process parameters as shown in table 5.13 to identify the significant and non significant parameters for heat affected zone width. From the table Adjusted R^2 value of 0.935 found which is examined to be approximate closed value of Predicted R^2: 0.911. The predicted most significant parameters found are cutting speed, laser power and reinforced particles.

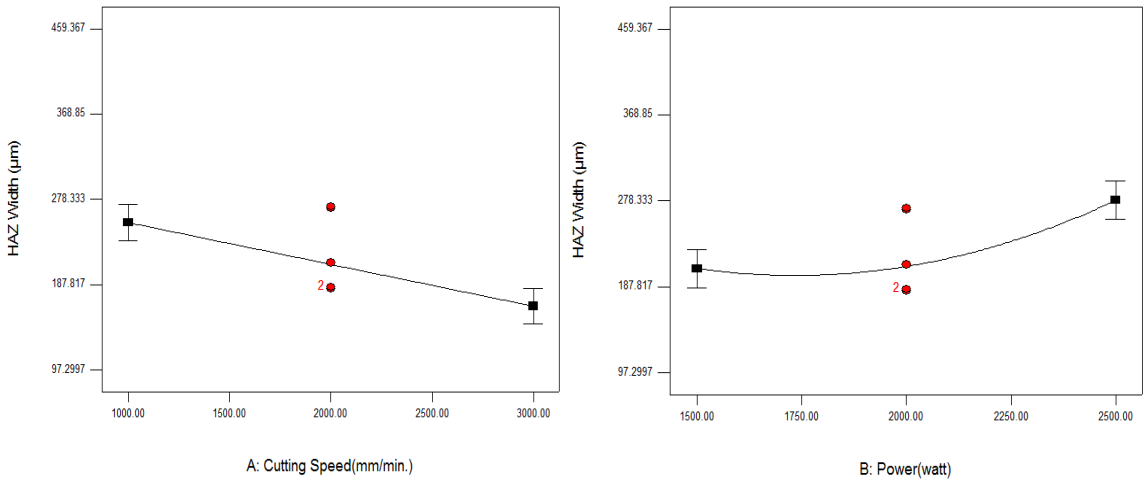

(a) **(b)**

Figure 5.50 Effect of cutting speed (a) and laser power (b) on heat affected zone width

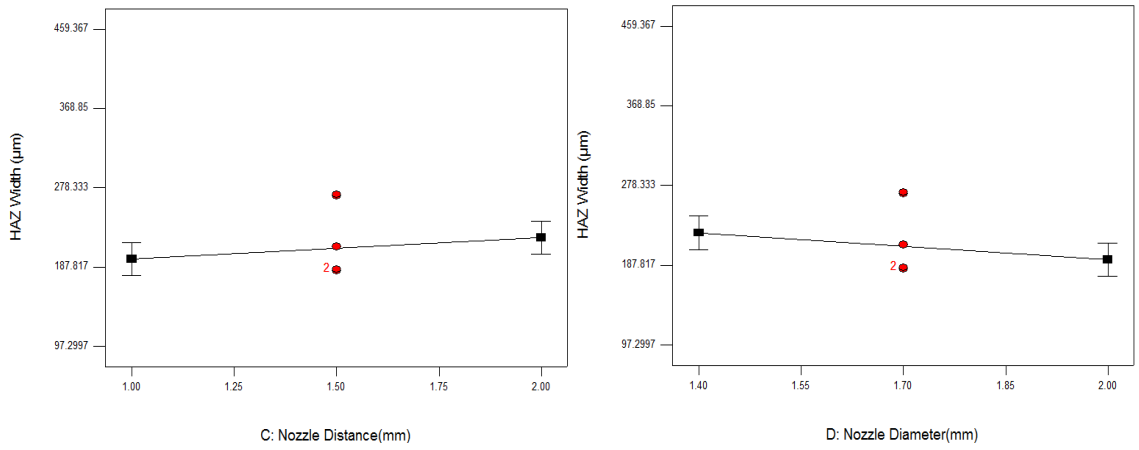

(a) **(b)**

Figure 5.51 Effect of nozzle distance (a) and nozzle diameter (b) on HAZ width

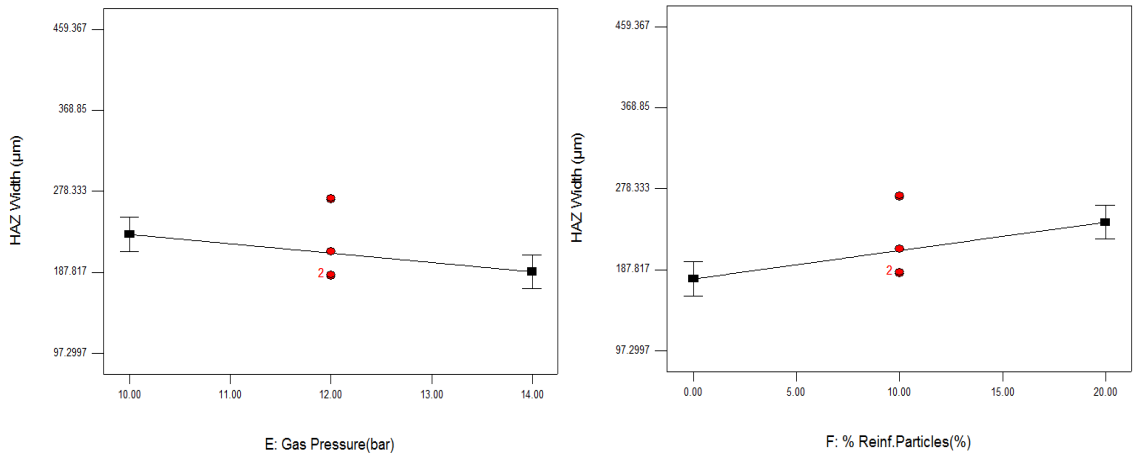

(a) **(b)**

Figure 5.52 Effect of gas pressure (a) and reinforced particles (b) on HAZ width

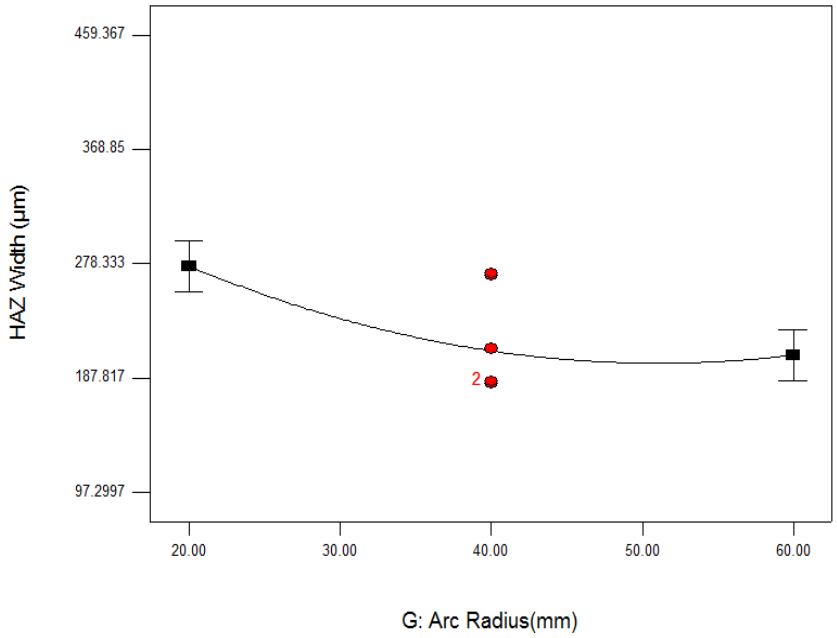

Figure 5.53 Effect of arc radius on heat affected zone width

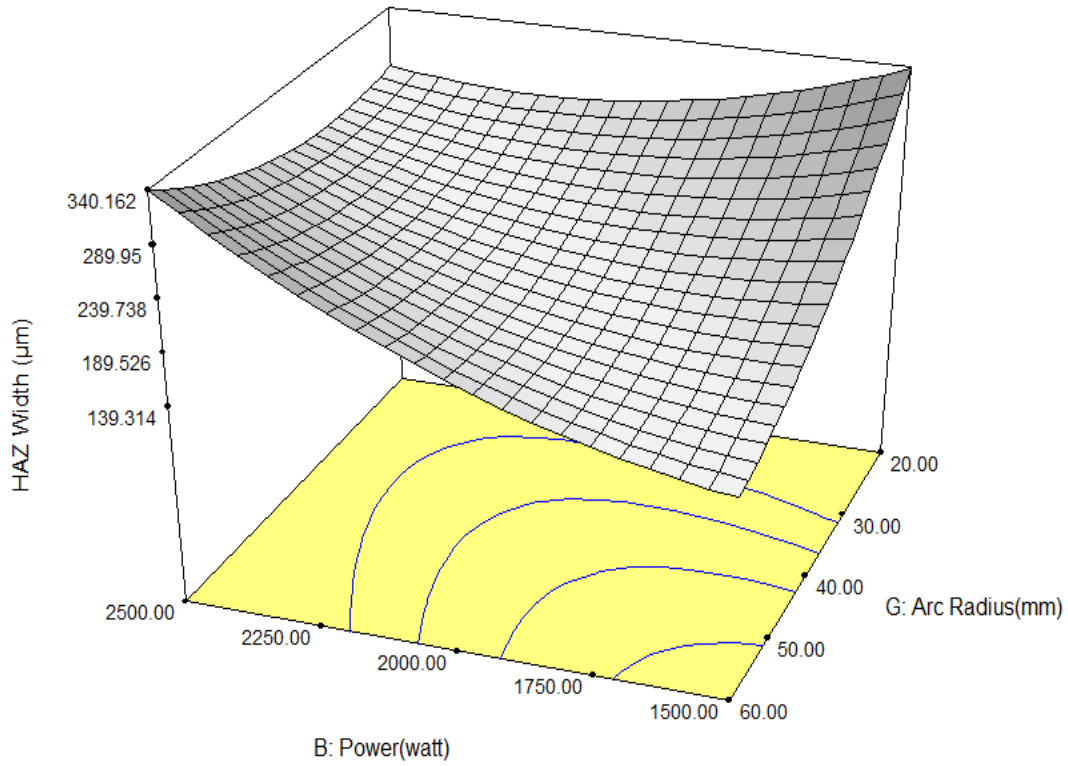

Figure 5.54 Interaction plot between arc radius and laser power for HAZ width

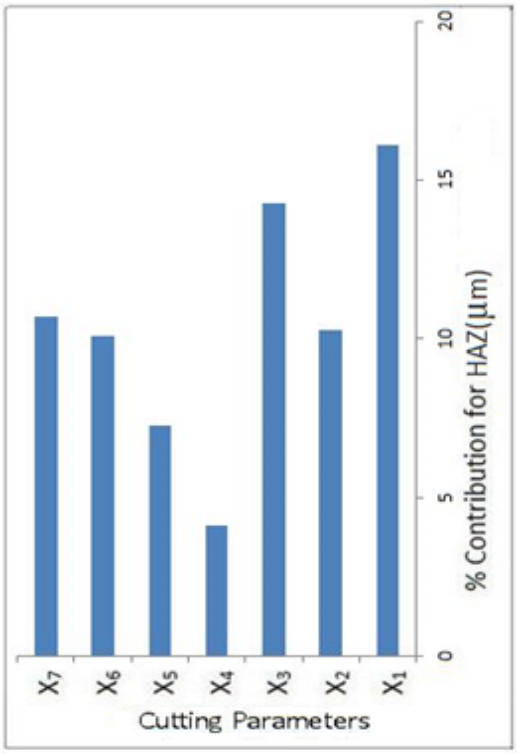

Figure 5.55 Percentage contribution of input parameters on heat affected zone width

The effect of various input parameters on heat affected zone width vary according to slope of the curves. From figure 5.50 (a) it was observed that as the cutting speed increased from 1000 mm/min to 3000 mm/min the slope of cutting speed decreased to lower level which signifies reduction in HAZ width. With the increase in laser power, the HAZ width increases to higher levels as shown in figure 5.50 (b). The distance between nozzle and specimen not proved to be significant as slope of standoff distance observed almost linear in nature. The slope of nozzle diameter decreases slightly to lower levels which signify the HAZ width has less significant effect of this factor as shown in figure 5.51 (b). The increase in value of gas pressure shows that width decreases to lower variation. From the plot it can also be observed that the increment in percentage SiC particles exhibits higher slope resulted into larger width of HAZ. The heat affected width examined to be increased with the higher quantity of SiC particles in vicinity of the kerf zone as shown in figure 5.52 (b). Due to the presence of these particles ejection of molten material becomes difficult and extension of molten material starts on the edge resulted into large heat affected zone width. A high extension and re-solidification of molten material can be decreased for less HAZ if gas pressure is set enough to drag out the viscous material (Riveiro A et al.., 2011). The deviation from the reference point of arc

radius depicted that with increase in arc radius from 20 mm to 60 mm the HAZ width decreases to less value. The cut profile also plays a prominent role in deciding the heat affected zone width. When the cut profile is more circular in nature, the HAZ width tend to increase to higher levels. The combined effects of laser power and arc radius are presented in figure 5.54 for constant values of cutting speed, standoff distance, nozzle diameter, gas pressure and arc radius at 2000 watt, 1.5 mm, 1.7 mm, 12 bar and 10 % wt respectively. From the response plot, it was analyzed that combination of higher value of laser power and lower value of arc radius increased the HAZ width. When the arc radius kept at 60 mm and laser power set to increase from 1500 watt to 2500 watt, the HAZ width increased from 139.28 µm to 340.16 µm. This is due to the higher power values which increases the energy levels in the cutting zone resulted into higher oxide layer. Moreover, the laser cut path also decides the width of HAZ as in this work when the arc radius decreases the width increases to higher levels. When arc radius set to decreased from 60 mm to 20 mm the HAZ width increased due to more complex cutting path of arc. Due to this ejection of molten material becomes difficult and heat penetration effect in the cutting zone increases resulted into large width of HAZ.

5.3.6 Effect of laser input variables on striation angle

The formation of striations along the cut edge is considered as undesirable factor. The surface roughness of the cut section is generally decided by the striation formation and inclination. The striation pattern increases with the increase in striation angle which resulted into higher stress concentration values. From the exhaustive literature review, it has been examined that the probable reasons for periodic striation formation are pulsation in the molten layer and the side burning phenomenon. The foremost theory is based on the perturbations effects of molten metal on cutting section which further solidifies in the form of periodic striation pattern. Moreover, the other explanations include the interaction of the assist gas with the molten material. The instabilities in the molten layer probably due to the effect of Kelvin-Helmholtz which develops due to the high velocity of assist gas. The mechanism of instability in the molten layer by assist gas was further discussed by Hirano et al.. . It was proposed that molten layer instability may be defined in terms of thermal dynamics and hydrodynamics. The effect of machining factors also plays a prominent role to enhance the origin of striations.

The normal probability plot of residuals for dross height is shown in figure 5.56. From the linearity of the graph, the adequacy of the model can be predicted. From the graph, it

can be predicted that residuals are normally distributed and scattered nearby the straight line resulted into less errors as shown in plot. It can also be observed that predicted values resembles with observed response values which shows the adequacy of the model and process parameters. The normal plots of residual values are shown in figure 5.57 which also shows the linearity of the model. The regression equation for striation angle is shown in equation 5.8.

$$\textit{Striation Angle (Degree)} = 74.04 - 0.012 \times X_1 - 0.0407 \times X_2 - 3.173 \times X_3 - 7.143 \times X_4 - 0.514 \times X_5 + 0.346 \times X_6 - 0.77785 \times X_7 + 1.527E\text{-}006 \times (X_1)^2 + 5.626E\text{-}006 \times (X_2)^2 + 3.969E\text{-}006 \times X_1 \times X_2 - 1.880E\text{-}004 \times X_2 \times X_7 + 0.22277 \times X_3 \times X_5 - 5.865E\text{-}003 \times X_2 \times X_7 \quad \text{.....(5.8)}$$

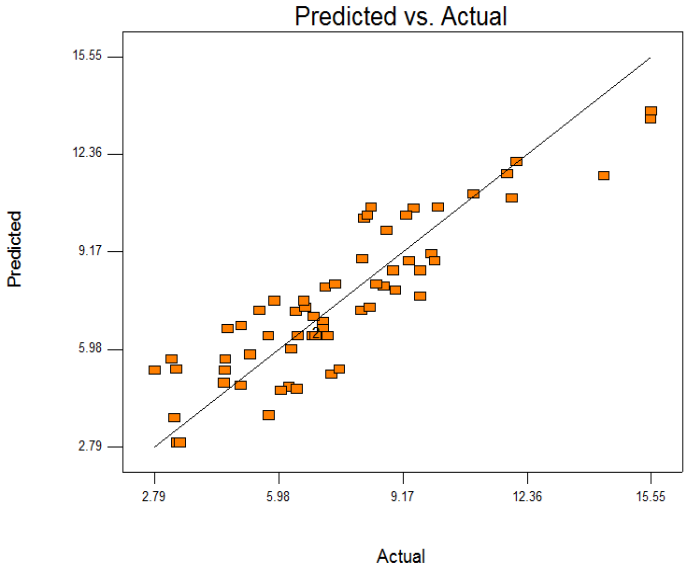

Figure 5.56 Plot of predicted versus actual for striation angle

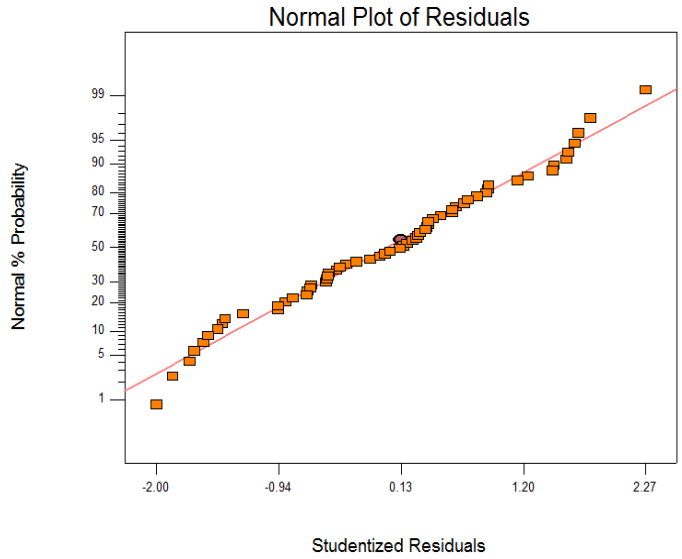

Figure 5.57 Normal probability plots of residuals for striation angle

Table 5.14 ANOVA for response surface of reduced quadratic model of striation angle

Source	Sum of Squares	Degrees of Freedom	Mean Square	F-Value	Prob. > F (p-value)	Remarks
Model	379.816	12	31.651	15.11012	< 0.0001	Significant
X_1	63.760	1	63.760	30.438	< 0.0001	Significant
X_2	46.684	1	46.684	22.287	< 0.0001	Significant
X_3	6.745	1	6.745	3.220	0.0789	Non-Significant
X_4	25.436	1	25.436	12.143	0.0010	Significant
X_5	30.172	1	30.172	14.404	0.0004	Significant
X_6	64.039	1	64.039	30.571	< 0.0001	Significant
X_7	34.042	1	34.042	16.251	0.0002	Significant
X_2^2	28.876	1	28.876	13.785	0.0005	Significant
X_7^2	31.517	1	31.517	15.046	0.0003	Significant
X_1X_5	28.292	1	28.292	13.506	0.0006	Significant
X_2X_7	14.292	1	14.292	6.823	0.0119	Significant
X_3X_6	11.011	1	11.011	5.256	0.0262	Significant
Predicted R^2 0.917						

***Legend: X_1: Cutting speed, X_2:* Laser power , *X_3:* Nozzle stand-off distance , *X_4:* Nozzle diameter , *X_5:* Gas pressure , *X_6:* Percentage reinforced particles, *X_7:* Arc radius**

The analysis of variance performed on various process parameters as shown in table 5.14 to identify the significant and non significant parameters for striation angle. From the table Adjusted R^2 value of 0.890 found which is examined to be approximate closed value of Predicted R^2: 0.917. The predicted most significant parameters found are cutting speed, laser power and reinforced particles. The effects of these variables have been analysed with the variation of slope of striation angle. From the plot, it was observed that striation angle increases with an increase in cutting speed from 1000 mm/min to 3000 mm/min as shown in figure 5.58 (a).

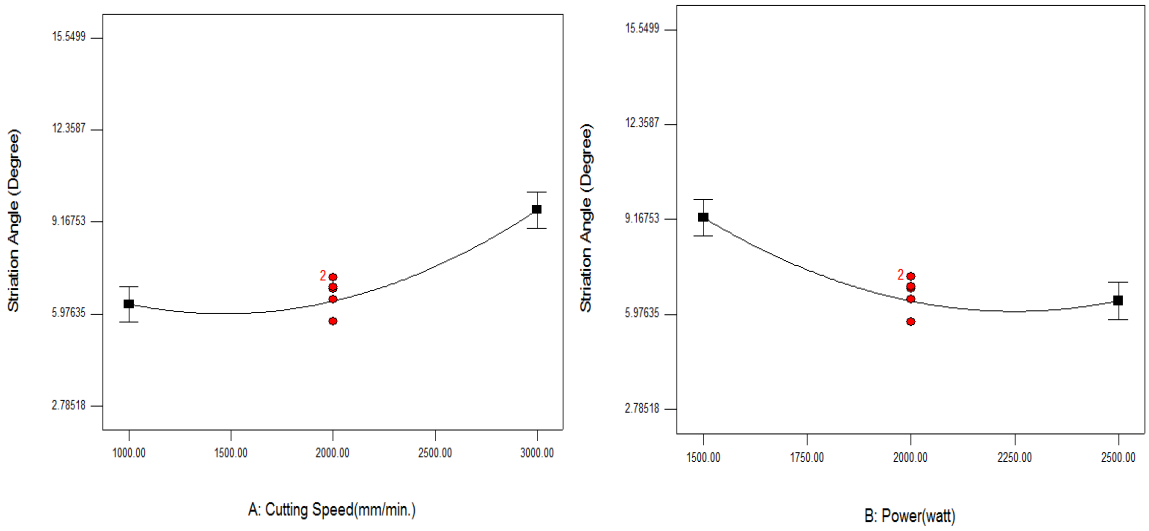

(a) **(b)**

Figure 5.58 Effect of cutting speed (a) and laser power (b) on striation angle

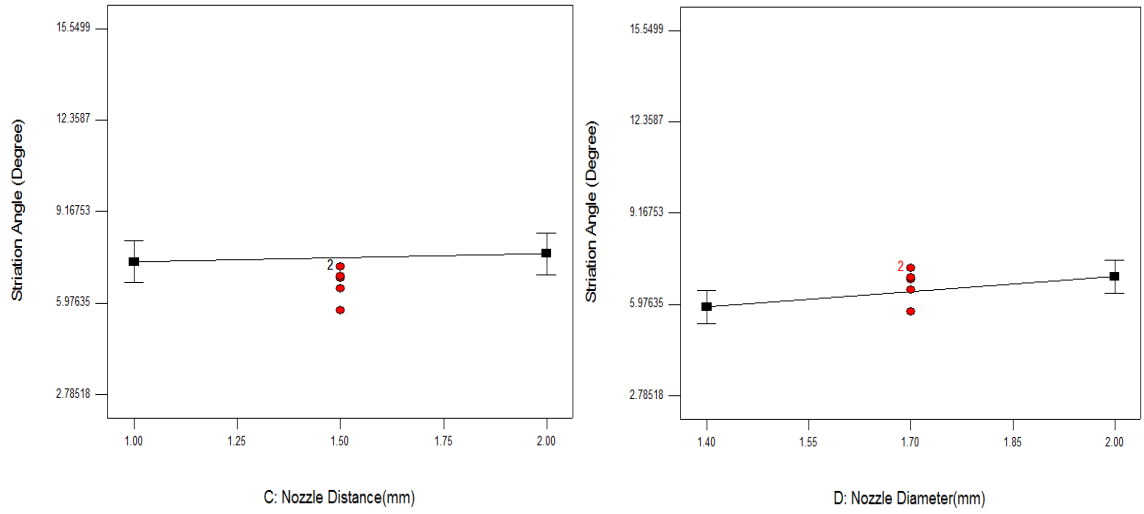

(a) **(b)**

Figure 5.59 Effect of nozzle distance (a) and nozzle diameter (b) on striation angle

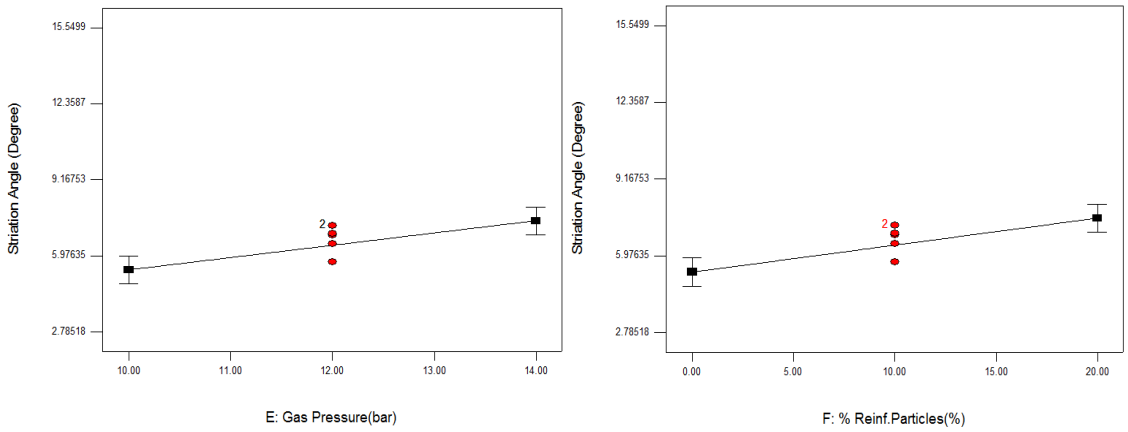

(a) **(b)**

Figure 5.60 Effect of gas pressure (a) and reinforced particles (b) on striation angle

The value of α_s decreased with increment in laser power from 1500 watt to 2500 watt as depicted in figure 5.58 (b). The variation in slope of standoff distance was linear in nature which resulted into less effect on α_s values. The effects on α_s values were slightly increased with increment in nozzle diameter values from 1.4 mm to 2.0 mm as reflected in figure 5.59 (b).

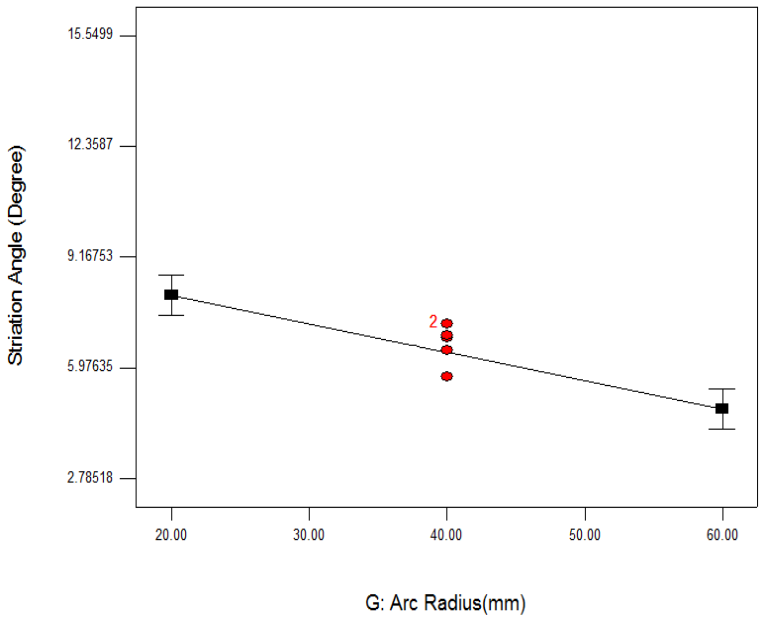

Figure 5.61 Effect of arc radius on striation angle

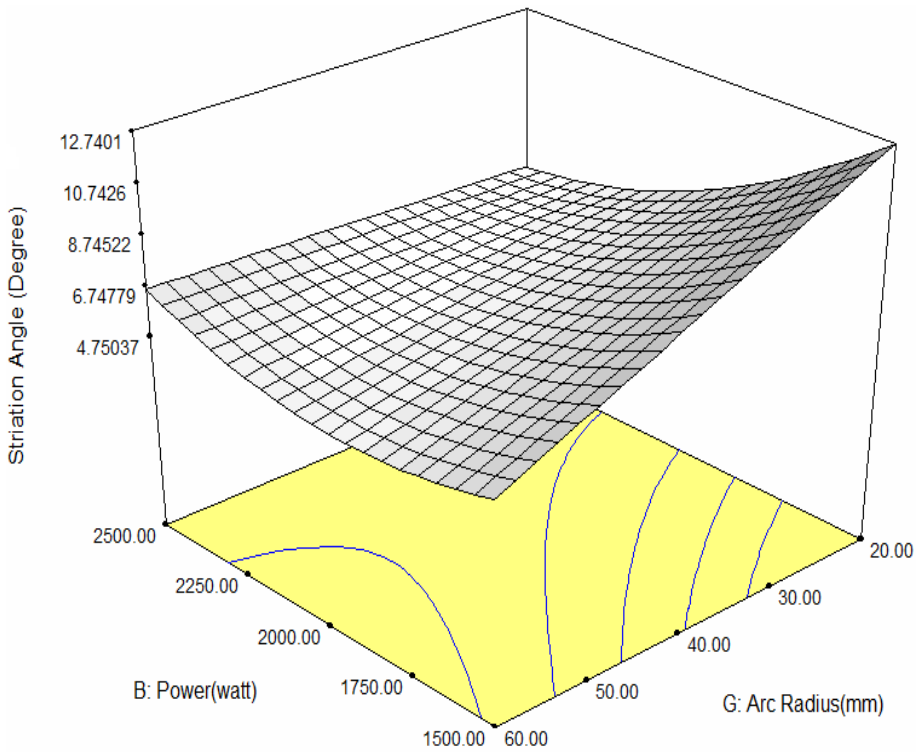

Figure 5.62 Interaction plot between laser power and arc radius for striation angle

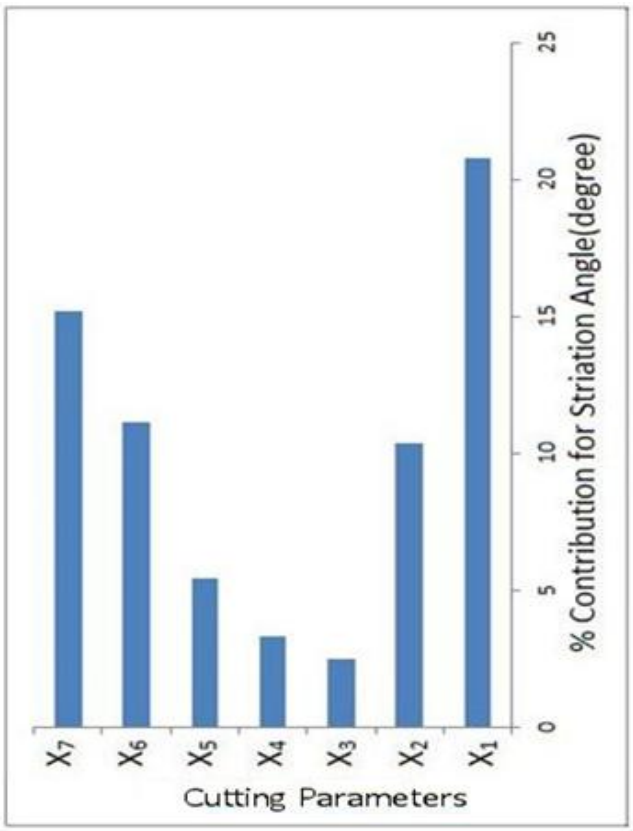

Figure 5.63 Percentage contributions of various factors on striation angle

With the increment in nitrogen gas pressure, α_s values increased to higher levels. The increment in percentage of reinforced particles resulted into increase in striation angle pattern with large variation. The slope of arc radius shows a large variation from the reference point which is sign of significant factor as shown in figure 5.61. As the arc radius increased from 20 mm to 60 mm, the striation angle pattern decreased to lower levels. The effect of variation of arc radius and laser power on striation angle has been examined as shown in figure 5.62. From the response plot, it was observed that striation angle increased with lower values of arc radius and laser power. When the laser power set at 1500 watt and arc radius set to decrease from 60 mm to 20 mm, the striation angle increased from 7.4 degree to 15.3 degree. With the decrease in arc radius, the cutting path becomes more complex in nature due to this ejection of molten material becomes difficult. This, in turns, accumulation of solidified material on cut surface in the form of angular striations (Sharma A. et al.., 2013). The percentage contribution of various factors on striation angle is shown in figure 5.63. It has been observed that cutting speed and arc radius has maximum significant contribution of 22 % and 15 % respectively. The least contribution of nozzle distance was predicted as 3 % on striation angle.

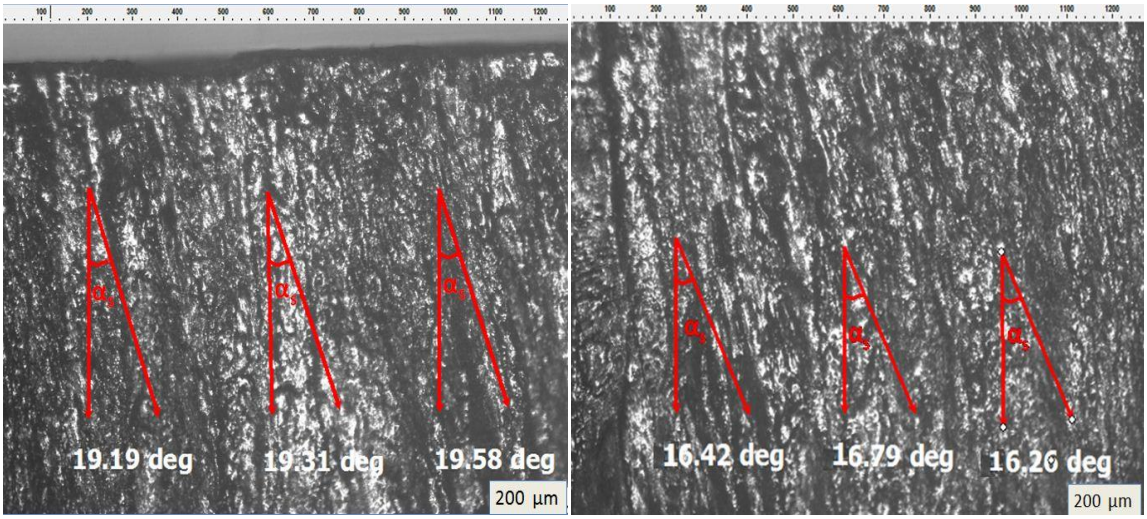

(a) (b)

Figure 5.64 Microscopic images (50×): (a) variation in striation angle for cutting speed: 3000 mm/min and arc radius: 20 mm, (b) striation angle for cutting speed: 2000 mm/min and arc radius: 20 mm

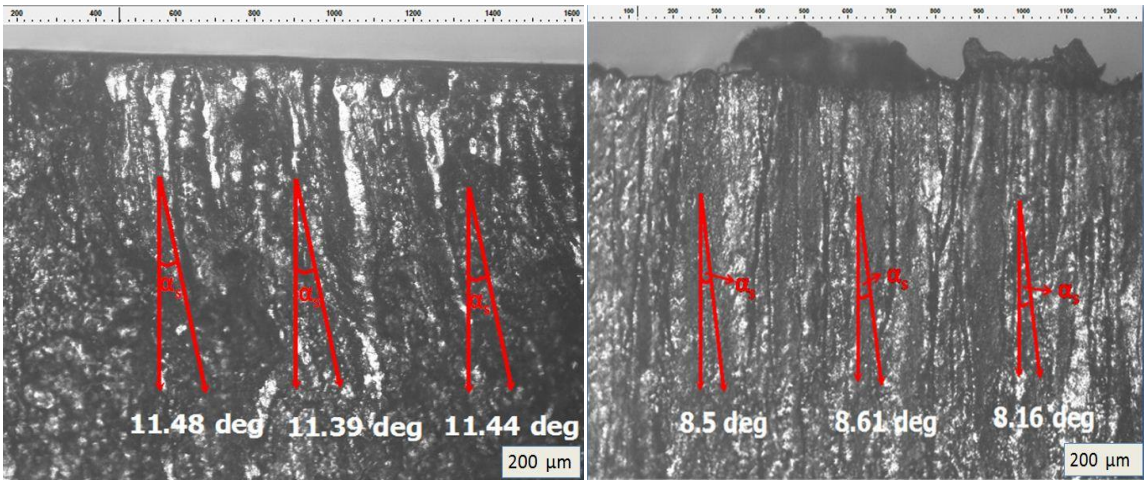

(a) (b)

Figure 5.65 Microscopic images (50×): (a) striation angle for cutting speed: 1000 mm/min and arc radius: 40 mm, (b) striation angle for cutting speed: 1000 mm/min and arc radius: 60 mm.

From figure 5.64 (b) the dramatic change in the striation inclinations (16.49˚) has been analyzed when cutting speed set at low level of 2000 mm/min. The inclinations value increased to 11.43˚ (average) when machining conditions set at cutting speed: 1000 mm/min, laser power: 1500 watt, standoff distance: 1.5 mm, nozzle diameter: 1.7 mm, gas pressure: 12 bar, ZrO_2 particles: 10 % and arc radius: 40 mm as shown in figure 5.65 (a).With the decrease in arc radius and increase in quantity of reinforced particles, the

value of α_s increased to higher levels. The striations inclinations of 8.42˚ (average) has been analyzed when machining conditions set at cutting speed: 1000 mm/min, laser power: 2000 watt, standoff distance: 1.5 mm, nozzle diameter: 1.7 mm, gas pressure: 12 bar, ZrO_2 particles: 20 % and arc radius: 60 mm as shown in figure 5.65 (b). The higher curvature of the striations is also due to the low pressure of the assist gas which insufficiently drag out the molten material. Moreover, oxidation of molten material continues due to its high temperature which resulted into irregular cut surface (Chen et al.., 1998). The lower inclinations were observed with lower values of cutting speed and higher arc radius values. From above discussions, it can be predicted that higher amount of energy is absorbed when the cut profile is more curvature in nature which resulted into deep striation pattern. Furthermore, the higher quantity of reinforced particles also increases the absorptance level of energy in the vicinity of kerf zone. The cutting speed has significant effect in the large variation of striation inclination patterns. The striation angles are more pronounced when the gas pressure is low of 10-12 bar range and reinforced particles is present in higher quantity of 20 %.

5.3.7 Effect of laser input variables on material removal rate

The material removal rate depends on various parametric conditions and material type. In the previous studies it has been examined that MRR increases with the decrease in material thickness when cutting process is conducted using CO_2 laser beam machining. The material removal rate depends on various factors of machining conditions. However, the main factor to be considered during laser cutting process is adaptability of laser beam for specimen, reflectivity of work material, elastic modulus of material, hardness etc. The material removal rate can be determine using following equation 5.9 in which the parameters such as cutting speed, loss of mass of specimen and length of cut is used. In this equation length of cut is taken as arc length.

MRR= (Loss of mass during the cut × cutting speed)/ length of cut …… (5.9)

The regression model for the material removal rate is shown in equation 5.10

Material Removal Rate (mg/min) = $-47.064 - 0.037\times X_1 + 0.090\times X_2 - 136.937\times X_3 - 120.26\times X_4 + 16.909\times X_5 - 1.160\times X_6 - 5.637\times X_7 + 0.0299\times (X_7)^2 - 3.309\text{E-}005\times X_1\times X_2 - 5.990\text{E-}003\times X_1\times X_5 + 0.114\times X_2\times X_4 + 1.279\text{E-}003\times X_2\times X_7 - 86.267\times X_3\times X_4$ ……(5.10)

Table 5.15 ANOVA for response surface of quadratic model of material removal rate

Source	Sum of Squares	Degrees of Freedom	Mean Square	F-Value	Prob. > F (p-value)	Remarks
Model	34492.86	14	2463.776	9.773	< 0.0001	Significant
X_1	8325.617	1	8325.617	33.025	< 0.0001	Significant
X_2	1132.002	1	1132.002	4.490	0.0394	Significant
X_3	566.433	1	566.433	2.246	0.1406	Non-significant
X_4	933.1613	1	933.161	3.701	0.0604	Significant
X_5	2331.437	1	2331.437	9.248	0.0038	Significant
X_6	3232.791	1	3232.791	12.823	0.0008	Significant
X_7	4464.541	1	4464.541	17.709	0.0001	Significant
X_1^2	3501.198	1	3501.198	13.888	0.0005	Significant
X_7^2	2095.11	1	2095.11	8.310	0.0059	Significant
X_1X_2	2190.628	1	2190.628	8.689	0.0050	Significant
X_1X_5	1148.362	1	1148.362	4.555	0.0381	Significant
X_2X_4	2357.376	1	2357.376	9.350	0.0037	Significant
X_2X_7	1310.088	1	1310.088	5.196	0.0272	Significant
X_3X_4	1339.564	1	1339.564	5.313	0.0256	Significant
Predicted R^2 0.946						
Legend: X_1: Cutting speed, X_2: Laser power , X_3: Nozzle stand-off distance , X_4: Nozzle diameter , X_5: Gas pressure , X_6: Percentage reinforced particles, X_7: Arc radius						

The analysis of variance performed on various process parameters as shown in table 5.15 to identify the significant and non significant parameters for material removal rate. From the table Adjusted R^2 value of 0.933 found which is examined to be approximate closed value of Predicted R^2: 0.946. The predicted most significant parameters found are cutting speed and arc radius.

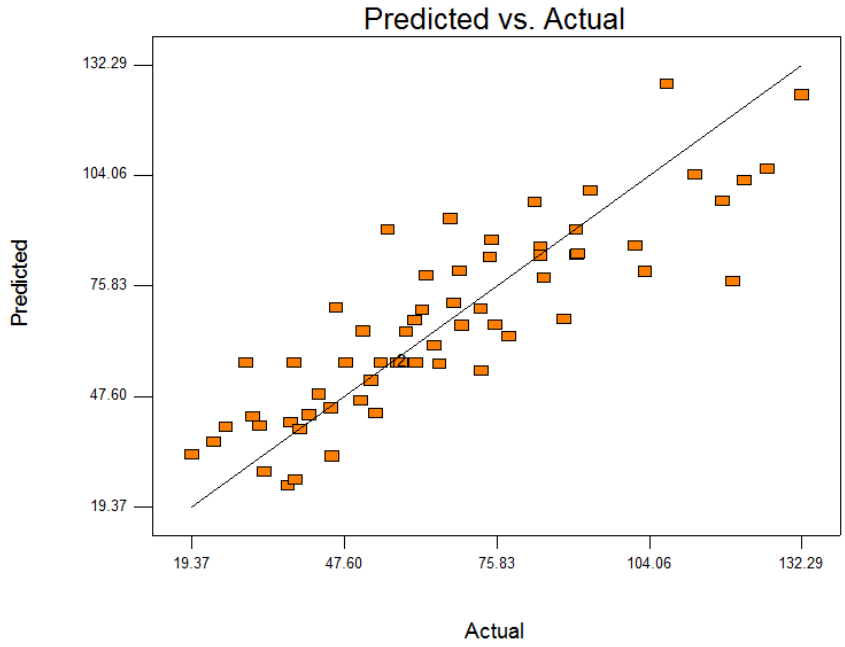

Figure 5.66 Plot of predicted versus actual for material removal rate

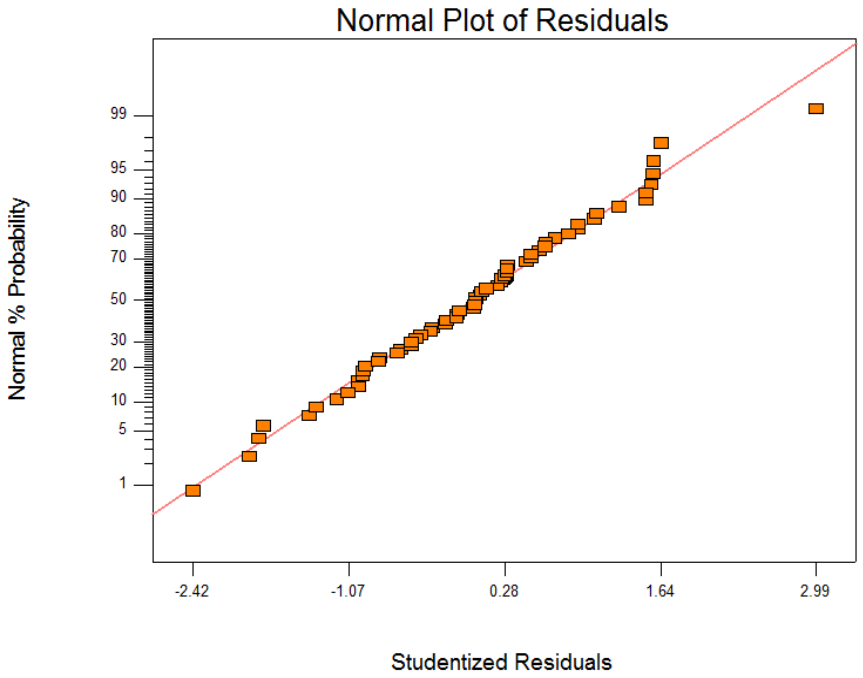

Figure 5.67 Normal probability plots of residuals for material removal rate

The normal probability plot of residuals for dross height is shown in figure 5.66. From the linearity of the graph, the adequacy of the model can be predicted. From the graph, it can be predicted that residuals are normally distributed and scattered nearby the straight line resulted into less errors as shown in plot. It can also be observed that predicted values resembles with observed response values which shows the adequacy of the model and

process parameters. The normal plots of residual values are shown in figure 5.67 which also shows the linearity of the model.

From the figure 5.68 (a), the effect of cutting speed has been analyzed on the material removal rate. The upward slope of plot predicted about the positive results of cutting speed on MRR. It was predicted when the cutting speed kept at 1000 mm/min the MRR reached to 52.93 mg/min whereas when the cutting speed increased to 3000 mm/min the MRR also increased to 90.18 mg/min. From the figure 5.68 (b) the effect of laser power on material removal rate can be predicted. It was explored from the plot that with increase in laser power from 1500 to 2500 watt, the MRR also increased by 49.20 mg/min 62.91 mg/min. This may be attributed to the fact that with increase in laser power the thermal energy in kerf zone increases resulted into higher material removal rate. With the increase in nozzle distance from 1.00 to 2.00 mm, the material removal rate increased by 51.21 to 60.9 mg/min. as shown in figure 5.69 (a). The same increasing trend has been analyzed with the nozzle diameter, when the diameter kept constant of 1.4 mm the MRR examined with lower vlaue of 49.80 mg/min.

On the other hand with increase in nozzle diameter to 2.0 mm the MRR increased to some higher levels. The probable reason for it may be the increased turbulence effect of gas resulted into higher MRR. The nitrogen gas pressure shown significant results for MRR as shown in figure 5.70 (a). With the increase in gas pressure from 10 to 14 bar the material removal rate increased significantly. As higher gas pressure able to produce higher drag force which removes the molten material in kerf zone quickly. The most significant parameter effected the material removal rate is examined as quantity of reinforced SiC particles. The decreasing slope of the curve of reinforced particles depicted the decrement of MRR. The figure 5.70 (b) shows that when the cutting process was executed with specimen of zero percentage SiC particles, higher material removal rate was reported of 67.68 mg/min. On the other hand, when the laser cutting executed with the work material having 20 % SiC particles, the MRR noted with lower value of 44.47 mg/min. The lower material removal rate achieved may be due to the higher reinforced particles, as these particles absorb large amount of energy which is required for material removal process. Thus, remaining part of energy is not sufficient to achieve the higher removal rate from the kerf zone. The cutting profile also plays an important role in deciding the material removal rate. It has been analyzed that with increase in the curvature of cut profile the laser travel larger distance as compared to lower curvature

path. From the figure 5.71 it can examined that when the arc radius kept at 20 mm the higher material removal rate achieved of 81.69 mg/min. On the other hand when the arc radius fixed at 60 mm the MRR decreased to 54.41 mg/min.

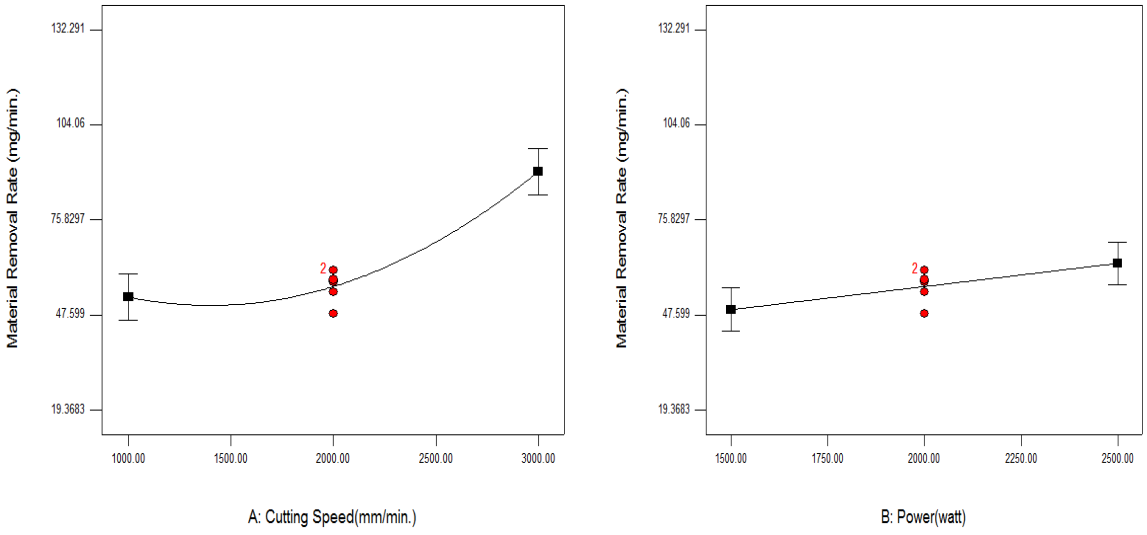

(a) **(b)**

Figure 5.68 Effect of cutting speed (a) and laser power (b) on material removal rate

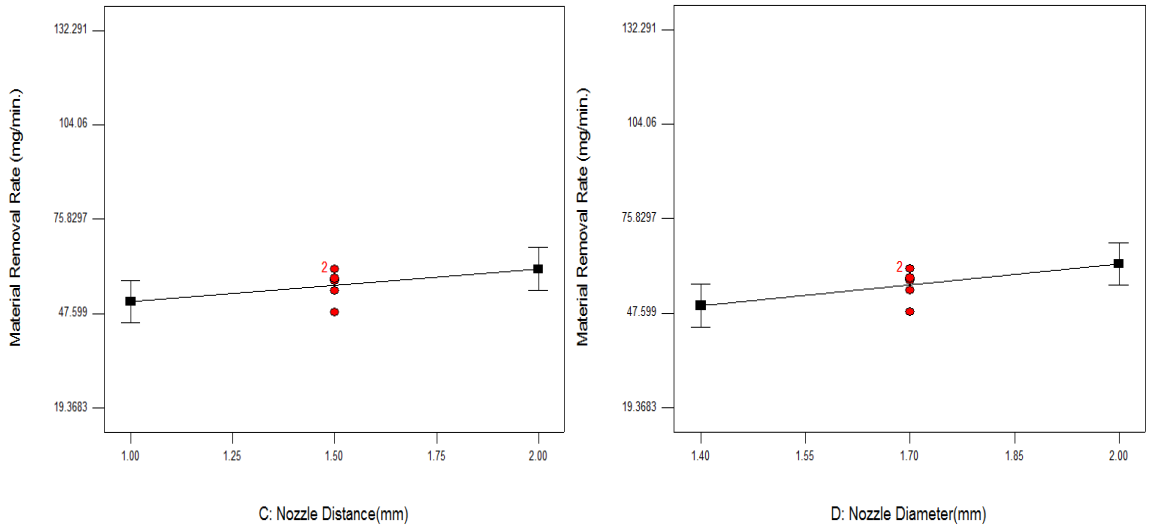

(a) **(b)**

Figure 5.69 Effect of nozzle distance (a) & nozzle diameter (b) on material removal rate

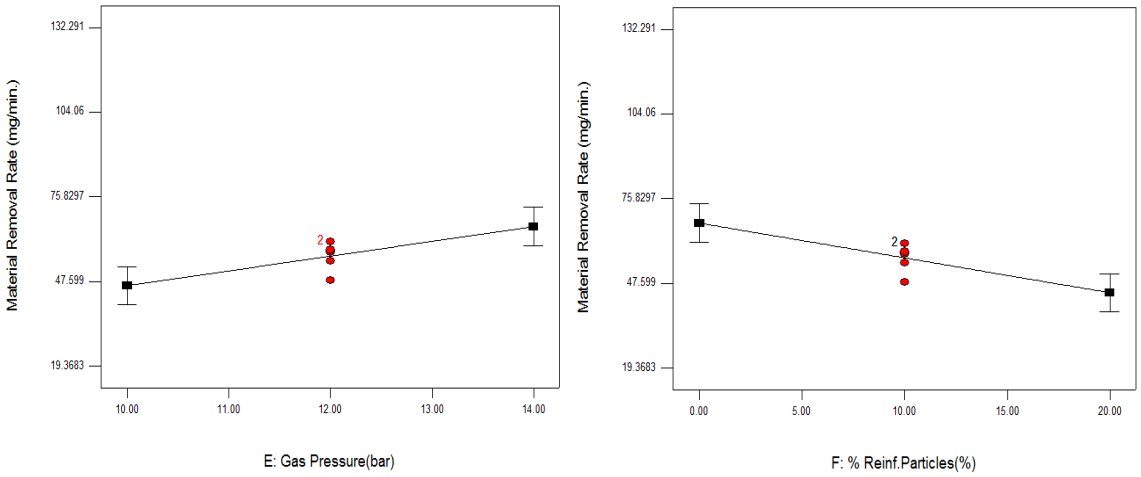

(a) **(b)**

Figure 5.70 Effect of gas pressure (a) & reinforced particles (b) on material removal rate.

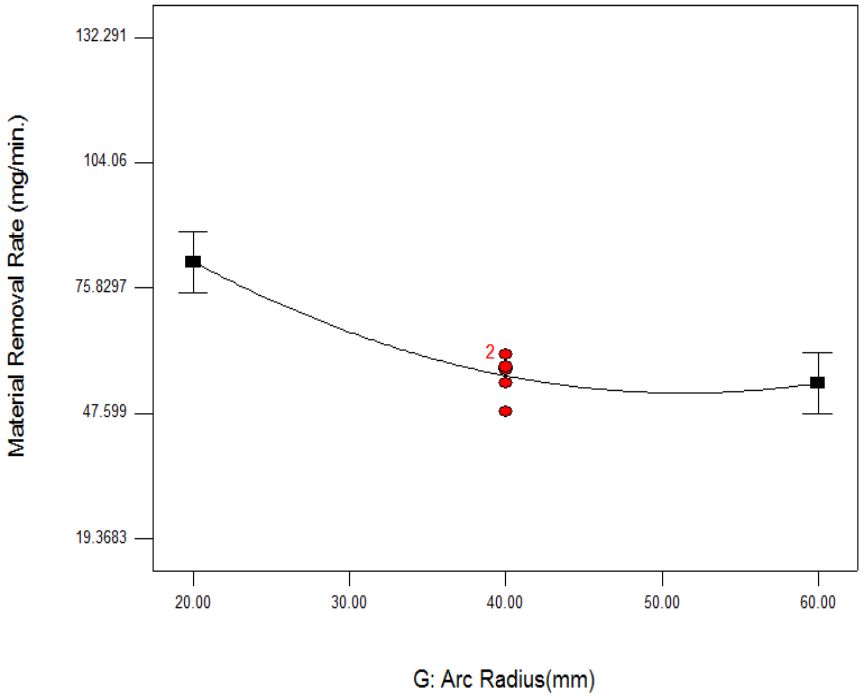

Figure 5.71 Effect of arc radius on material removal rate

The results of interaction of process parameters is shown in figure 5.72 with the help of 3-D response surface plot. It was analyzed that when the gas pressure kept constant at 10 bar and cutting speed set to increase from 1000 to 3000 mm/min the material removal rate increased from 31.10 mg/min to 92.32 mg/min. This increase in higher value of material removal rate is due to the increase in cutting speed resulted into prevention of backward flow of molten material. The percentage contributions of various process parameters is

shown in figure 5.73 for material removal rate. The cutting speed has higher contribution has compared to other factors.

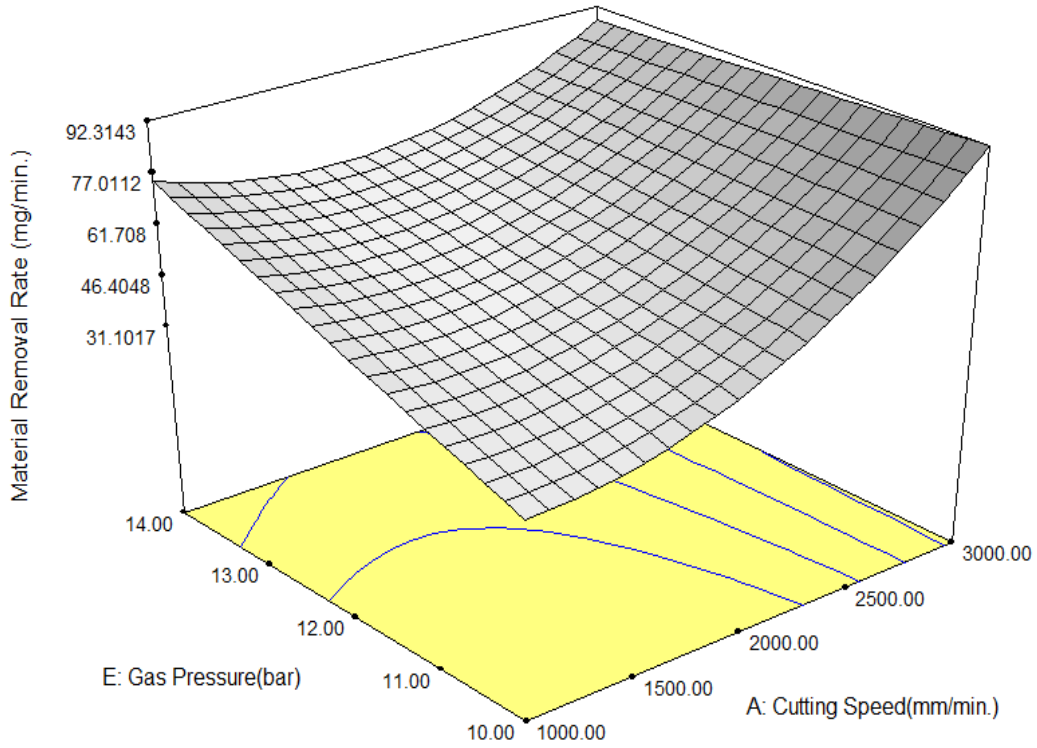

Figure 5.72 Interaction plot between gas pressure and reinforced particles on MRR

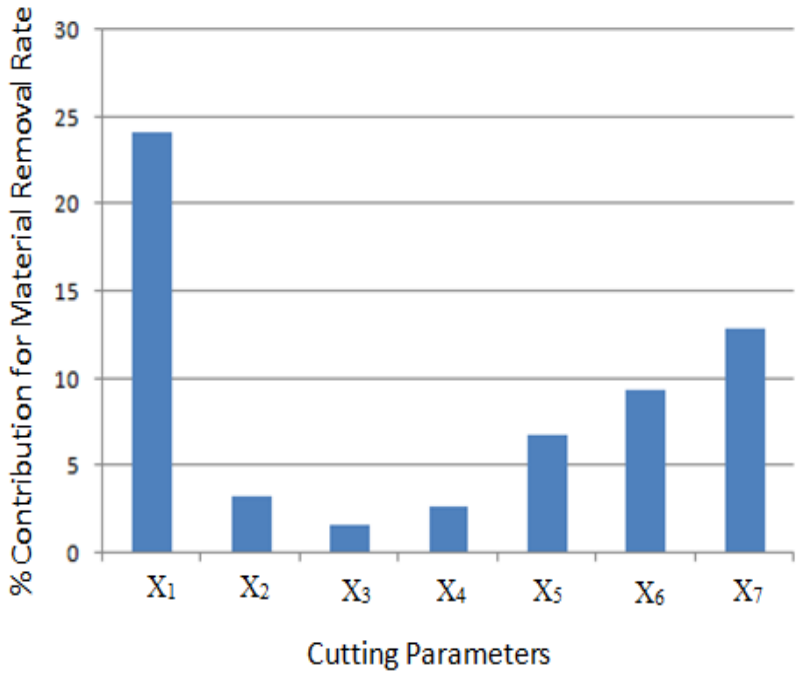

Figure 5.73 Percentage contributions of various factors on MRR

5.3.8 Effect of laser input variables on energy losses

When the laser beam is focused on the work material for initiating the cutting process, then there may be number of losses can occur which reduces the efficiency of the process. The energy losses are divided into two components such as primary and secondary losses based on the conduction, convection and radiation process. The energy losses also depend on the material type and material thickness used for cutting operation. The primary energy losses occur when the laser beam of 10.6 μm leave the kerf zone as they entered. This type of energy losses include only reflected and transmitted laser light. The secondary losses includes the losses occurred due to thermal transformation of the material of kerf zone. These types of energy losses include losses due to conduction, convective and radiative losses from the machined surface to the atmosphere. It has been investigated that conductive losses are higher than radiative and convective losses. The radiative and convective losses have least contribution in the energy balance equation. The present research work is focused to determine the energy power losses with the help of volumetric ablation energy of the acrylic block A.

To measure the energy losses equation 5.11 has been used, which shows the energy power losses.

$$E_{LOSS} = A \cdot Vp \qquad \ldots\ldots\ldots\ldots\ldots\ldots (5.11)$$

A= volumetric ablation energy of the acrylic block,

Vp = mode print volume developed by the laser beam on acrylic block

The energy losses in terms of power losses is expressed in equation 5.12.

$$P_{LOSS} = A \times Vp / t \qquad \ldots\ldots\ldots\ldots\ldots\ldots (5.12)$$

t = time taken

The mode print volume is calculated using equation 5.13.

$$Vp = m/\rho \qquad \ldots\ldots\ldots\ldots (5.13)$$

ρ = mass density of PMMA (1190 kg/m^3)

m = mass of the print volume

$$m = m_{init} - m_{fin} = \Delta m \qquad \ldots\ldots\ldots\ldots (5.14)$$

m_{init} = initial mass of acrylic block A

m_{fin}= final mass of acrylic block A after laser impinges on the block A.

$$l = v \cdot t \qquad \text{..... (5.15)}$$

l is taken as imprinting arc length l on acrylic block A

v is laser cutting speed fixed as layout

$$P_{LOSS} = A \cdot \Delta m / \rho \times v / l \qquad \text{..... (5.16)}$$

The regression equation for energy losses is formulated using response surface methodology as shown in below equation 5.17.

$$\textit{Energy Losses (watt)} = 8556.446 - 0.495 \times X_1 + 0.047 \times X_2 - 1241.093 \times X_3 - 1836.136 \times X_4 + 178.230 \times X_5 - 45.214 \times X_6 - 112.273 \times X_7 + 0.0299 \times (X_7)^2 - 9.690E\text{-}003 \times X_1 \times X_6 + 6.932E\text{-}003 \times X_1 \times X_7 + 0.019 \times X_2 \times X_6 + 760.321 \times X_3 \times X_4 + 20.556 \times X_3 \times X_7 + 2.435 \times X_5 \times X_6 \qquad \text{.....(5.17)}$$

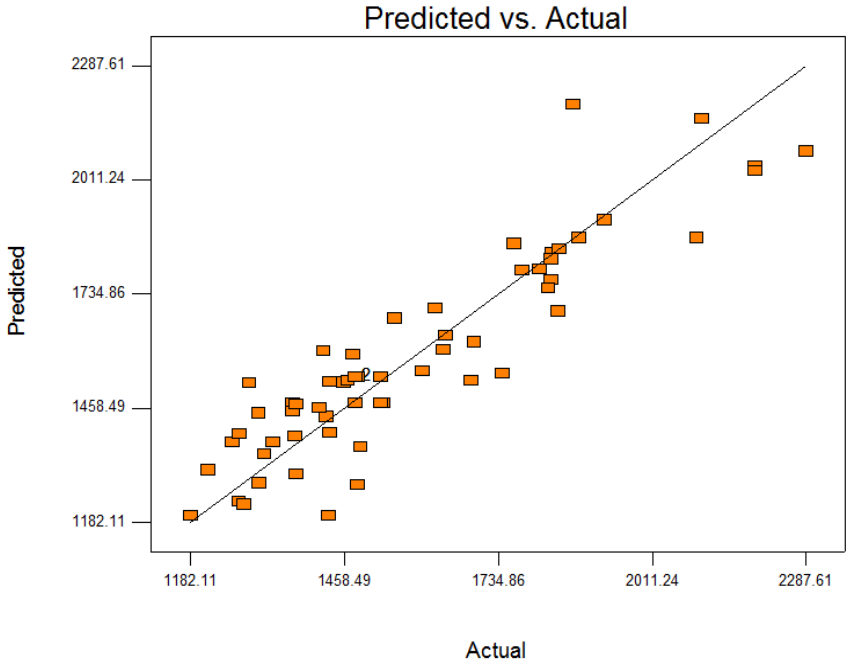

Figure 5.74 Plot of predicted versus actual for energy losses

The normal probability plot of residuals for energy losses is shown in figure 5.74. From the linearity of the graph, the adequacy of the model can be predicted. From the graph, it can be predicted that residuals are normally distributed and scattered nearby the straight line resulted into less errors as shown in plot.

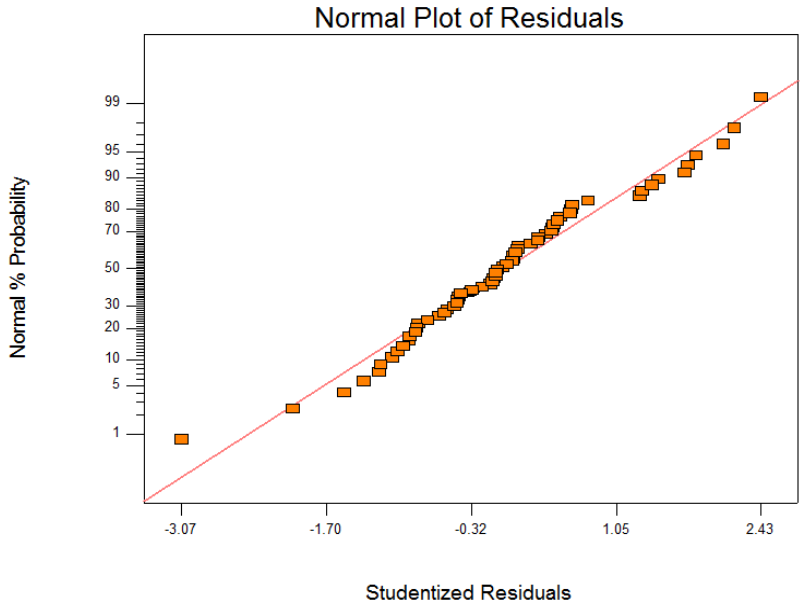

Figure 5.75 Normal probability plots of residuals for energy losses

It can also be observed that predicted values resembles with observed response values which shows the adequacy of the model and process parameters. The normal plots of residual values are shown in figure 5.75 which also shows the linearity of the model. The analysis of variance performed on various process parameters as shown in table 5.16 to identify the significant and non significant parameters for energy losses. From the table Adjusted R^2 value of 0.901 found which is analyzed to be approximate closed value of Predicted R^2: 0.929. The predicted most significant parameters found are cutting speed, gas pressure, reinforced particles and arc radius.

Table 5.16 ANOVA for response surface of reduced quadratic model of energy losses

Source	Sum of Squares	Degrees of Freedom	Mean Square	F-Value	Prob. > F (p-value)	Remarks
Model	3450311	14	246450.8	15.731	< 0.0001	Significant
X_1	354083.3	1	354083.3	22.601	< 0.0001	Significant
X_2	135620.1	1	135620.1	8.656	0.0050	Significant
X_3	15884.32	1	15884.32	1.0139	0.319	Not-significant
X_4	34615.52	1	34615.52	2.209	0.143	Significant
X_5	626911	1	626911	40.016	< 0.0001	Significant
X_6	449468.6	1	449468.6	28.689	< 0.0001	Significant

Source	Sum of Squares	Degrees of Freedom	Mean Square	F-Value	Prob. > F (p-value)	Remarks
X_7	1013943	1	1013943	64.720	< 0.0001	Significant
X_7^2	211116.2	1	211116.2	13.475	0.0006	Significant
X_1X_6	75125.24	1	75125.24	4.795	0.0335	Significant
X_1X_7	153781.7	1	153781.7	9.815	0.0030	Significant
X_2X_6	78085.37	1	78085.37	4.984	0.0304	Significant
X_3X_4	104055.9	1	104055.9	6.641	0.0132	Significant
X_4X_7	121696.4	1	121696.4	7.767	0.0076	Significant
X_4X_7	75924.95	1	75924.95	4.846	0.0327	Significant
Predicted R^2 0.929						

***Legend: X_1: Cutting speed, X_2:* Laser power , *X_3:* Nozzle stand-off distance , *X_4:* Nozzle diameter , *X_5:* Gas pressure , *X_6:* Percentage reinforced particles, *X_7:* Arc radius**

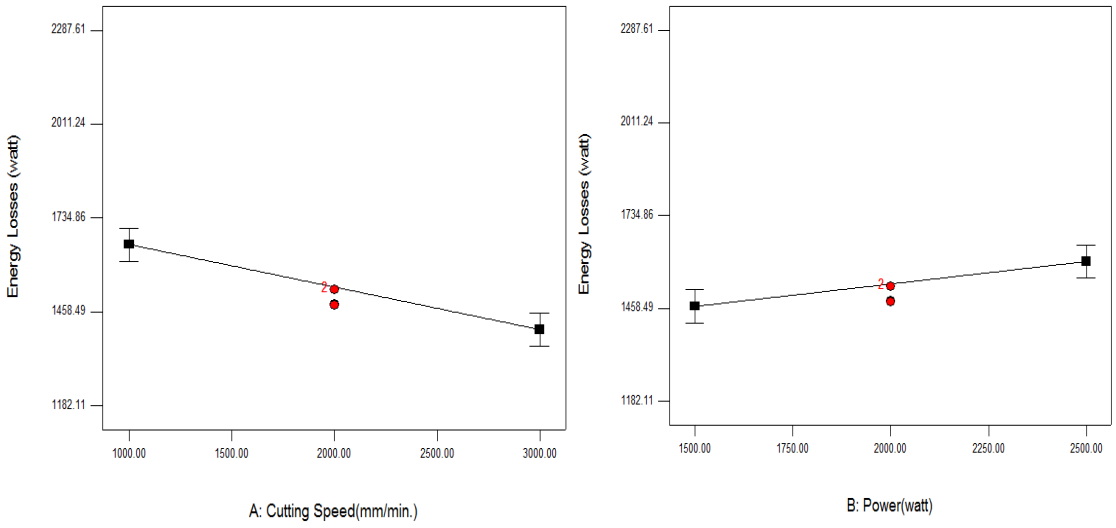

(a) **(b)**

Figure 5.76 Effect of cutting speed (a) and laser power (b) on energy losses

The main process parameters effects have been shown in figure 5.76 - 5.79 on the energy losses. From the figure 5.75 (a) the effect of cutting speed can be examined which revealed that with increasing cutting speed from 1000 to 3000 mm/min the energy losses

decreases to lower levels. When the laser power increased to 2500 watt, the energy losses increased to 1609 watt as shown in figure 5.75 (b).

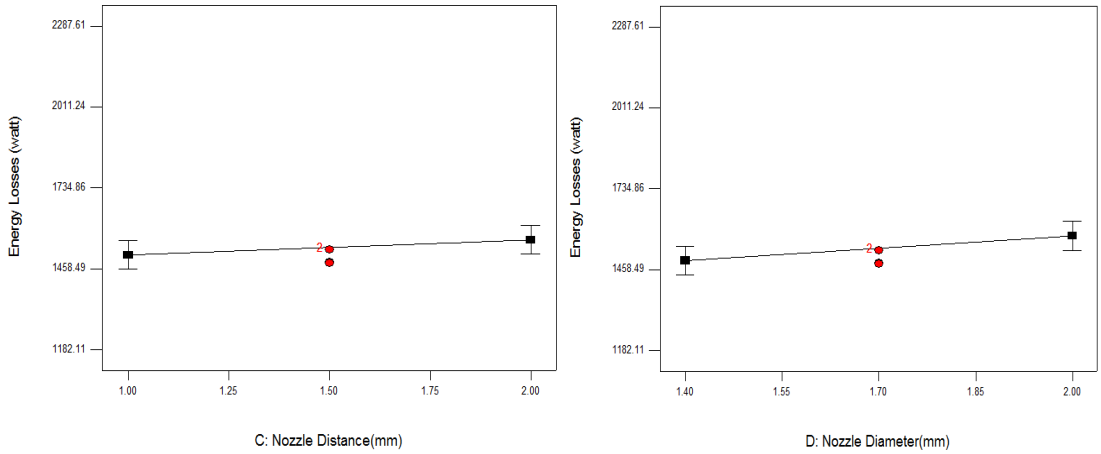

(a) **(b)**

Figure 5.77 Effect of nozzle distance (a) and nozzle diameter (b) on energy losses

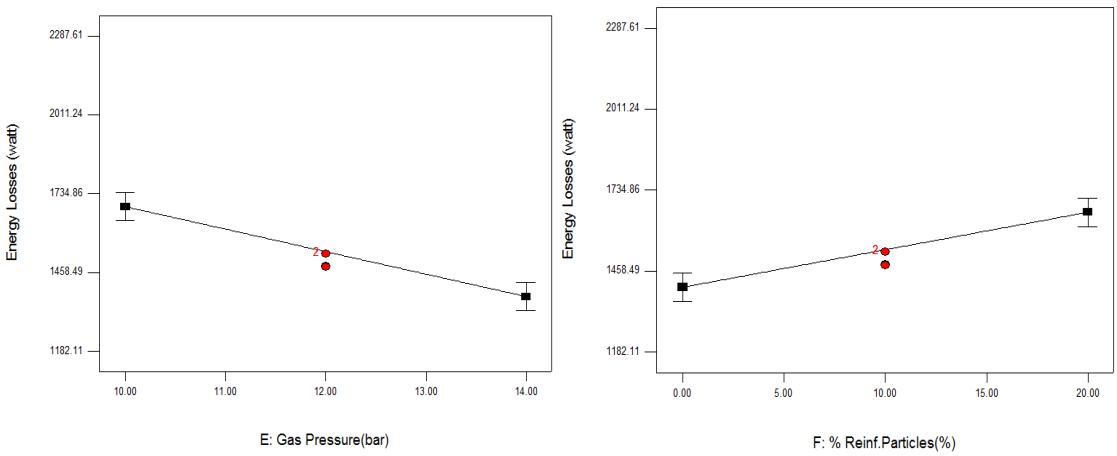

(a) **(b)**

Figure 5.78 Effect of gas pressure (a) and reinforced particles (b) on energy losses

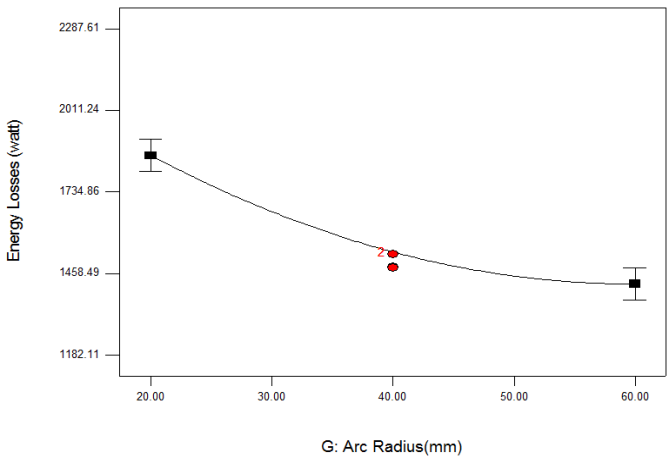

Figure 5.79 Effect of arc radius on energy losses

The probable reason for this process may be the high power and low curvature cut in which power losses remains higher. On the other hand, nozzle stand-off distance has shown negligible effect on the energy losses.

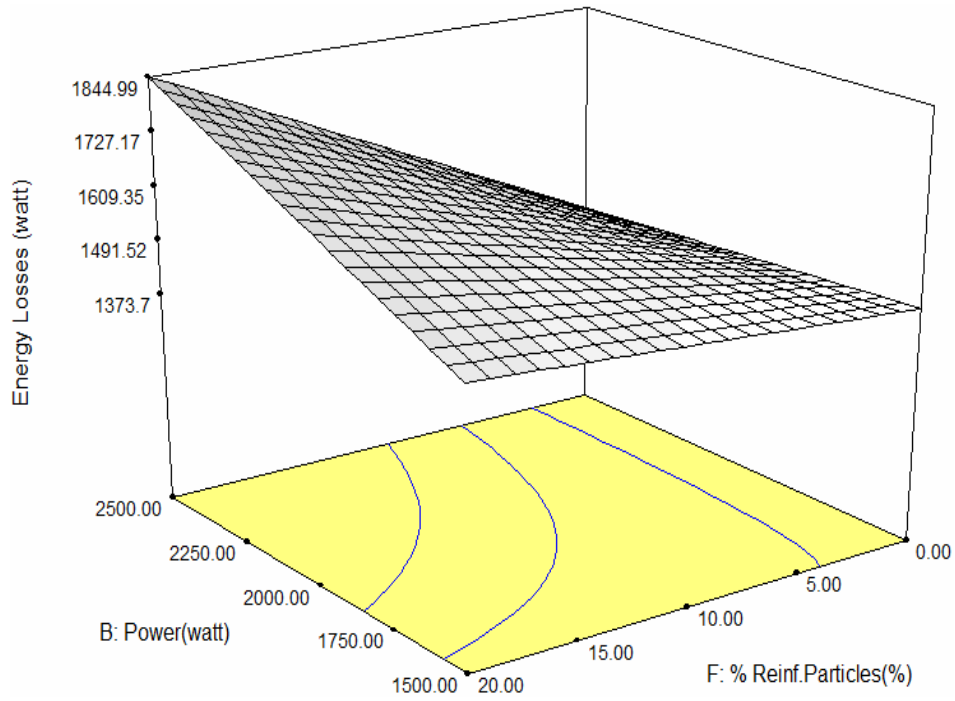

Figure 5.80 Interaction plot between laser power and reinforced particles for energy losses

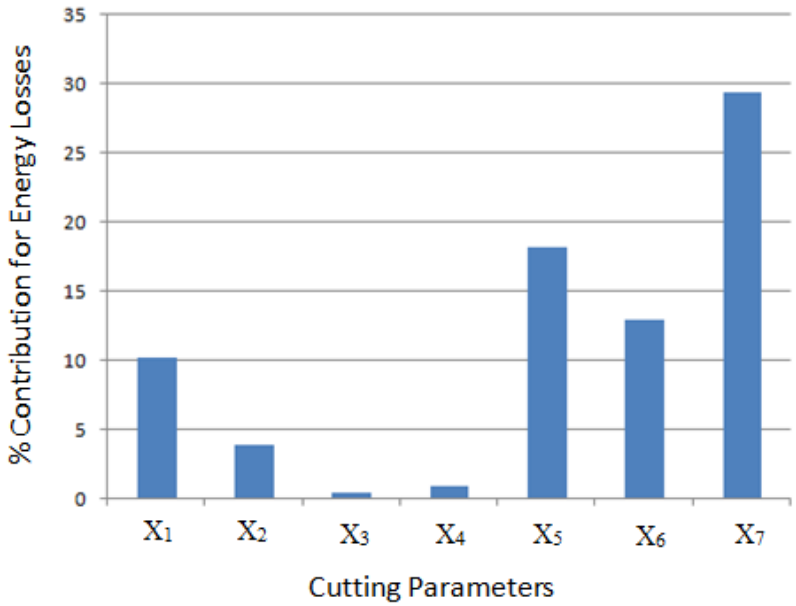

Figure 5.81 Percentage contributions of various factors on energy losses

From the figure 5.77 (a), the linearity of plot can be analyzed which shows that higher and lower nozzle distance value not having any significant effect on energy losses. The higher nozzle diameter has shown incremental energy losses as shown in figure 5.77 (b). The nozzle diameter of 2.00 mm has shown higher impact on the energy losses due to occurrence of turbulence effect. The gas pressure has shown significant effect on energy losses as shown in figure 5.78 (a). With increase in gas pressure from 10 to 14 bar, the energy losses decreased to 1372.55 watt. It may be due to exothermic reaction induced by the higher pressure which utilized maximum energy in the removal of molten material from kerf zone. The quantity of reinforced particles has significant effect on energy losses. The figure 5.78 (b) shows that as the reinforced particles increased in the specimen the energy losses also increased to higher levels. The presence of higher quantity of reinforced particles have higher accumulation of particles due to which conductive losses increases resulted into increase in power energy losses. The laser cut profile also has significant effect on the power energy losses. The energy loss increases with the more complicated path as laser has to travel large distance with low cutting speed. From the figure 5.79 the downward slope of curve plot shows that when the cut profile having 60 mm radius the energy losses has lower values. When the cut profile having arc radius of 20 mm the energy losses shown higher values of 1859.52 watt. Figure 5.80 shows the interaction plot between laser power and reinforced particles for energy losses. From the plot it can be analyzed that when the work material reinforced with higher quantity of 20 % and laser power set to increase from 1500 to 2500 watt, the energy losses also shown incremental behavior. The percentage contributions of various factors on energy losses is shown in figure 5.81.

5.4 EFFECT OF PROCESS PARAMETERS ON THE SPECIMEN Al5052/Al_2O_3 USING PERTURBATION AND INTERACTION PLOTS

5.4.1 Effect of various process parameters on dross height

For the specimen of Al5052/Al_2O_3 metal matrix composite, the quality characteristics results for the material have not shown large variation with respect to the specimen of Al5052/SiC, Al5052/ZrO_2 MMC work material. The effect of various process parameters has shown significant results on various output responses. With the help of perturbation plot the effect of various input control factors can be analyzed in a single plot. All the

results are analyzed with the help of reference point which lies at the middle of the curves.

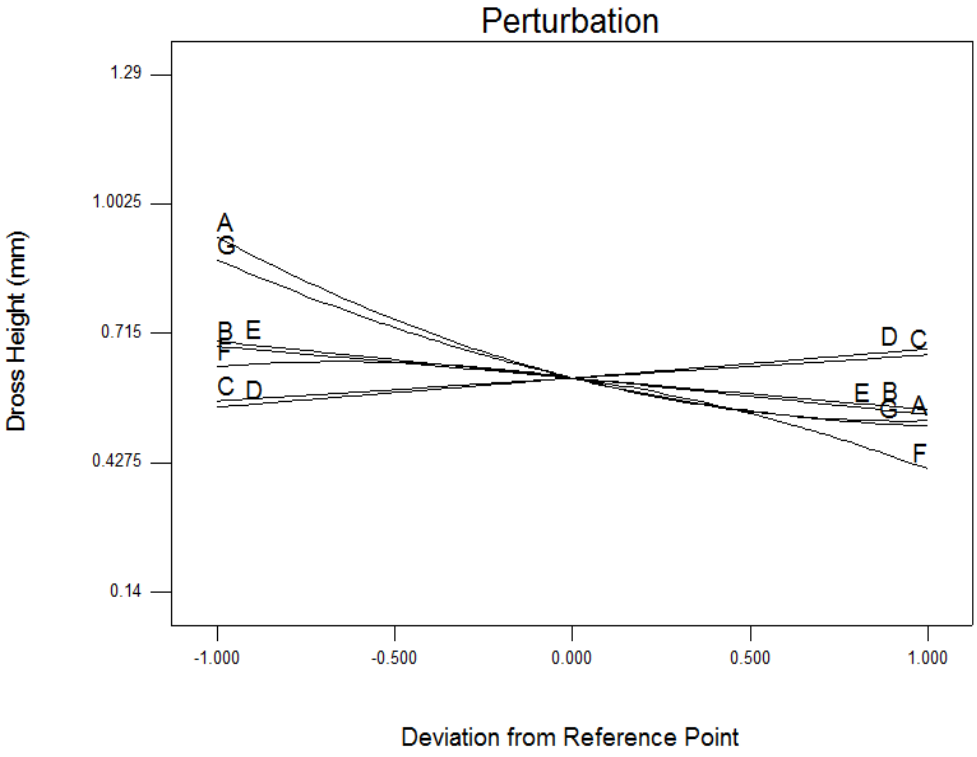

Figure 5.82 Perturbation plot of process parameters for dross height

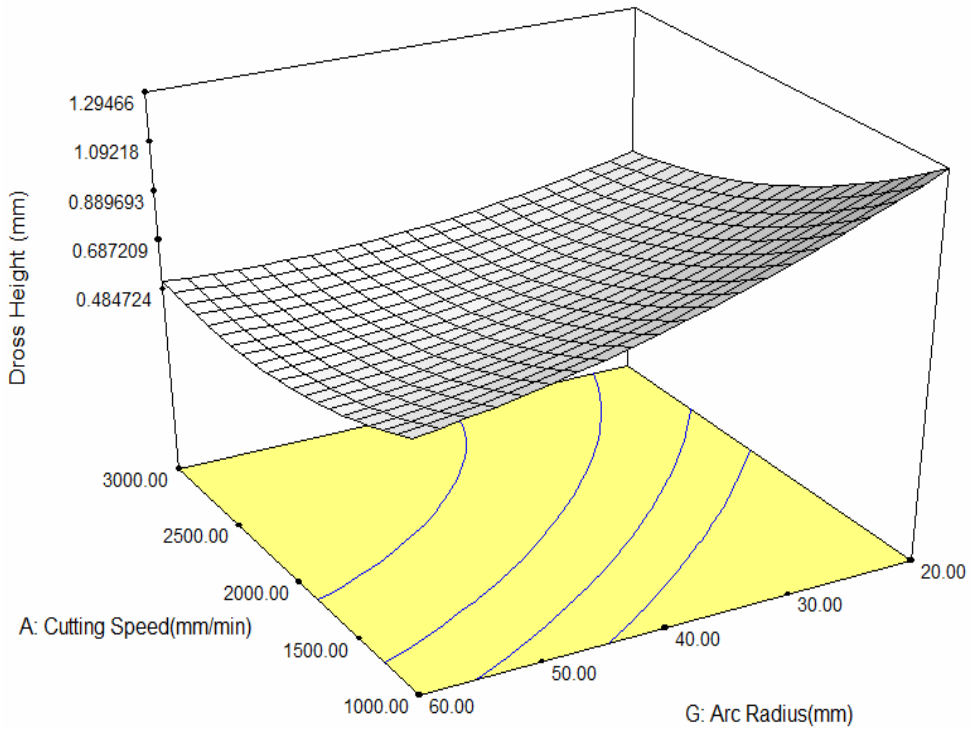

Figure 5.83 Interaction plot between laser power and reinforced particles for dross height

In order to examine the effect of various parameters on dross height, the perturbation plot has been depicted for the dross height as shown in figure 5.82. The deviation of the results can be predicted from reference point. The plot exhibits about the behavior of various input variables which are denoted by the different lines like X_1 (Cutting Speed), X_2 (Laser Power), X_3 (Nozzle Stand-off Distance), X_4 (Nozzle Diameter), X_5 (Gas Pressure), X_6 (% Reinforced Particles) and X_7 (Arc Radius). From the plot it can be easily predicted that dross height decreases with an increment in cutting speed from 1500 mm/min to 3000 mm/min. The value of D_t decreases slightly with increment in laser power from 1500 watt to 2500 watt. The middle values of nozzle distance and nozzle diameter found suitable for decreased values of D_t. With the increment in nitrogen gas pressure the D_t value decreased to higher extent. The lower arc radius proved to be significant for higher values of D_t. The arc of lower radius is of more circular in nature which caused the variation in dross height. Also with increase in percentage volume of reinforced particles the pattern of dross height reduces to lower rate. Because the presence of unburned Al_2O_3 develops more viscosity level resulted into restricted metal flow in downward direction. The interaction plot between laser power and reinforced particles for dross height is shown in figure 5.83. It was analyzed that at constant cutting speed of 1000 mm/min with decrease of arc radius from 60 to 20 mm the dross height increased to higher levels.

5.4.2 Effect of various process parameters on kerf taper

The effect of various input parameters is depicted in perturbation plot as shown in figure 5.84 for the kerf taper. It was analysed that cut arc of less radius has higher kerf taper as compared to arc of higher radius which also agrees with Rao R. et al.., (2009). With increase in cutting speed and gas pressure the kerf taper reduced to lower levels. The effect of nozzle distance not developed any positive results on the kerf taper. With increase in % volume of SiC reinforced particles (X_6) the kerf taper also increased to higher levels which may be caused due to temperature differences developed in between kerf zones resulted into large K_t value.

The interaction plot between gas pressure and arc radius for kerf taper is shown in figure 5.85. It was analyzed that at constant arc radius of 20 mm and gas pressure set to increase from 10 to 14 bar the kerf taper decreased to lower levels.

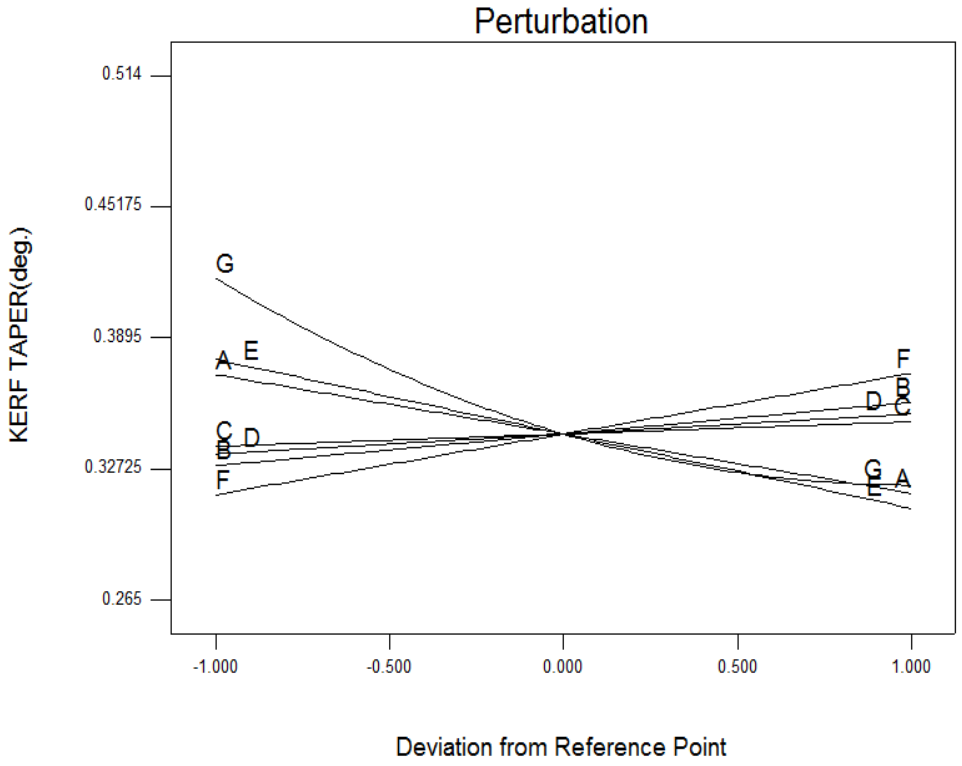

Figure 5.84 Perturbation plot of process parameters for kerf taper

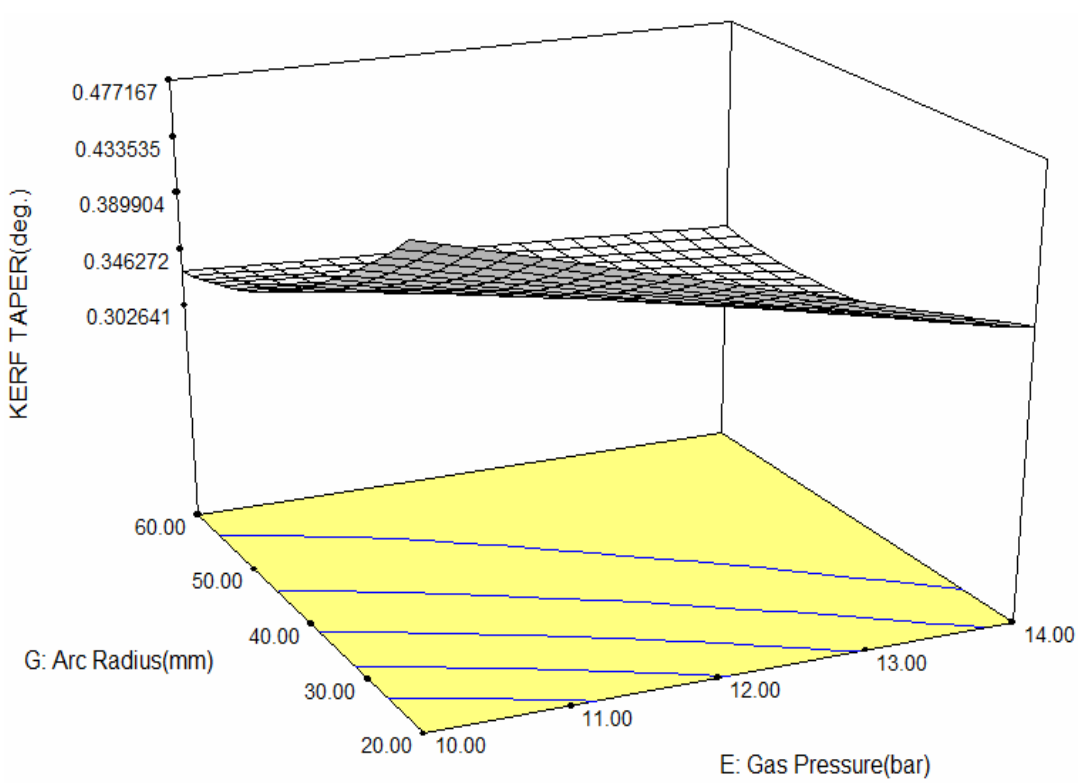

Figure 5.85 Interaction plot between gas pressure and arc radius for kerf taper

5.4.3 Effect of various process parameters on surface roughness

Surface finish is considered as important quality parameter for laser machined specimens. Surface finish, striation formation and crack propagation are related to each other which define the surface roughness of machined surface. From the perturbation plot of surface roughness as depicted in figure 5.86, the deviation from reference point of different variables can be easily explored. Here, the reference point is considered as deviation point through which the effect of various parameters can be analysed on the particular output response. It has been observed that with increment in cutting speed from 1000 mm/min. to 3000 mm/min. the R_z value reduced to significant levels. This mechanism of low roughness with increasing cutting speed also agreed with Dong et al.. 2009. The linearity of nozzle distance and diameter lines predict about less effect on R_z values. Only the lower values of both parameters found optimum for lower R_z values. With the increment in laser power from 1500 W to 2500 W the surface roughness decreased as sufficient energy is deported to cutting zone for clear cut. On the other hand, high gas pressure reduced the surface roughness of the cutting zone. The higher quantity of SiC reinforced particles (X_6) in specimen increases the roughness of the surface as depicted in the plot. It may be due to the presence of high quantity of ceramic particles modified the cutting front dynamics.

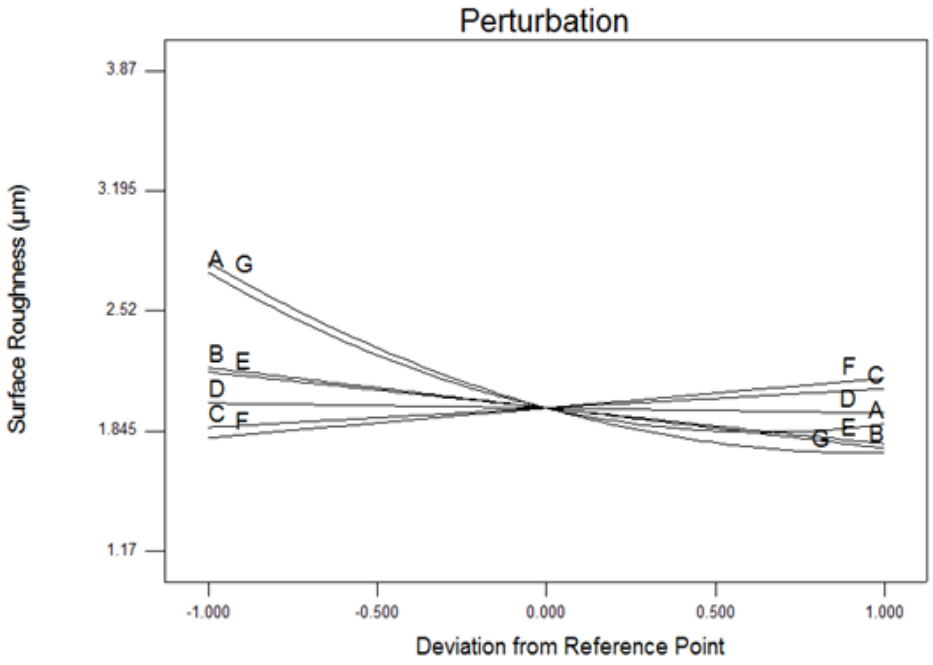

Figure 5.86 Perturbation plot of process parameters for surface roughness

The most significant factor for R_z value is cut profile arc radius. With decrease in arc radius upto20 mm the roughness of the surface increases dramatically as compare to 60 mm arc radius. The interaction plot between gas pressure and cutting speed for surface roughness is shown in figure 5.87. It was analyzed that when the gas pressure set constant at 14 bar and cutting speed set to increase from 1000 to 3000 mm/min the surface roughness decreased to lower levels. It may be due to combination og higher cutting speed and gas pressure able to drag out the molten material completely for better surface finish.

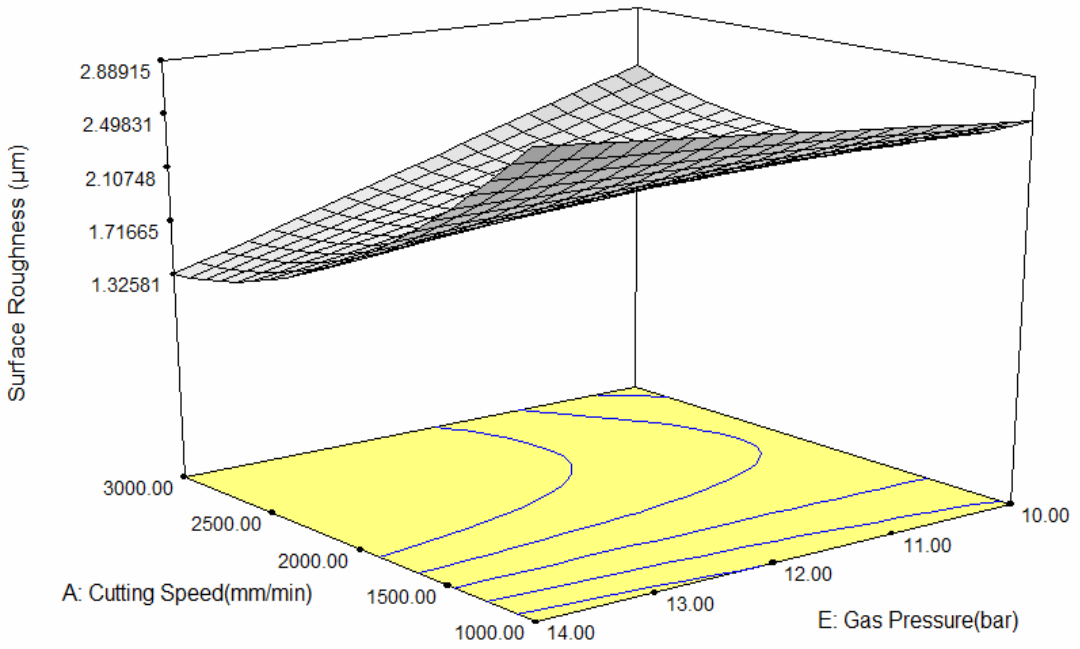

Figure 5.87 Interaction plot between cutting speed and gas pressure for surface roughness

5.4.4 Effect of various process parameters on kerf deviation

The significant and non-significant parameters can be observed from the perturbation plot as shown in figure 5.88 for the kerf deviation. The deviation of the results can be predicted from reference point on the plot. With increase in laser cutting speed from 1000 mm/min. to 3000 mm/min. the kerf deviation decreased to large extent due to less interaction time between specimen and laser beam. The value of K_d increases with increment in laser power from 1500 watt to 2500 watt. The nozzle diameter line has a mirror image from the centre point which depicted about non-significant parameter, also confirmed from the ANOVA results for kerf deviation.

The middle value of nozzle diameter found suitable for minimum K_d value. With the increase in gas pressure and percentage reinforced particles the deviation in the kerf also

increased to large limit. The unevenness in the kerf width increases due to presence of SiC particles and these particles remain in unburned state. Due to this proper exothermic reaction does not takes place which further gives rise to unevenness in kerf zone. The interaction plot between cutting speed and gas pressure for kerf deviation is shown in figure 5.89. It was analyzed that when the cutting speed set constant at 3000 mm/min and laser power increased 2500 watt the kerf deviation increased to 0.099 mm.

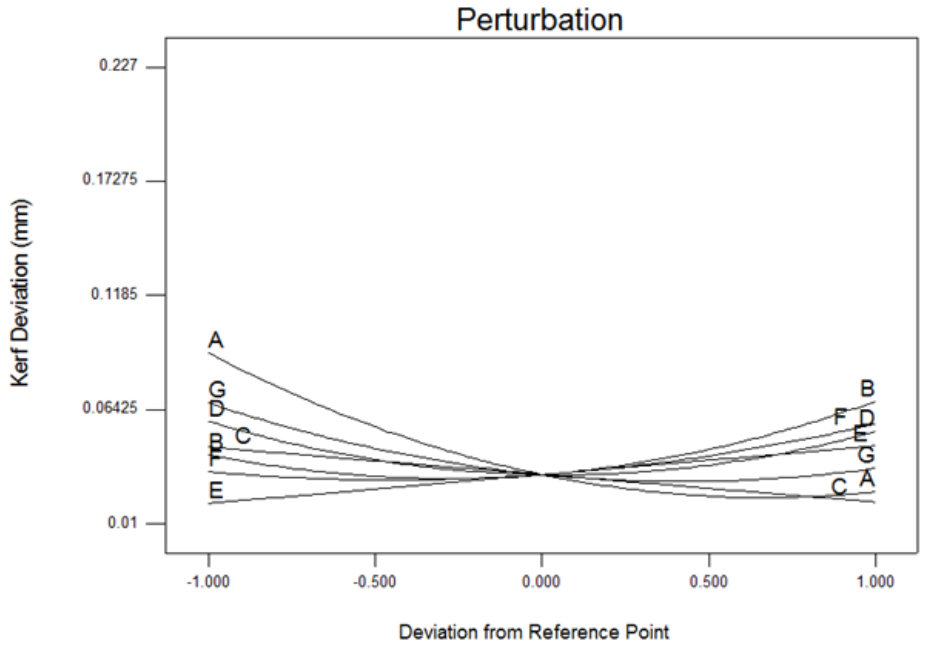

Figure 5.88 Perturbation plot of process parameters for kerf deviation

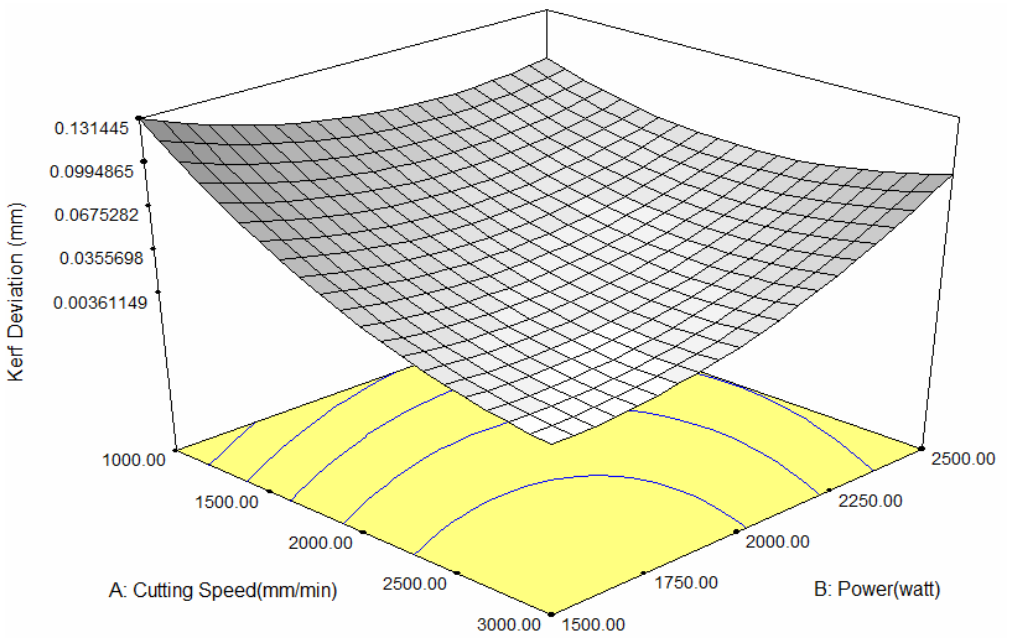

Figure 5.89 Interaction plot between cutting speed and gas pressure for surface roughness

5.4.5 Effect of various process parameters on heat affected zone width

To study the effect on heat affected zone width, the various parameters effects are depicted in the perturbation plot as shown in figure 5.90. The effect of various input parameters on heat affected zone width vary according to slope of the curves. It was observed that as the cutting speed increased from 1000 mm/min to 3000 mm/min the slope of cutting speed decreased to lower level which signifies reduction in HAZ width. With the increase in laser power, the HAZ width increases to higher levels. The distance between nozzle and specimen not proved to be significant as slope of standoff distance observed almost linear in nature. The slope of nozzle diameter decreases slightly to lower levels which signify the HAZ width has less significant effect of this factor. The increase in value of gas pressure shows that width decreases to lower variation.

From the plot it can also be observed that the increment in percentage Al_2O_3 particles exhibits higher slope resulted into larger width of HAZ. The heat affected width examined to be increased with the higher quantity of Al_2O_3 particles in vicinity of the kerf zone. The interaction plot between arc radius and laser power for heat affected zone width is shown in figure 5.91. From the interaction plot it can be analyzed that higher arc radius of 60 mm shown less heat affected zone width. When the arc radius set to 20 mm for the cut profile with constant laser power of 1500 watt, the heat affected zone width shown higher value of 349.913 µm.

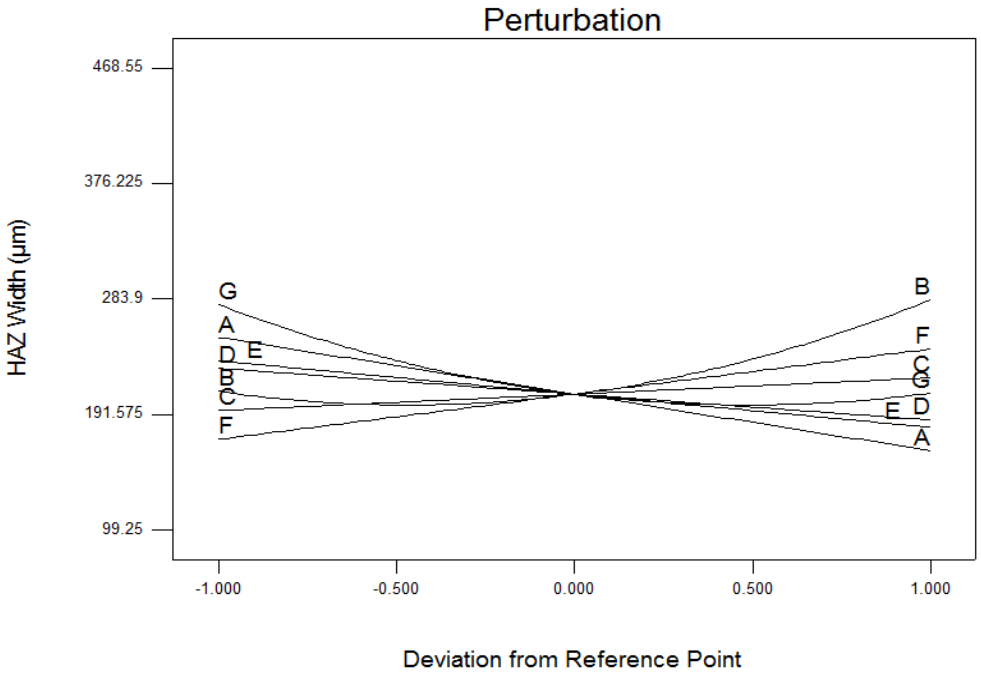

Figure 5.90 Perturbation plot of process parameters for HAZ width

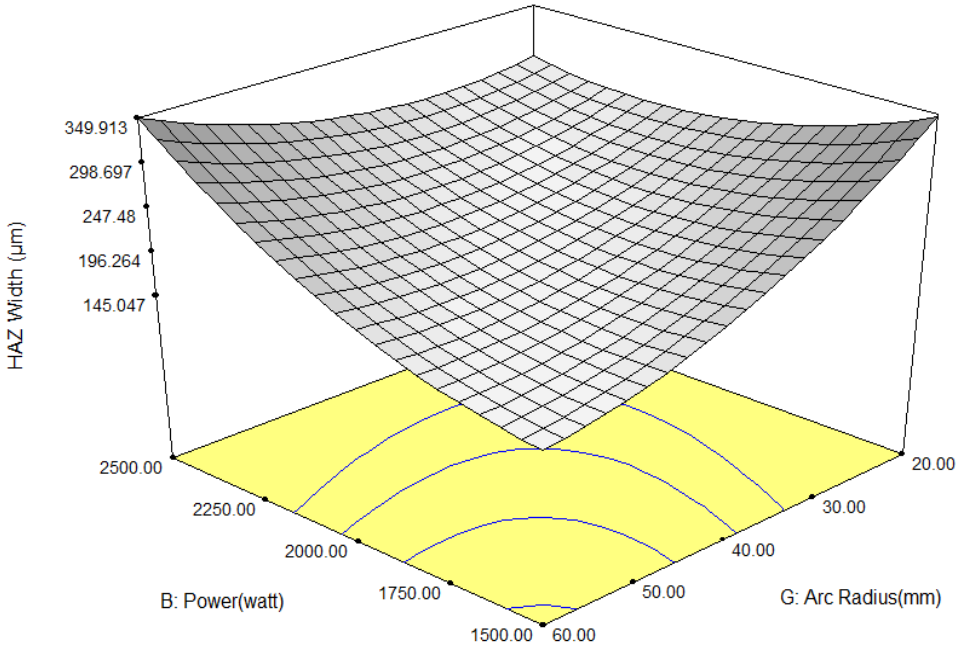

Figure 5.91 Interaction plot between cutting speed and gas pressure for HAZ width

5.4.6 Effect of various process parameters on striation angle

To analyze the effect on striations, the perturbation plot has been used as shown in figure 5.92. The slope of various input parameters cutting speed, laser power, standoff distance, nozzle diameter, gas pressure, Al_2O_3 particles and arc radius varied from the reference point. The effects of these variables have been analysed with the variation of slope of striation angle. From the plot, it was observed that striation angle increases with an increase in cutting speed from 1000 mm/min to 3000 mm/min. The value of α_s decreased with increment in laser power from 1500 watt to 2500 watt. The variation in slope of standoff distance was linear in nature which resulted into less effect on α_s values. The effects on α_s values were slightly increased with increment in nozzle diameter values from 1.4 mm to 2.0 mm. With the increment in nitrogen gas pressure, α_s values increased to higher levels. The increment in percentage of Al_2O_3 reinforced particles resulted into increase in striation angle pattern with large variation. The slope of arc radius shows a large variation from the reference point which is sign of significant factor. As the arc radius increased from 20 mm to 60 mm, the striation angle pattern decreased to lower levels. The interaction plot between arc radius and laser power for striation angle is shown in figure 5.93. The effect of laser power has not shown much significant effect on the variation of striation angle. It was examined that when the laser power set constant at

1500 watt and arc radius set to decrease from 60 to 20 mm the trend of striation angle increased to higher levels. It was explored that when the arc radius set at 20 mm radius the striation angle shown higher value of 7.28 degree which also resulted into higher surface roughness.

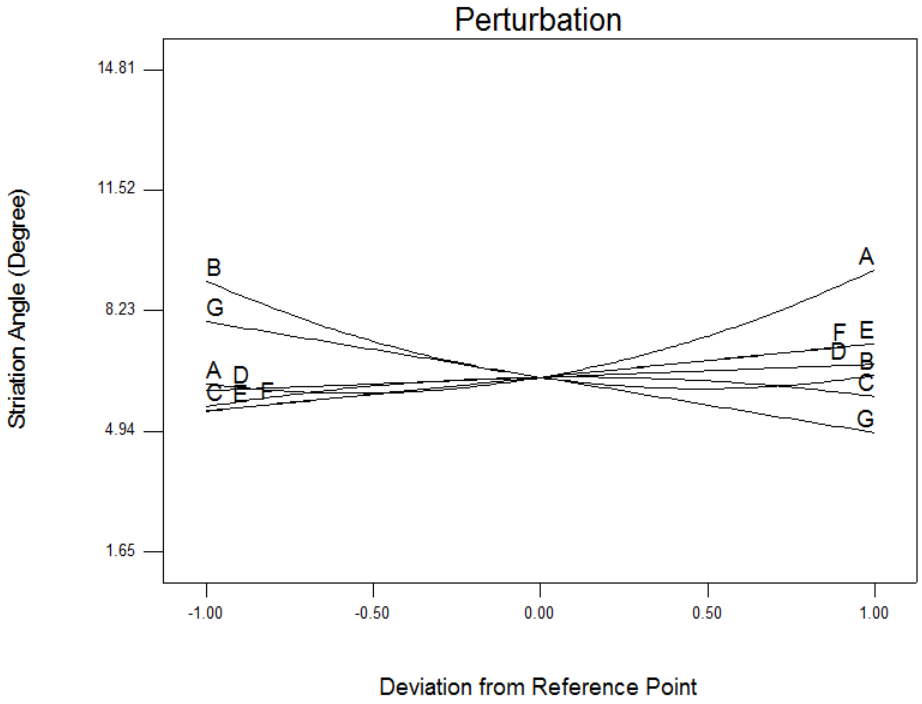

Figure 5.92 Perturbation plot of process parameters for striation angle

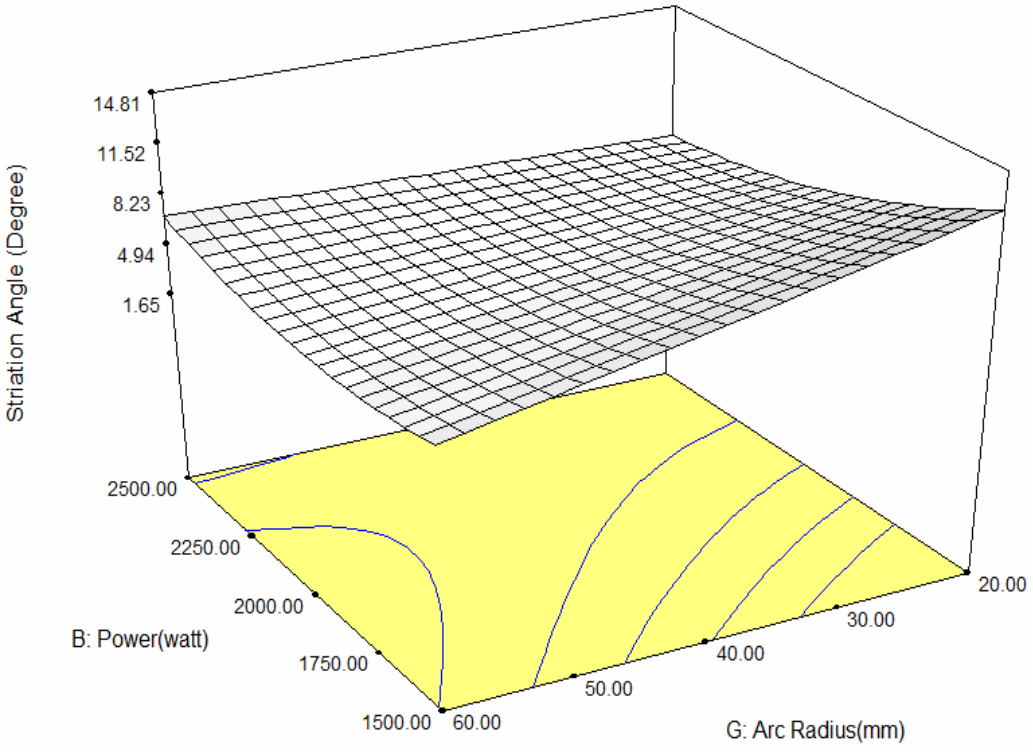

Figure 5.93 Interaction plot between cutting speed and gas pressure for striation angle.

5.4.7 Effect of various process parameters on material removal rate

The effect of input process parameters on material removal rate has been examined using perturbation plot as shown in figure 5.94. It was predicted when the cutting speed kept at 1000 mm/min the MRR reached to lower levels whereas when the cutting speed increased the MRR also increased to higher values. From the plot, the effect of laser power on material removal rate can be predicted. It was explored from the plot that with increase in laser power, the MRR also increased. With the increase in nozzle distance from 1.00 to 2.00 mm, the material removal rate increased to significant levels as shown in plot.

The same increasing trend has been analyzed with the nozzle diameter whereas with increase in nozzle diameter to 2.0 mm the MRR increased to some higher levels. The gas pressure predicted significant results for MRR. With the increase in gas pressure from 10 to 14 bar the material removal rate increased significantly. The most significant parameter effected the material removal rate is examined as quantity of reinforced Al_2O_3 particles. The decreasing slope of the curve of reinforced particles depicted the decrement of MRR. The lower material removal rate achieved may be due to the higher reinforced particles, as these particles absorb large amount of energy which is required for material removal process. Thus, remaining part of energy is not sufficient to achieve the higher removal rate from the kerf zone. The cutting profile also plays an important role in deciding the material removal rate. It has been analyzed that with increase in the curvature of cut profile the laser travel larger distance as compared to lower curvature path.

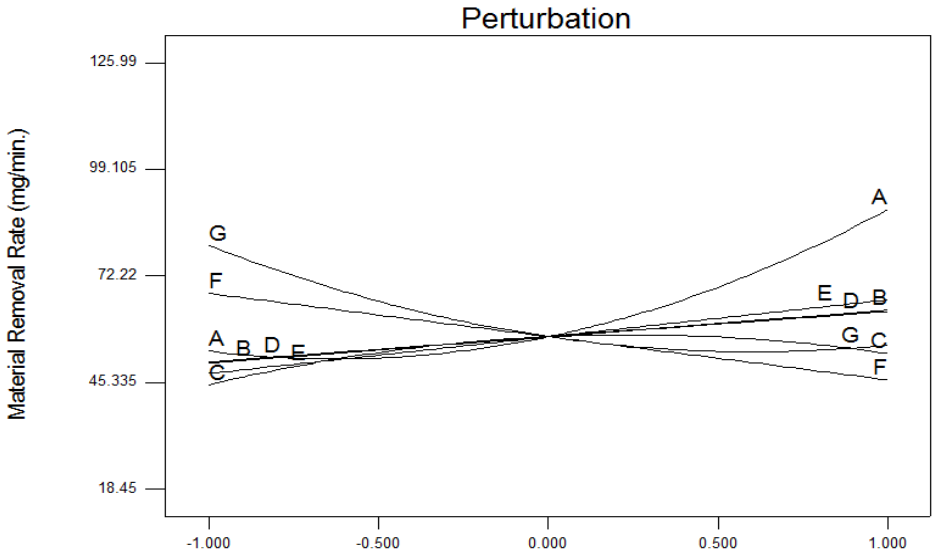

Figure 5.94 Perturbation plot of process parameters for MRR

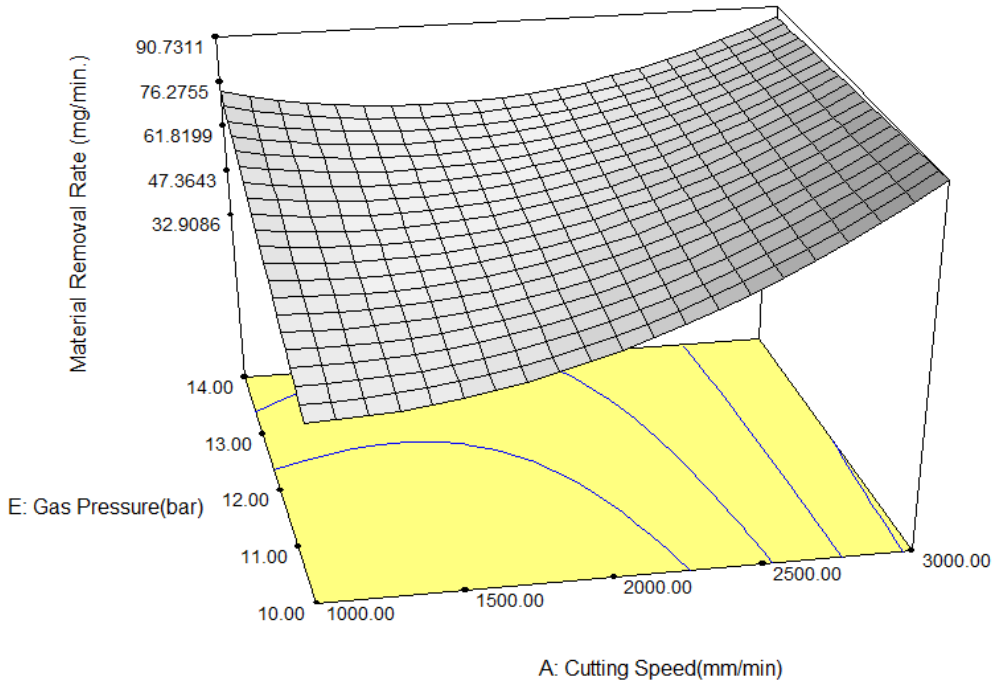

Figure 5.95 Interaction plot between cutting speed and gas pressure for MRR

The interaction plot between arc radius and laser power for striation angle is shown in figure 5.95. The effect of laser power has not shown much significant effect on the variation of striation angle. It was examined that when the laser power set constant at 1500 watt and arc radius set to decrease from 60 to 20 mm the trend of striation angle increased to higher levels.

5.4.8 Effect of various process parameters on energy losses

The main process parameters effects have been shown using perturbation plot as shown in figure 5.96 for the energy losses. The effect of cutting speed revealed that with increasing cutting speed the energy losses decreases to lower levels. When the laser power increased to maximum limit, the energy losses predicted with incremental values. The probable reason for this process may be the high power and low curvature cut in which power losses remains higher.

On the other hand, nozzle stand-off distance has not shown significant effect on the energy losses. The higher nozzle diameter has shown incremental energy losses as shown in plot. The nozzle diameter of 2.00 mm has shown higher impact on the energy losses due to occurrence of turbulence effect. The gas pressure has shown significant effect on energy losses. It may be due to exothermic reaction induced by the higher pressure which utilized maximum energy in the removal of molten material from kerf zone. The quantity

of reinforced particles has significant effect on energy losses. The presence of higher quantity of reinforced particles have higher accumulation of particles due to which conductive losses increases resulted into increase in power energy losses. The laser cut profile also has significant effect on the power energy losses. The energy loss increases with the more complicated path as laser has to travel large distance with low cutting speed.

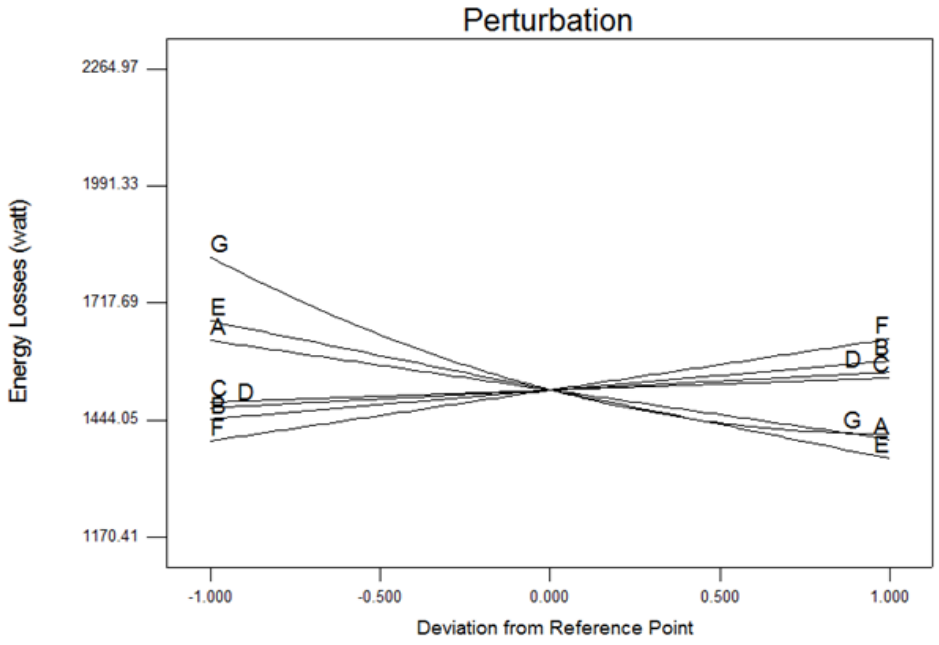

Figure 5.96 Perturbation plot of process parameters for energy losses

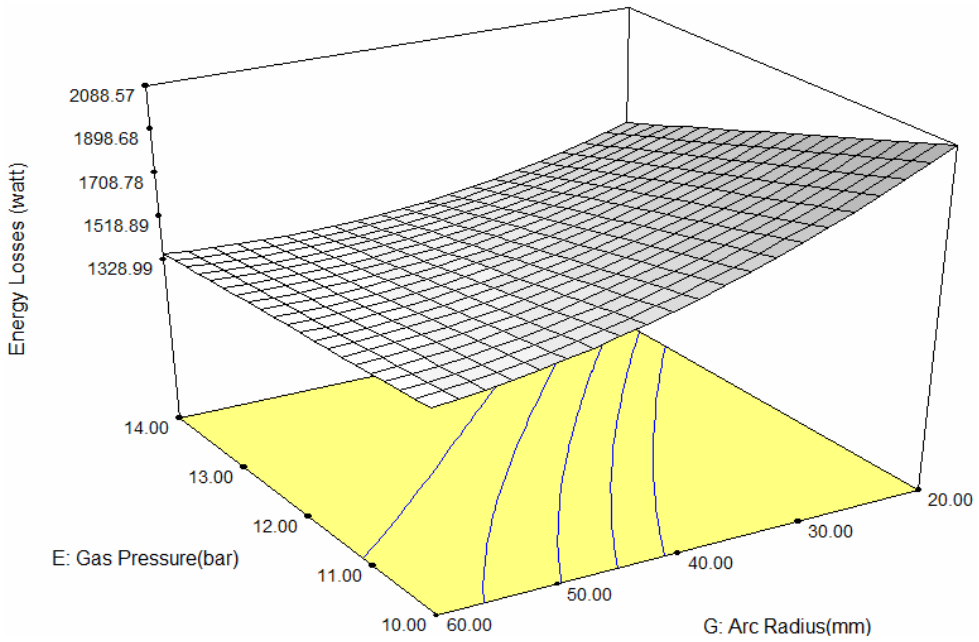

Figure 5.97 Interaction plot between cutting speed and gas pressure for energy losses

When the cut profile having arc radius of 20 mm the energy losses shown higher values. The significant effect has been examined with the help of the interaction plot between arc radius and gas pressure for energy losses as shown in figure 5.97. The effect of increasing gas pressure has not shown much significant effect on the variation of energy losses. It was examined that when the gas pressure set at 10 bar and arc radius set to decrease from 60 to 20 mm the trend of energy losses increased to higher levels.

5.5 EFFECT OF PROCESS PARAMETERS ON THE SPECIMEN Al5052/ZrO_2 USING PERTURBATION PLOTS

5.5.1 Effect of various process parameters on dross height

In order to examine the effect of control factors on dross height for the work material of Al5052/ZrO_2, the perturbation plot has been depicted as shown in figure 5.98. From the plot it can be easily predicted that dross height decreases with an increment in cutting speed. However, it can be examined that slope of curve is lower as compared to slope of the curve in case of specimens of Al5052/SiC, Al5052/Al_2O_3. The value of D_t decreases slightly with increment in laser power. The middle values of nozzle distance and nozzle diameter found suitable for decreased values of D_t. With the increment in nitrogen gas pressure the D_t value decreased to higher extent.

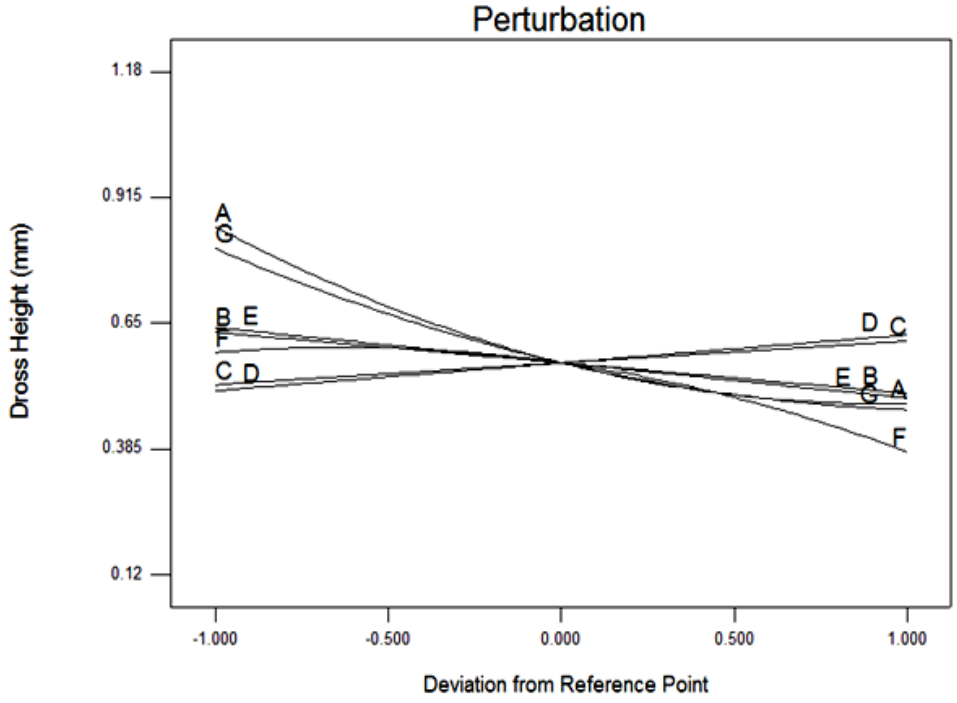

Figure 5.98 Perturbation plot of process parameters for dross height

The lower arc radius proved to be significant for higher values of D_t. The arc of lower radius is of more circular in nature which caused the variation in dross height. Also with increase in percentage volume of reinforced particles the pattern of dross height reduces to lower rate. It was analyzed that at constant cutting speed of 1000 mm/min with decrease of arc radius from 60 to 20 mm the dross height increased to higher levels.

5.5.2 Effect of various process parameters on kerf taper

It can be analyzed from the perturbation plot that the kerf taper has higher values as compared to values of the specimens Al5052/SiC, Al5052/Al_2O_3. The effect of various input parameters is depicted in perturbation plot as shown in figure 5.99 for the kerf taper. The increase in cutting speed from 1000 to 3000 mm/min shown lower values of kerf taper. It was analysed that cut arc of less radius has higher kerf taper as compared to arc of higher radius**.**

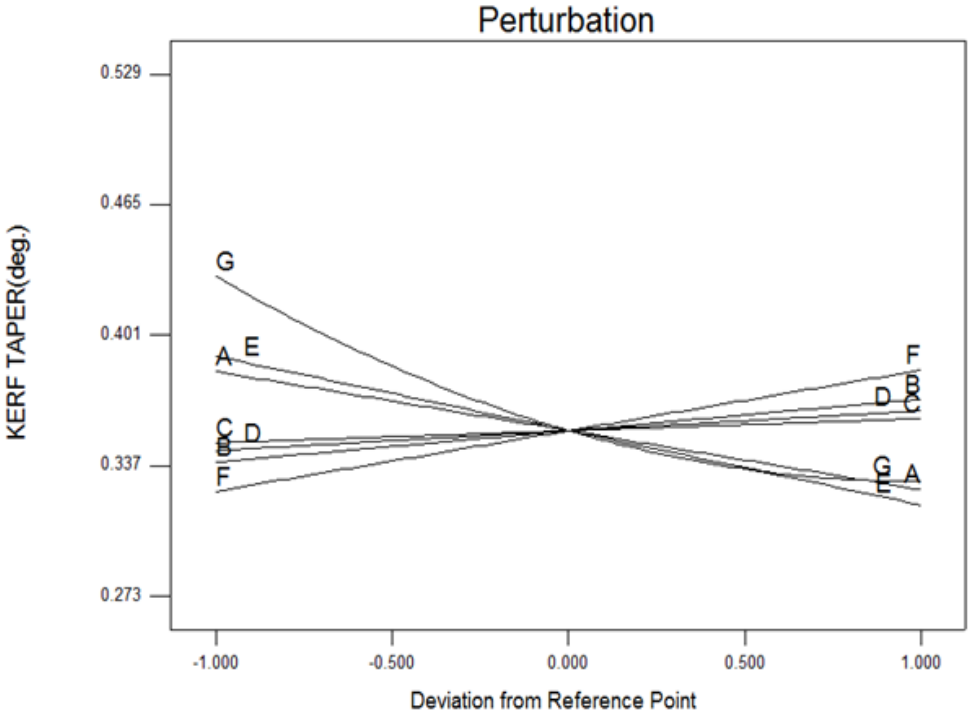

Figure 5.99 Perturbation plot of process parameters for kerf taper

With increase gas pressure the kerf taper reduced to lower levels. The effect of nozzle distance not developed any positive results on the kerf taper. With increase in percentage quantity of ZrO_2 reinforced particles the kerf taper also increased to higher levels which may be caused due to temperature differences developed in between kerf zones resulted into large K_t value.

5. 5.3 Effect of various process parameters on surface roughness

It has been observed that with increment in cutting speed from 1000 mm/min. to 3000 mm/min. the R_z value reduced to significant levels as shown in figure 5.100. The linearity of nozzle distance and diameter curves examined with lower effect on R_z values. With the increment in laser power the surface roughness decreased to lower levels as sufficient energy is deported to cutting zone for clear cut whereas high gas pressure reduced the surface roughness of the cutting zone. The higher quantity of ZrO_2 reinforced particles in specimen increases the roughness of the surface as depicted in the plot. The most significant factor for R_z value is cut profile arc radius.

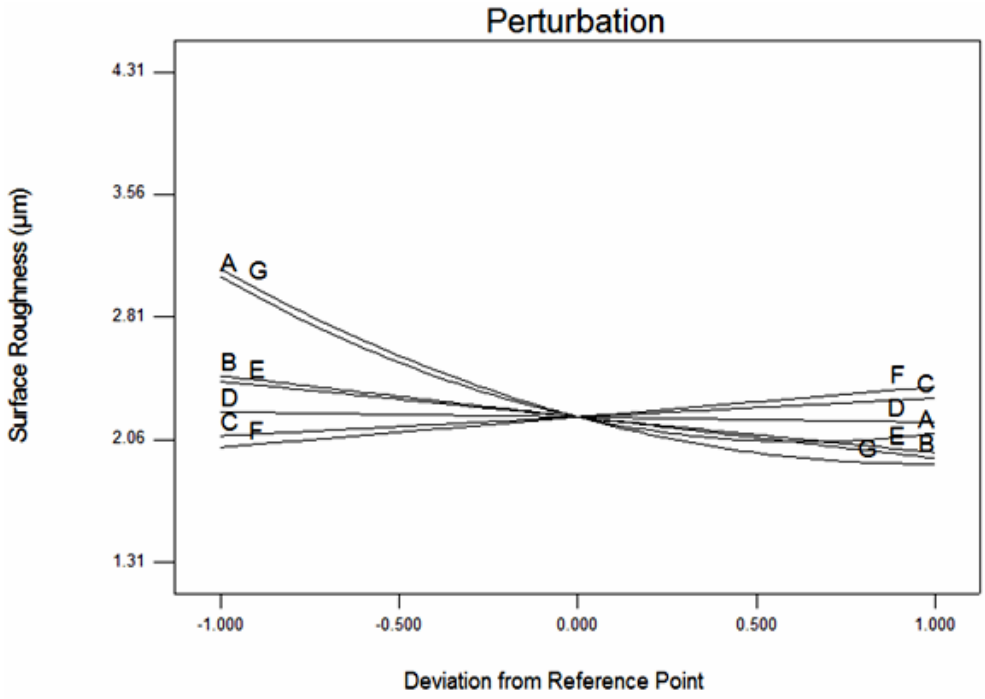

Figure 5.100 Perturbation plot of process parameters for surface roughness

With decrease in arc radius upto 20 mm the roughness of the surface increases dramatically as compare to 60 mm arc radius. It can be explored after comparing the slopes of the curves of various specimens that Rz values are in higher range for the specimen of Al5052/ZrO_2**.**

5. 5.4 Effect of various process parameters on kerf deviation

The variation of the results can be predicted from deviation point on the plot. With increase in laser cutting speed the kerf deviation decreased to higher levels as shown in figure 5.101. The value of K_d increases with increment in laser power. The nozzle distance has not shown any significant results for the variation of kerf deviation value.

The middle value of nozzle diameter found suitable for minimum K_d value. With the increase in gas pressure and percentage reinforced particles the deviation in the kerf also increased to large limit. The unevenness in the kerf width increases due to presence of ZrO_2 reinforced particles. The increase in arc radius from 20 mm to 60 mm shown decrement values of kerf deviation.

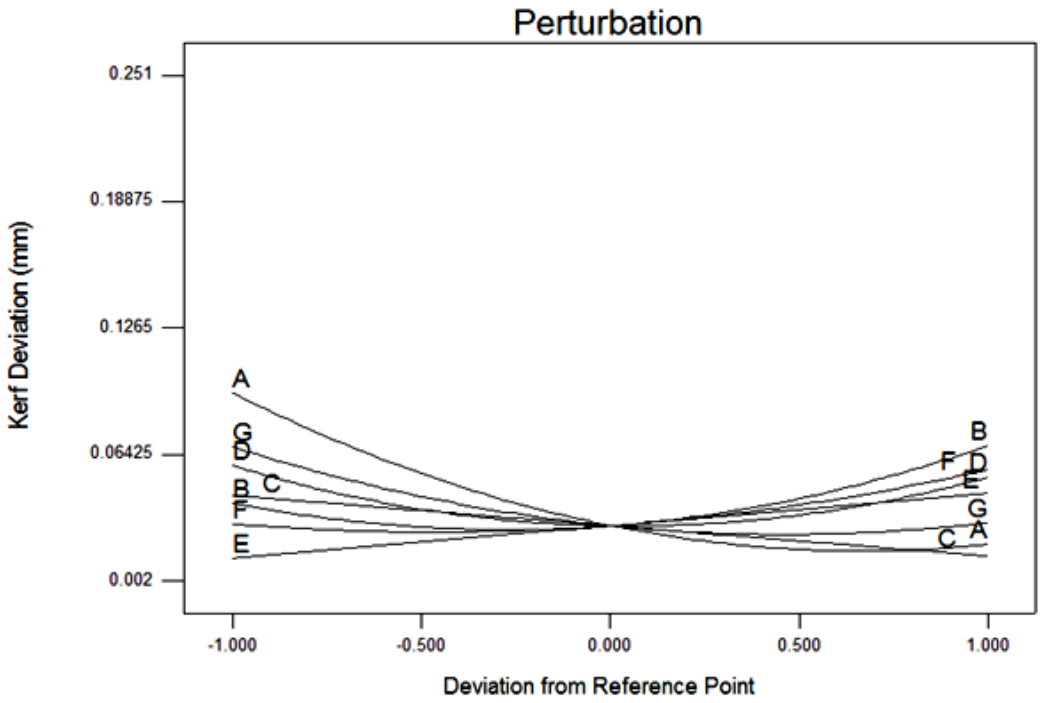

Figure 5.101 Perturbation plot of process parameters for kerf deviation

5. 5.5 Effect of various process parameters on heat affected zone width

The effect of various input parameters on heat affected zone width vary according to slope of the curves as shown in figure 5.102. It was observed that as the cutting speed increased the slope of cutting speed decreased to lower level which signifies reduction in HAZ width. With the increase in laser power, the HAZ width increases to higher levels. The distance between nozzle and specimen not proved to be significant as slope of standoff distance observed almost linear in nature. When the value of nozzle diameter decreases slightly to lower levels, HAZ width has not shown any significant effect of this factor. The increase in value of gas pressure shows that width decreases to lower variation. From the plot it can also be observed that the increment in percentage ZrO_2 particles exhibits higher slope resulted into larger width of HAZ. The heat affected width examined to be increased with the higher quantity of ZrO_2 particles in vicinity of the kerf zone.

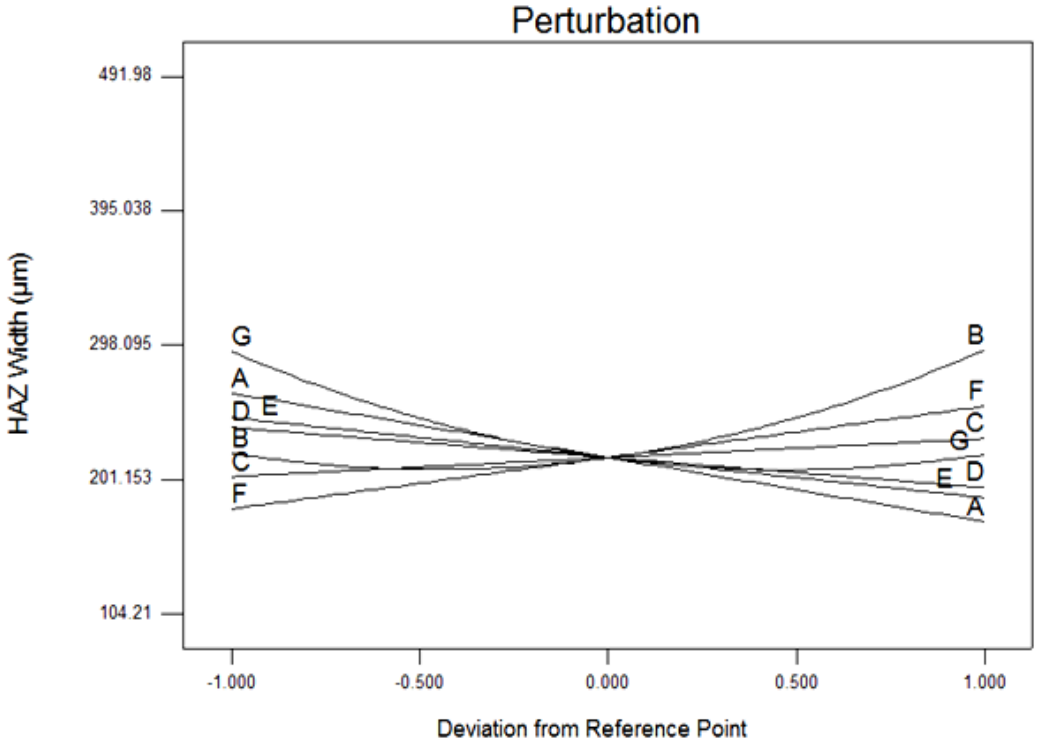

Figure 5.102 Perturbation plot of process parameters for HAZ width

5. 5.6 Effect of various process parameters on striation angle

From the plot as shown in figure 5.103, it was observed that striation angle increases with an increase in cutting speed. The value of striation angle decreased with increment in laser power. The variation in slope of standoff distance was linear in nature which resulted into less effect on α_s values.

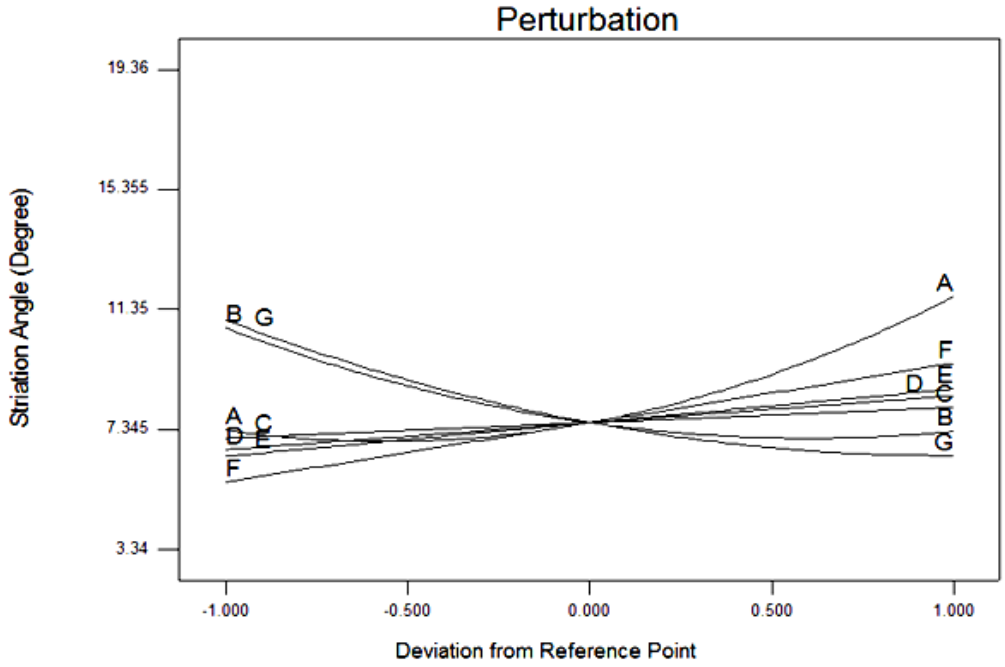

Figure 5.103 Perturbation plot of process parameters for striation angle

The effects on striation angle were slightly increased with increment in nozzle diameter values from 1.4 mm to 2.0 mm. With the increment in nitrogen gas pressure, α_s values increased to higher levels. The increment in percentage of ZrO_2 reinforced particles resulted into increase in striation angle pattern with large variation. The slope of arc radius shows a large variation from the reference point which is sign of significant factor.

5. 5.7 Effect of various process parameters on material removal rate

The increase in cutting speed improved the material removal rate to higher levels. It was examined from the plot that with increase in laser power, the material removal rate also increased as shown in figure 5.104. With the increase in nozzle distance from 1.00 to 2.00 mm, the material removal rate also increased to significant levels. The same increasing trend has been analysed with the nozzle diameter whereas with increase in nozzle diameter to 2.0 mm the MRR increased to some higher levels. The gas pressure predicted significant results for MRR.

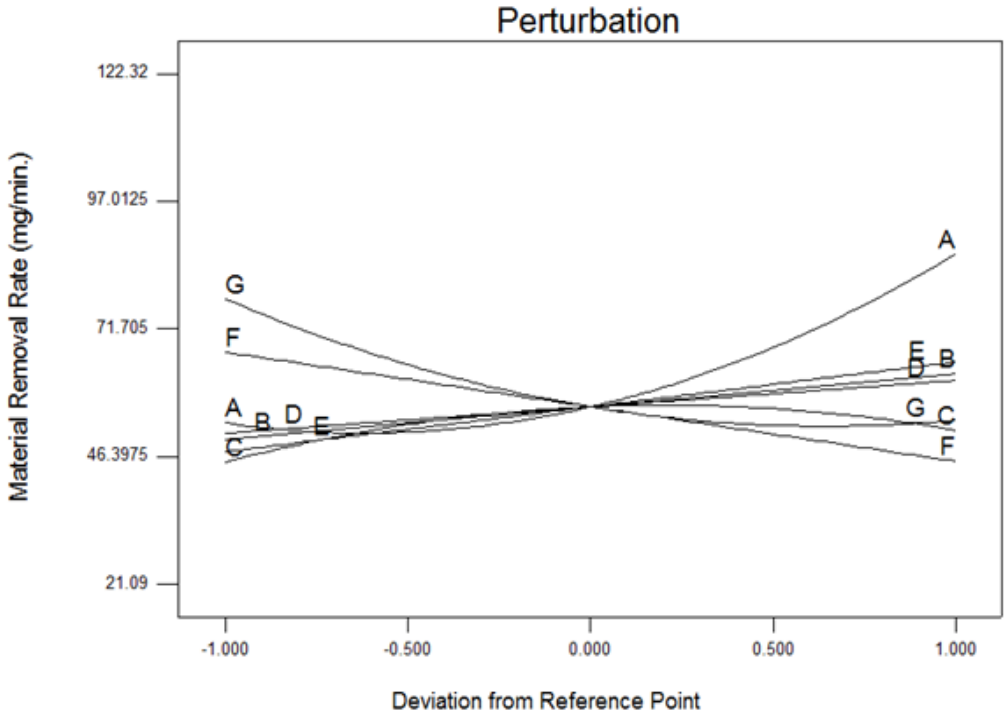

Figure 5.104 Perturbation plot of process parameters for MRR

With the increase in gas pressure the material removal rate increased significantly. The most significant parameter effected the material removal rate is examined as quantity of reinforced ZrO_2 particles. The decreasing slope of the curve of reinforced particles depicted the decrement of MRR. The lower material removal rate achieved may be due to the higher reinforced particles, as these particles absorb large amount of energy which is

required for material removal process. It has been analyzed that with increase in the curvature of cut profile the laser travel larger distance as compared to lower curvature path.

5. 5.8 Effect of various process parameters on energy losses

The energy losses decreases to lower levels with the increase in cutting speed as shown in perturbation plot of figure 5.105. When the laser power increased to maximum limit, the energy losses predicted with incremental values. The probable reason for this process may be the high power and low curvature cut in which power losses remains higher. On the other hand, nozzle stand-off distance has linearity of curve slope which not shown any significant effect on the energy losses. The higher nozzle diameter has shown incremental energy losses as shown in plot. The gas pressure has shown significant effect on energy losses. It may be due to exothermic reaction induced by the higher pressure which utilized maximum energy in the removal of molten material from kerf zone.

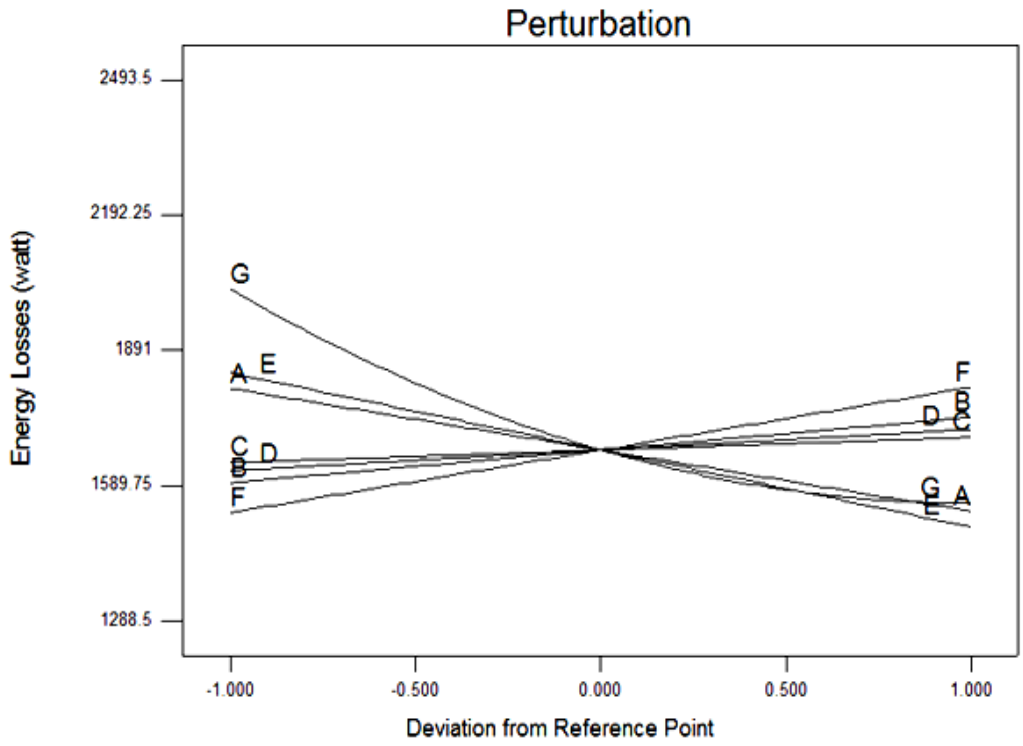

Figure 5.105 Perturbation plot of process parameters for energy losses

The quantity of reinforced particles has significant effect on energy losses. The laser cut profile also has significant effect on the power energy losses. When the cut profile having arc radius of 20 mm the energy losses shown higher values.

5.6 MULTI-RESPONSE OPTIMIZATION USING DESIRABILITY FUNCTION

For obtaining the optimized process parameters, various combinations have been determined for dross height, kerf taper and kerf width. With the help of desirability function approach, desirability value and target limit value of each parameter have been examined. A desirability function approach is one of the most important and useful approach due to its ability to perform simultaneous optimization for the process. By using this approach, target limit and desirability value of each input factor have been analysed. According to this approach, each input parameter has to be defined by individual desirability function (di) which varies between 0≤ di ≤1. If target value of di reaches to zero then it is considered as acceptable range.

In the present study, the Design Expert 6.0 software has been used to develop the RSM model. The optimized values of various input parameters have been determined with the help of predicted model. The output responses values have been minimized within the desired limit.To determine the optimized parameters with a large number of output responses become a typical work hence desirability function approach is applied to solve the purpose. This approach is also known by the name of simultaneous optimization technique.

The individual desirability can be determined as below when the response value is to be maximize:

The equation 5.18 is a geometric mean of all responses (d_1,d_2….d_n) which are transformed and equal to simultaneous objective function D

$$D=(d_1\times d_2\times d_3\times \ldots\ldots\ldots\ldots\ldots\times d_n)^{1/n}=\left(\prod_{i=1}^{n} di\right)^{1/n} \quad \ldots\ldots\ldots\ldots\ldots(5.18)$$

Where, n is the number of responses in the measure.

Each response must be represented by high and low value linked with each goal. Here the Goal for different responses must have five options to select like in range, none, maximum, minimum and target. Each input variable of the process for the optimization must have design range by maximum, minimum and default of target goal.

The optimization for a particular process is considered by following points:

i. To obtain the value of‘d’ for every response.
ii. Summation of all the individual desirabilities.
iii. To combine the composite desirability (D); and

iv. To get the maximum value of 'D' and to obtain the optimal input parameters settings.

The goal parameters can be easily understand by following form :

Maximum

di = 0 if response < low value

1≤di≤0 as response varies from low to high

di = 1 if response > high value

Minimum:

di = 1 if response < low value

1 ≥ di ≥ 0 as response varies from low to high

di = 0 if response > high value

Target:

di = 0 if response < low value

0 ≤di ≤ 1 as response varies from low to target

1 ≥di ≥ 0 as response varies from target to high

di = 0 if response > high value

Range:

di = 0 if response < low value

di = 1 as response varies from low to high

di = 0 if response > high value

The total desirability is considered with maximum value for various process optimal parameter settings. The desirability function is applied to examine the optimum parameter combinations for optimization of dross height, kerf taper, edge surface roughness, kerf deviation, striations, heat affected zone width, material removal rate, energy losses.

Table 5.17 shows the constraints for performing the optimization of quality characteristics such as dross height, kerf taper, edge surface roughness, kerf deviation, striations, heat affected zone width, material removal rate, energy losses. To examine the influence of each output response on individual desirability, the target value and limits for process parameters are developed by considering the conditions of goals to maximize or minimize. The target value is given importance by the assigned weights after considering the upper and lower bounds. The default value '3' and '4' assigned via design expert software to consider the objective function importance.

Table 5.17 Constraints of input parameters and responses

Parameters	Target	Lower limit	Upper limit	Lower weight	Upper weight	Importance
Cutting Speed	is in range	1000	3000	1	1	3
Power	is in range	1500	2500	1	1	3
Nozzle Distance	is in range	1	2	1	1	3
Nozzle Diameter	is in range	1.4	2	1	1	3
Gas Pressure	is in range	10	14	1	1	3
% Reinf.Particles	is in range	0	20	1	1	3
Arc Radius	is in range	20	60	1	1	3
Dross Height	minimize	0.14	1.33	1	1	4
KERF TAPER	minimize	0.257	0.498	1	1	3
Surface Roughness	minimize	1.21	3.99	1	1	4
Kerf Deviation	minimize	0.011	0.26	1	1	3
Striation Angle	minimize	2.785	15.54	1	1	3
HAZ Width	minimize	97.29	459.3	1	1	4
Material Removal Rate	maximize	19.36	132.2	1	1	3
Energy Losses	minimize	1182.1	2287.6	1	1	3

The experimental data is used for performing the multi-objective optimization by considering the various process parameters. The constraints, target values of input parameters and responses are tabulated in table 5.17. The application of desirability functional approach provides the different optimum levels of input parameters. Further the predicted and experimental results were compared to find out the percentage error. The confirmatory experiments were executed to validate the adequacy of the predicted model. It was analyzed that both predicted model and experimental results were reasonable agreed with minimal difference. Different input optimized variables combinations for high value of desirability are shown in table 5.18 and 5.19. From the RSM model 25 optimal desirability solutions has been predicted for the various output responses. Out of 25 predicted experiments, various experiments were selected and performed to analyze the percentage error. From the plot it is seen that desirability values lies approximate along a straight line with respect to increasing experimental numbers. The approximation of each curve with respect to each other shows the less difference in percentage error values.

Table 5.18 Optimal solutions for dross height, kerf taper, surface roughness and kerf deviation

Exp. No.	X_1	X_2	X_3	X_4	X_5	X_6	X_7	D_t	K_t	R_z	K_d	Desirability
1	3000	2263	1.2	1.4	13	0.00	60	0.350	0.246	0.233	0.085	0.893
2	2971	2206	1.1	1.5	13	0.00	60	0.382	0.257	0.424	0.065	0.892
3	3000	2202	1.0	1.4	12	0.00	60	0.438	0.258	0.456	0.069	0.892
4	2999	2293	1.0	1.5	13	0.69	60	0.373	0.258	0.347	0.087	0.892
5	2960	2232	1.5	1.5	14	0.00	60	0.269	0.236	0.106	0.080	0.889
6	3000	2273	1.6	1.4	14	0.73	60	0.227	0.228	0.061	0.085	0.888
7	3000	2188	1.5	1.6	14	0.00	60	0.307	0.249	0.188	0.064	0.888
8	3000	2310	1.5	1.5	14	0.02	54	0.252	0.232	0.151	0.093	0.886
9	3000	2330	1.0	1.6	13	0.28	58	0.366	0.261	0.527	0.077	0.885
10	3000	2208	1.4	1.6	14	0.00	60	0.308	0.258	0.207	0.068	0.885
11	3000	2183	1.4	1.6	14	0.27	60	0.345	0.260	0.344	0.061	0.883
12	3000	2166	1.0	1.6	14	0.03	60	0.343	0.258	0.333	0.071	0.881
13	3000	2098	1.0	1.6	12	0.00	58	0.415	0.268	0.746	0.033	0.881
14	3000	2240	1.0	1.7	12	0.00	58	0.384	0.271	0.795	0.048	0.875
15	3000	2119	1.9	1.5	14	0.18	49	0.236	0.226	0.336	0.055	0.868
16	2959	2185	1.8	1.7	14	0.00	52	0.347	0.257	0.362	0.060	0.860
17	3000	2156	2.0	1.4	14	0.00	43	0.247	0.221	0.604	0.064	0.850
18	2986	1999	1.0	1.7	14	0.00	51	0.311	0.247	0.569	0.060	0.846
19	2548	1986	2.0	1.6	14	0.31	60	0.358	0.258	0.517	0.034	0.836
20	2996	2273	1.0	2.0	11	0.00	50	0.327	0.277	1.320	0.078	0.834
21	2998	2408	1.0	1.7	12	1.71	40	0.359	0.270	1.210	0.105	0.829
22	3000	2092	2.0	1.4	14	15.78	52	0.102	0.261	1.304	0.037	0.817
23	3000	1689	1.0	1.9	12	0.02	48	0.362	0.268	1.340	0.038	0.808
24	3000	2444	1.5	1.4	14	12.84	35	0.208	0.299	1.256	0.134	0.770
25	2112	2500	2.0	1.4	14	9.02	42	0.174	0.275	1.368	0.105	0.759

Multi-optimal variable settings recorded for output parameters are tabulated in table 5.18 and 5.19. It was investigated that percentage error for all the output responses lies in between the range of 7 % which confirms the validation of predicted optimal model. Figure 5.106 depicted the 3D surface plot of composite desirability for all responses using two parameters such as cutting speed and laser power.

Table 5.19 Optimal solutions for striation angle, HAZ width, MRR and energy losses

Exp. No.	X_1	X_2	X_3	X_4	X_5	X_6	X_7	S.A	HAZ	MRR	E.L	Desirability
1	3000	2263	1.2	1.4	13	0.00	60	5.92	97.31	123.784	1130.28	0.893
2	2971	2206	1.1	1.5	13	0.00	60	5.88	97.30	115.559	1179.93	0.892
3	3000	2202	1.0	1.4	12	0.00	60	5.48	107.99	122.464	1182.11	0.892
4	2999	2293	1.0	1.5	13	0.69	60	5.86	97.30	125.99	1183.04	0.892
5	2960	2232	1.5	1.5	14	0.00	60	6.34	97.30	114.298	1081.55	0.889
6	3000	2273	1.6	1.4	14	0.73	60	6.29	118.79	118.095	1043.97	0.888
7	3000	2188	1.5	1.6	14	0.00	60	6.61	97.30	111.876	1142.6	0.888
8	3000	2310	1.5	1.5	14	0.02	54	6.63	97.31	120.163	1062.18	0.886
9	3000	2330	1.0	1.6	13	0.28	58	5.63	132.88	124.099	1197.78	0.885
10	3000	2208	1.4	1.6	14	0.00	60	6.76	99.20	112.945	1182.15	0.885
11	3000	2183	1.4	1.6	14	0.27	60	6.60	97.31	110.958	1193.46	0.883
12	3000	2166	1.0	1.6	14	0.03	60	6.46	46.61	111.066	1182.11	0.881
13	3000	2098	1.0	1.6	12	0.00	58	5.98	97.92	104.586	1229.22	0.881
14	3000	2240	1.0	1.7	12	0.00	58	5.54	138.52	112.11	1243.25	0.875
15	3000	2119	1.9	1.5	14	0.18	49	7.80	97.31	98.416	1036.05	0.868
16	2959	2185	1.8	1.7	14	0.00	52	7.64	128.07	108.77	1179.57	0.860
17	3000	2156	2.0	1.4	14	0.00	43	7.87	135.50	98.749	1013.22	0.850
18	2986	1999	1.0	1.7	14	0.00	51	7.92	2.21	91.362	1134.59	0.846
19	2548	1986	2.0	1.6	14	0.31	60	6.75	151.52	81.417	1182.18	0.836
20	2996	2273	1.0	2.0	11	0.00	50	6.14	118.77	95.3146	1271.71	0.834
21	2998	2408	1.0	1.7	12	1.71	40	7.12	133.15	111.891	1238.23	0.829
22	3000	2092	2.0	1.4	14	15.78	52	9.14	97.30	72.314	1196.07	0.817
23	3000	1689	1.0	1.9	12	0.02	48	8.56	29.18	78.663	1230.29	0.808
24	3000	2444	1.5	1.4	14	12.84	35	9.17	138.01	116.18	1369.78	0.770
25	2112	2500	2.0	1.4	14	9.02	42	6.73	239.77	79.4385	1259.85	0.759

Figure 5.107 shows the ramp graph for various optimized input parameters values within the desired range of output quality characteristics. From graph, it can be observed that HAZ, kerf taper, energy losses, material removal rate and surface roughness has maximum desirability whereas striation angle and kerf deviation has less value as compared to other output responses. The various limit values of input parameters and output responses are shown in table 4. The upper limit for the striation angle, heat

affected zone and kerf deviation was observed as 18.659˚, 491.98 µm and 0.251 mm respectively. The comparison of predicted and experimental values is shown using percentage error method as shown in table 5.20. The bar graph shows the desirability values of all output responses as shown in figure 5.108.

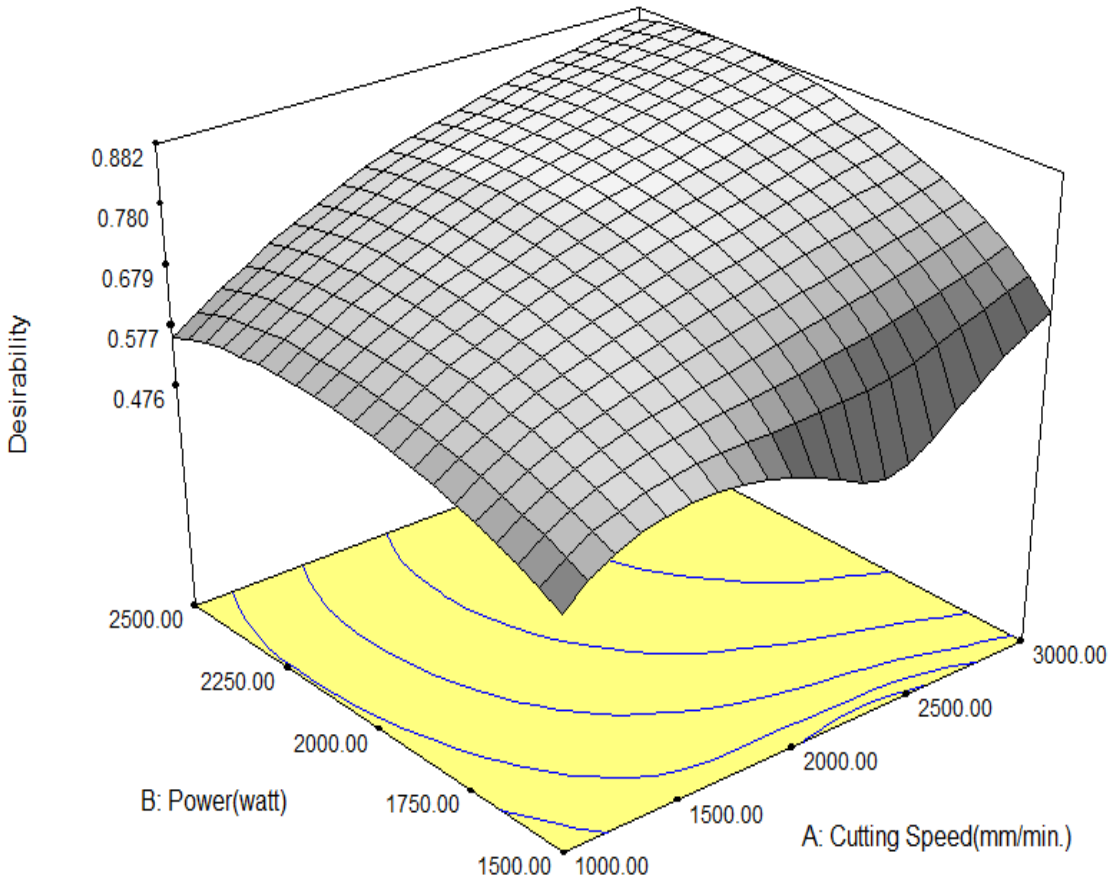

Figure 5.106 3D surface plot of composite desirability for all responses

Table 5.20 Experimental validations of developed models with optimal parameter settings

Responses		Predicted	Experimental	Error (%)	Desirability
Dross Height	(mm)	0.146	0.140	4.10	0.828
Kerf taper	(deg.)	0.233	0.224	4.137	0.989
Surface roughness	(µm)	1.25	1.210	3.2	0.981
Kerf Deviation	(mm)	0.0148	0.014	5.4	0.651
Striation Angle	(deg.)	3.09	3.35	7.76	0.763
HAZ	(µm)	104.2	110.50	5.70	0.984
MRR	(mg/min)	79.4385	84.56	6.06	0.688
Energy losses	(watt)	1130.28	1209.36	6.53	0.665

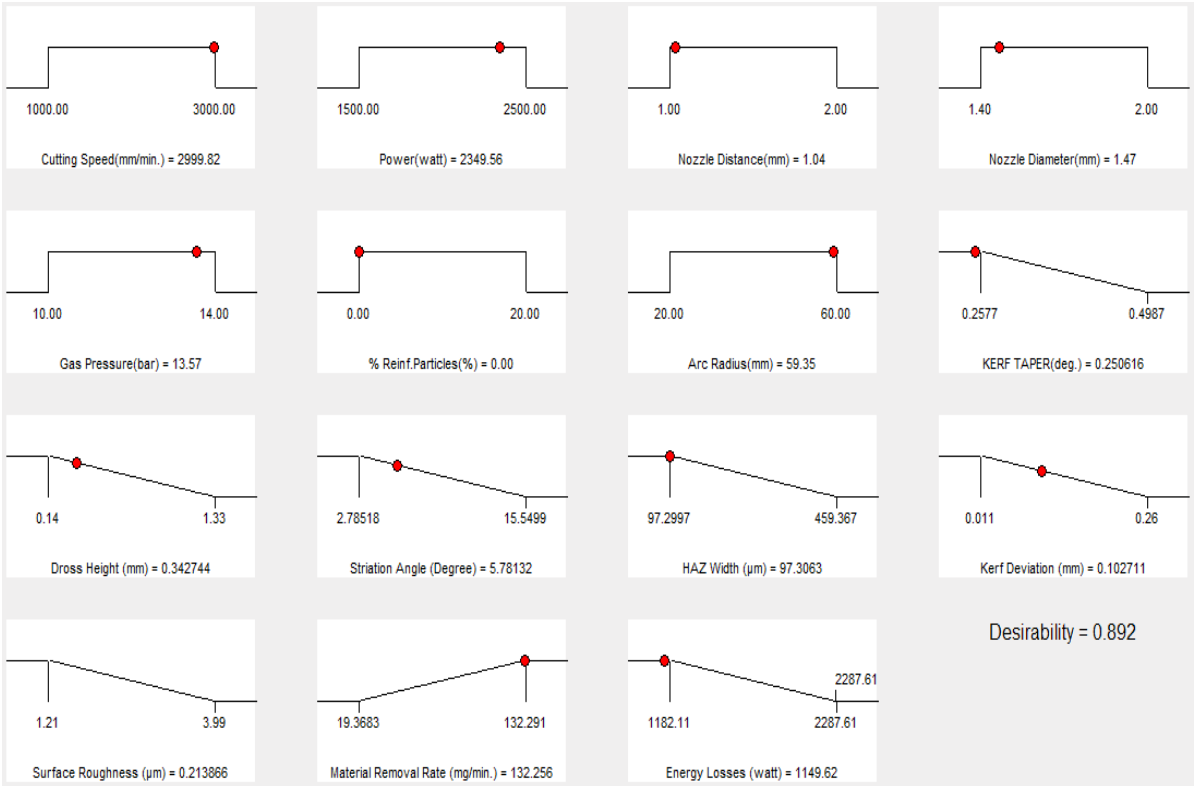

Figure 5.107 Ramp graph of optimal setting for all responses

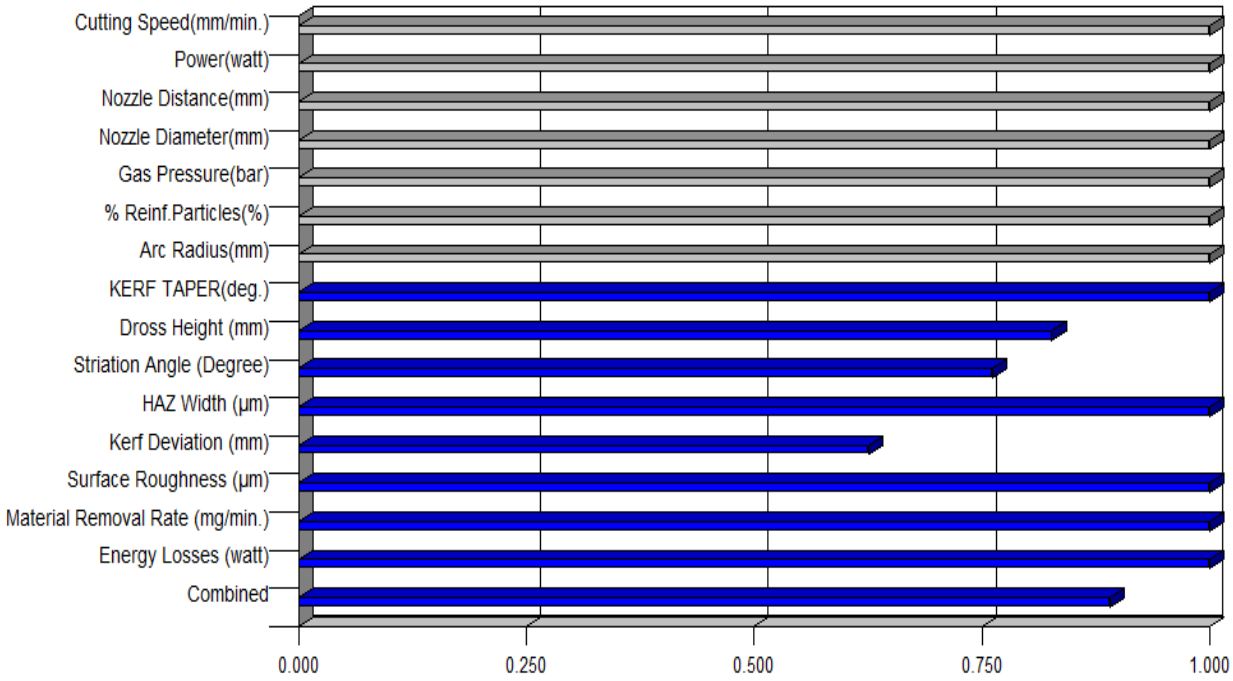

Figure 5.108 Bar histogram plot of composite desirability for all responses

5.7 MICROSTURCTURE ANALYSIS OF MACHINED SURFACES

The thermal behavior of aluminium metal matrix material changes after machining with laser beam machining process due to different melting point of base metal aluminium 5052 and reinforced particles. It is necessary to identify the machining parameters which affect the quality of the machined surface. The various experimental results has shown that cutting speed, laser power, reinforced particles and arc radius are the most significant parameters for all the output responses. Laser beam machining is thermal cutting process; due to this machined specimens may have variation in microstructure properties. Stress concentration is a basic process for the development of crack formation. It may occur when it exceeds the plastic deformation and fracture strength of material. Further the development of micro-cracks can be caused by machining parameters and different material properties like thermal expansion coefficient, thermal conductivity, tensile strength and Young's modulus. In case of aluminium alloy MMCs material reinforced with SiC particles the crack formation is associated with un-burned particles. These un-burned SiC particles cause the de-bonding between constituents which further enhances the crack formation on the machined surface. In addition to that, higher surface roughness may promote stress concentration resulted into crack formation which spoils the quality of the surface. The presence of un-burned SiC particles can be seen on the cut edge surface as depicted in figure 5.109 (a). When the laser beam displaces and cut the edge, the molten material flows from top to bottom direction. Higher surface roughness and dross height occurs when the viscosity and surface tension of the molten material increases due to unburned SiC particles. Due to this nature the chances of restricted flow increases which resulted into increment in striation formation as depicted in figure 5.109 (a). Figures 5.110(a, b), 5.111 (a) exhibits the formation of micro-cracks and recast layer on the laser cut surfaces. The tendency of crack formation and recast layer increases due to presence of ceramic particles in the vicinity of the surfaces and low nitrogen gas pressure. As low gas pressure not able to create the sufficient drag force to expel out the molten material with unburned SiC particles. Consequently, the development of large number of cracks and voids on the cut edge surface formed. The presence of SiC particles were seen in vicinity of recast layer when MMC specimen was machined by laser beam machining and electric discharge machine. Figure 5.111 (b) reflects the top section of cut edge where the displacement of SiC particles has been noticed.

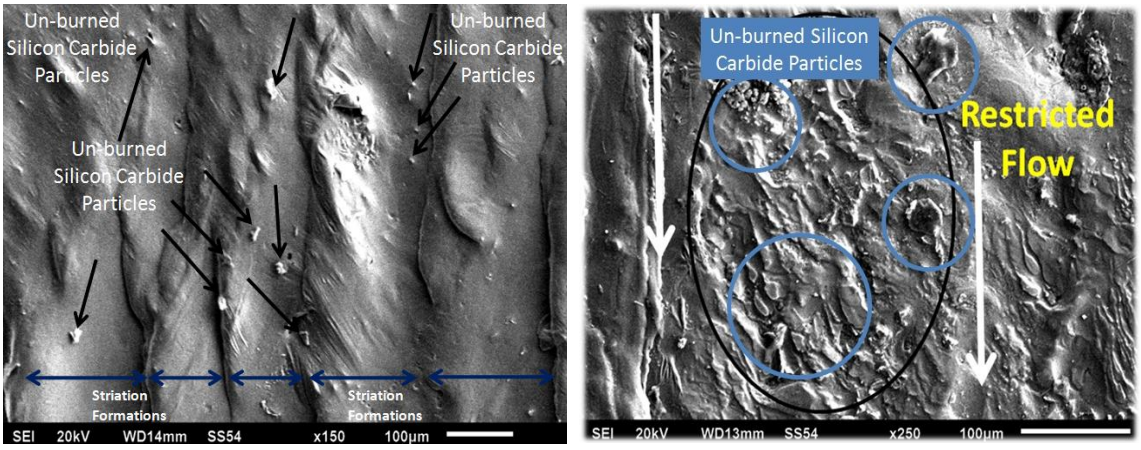

a) b)

Figure 5.109 SEM micrograph showings striation formation due to restricted flow (a) unburned particles (b)

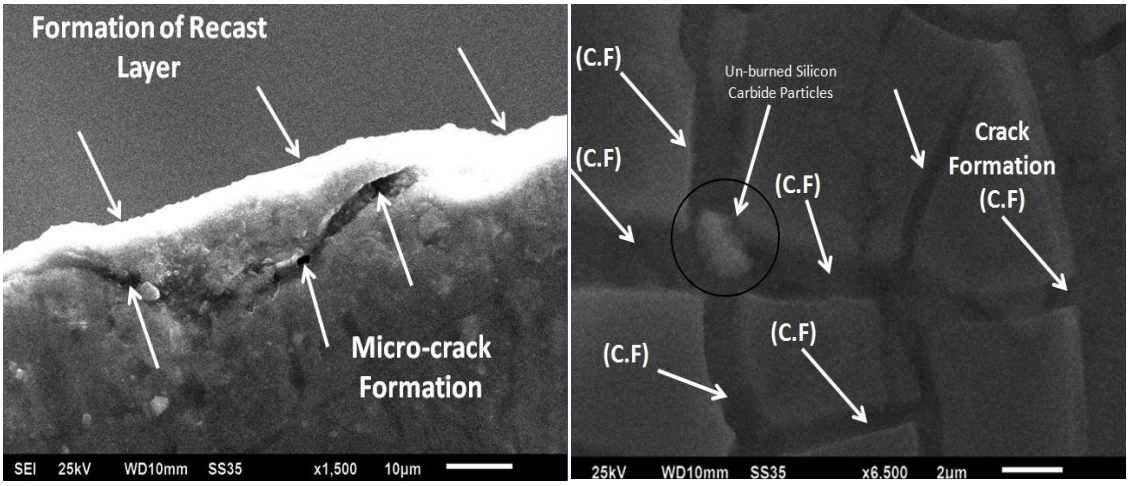

a) b)

Figure 5.110 Crack and recast layer formation(a, b)

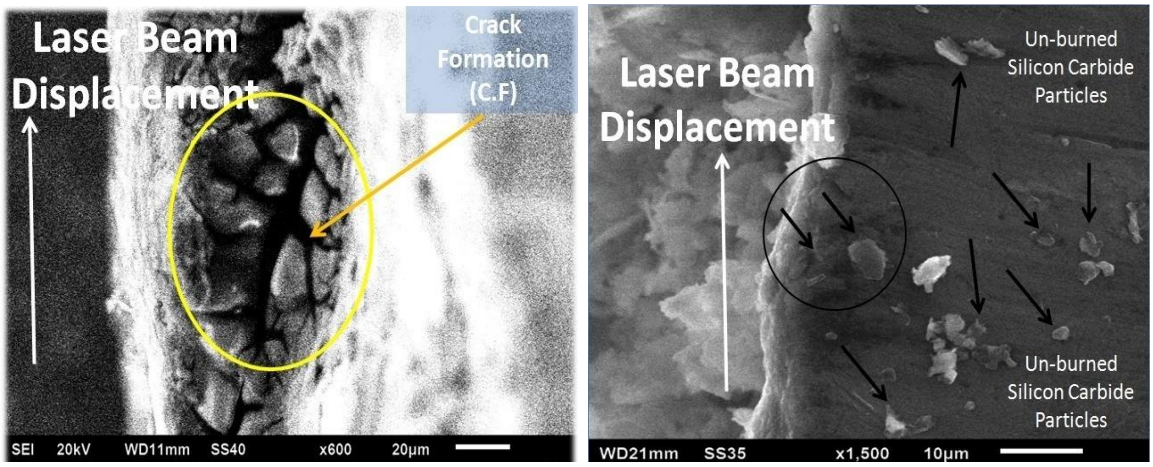

a) b)

Figure 5.111 Crack formation and presence of un-burned SiC particles on edge (a, b)

The presence of ceramic particles in vicinity and on the surfaces is clear evidence of large formation of cracks, recast layer, surface roughness and striation formation. After laser beam cutting operations, the machined specimens were analyzed with help of scanning electron microscope (SEM). As the laser beam process cut the material with the help of thermal effect and due to this it may change the microstructure of machined surface. In these images the information about presence of SiC particles, restricted flow, crack and recast layer formation can be obtained. The presence of un-burned SiC particles (marked in circular dash line) and restricted flow of molten material depicted into downward direction. This type of microstructure suggests about large number of striations formation on the edge surface.

As the expulsion of molten material becomes difficult due to presence of small un-burned SiC particles on the edge surface resulted into large striations. Moreover, this restriction might become more pronounced when the cut profile is more circular in nature. The accumulation of reinforced particles and high viscosity of molten material restricts the movement in the downward direction as shown in figure 5.112 (a). The formation of recast layer is shown in figure 5.112 (b). Figure 5.113 depicted the dross and striation formation at cutting conditions X_1: 1000 mm/min., X_2: 2000 watt, X_3: 2.0 mm, X_4: 1.4 mm, X_5: 14 bar, X_6: 0 % and X_7: 20 mm.

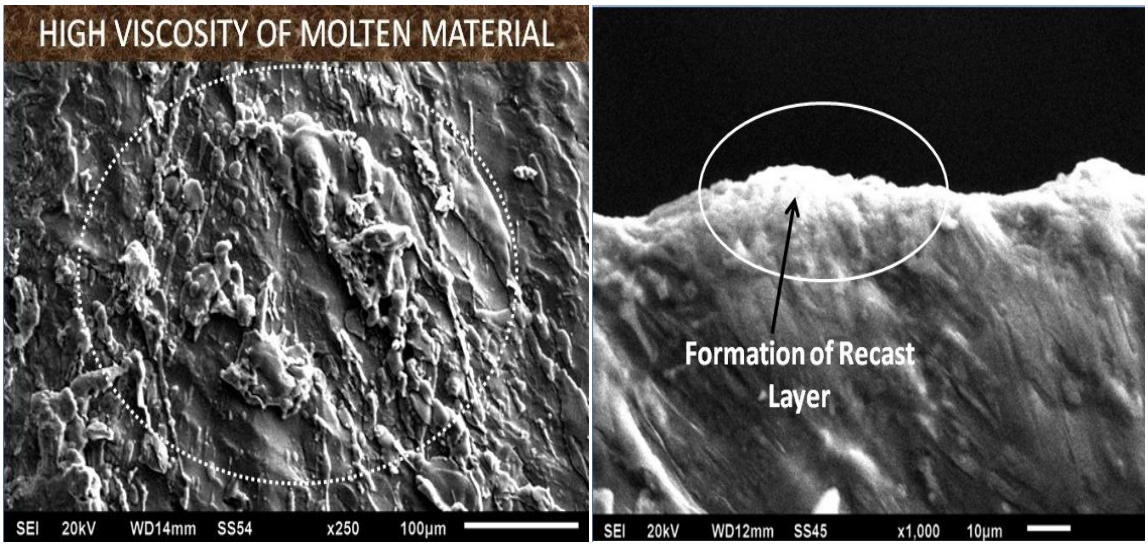

(a) **(b)**

Figure 5.112 Accumulation of molten material due to presence of SiC particles (a), formation of recast layer (b)

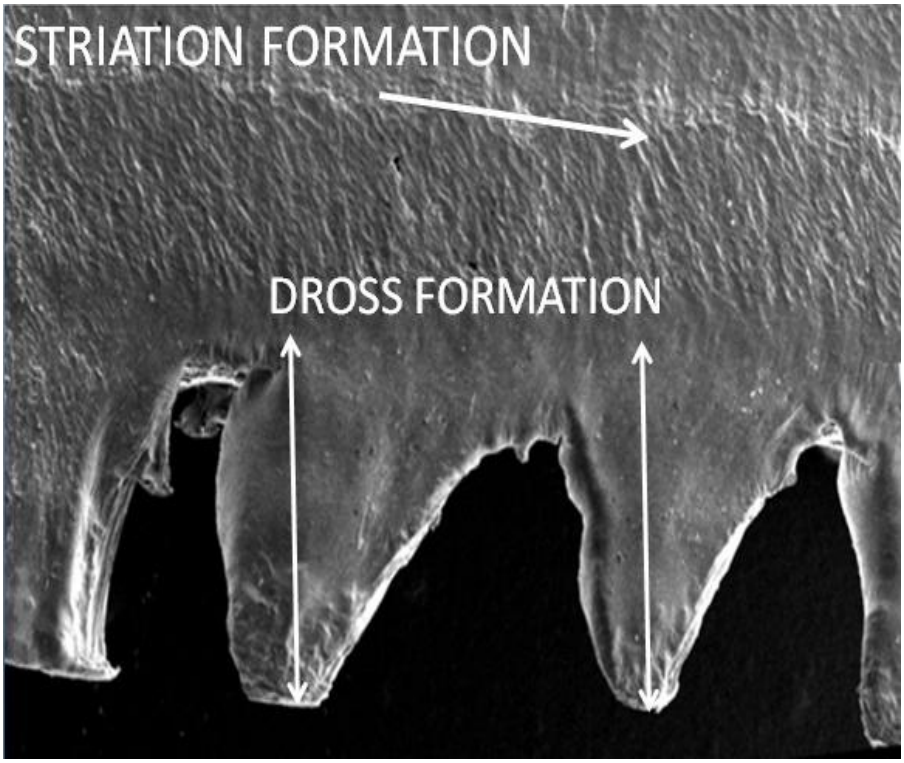

Figure 5.113 Dross and striation formation on the Al5052/SiC MMC machined surface

It was examined that thickness of recast layer increased when the specimen material was reinforced with SiC particles. In case of non-reinforced specimens (0 % SiC) the recast layer thickness was less. The probable reason for this may be increased levels of viscosity. Due to this, removal of molten material from the vicinity of kerf zone becomes difficult. The phenomenon of crack formation may rise due to high quantity of SiC particles and circular nature of cut profile. The presence of SiC particles may initiate the stress concentration and de-bonding of matrix and base material resulted into large number of void and cracks. Due to this surface roughness of edge may rise to large extent. It was proposed that these particles were regularly fractured by the fast flow of molten material resulted into mix up with melt due to this high viscosity and large surface tension induced into the melt. Therefore reduced melt flow velocity caused the formation of large striation resulted into large surface roughness (Yigezu B.S et al.., 2013). The thermal effects induced on the surface changes the micro structural properties due to the laser cutting operations. The developed stresses reflected on the cut kerf surfaces in the form of recast layer and heat affected zone width which is analysed using scanning electron microscope and electron dispersive technique.

The distribution of ZrO_2 particles on the surface were predicted using both techniques. It was found that scattering of particles was more pronounced when specimen of 20 % selected for testing. The presence of ZrO_2 particles absorbs large amount of beam energy which resulted into creation of high density energy zone. Due to this heat affected zone of double layers exists near the edge where the reinforced ZrO_2 particles quantity is higher in nature. The absorptivity behaviour of specimen depends on the constituents like base metal aluminium and matrix material.The local absorption of the laser light depends upon the constituents of specimen which have different melting temperature and absorptivity property. Figure 5.114 (a) shows the surface structure having ZrO_2 particle distribution of 20 % in metal matrix composite specimen. It was analysed that cut profile having arc radius of 2 cm exhibited with large heat affected zone width and recast layer. Figure 5.114 (b) shows schematic diagram of the recast layer and heat affected zone width.

From the figure 5.115, the various zones were analysed as zone 1, zone 2 and zone 3. The machined surface was processed at cutting speed: 1000 mm/min, laser power: 2000 watt, standoff distance: 1.5 mm, nozzle diameter: 1.7 mm, gas pressure: 12 bar, ZrO_2 particles: 20 % and arc radius: 20 mm. The zone 1 and zone 2 were analysed purely as heat affected zone whereas zone 3 as recast layer zone. In heat affected zone 1, the presence of some un-burned ZrO_2 reinforced particles was examined using SEM micrographs.

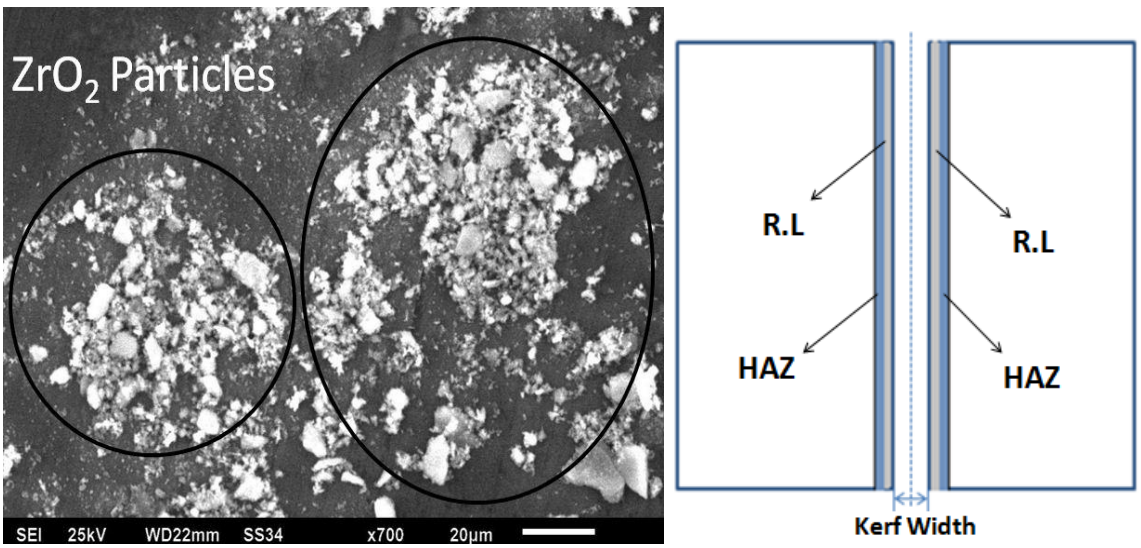

(a) **(b)**

Figure 5.114 SEM micrographs: (a) presence of 20 % ZrO_2 particles in sepecimen, (b) schematic diagram of recast layer and HAZ

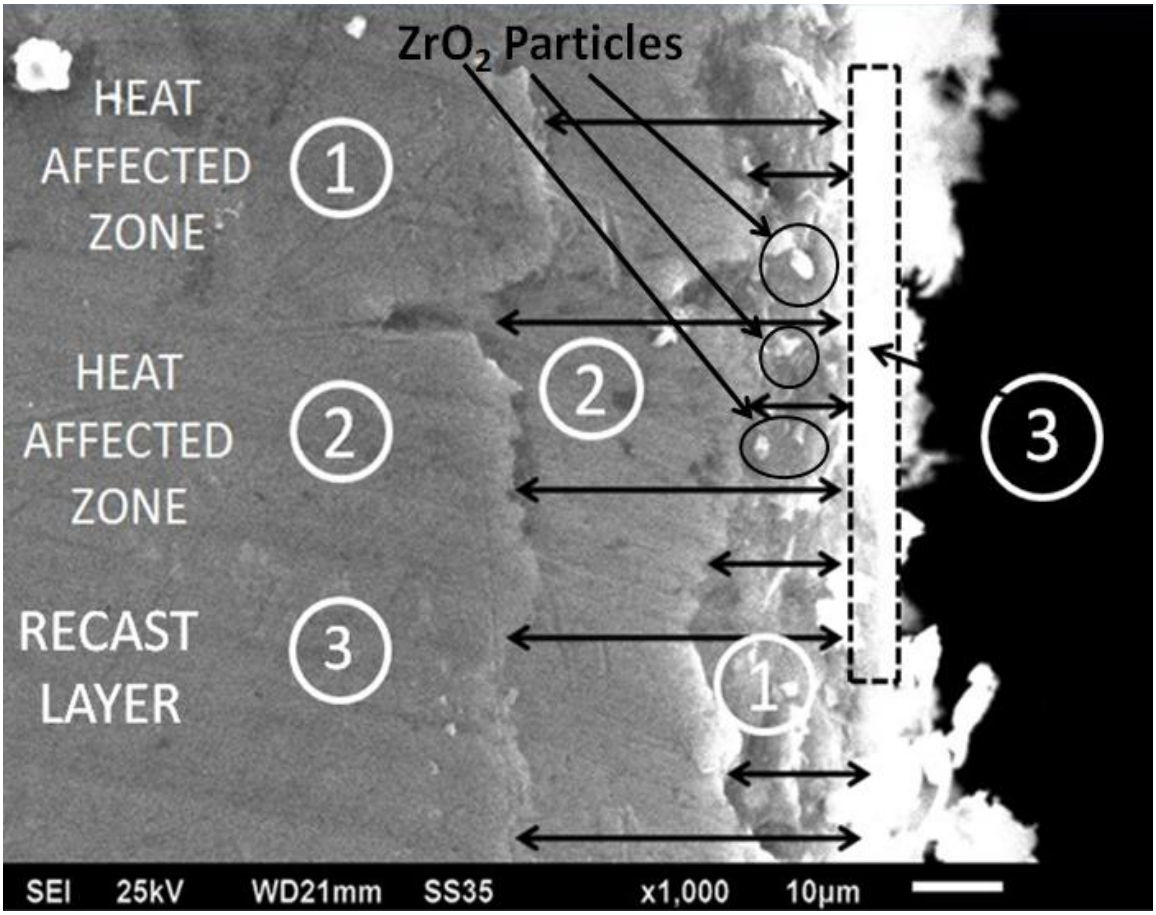

Figure 5.115 Sub-layers of HAZ for machining condition at X_1: 1000 mm/min, X_6: 20 %, X_7: 20 mm

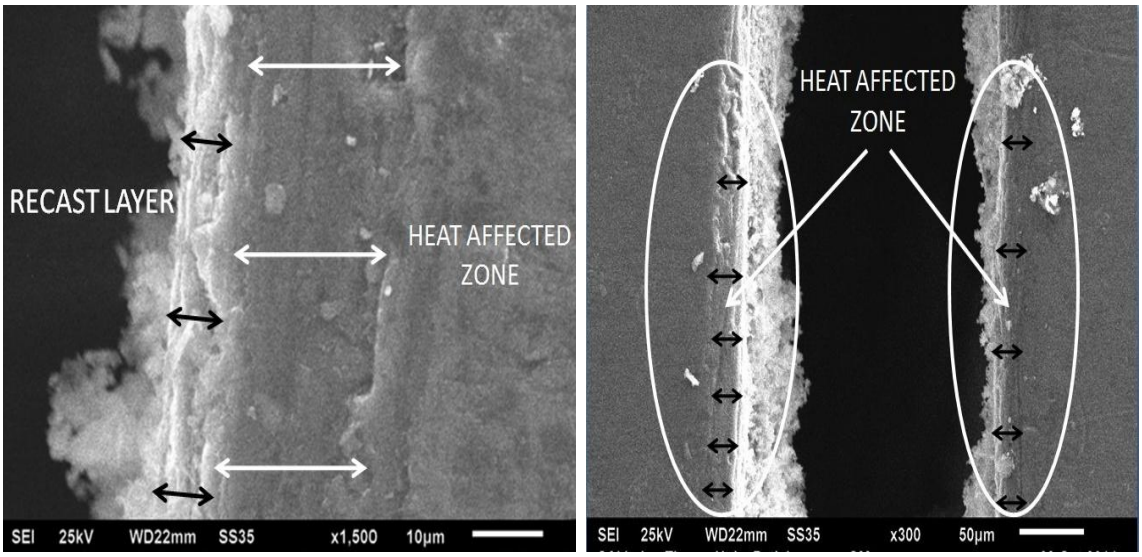

(a) (b)

Figure 5.116 Heat affected zone width and recast layer (a) heat affected zone width for Al/ZrO_2 MMC(b)

It can be revealed that due to these particles the absorbed energy is higher in this region and this higher energy melted the reinforced particles to some levels. The remaining reinforced particles helps to increase the viscosity of the molten material. Consequently, re-solidification of molten material and high extension of molten material on the cut edge takes place which increases the HAZ width.

The remaining energy of zone 1 is transmitted to zone 2. The heat affected zone width (average of zone 1 and 2) measured as 395.79 µm which is highest value based on observations. The other probable reason for higher energy absorption may be due to more circular nature of laser cut. As during complex cut the laser beam has to travel large distance and due to this interaction time increases which increases the energy levels in the kerf zone. The zone 3 is recast layer which occurs due to presence of reinforced particles in the vicinity of kerf zone (Muller F. et al.., 2001). The thickness of recast layer increases if machining conditions are not in optimized state and it also depends on the material composition. The thickness also increases due to re-solidification of the molten material in the kerf zone.

When curvature of cut increases (20 mm), laser has to travel large distance as compare to laser cut of 40 mm and 60 mm. Due to this reason the induced stress and heat affected zone is higher in case of curved trajectories i.e. 20 mm arc radius. The presence of higher quantity of ZrO_2 particles also absorbs higher energy which resulted into higher heat affected zone width and formation of recast layer. Figure 5.116 (a) shows the recast layer and heat affected zone when machining condition set at cutting speed: 1000 mm/min, laser power: 2500 watt, standoff distance: 1.5 mm, nozzle diameter: 1.4 mm, gas pressure: 12 bar, ZrO_2 particles: 10 % and arc radius: 40 mm.
The measured HAZ width for this machined surface as 311.82 µm.Figure 5.116 (b) exhibits the heat affected zone when the machining condition set at cutting speed: 2000 mm/min, laser power: 1500 watt, standoff distance: 1.5 mm, nozzle diameter: 1.7 mm, gas pressure: 10 bar, ZrO_2 particles: 10 % and arc radius: 20 mm. From the above discussions it can be concluded that higher quantity of reinforced particles and lower arc radius is responsible factors to increase the heat affected zone width and formation of recast layer. In the figures 5.117 and 5.118 the SEM micrographs of machined and un-machined work samples of Al/ZrO_2 MMCs has been shown which depicted the presence of aluminium oxide particles.

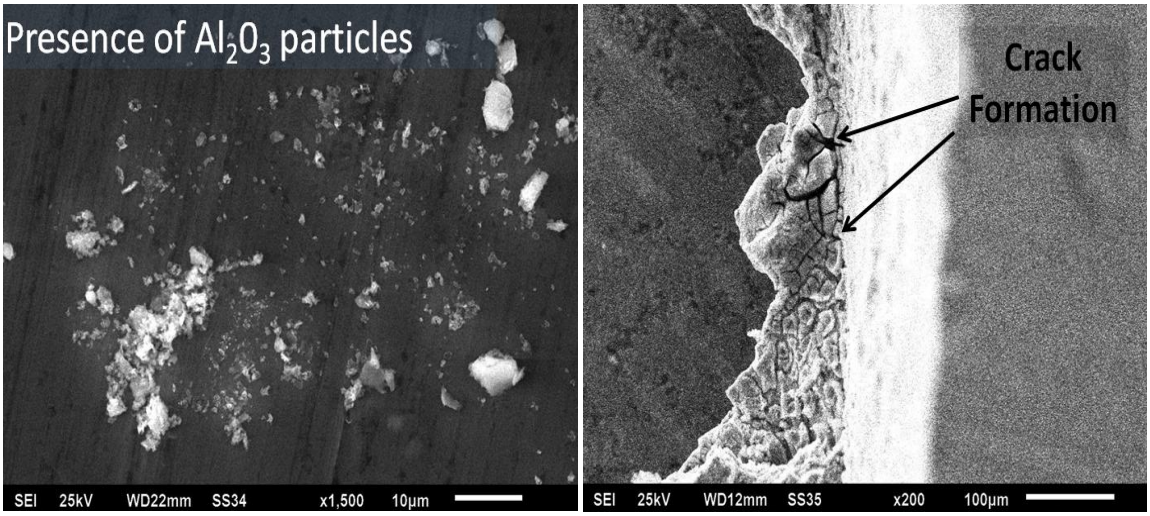

(a) (b)

Figure 5.117 SEM micrographs shows presence of Al_2O_3 reinforced particles in Al5052/Al_2O_3 MMC(a), crack formation on the edge machined surface (b)

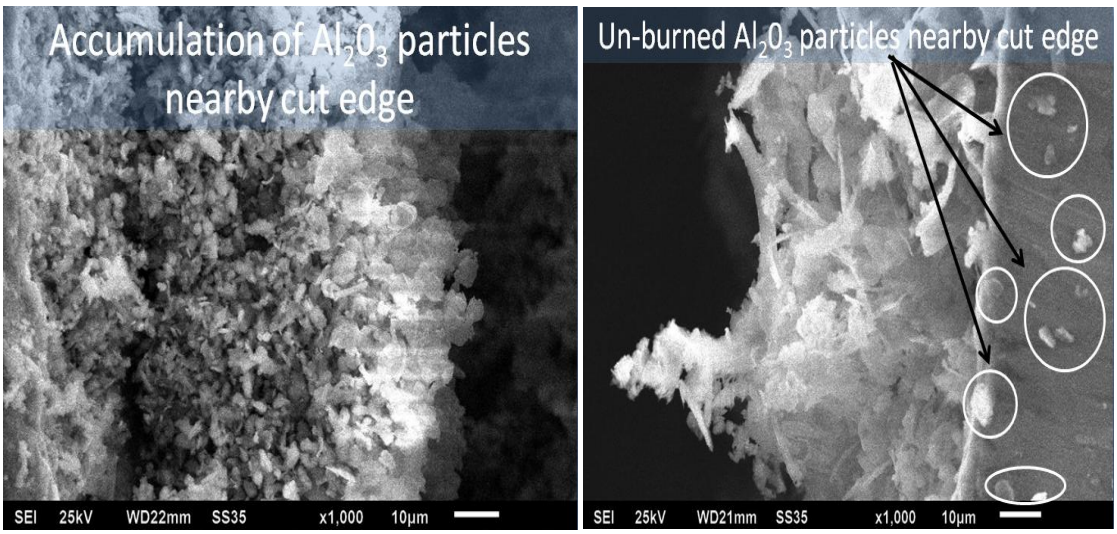

(a) (b)

Figure 5.118 Accumulation of Al_2O_3 reinforced particles nearby cut edge (a), presence of un-burned Al_2O_3 reinforced particles (b)

5.7.1 XRD and EDX Analysis

Selected machined specimens were prepared for XRD and EDX analysis to examine the changes in crystalline phases. For this purpose few samples were selected for x-ray diffraction. The machined specimen diffraction results revealed for new phase formation of Al_4C_3. The machined specimen was operated by machining conditions at X_1: 1000 mm/min., X_2: 2000 watt, X_3: 1.5mm, X_4: 1.7mm, X_5: 12 bar, X_6: 20mm and X_7: 20 %. The formation of new compound Al_4C_3 may be caused due to large amount of heat in the

cutting zone which forced the SiC particle to breakdown. The carbide content of SiC reacted with aluminium to form new compound Al_4C_3. From the previous studies it was found that this compound is undesirable which diminish the quality characteristics in form of large stress formation in metal matrix composite material (Yigezu B. et al.., 2013).

The specimens were made ready for the X-ray energy dispersive spectroscopy (EDS) and X-ray diffraction (XRD) to examine change in the composition of crystalline phases. The results of X-ray diffraction were compared for laser machined specimen and non-machined specimen. The XRD plot is shown in figure 5.119 (a, b) for the laser machined specimen. From the plot, the highest peaks of aluminium were observed whereas peaks of other compounds also seen in the plot. The highest peak is observed at 2θ value of 38.89˚ for the aluminium element. For the silicon carbide the value of 2θ was analysed as 52.4˚ and 68.1˚. Due to large heat produced in the cut kerf area resulted into breakdown of SiC particles to some extent. This phenomenon supported the carbon (C) to react with aluinium (Al) to form a new compound as Al_4C_3. The newly formed compound Al_4C_3 having 2θ value at 42.1˚ and 48.9˚.

From below equation 5.19, it can be seen via chemically that how both elements reacted with each other to form new compound.

$$4Al+3SiC \longrightarrow Al_4C_3+3Si \qquad \text{……..….(5.19)}$$

It has been observed that peaks of SiC have higher altitude when the surface was not machined by the laser whereas peaks reduced to low levels when the surface was machined using laser operation. It means that SiC particles crack down to some extent due to high temperature. Although the presence of Al_4C_3 type of compounds weakens the bond between reinforcement and matrix material. Due to this process microstructure may have cracks on the surface which ultimately deteriorates the cut edge quality. Different phases also seen during analysis of EDX analysis like iron (Fe), chromium (Cr), magnesium (Mg), aluminium (Al), oxygen (O), and silicon (Si). It can also be examined that there is existence of oxygen which may be due to the oxidation process of the laser cut surface. From the EDX results as shown in figure 5.120 (a, b) different phases of elements can be seen like iron (Fe), chromium (Cr), magnesium (Mg), aluminium (Al), oxygen (O) and silicon (Si). It was confirmed that silicon and carbon elements present

into the specimen material resulted in the formation of Al_4C_3 compound. From the EDX results it can be concluded that silicon and carbon elements presented into the AA5052/SiC composite material. The lower peaks of iron (Fe) and magnesium (Mg) also observed through the EDS results.

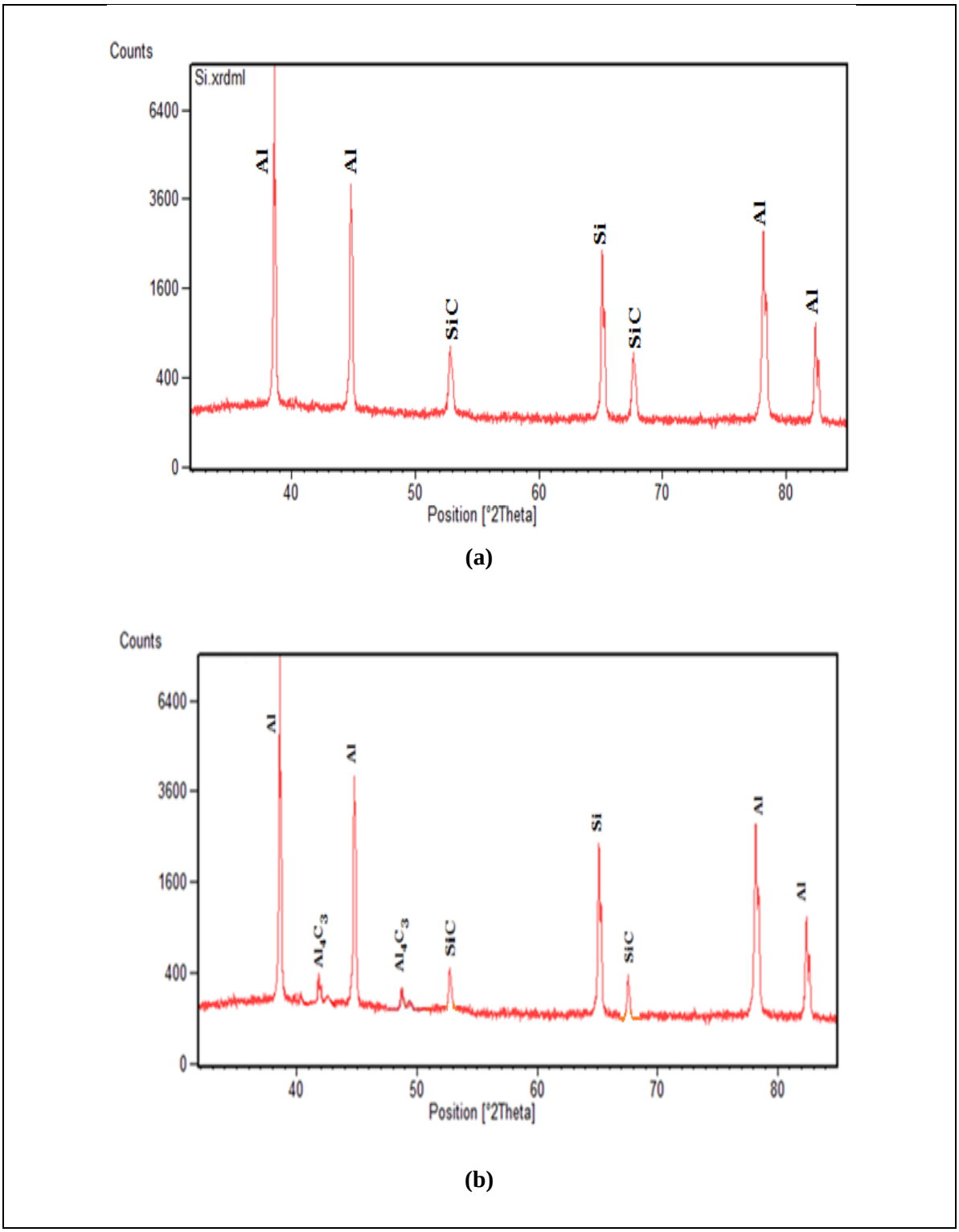

Figure 5.119 XRD analysis of un-machined AA5052/SiC MMC(a) XRD pattern of machined AA5052/SiC MMC (b)

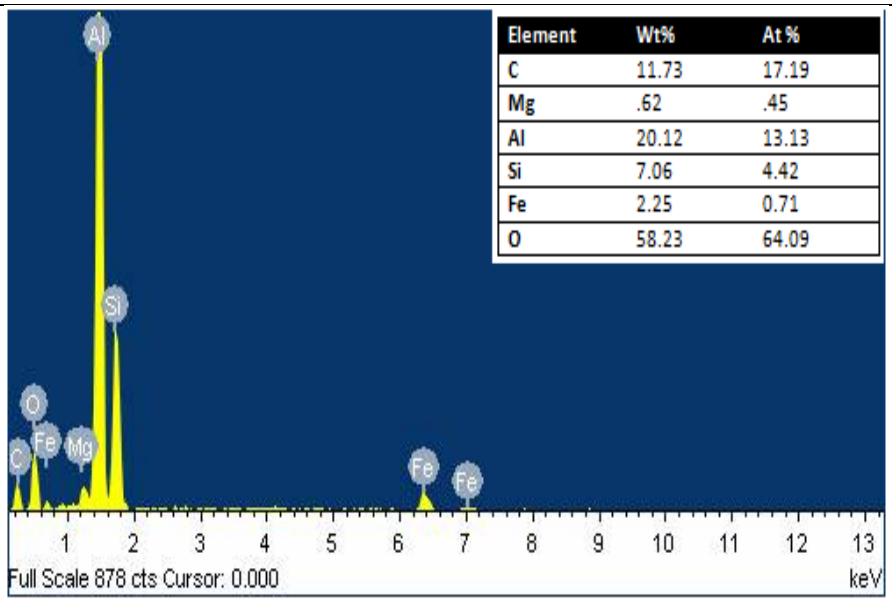

(a)

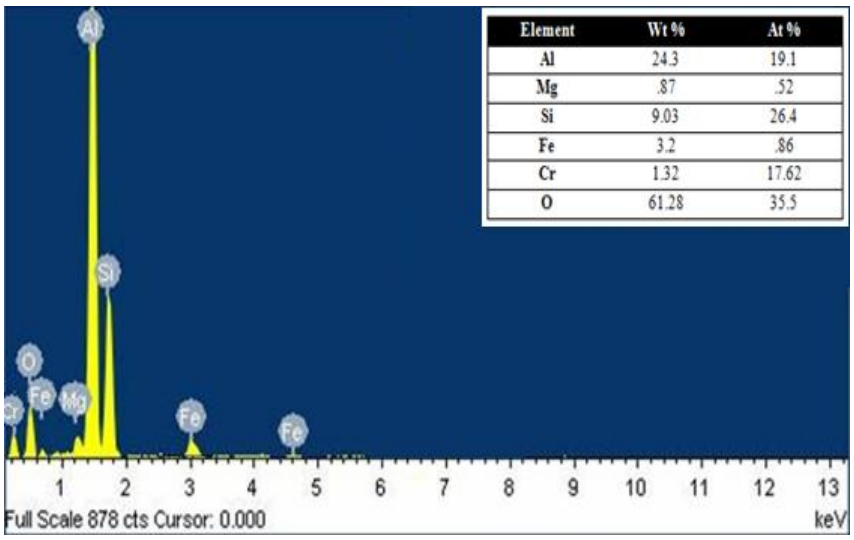

(b)

Figure 5.120 EDX analysis of laser machined surface of AA5052/SiC MMC (a), (b)

The presence of reinforced particles and various elements is shown in figure 5.117 with the help of SEM and EDS plot. From the figure 5.121, the distribution of 10 % ZrO_2 particles has been shown with the help of SEM micrograph. The presence of various elements like chromium, iron, nickel, zirconium and carbon has been presented with the help of EDS technique. The verification of zirconium reinforced particles of SEM micrograph is executed with the help of EDS plot.

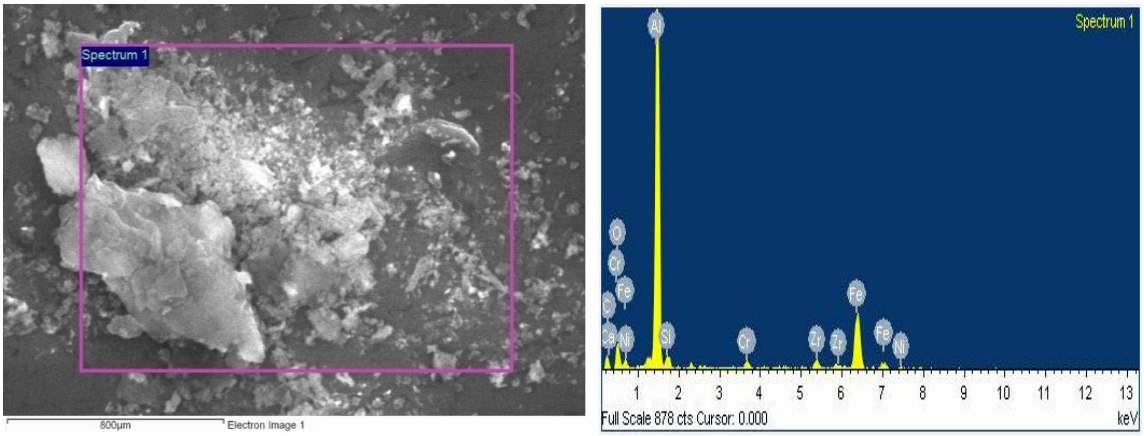

(a) **(b)**

Figure 5.121 SEM micrograph showing presence of 10 % ZrO_2 particles(a), EDS graph depicted the various elements of surface of specimen (b)

5.8 COMPARISON OF VARIOUS OUTPUT RESPONSES FOR DIFFERENT METAL MATRIX COMPOSITE WORK MATERIALS

In the present research work, the importance has been given to analyse the effect of laser input process parameters on various output responses. The experimental runs have been performed according to Box-Bhenken Design for various MMCs such as Al5052/SiC, Al5052/Al_2O_3, A5052/ZrO_2. For various metal matrix composite materials the effect of various parameters has been compared for output responses such as dross height, kerf taper, edge surface roughness, kerf deviation, striations, heat affected zone width, material removal rate, energy losses. The various work materials influenced with process parameters has shown variable results. The effect of process parameters has been denoted by the rank 1, rank 2 and rank 3. Here, rank 1 signifies for the lower effect and rank 3 for higher effect of parameters on the particular quality characteristics. The rank 2 denotes the middle values between rank 1 and 3. From the detailed investigations it has been analyzed that Al5052/SiC MMC has shown higher dross height as compared to other metal matrix composite materials and it has been ranked 3 as shown in graph using figure 5.122. The rank 2 has been attained by the Al5052/Al_2O_3 material whereas rank 1 achieved by the A5052/ZrO_2 MMC material. This may attributed to the fact that agglomerated of particles resulted into higher viscosity which prevents the molten metal to flow down the kerf edge.

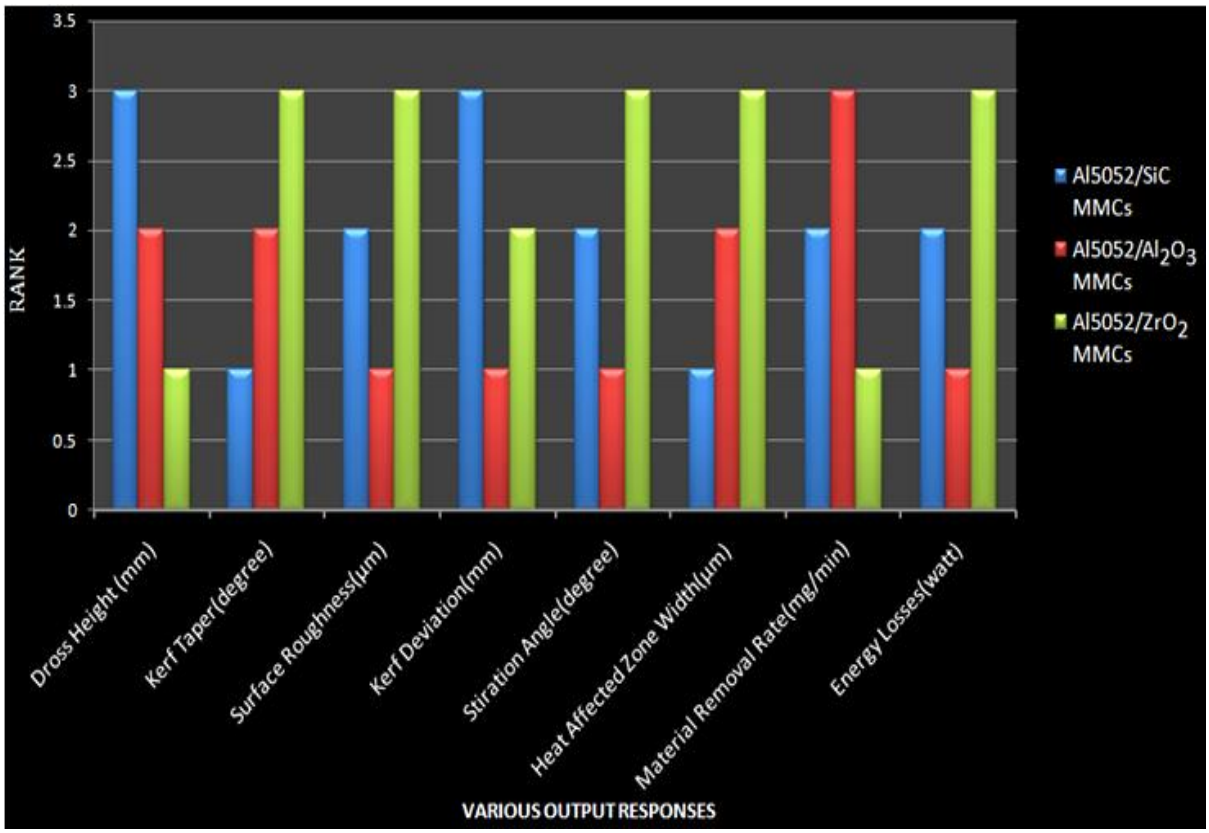

Figure 5.122 Comparison of quality characteristics of various metal matrix composites work material

This trend has been examined more in A5052/ZrO_2 MMC work material where cluster of reinforced particles increase the viscosity resulted into lower dross height. From the bar graph it can be analyzed that A5052/ZrO_2 MMC work material has higher impact on the output quality characteritics as compared to other materials. Moreover, from the SEM micrograph it can analysed that cluster of reinforced particles is lower in case of Al5052/SiC MMC work material. Thus, due to this fact the output responses results has been depicted with lower values. From the bar graph it can be predicted that Al5052/Al_2O_3 MMC work material has lower impact as compared to other MMCs. It has been given rank 2, 2, 1, 1, 1, 2, 3 and 1 for dross height, kerf taper, surface roughness, kerf deviation, striation angle, heat affected zone, material removal rate and energy losses respectively.

For the same machining conditions it has been analyzed for A5052/ZrO_2 MMC work material that rank 3 has been attained for maximum number of output responses. The probable reason for it may be the reinforced particle which has higher tendency for cluster process and the higher hardness of work material as compared to other materials. It can be

analysed from the graph that in case of Al5052/SiC MMC work material, the material removal rate analysed higher as compared to other materials. It may be due to lower agglomerated of the SiC reinforced particles which easily gained the melting temperature and thus removes quickly by the exothermic reaction of nitrogen gas pressure.

5.8.1 Comparison of literature review data with respect to experimental data

The current research data has been compared with the literature review data with the help of various parametric conditions. The comparison of parametric condition with the experimental condition has been shown in tables 5.21 and 5.22. The figures 5.123 and 5.124 predicted the graph of various output quality characteristics using various parametric conditions.

Table 5.21 Parametric conditions for comparison of values

Literature Values				Experimental Values			
Cutting Speed (mm/min)	Laser Power (Watt)	Gas Pressure (bar)	Nozzle Diameter (mm)	Cutting Speed (mm/min)	Laser Power (Watt)	Gas Pressure (bar)	Nozzle Diameter (mm)
Range: 1000-3000	1000 - 3000	08-15	1-2	1000-3000	1500-2500	10-14	1.4-2.0

Table: 5.22 Parametric conditions for literature and experimental data

Literature Values				Experimental Values			
Cutting Speed (mm/min)	Laser Power (Watt)	Gas Pressure (bar)	Pulse Frequency (Hz)	Cutting Speed (mm/min)	Laser Power (Watt)	Gas Pressure (bar)	Pulse Frequency (Hz)
1500-1800	2000-4000	04-14	8000-10000	1000-3000	1500-2500	10-14	5000

The desirability with respect to predicted experiment number is shown in figure 5.25 (a) and plots between predicted & experimental values is depicted in figure 5.25 (b-d). It has been analyzed from the various graphs that the deviation of predicted curve is very low as compared to experimental data curve. The calculated prediction error for all the output responses has shown lower values. Due to these lower values the adequacy of the predicted model also has been confirmed.

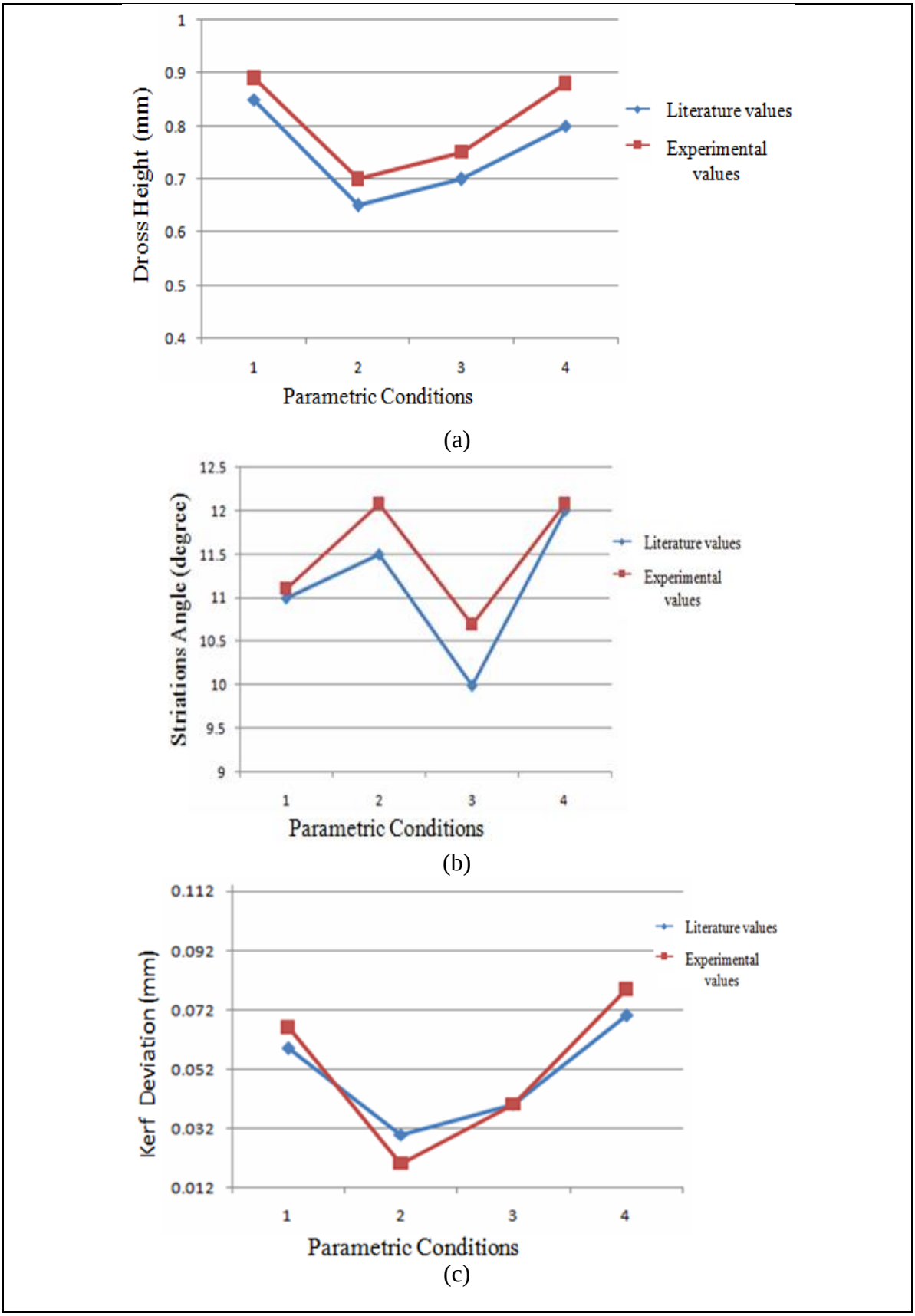

Figure 5.123 Variation of dross height, striation angle and kerf deviation values w.r.t to various parametric conditions

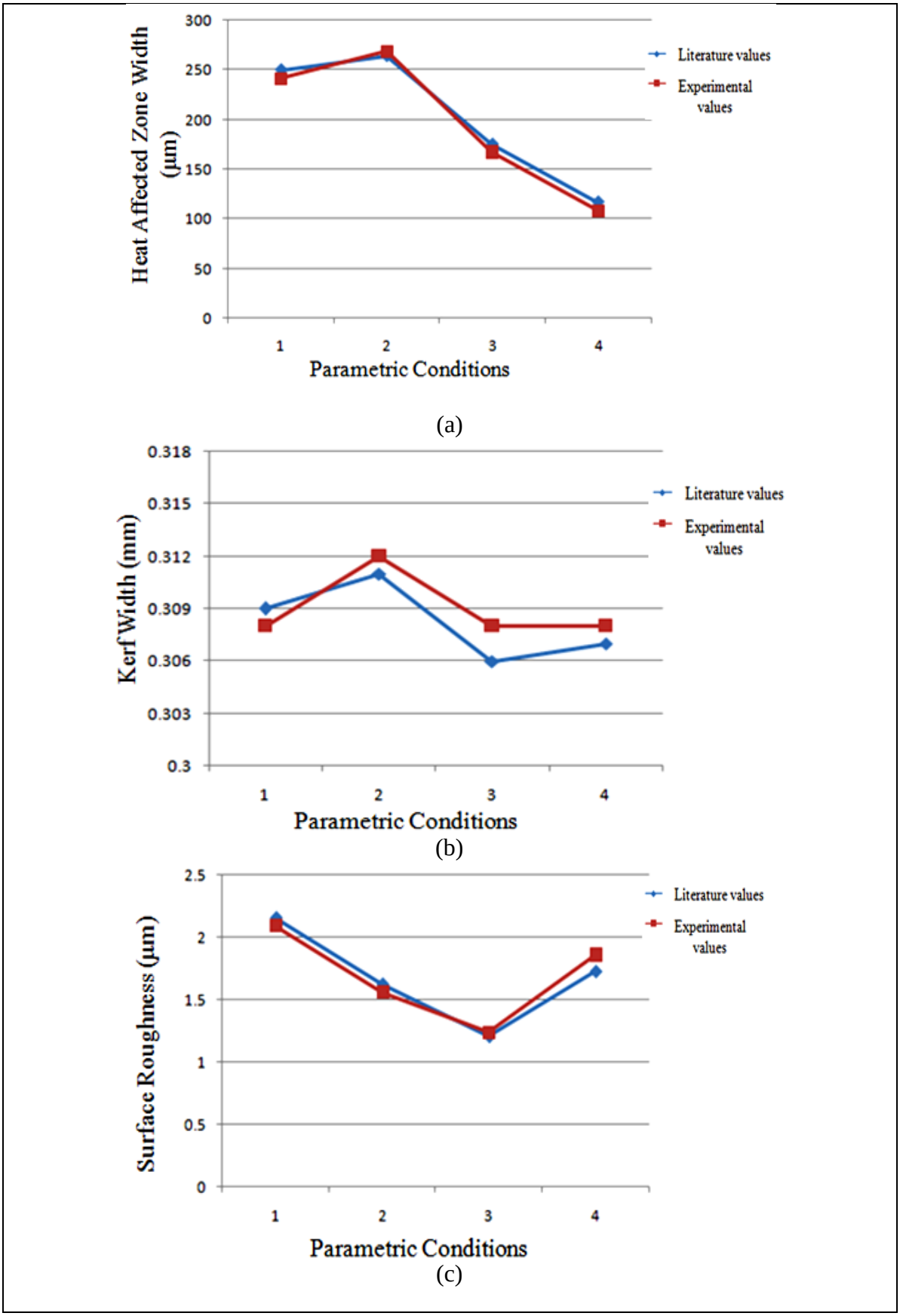

Figure 5.124 Variation in heat affected zone width, kerf width and surface roughness values by comparing literature and experimental data

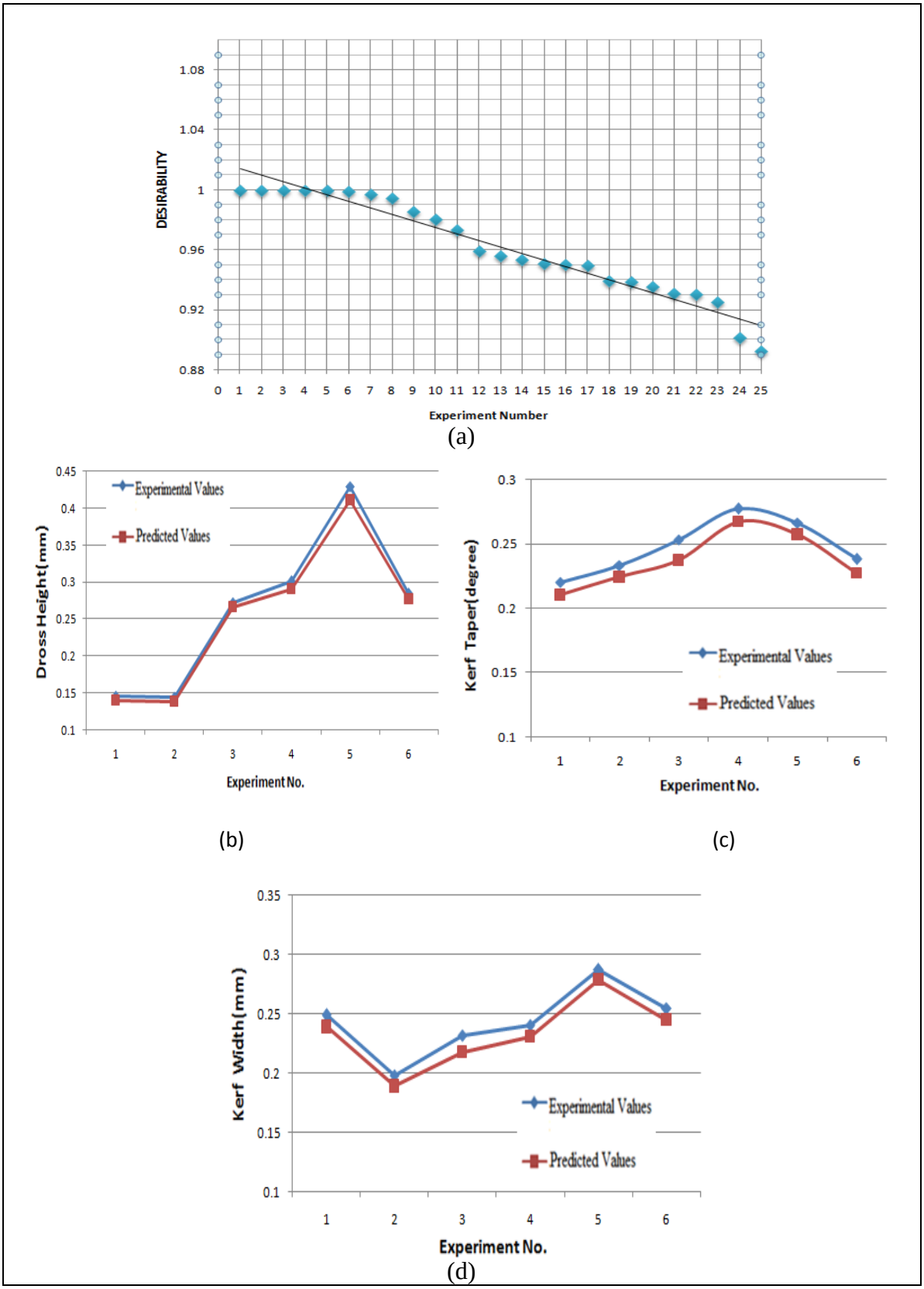

Figure 5.125 Desirability w.r.t predicted experiment number (a), plots between predicted & experimental values (b-d).

CHAPTER 06

FINITE ELEMENT METHOD

6.1 INTRODUCTION

FEM is a computer-based numerical method for calculating the strength and behavior of engineering structures based on different conditions. The purpose of an FE analysis is to model the behavior of structure under a system a loads such as variation in thermal conditions. In order to do so, influencing factors must be considered and determined whether their effects are considerable or negligible on the final result. In current industrial era, the finite element method (FEM) is one of the most useful tools to identify the various parametric, in-house process and structural conditions before implementation of project. Moreover, using this tool simulation of interactions of various models can be developed viz. fluid dynamics, thermal, modal, physics, bio-mechanical etc. For carrying out FEM for any process a manual or mathematical modeling can be done. However, for the complicated physical models the use of software is more feasible due to less execution of time.

The finite element method works on the basis of representation of physical structure in to sub-divisions. The collection of these sub-divisions also called as finite elements. The FEM also interprets the partial differential equation problems and convert into linear algebraic equations for the analysis work.

$$[K]\{q\}= \{F\} \quad \ldots\ldots\ldots\ldots\ldots\ldots (6.1)$$

where K is the stiffness matrix, q is nodal displacement vector and F is nodal vector force[1972].

In the present work, the FEM model has been developed using Ansys 12.0 software for performing the transient thermal analysis using structural analysis data. It is assumed that for solving the thermal field problems the partial differential equations for the conduction has to be considered in the model. The thermal stress analysis has been performed for various arc radius of 20, 40 and 60 mm by considering various assumptions for the metal matrix composite material and transient thermal stress analysis. This finite model consists of thermal and structural involved a great deal of complexity as the results of one model are to be inserted as the input of other model. To perform the thermal analysis, the transient analysis has been performed. The result of transient analysis conducted in the form of heat flux and temperature variation.

The basic procedure has been implemented for FEM analysis from geometry construction to final results. The finite element method fundamentally follows three steps such as:

1. Pre-process or modeling the structure
2. Analysis
3. Post processing

However, the detailed procedure follows the basics step of geometry construction to the analyzed results. Figure 6.1 shows the basic steps to implement the finite element method.

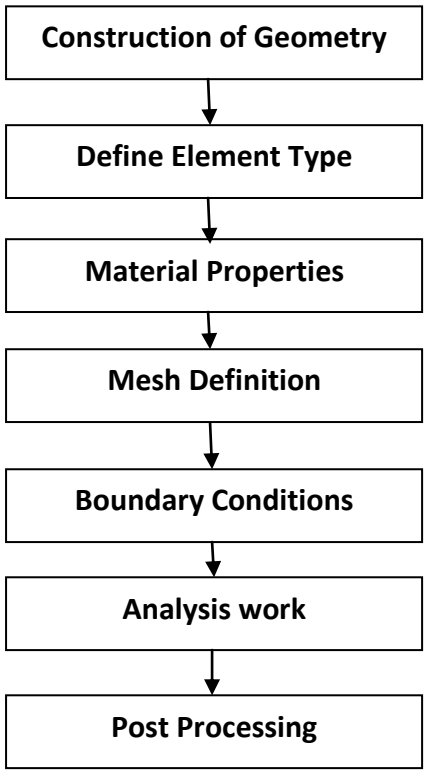

Figure 6.1 Procedure to apply the FEM from initial to post processing phase

6.1.1 Assumptions used in the laser source model

1. The laser beam spatial distribution is in Gaussian at TEM00 mode.
2. The radiation losses during the cutting process for the workpiece have been ignored.
3. It is assumed that Rate of molten evaporation is equal to the rate of ejected material.
4. Due to the use of assist gas the effect of cooling has been ignored.
5. The vaporization effect has been ignored as assist gas remove the molten material.
6. The reflective losses during the cutting have been assumed to be constant.

Table 6.1 Physical properties of the Al5052 and laser mode properties

S.No.	Properties	Units	Values
1	Absorption Coefficient	1/cm	0.20
2	Beam Mode	--	TEM_{00}
3	Convective heat transfer coefficient	W/m^2K	25
4	Density	g/cm^3	2.68
5	Melting Point	°C	605
6	Thermal Expansion	/K	23.7×10^{-6}
7	Modulus of Elasticity	GPa	70
8	Thermal Conductivity	W/m.K	138
9	Electrical Resistivity	Ω .m	0.0495×10^{-6}

6.2 HEAT TRANSFER MODEL AND ANALYSIS

The heat source model of the laser cutting process is totally based on heat transfer analysis which is modeled as two dimensional transient analyses. The Physical properties of the Al5052 work material and laser mode properties used in the FEM model is tabulated in the table 6.1. To determine the two dimensional heat conduction model, the spatial and temporal distribution T(x, y, t) must satisfy the following equation as also applied by [Sowdari and Mahumdar, 2010]. The heat analysis model is based on governing equations of Fourier law of heat conduction as shown below:

$$\partial/\partial x \left[k\,(T)\,\partial T/\partial x\right] + \partial/\partial y \left[k\,(T)\,\partial T/\partial y\right] + Q_{int} = \rho\, c\,(T)\,\partial T/\partial t \ldots\ldots\ldots (6.2)$$

where

$\partial T/\partial x$ = temperature in x- direction

$\partial T/\partial y$ = temperature in y- direction

c = specific heat

k = thermal conductivity of the work material

The boundary and initial conditions are applied for heat source model for variation in temperature and heat flux in the kerf zone. The solution of above Governing equation is also determined with the help of boundary and initial conditions.

The initial and boundary conditions are shown below:

1. The initial conditions:

$T(x, y, 0) = T_0$ for $(x, y) \in D$ …….. (6.3)

The essential boundary condition: T (0, y, t) = T …….. (6.4)

The above condition describes the nodal temperature at different nodes for inlet flow condition of heat.

The natural boundary condition imposed on the upper surface of work material:

q_0= h. (T_{ext} -T) …….. (6.5)

on the boundary S_2 for (x, y) ϵ S_2 and t>0. S_2 is surface where boundary condition is applied by fixing convection coefficient.

6.2.1 Thermal stress analysis for laser source model

The thermal stress develops in the specimen due to temperature variation on the surface during laser cutting process. The thermal stress occurs rapidly if the workpiece has higher tendency of rapid cooling and also it depends on the cutting environment. The thermal stress due to temperature variation is given by below equation:

$$\sigma = \frac{E\ \alpha \Delta T}{(1-\nu)} \qquad \text{…… (6.6)}$$

$\sigma = \sigma(\text{thermal stress})$
α = coefficient of expansion

ΔT = temperature difference

The structural analysis is conducted using von-misses stress analysis and determined using below equation:

$$\sigma_m = \frac{\sqrt{[(\sigma_1-\sigma_2)^2+(\sigma_2-\sigma_3)^2+(\sigma_3-\sigma_1)^2}}{2} \qquad \text{……(6.7)}$$

where

$\sigma_{1,2,3}$ = stresses induced at various sections

6.2.2 Global equation for heat transfer analysis

The global equation for the thermal analysis is developed using the finite element formulation as shown below:

[C (T)] {T}+ [K (T)]{ T }+{ V } = { Q (T) } ……. (6.8)

For the mechanical analysis the global equation is shown below:

[K (T)] {u (t)}+ {F (t)] + {F_{th} (t) } = 0 ……. (6.9)

6.3 STRESS, TEMPERATURE AND HEAT FLUX ANALYSIS

The laser cutting process is thermal process which may develop high thermal stress which depends on machining conditions and material type. In the present work, with the use of finite element method a numerical simulation model has been developed to examine the stress and temperature raised in the specimen. The heat source model is one of most important component for analyzing the results of laser cutting process. The results have been depicted numerically using ANSYS finite element code. The heat flux produced in the specimen also has been analyzed for various arc radius 2, 4 and 6 cm. For the numerical simulation, the properties of Al5052 workpiece have been used. For the numerical simulation model and analysis work, the Fourier law of conduction has been used. Moreover, the formulation of the model also considered using Gaussian distribution as using the Gaussian energy distribution mode a small diameter can be analysed with the help of high laser power. To determine the results related to the stress and temperature analysis two models has been used viz. static structural and transient thermal model. For the input loading conditions of static structural model, the output of transient thermal model has been used.

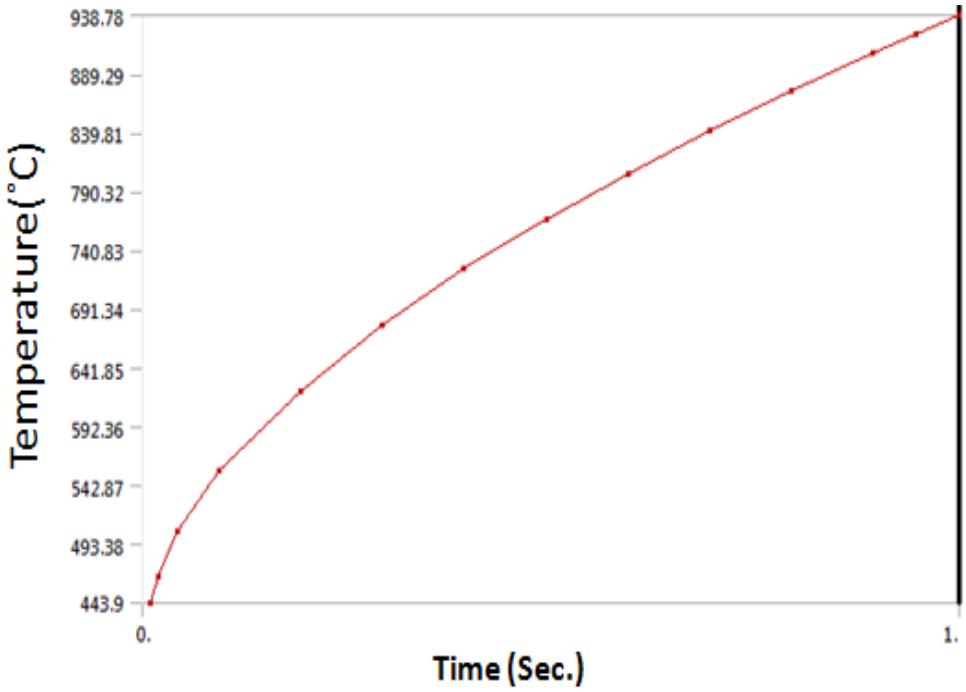

Figure 6.2 Analysis of temperature variation w.r.t time for 20 mm arc radius

6.3.1Thermal analysis for 20 mm arc radius

The present work is more focused on the curve cutting using laser cutting process for various curvature arcs. It has been analyzed experimentally that cutting of typical profile using laser process develop higher values of various output responses. This increase in higher values may be responsible due to the curvature cut of arc radius. It was predicted from the analysed work that arc radius of 20 mm has higher values of output responses except material removal rate as compared to 60 mm arc radius.

The various plots has been predicted for determining the relation between heat flux, temperature and time. It was examined that during laser cutting time of 1 second the temperature raised from 443.9 C to 938.78 ˚C as shown in figure 6.2. The rise in temperature may be due curvature path of the cut profile. With the same trend the heat flux also increased from 5620 × 10^3 to 9324 × 10^3 watt/m^2 as reflected in the figure 6.3. The raise in heat flux may be attributed to the fact that cut profile of 20 mm arc radius has large curvature resulted into large travel of laser energy in the kerf zone.It was observed from the shown figure 6.4 that arc of 20 mm has maximum value of von-misses stress of 2077 MPa. The probable reason for it may be the more curvature nature of the arc, as laser source has to travel large distance resulted into accumulation of heat in the cut profile.

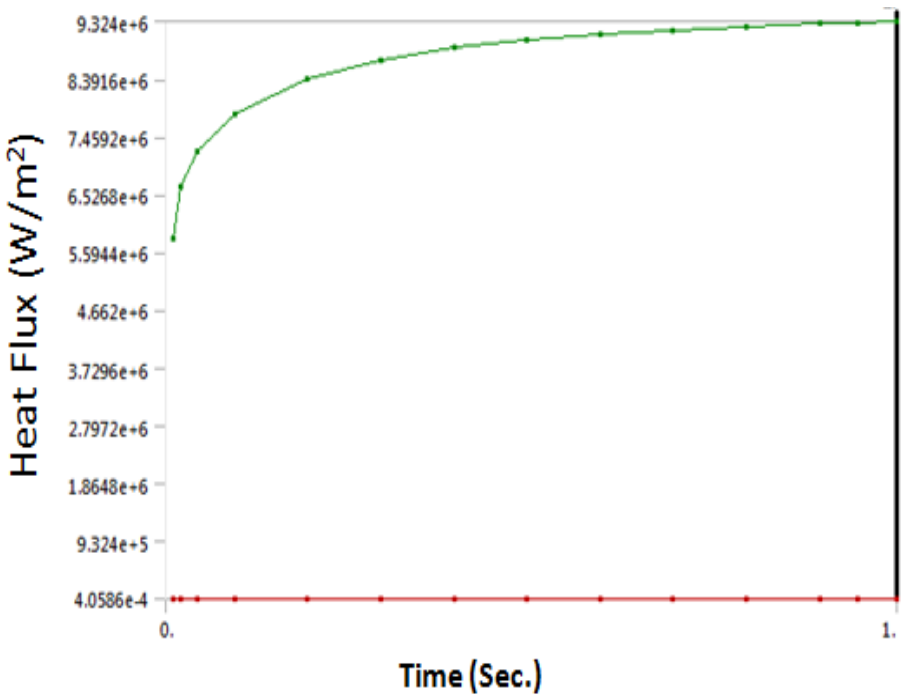

Figure 6.3 Analysis of heat flux variation w.r.t time for 20 mm arc radius

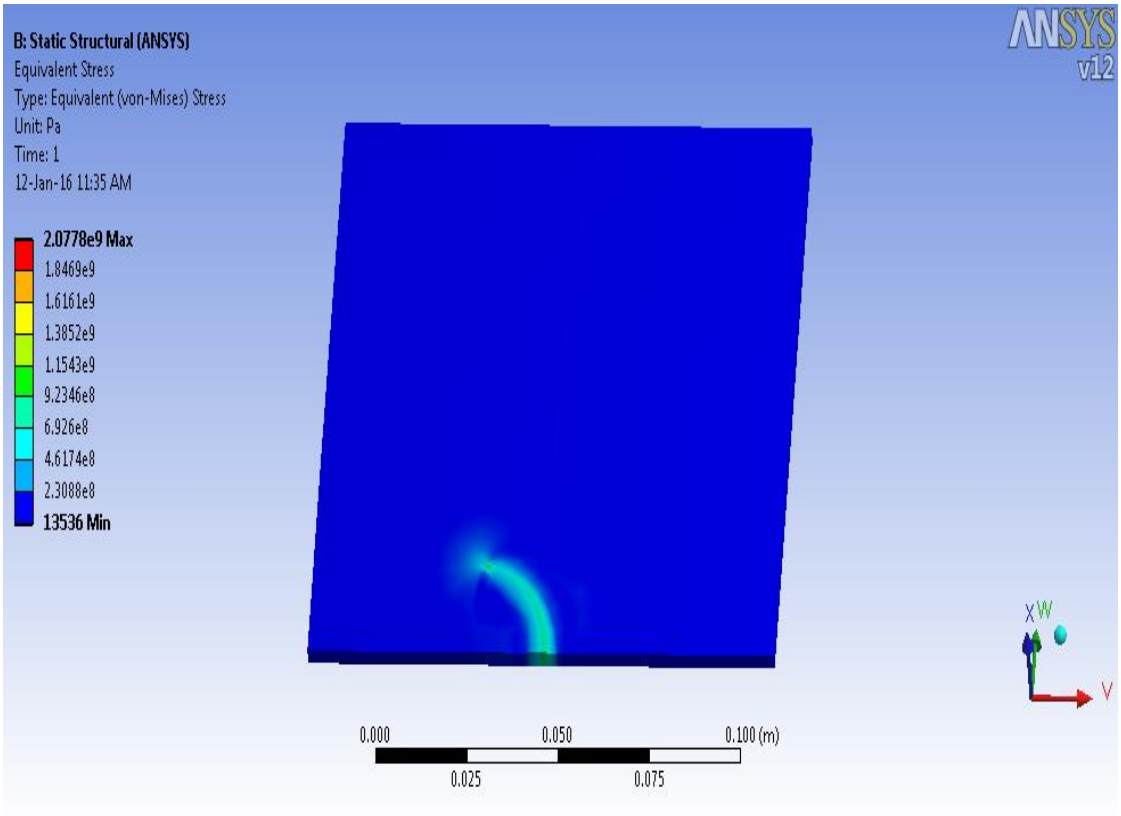

Figure 6.4 Von-mises stress analysis using transient analysis model for 20 mm arc radius

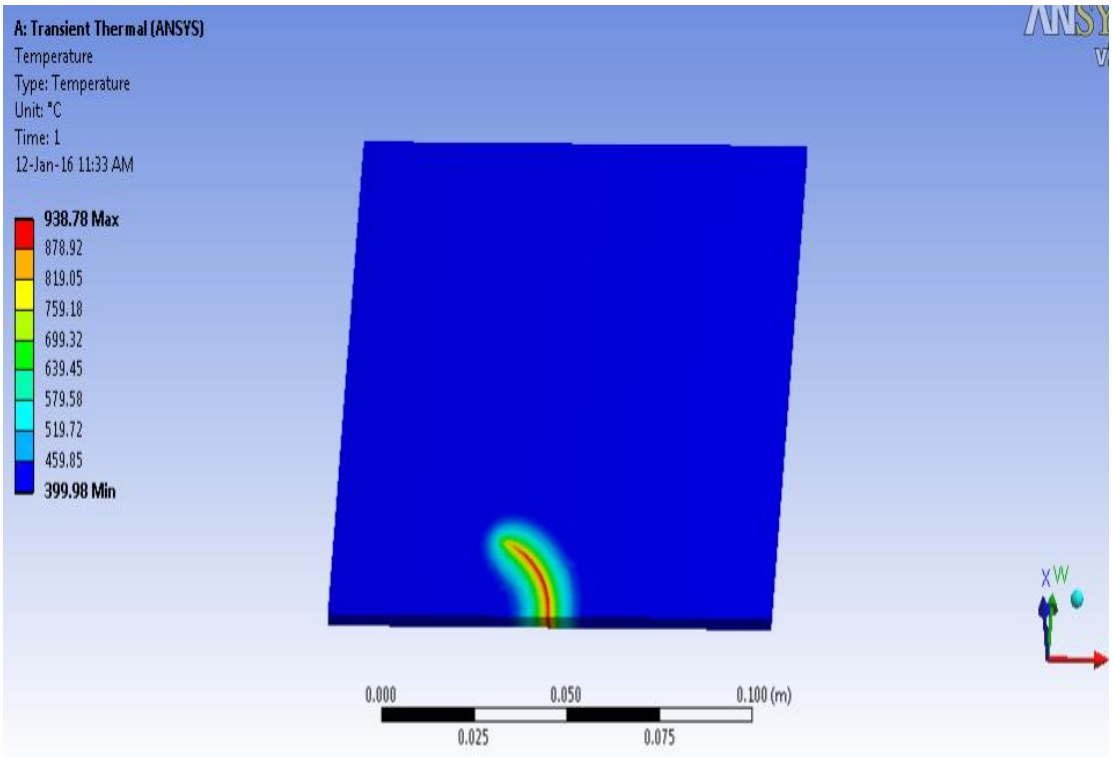

Figure 6.5 Temperature analysis for 20 mm arc radius

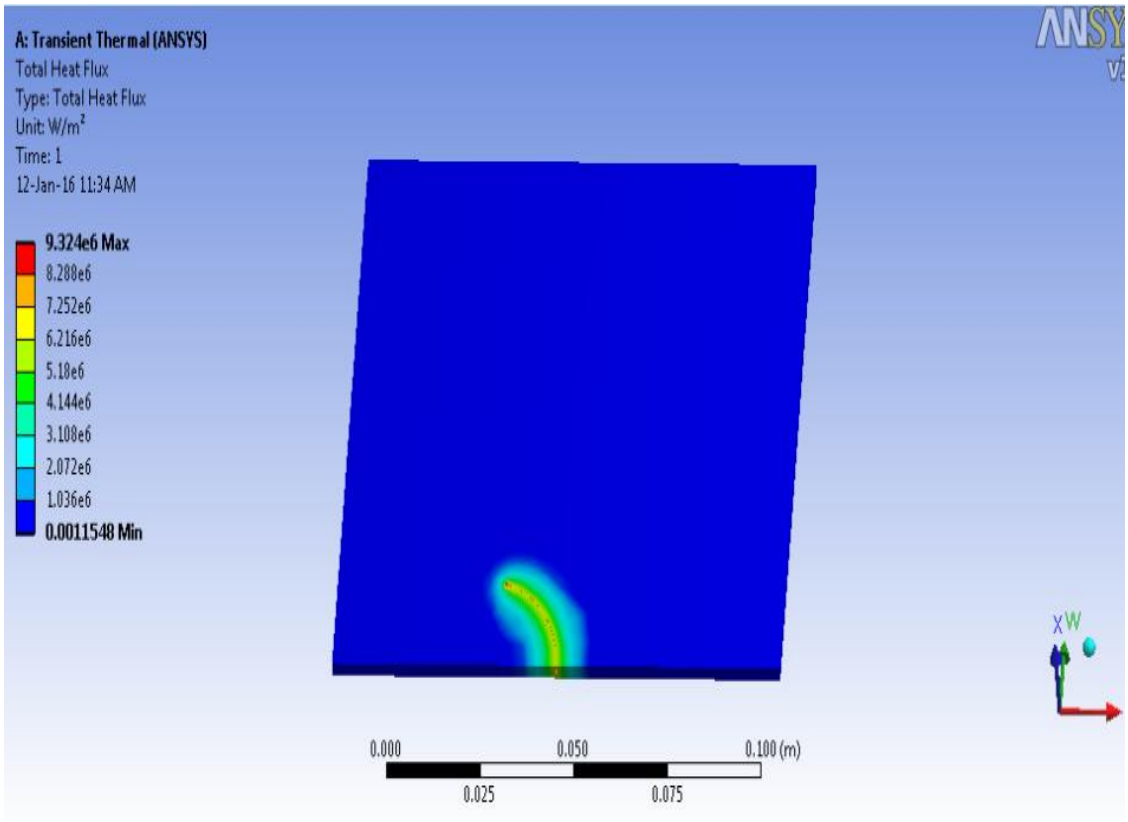

Figure 6.6 Variation of heat flux for cutting profile of 20 mm arc radius

Due to the accumulation of heat, the kerf zone develops more stresses as compared to other curvature having higher radius. The rise in temperature for the 20 mm arc radius can be examined from the figure 6.5. It has been analysed that during cutting process the maximum rise in temperature observed was 938.78 ˚C which is the highest recorded value. This may be attributed to the fact that during cutting of typical cut profile the cutting speed slowdowns. Due to this interaction time between specimen and laser source increase resulted into rise in temperature in the kerf zone. In the similar pattern the heat flux in the kerf zone examined as highest for 20 mm arc radius as shown in figure 6.6.

6.3.2 Thermal analysis for 40 mm arc radius

The comparison between the 20 mm and 40 mm arc radius is the curvature of both the curves. The 20 mm arc radius has more curvature than 40 mm arc radius which decides the energy levels within the kerf zone of respective kerf. The curvature or slope of cut profile decides the energy accumulation in the kerf zone which further effects heat flux, stress and temperature values. Figure 6.7 illustrates that when the laser beam initiate to cut the initial temperature increased to 443.08 ˚C whereas at the end of cutting the

temperature raised to 919.84 ˚C which is lower temperature as compared to 20 mm arc radius.

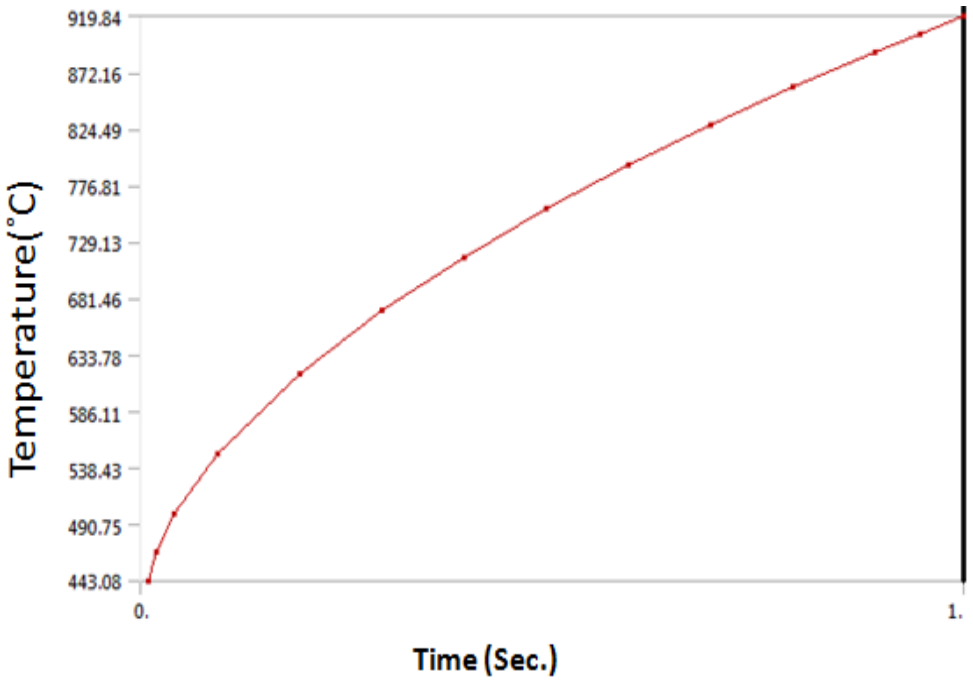

Figure 6.7 Analysis of temperature variation w.r.t time for 40 mm arc radius

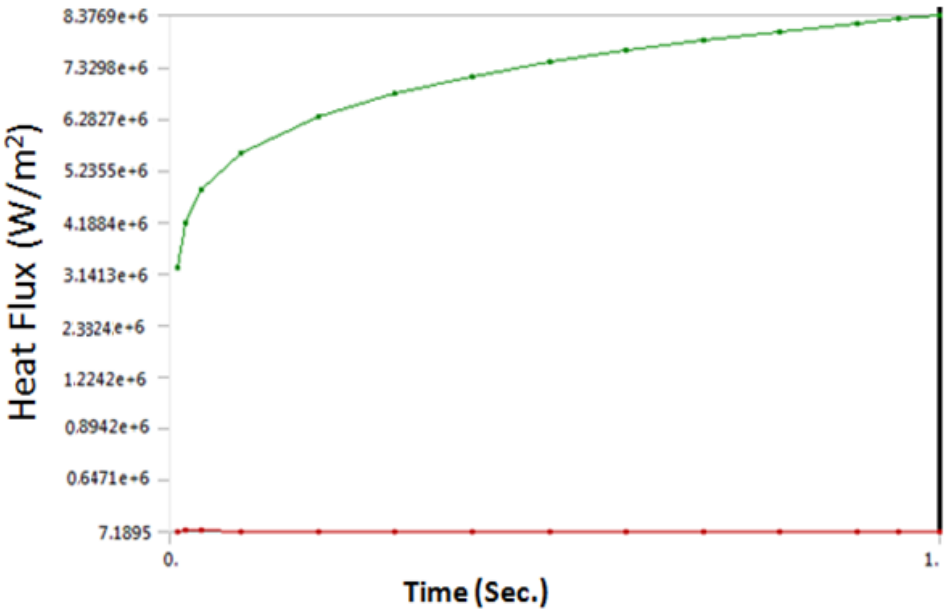

Figure 6.8 Analysis of heat flux variation w.r.t time for 40 mm arc radius

The heat flux plot is shown in figure 6.8 which depicted the heat flux values lower than the 20 mm arc radius profile. In this case, the heat flux values raised to 8376 × 10^3 watt/m^2 which is lower due to lower curvature of 40 mm arc radius as compared to 20 mm. The von-Mises stress value for 40 mm arc radius raised to 1331 MPa which is lower than the 20 mm arc radius stress value.

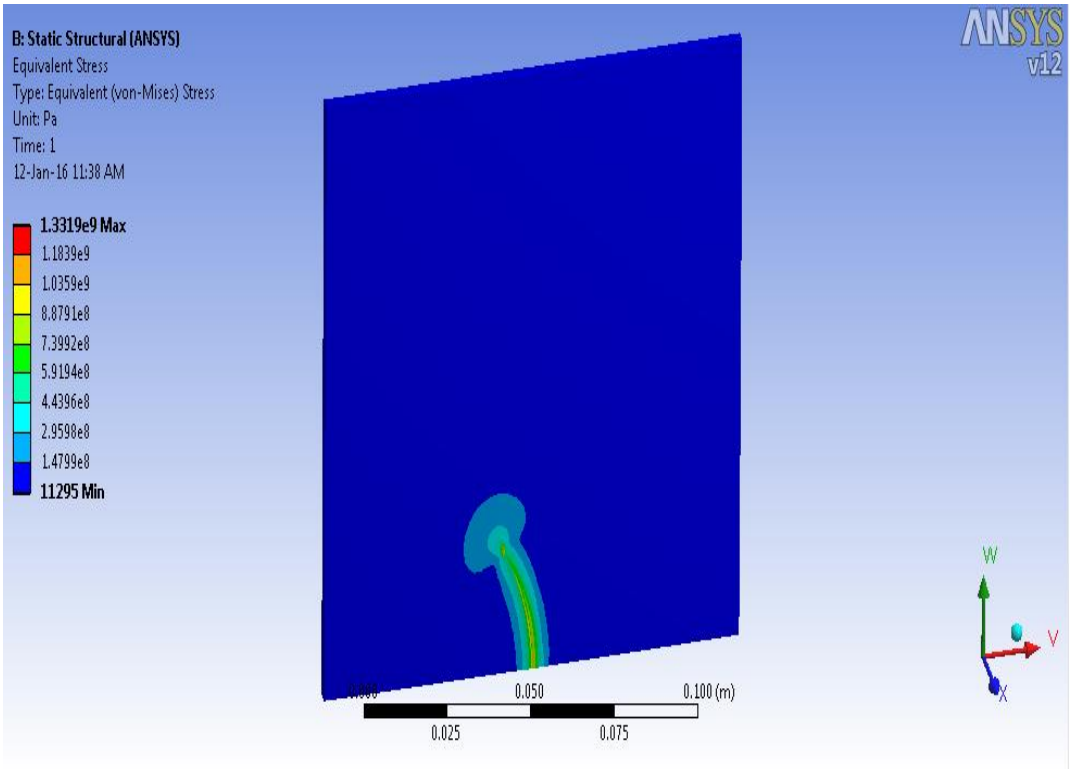

Figure 6.9 Von-mises stress analysis using transient analysis model for 40 mm arc radius

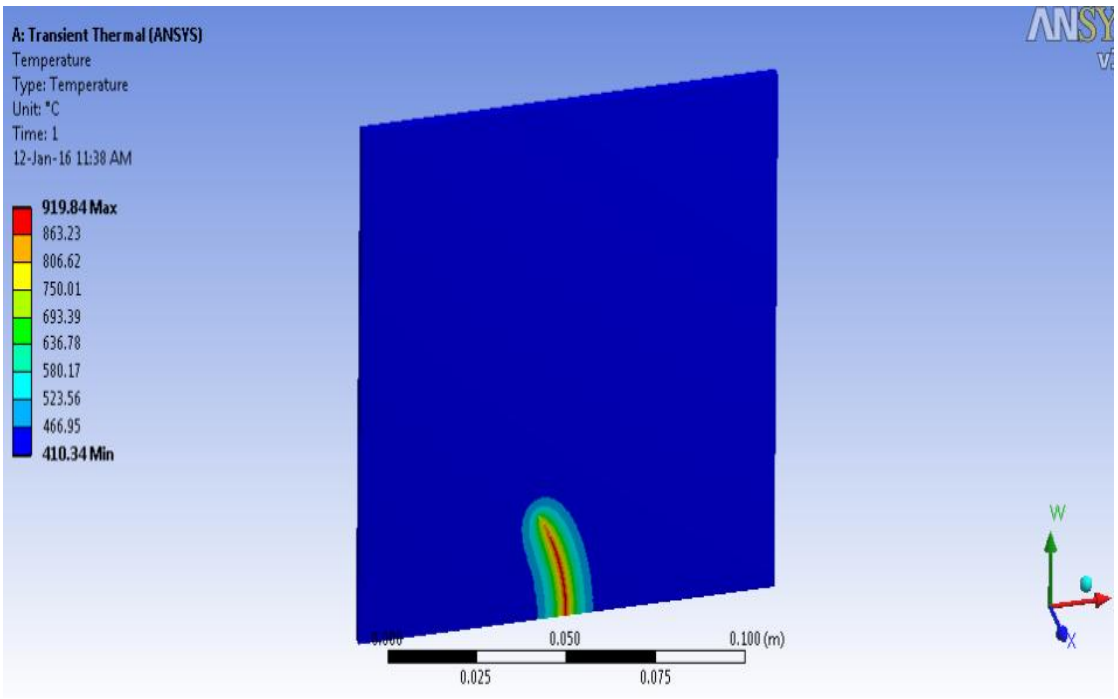

Figure 6.10 Temperature analysis for 40 mm arc radius

The energy level in the 40 mm arc radius is less than 20 mm arc radius resulted into less stress induced in the kerf zone. The temperature in the kerf zone can be analyzed as

919.84 ˚C as shown in figure 6.10. The raised temperature of 40 mm arc radius is lower than highest value of temperature of 938.78 ˚C. The heat flux value in the kerf zone is recorded with lower value as compared to the value of arc radius of 20 mm as shown in figure 6.11.

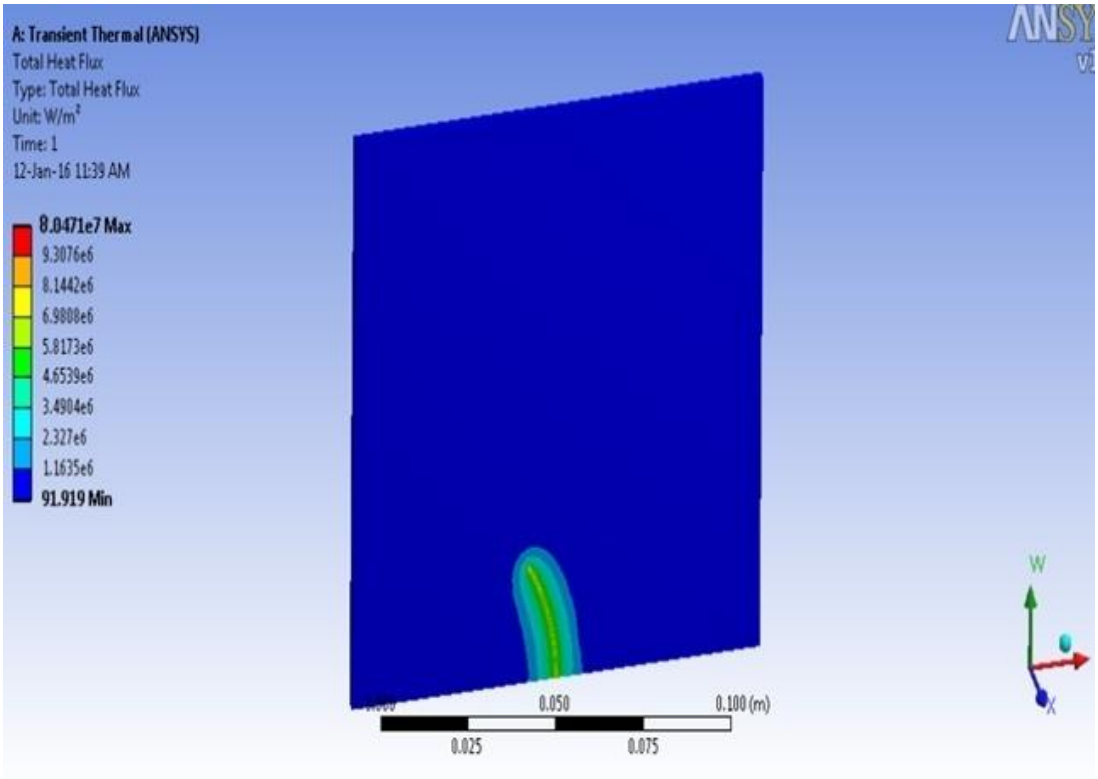

Figure 6.11 Variation of heat flux for cutting profile of 40 mm arc radius

6.3.3 Thermal analysis for 60 mm arc radius

The curvature of 60 mm arc is less circular in nature as compared to both the curves of 20 mm and 40 mm arc radius. Due to this less circular nature of the curve heat accumulation factor is less pronounced in this curve.

The heat flux plot is shown in figure 6.12 which depicted the heat flux values lower than the 20 mm and 40 arc radius profile. In this case, the heat fluxe values raised to 7122 × 10^3 watt/m^2 which is lower due to lower curvature of 60 mm arc radius as compared to 20 mm and 40 mm arc radius. The von-Mises stress value for 60 mm arc radius predicted value of 1013 MPa as shown in figure 6.14 which is lower than the 20 mm and 40 mm arc radius stress value. The energy level in the 60 mm arc radius is less than 20 mm and 40 mm arc radius resulted into less stress induced in the kerf zone. The temperature in the kerf zone can be analyzed as 899.99 ˚C as shown in figure 6.15. The raised temperature of 60 mm arc radius is lower than highest value of temperature of 938.78 ˚C in case of 20

mm arc radius. The heat flux values in the kerf zone are recorded lower value as compared to the value of both arc radius.

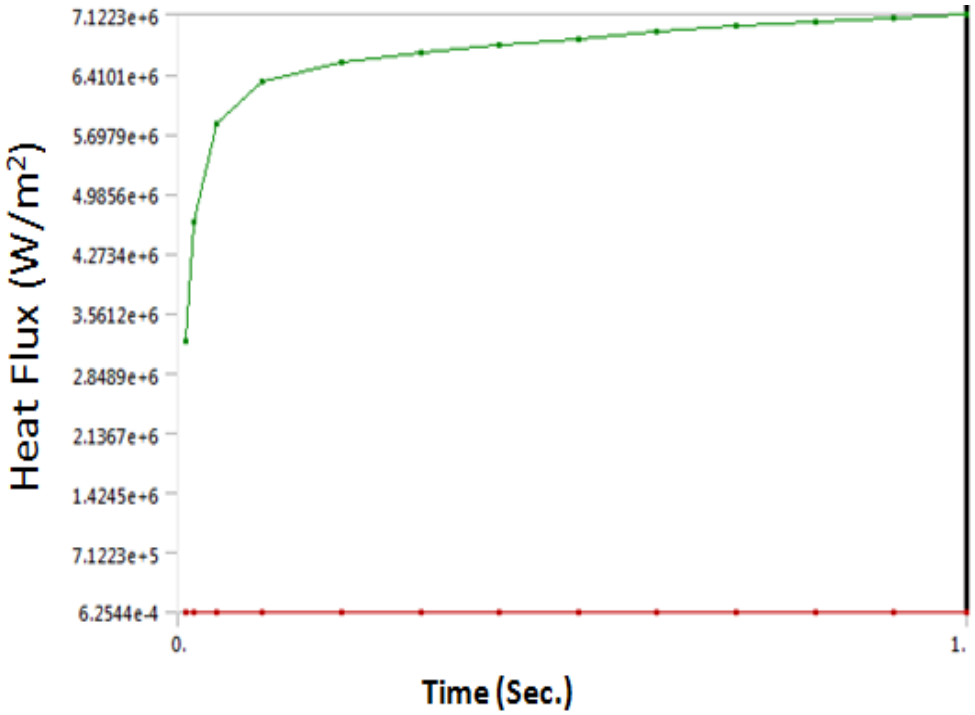

Figure 6.12 Analysis of temperature variation w.r.t time for 60 mm arc radius

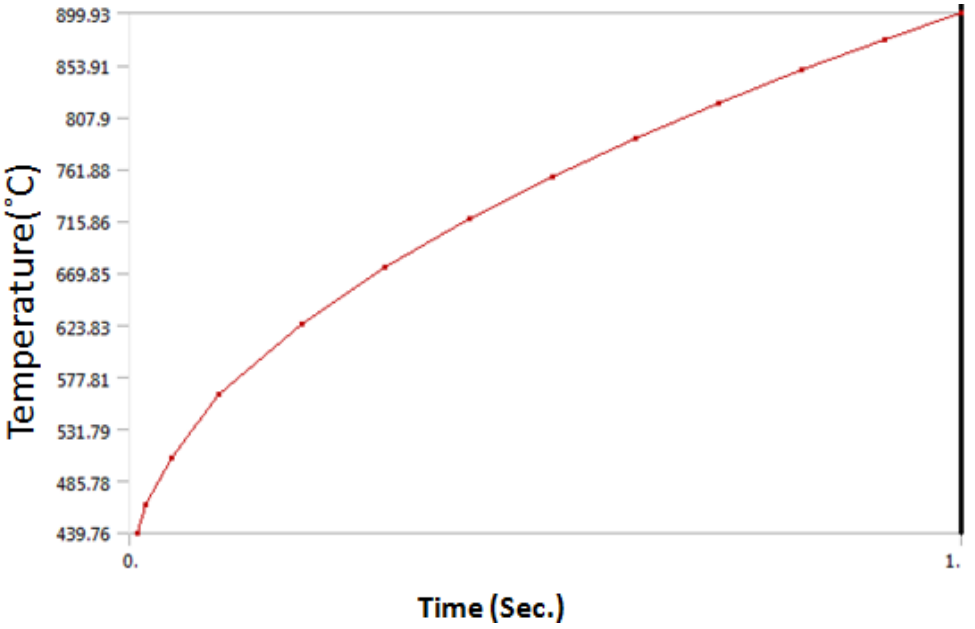

Figure 6.13 Analysis of heat flux variation w.r.t time for 60 mm arc radius

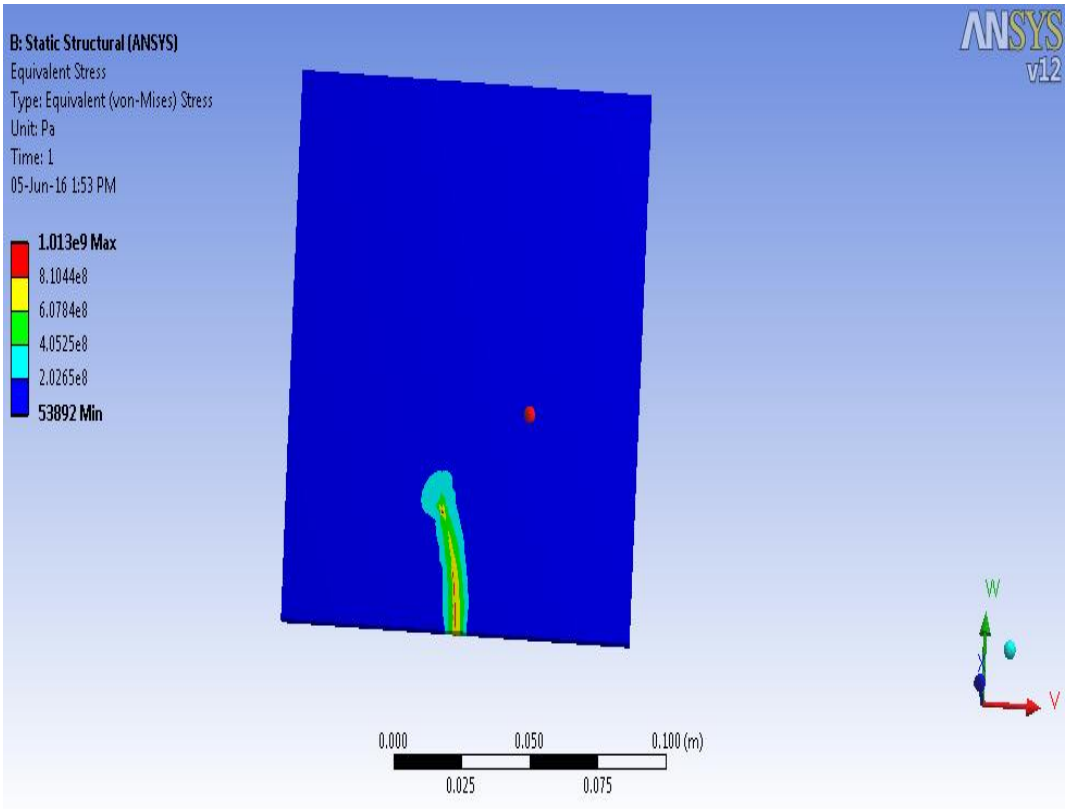

Figure 6.14 Von-mises stress analysis using transient analysis model for 60 mm arc radius

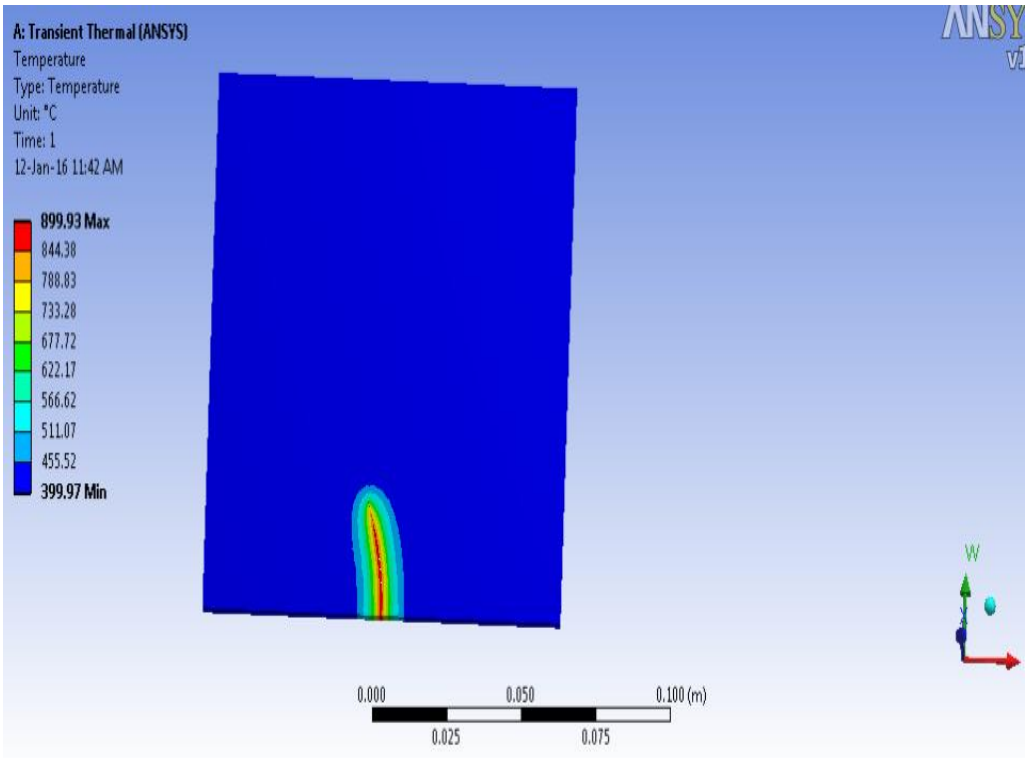

Figure 6.15 Temperature analysis for 60 mm arc radius

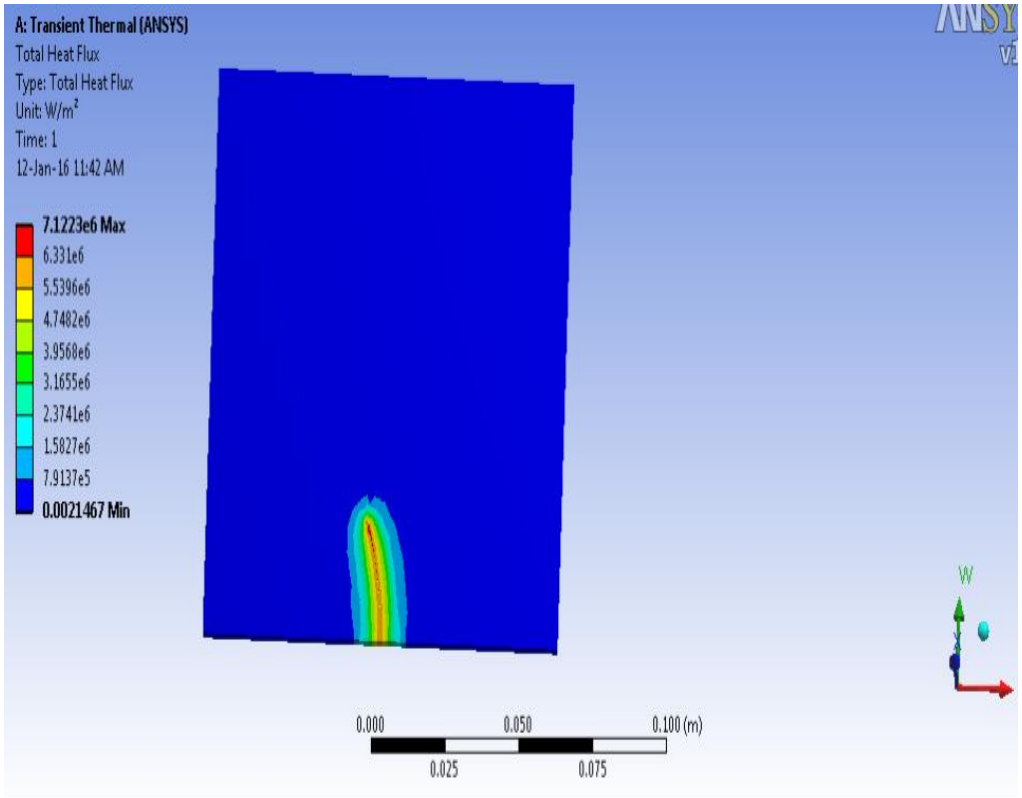

Figure 6.16 Variation of heat flux for cutting profile of 60 mm arc radius

CHAPTER 7

CONCLUSIONS AND SCOPE FOR FUTURE WORK

7.1 CONCLUSIONS

In the previous chapters, the details of process parameters and output responses are presented. The range of process parameters are reported using preliminary investigations of LBM process. Further, the main experimentation has been performed using Box-Behnken Design approach. The multi-optimization of various process parameters has been done using response surface methodology and desirability functional approach. The present work and investigations on various process parameters have been done successfully by identifying optimized parameters range of laser beam process for machining of aluminium MMC materials. This chapter summarizes about the present research work and effect of process parameters on output quality characteristics. The scope of future work in the field of laser machining is also discussed.

The response surface model was applied and found adequate using desirability functional approach for output responses like material removal rate, kerf deviation, kerf taper, striations, heat affected zone, surface roughness, dross height and energy losses. The percentage error was determined from the optimal input parameters setting between predicted and experimental results.

1. The percentage contribution of each parameter is evaluated for various output quality characteristics. The results revealed that cutting speed, arc radius and percentage reinforced particles are the most significant parameters for dross height and kerf width. The most prominent parameters for kerf taper found are arc radius, gas pressure and reinforced particles.
2. The percentage contribution of various input variables is determined for various output responses. The results concluded that cutting speed, arc radius and ZrO_2 reinforced particles had contribution of 22 %, 15% and 11 % respectively on striation angle.
3. The percentage contribution of cutting speed, stand-off distance and arc radius for HAZ width investigated as 16 %, 14 % and 10 % respectively. In case of kerf deviation, cutting speed and arc radius had maximum significant contribution of 39 % and 9 %.

4. The optical microscope images shows increase in striation angle from 8˚ to 19˚ with the increase in ZrO_2 reinforced particles (20 %) and cutting speed (3000 mm/min). Moreover, the lower values of arc radius of 20 mm also resulted into increase in striation angle within the range from 6˚ to 13˚.
5. The material removal rate was examined to be increased with decrease in arc radius and percentage reinforced particles (Al/Al_2O_3, Al/SiC and Al/ZrO_2).
6. The heat affected zone width found to be increased from 150 µm to 300 µm with the decrease in arc radius from 60 mm to 20 mm. The SEM micrographs shows the formation of recast layer and double layer of HAZ when machining condition set at cutting speed 1000 mm/min, 20 mm arc radius and 20 % ZrO_2 particles.
7. It was analysed from the ANOVA and regression coefficients that linear and square effects of input variables are significant for all output models. The co-efficient of regression R-Squared: 0.914 is well matched with adj. R-Squared: 0.891 for dross height, R- Squared: 0.884 is agreed with adj. R-Squared: 0.861for kerf taper and for kerf width R- Squared: 0.912 is matched with adj. R-Squared: 0.892.
8. The formation of recast layer and cracks were observed using SEM. The presence of un-burned SiC particles found in the kerf zone which further enhances the recast layer and crack formation due to the stress concentration.
9. EDS analysis confirmed the presence of carbon which reacted with aluminium under high temperature condition to form a new compound named as Al_4C_3.Also the existence of some elements like iron (Fe), chromium (Cr), magnesium (Mg), aluminium (Al), oxygen (O), and silicon (Si) of aluminium alloy 5052 was observed using EDS.
10. With the increase in cutting speed from 1000 mm/min to 3000 mm/min, the heat affected zone decreased within the range from 300 µm to 100 µm. The higher interaction time between laser beam and specimen increases the energy levels in kerf zone which resulted into higher heat affected zone width.
11. For energy losses, the most significant parameters were analysed as arc radius and percentage reinforced particles. It was found that energy losses decreased with the increase in quantity of reinforced particles and arc radius.
12. The presence of reinforced aluminium oxide particles also showed comparable results as reinforced SiC and ZrO_2 particles for all the output quality characteristics.

13. It was concluded after comparison of output quality characteristics results that work material Al5052/ZrO_2 has highest values for the kerf taper, surface roughness, striation angle, heat affected zone width and energy losses. However, Al5052/SiC work material has highest values for the dross height and kerf deviation and Al5052/Al_2O_3 work material has shown highest values for material removal rate.
14. The transient thermal model has been developed using the static structural model. It was concluded that the numerical simulation results for temperature variation has shown highest values for the arc radius of 20 mm as compared to 40 and 60 mm arc radius. Moreover, the von-Mises stress and heat flux values also examined with sharp rise in the values for 20 mm arc radius.

7.2 SCOPE FOR FUTURE WORK

Although the LBM process has been investigated thoroughly for Al/Al_2O_3, Al/SiC and Al/ZrO_2 MMC work materials. However, there is still scope for research work in the field of laser beam machining and work materials. The various points related to future work are as follows:

1. In the future work, the optimized machining conditions for titanium and their carbides as a work material may be investigated.

2. The thick sheets of metal matrix composites can be used as work material for investigations on LBM process.

3. The laser micromachining of advanced hybrid and difficult-to-cut material can be part of future research work.

4. The various optimization techniques other than RSM and desirability functional approach can be applied such as genetic algorithm, neural network, particle swarm optimization etc.

5. The issues related to high temperature and residual stress can be investigated using physical setups during laser curve cutting.

6. The optimum parameters of three dimensional laser beam machining may be investigated for various materials and typical cutting profiles.

REFERENCES

1. Arif A.F.M., Yilbas B.S., Aleem B.J., Laser cutting of thick sheet metals Residual stress analysis, Optics & Laser Technology, 41, 2009, 224–232

2. Allmen M., Blatter A., Laser-Beam Interactions with Materials, Springer, 1995.

3. Al-Sulaiman F.A., Yilbas B.S., Ahsan M., CO_2 laser cutting of a carbon/carbon multi-lamelled plain-weave structure, Journal of Materials Processing Technology, 173, 2006, 345–351

4. Antony, Design of experiments for engineers and scientists, Butterworth and Heinman, USA, 2003

5. Arata Y., Maruo H., Miyamoto I., Takeuchi S., Quality in laser-gas-cutting stainless steel and its improvement. Transactions of JWRI, 10, 1981, 129–139.

6. Araujo D, Carpio J., Mendez D., et al.., Microstructural Study of CO_2 Laser Machined Heat Affected Zone of 2024 Aluminum Alloy. Appl Surf Sci, 208, 2007, 210–217.

7. Arif A., Yilbas B. Thermal stress developed during the laser cutting process: consideration of different materials. J Adv Manuf Technol, 2008, 37, 698–704.

8. Bandyopadhyay S., Sundar J.K., Sundararajan G., et al.., Geometrical features and metallurgical characteristics of Nd:YAG laser drilled holes in thick IN718 and Ti–6Al–4V sheets, Journal of Materials Processing Technology,127 , 2002, 83–95

9. Banea M. D., Silva da L.F.M., Raul Campilho, Effect of Temperature on tensile strength and mode fracture toughness of a high temperature epoxy adhesive, Journal of Adhesion Science and Technology, 26, 2012, 939-953

10. Black S.A, Livingstone J., Chua K.L., A laser beam machining database for the cutting of ceramic tile, Journal of Materials Processing Technology ,84 , 1998, 47–55

11. Box P., Behnken D., Technometrics, 1960, Taylor & Francis, United Kingdom

12. Carpinteri A., Cornetti P., Pugno N., Sapora A., Taylor D., Generalized fracture toughness for specimens with re-entrant corners: Experiments vs. theoretical predictions, Structural Engineering and Mechanics, 32, 2009, 609-620

13. Caydas U., Hascalik A., Use of grey relational analysis to determine optimum laser cutting parameters with multi-performance characteristics. Optics and Laser Tech, 40, 2008, 987–94.

14. Chen Shang-Liang, The effects of gas composition on the CO2 laser cutting of mild steel. Journal of Materials Processing Technology, 73, 1998, 147–159

15. Chen-Hao Li, Ming-Jong Tsai, Ciann-Dong Yang, Study of optimal laser parameters for cutting QFN packages by Taguchi's matrix method, Optics & Laser Technology,39 , 2007, 786–795

16. Chong Zhian Syn, Mohzani Mokhtar, Chin Jeng Feng , Yupiter H.P. Manurung, Approach to prediction of laser cutting quality by employing fuzzy expert system, Expert Systems with Applications,38 , 2011, 7558–7568

17. Choudhury I.A., Shirley S., Laser cutting of polymeric materials an experimental investigation Optics & Laser Technology, 42, 2010, 503–508

18. Chryssolouris G., Laser Machining: Theory and Practice. Mechanical Engineering, ed. F.F. Ling. 1991: Springer-Verlag.

19. Chun-Hao Li, Ming-Jong Tsai, Multi-objective optimization of laser cutting for flash memory modules with special shapes using grey relational analysis, Optics & Laser Technology ,41 , 2009, 634–642

20. Cicala E., Soveja A., Sallamandb P., et al.., The application of the random balance method in laser machining of metals. Journal of Materials Processing Technology,196, 2008, 393–401

21. Ciftci I., Turker M., Seker U., Evaluation of tool wear when machining SiCp-reinforced Al-2024 alloy matrix composites, Materials and Design, 25, 2004, 251-255.

22. Cihan Karatas, Omer Keles, Ibrahim Uslan, Yusuf Usta, Laser cutting of steel sheets: Influence of workpiece thickness andbeam waist position on kerf size and striation formation, Journal of Materials Processing Technology, 172, 2006, 22–29

23. Dabade U., Joshi S., Analysis of chip formation mechanism in machining of Al/SiCp metal matrix composites. Journal of Materials Processing Technology, 209, 2009, 4704-4710.

24. Dahotre Narendra, Harimkar Sandip, Laser Fabrication and Machining of Materials, Springer, 2007, 1-555.

25. Das S., Joshi S.S., Modeling of spark erosion rate in micro wire-EDM, International Journal of Advanced Manufacturing Technology, 48, 2010, 581-596.

26. Davim J.P, Mranhao C., et al., Performance of cutting tools in machining Cu/W alloys for application in EDM electrodes, Int. J. Refractory Metals and Hard Materials, 27, 2009, 676-682

27. Davim Paulo, Barricasa Nuno, Marta Conceic, Carlos Oliveira, Some experimental studies on CO_2 laser cutting quality of polymeric materials, Journal of materials processing technology , 198, 2008, 99–104

28. Derringer G., Suich R., Simultaneous optimization of several response variables. J Qual Technol, 12, 1980, 214–219

29. Dharani Sowdari, Pradip Majumdar, Finite element analysis of laser irradiated metal heating and melting processes, Optics & Laser Technology, 42 , 2010, 855–865

30. Dirk Herzog, Peter Jaeschke, Oliver Meier, Heinz Haferkamp, Investigations on the thermal effect caused by laser cutting with respect to static strength of CFRP International Journal of Machine Tools & Manufacture ,48 , 2008, 1464– 1473

31. Dong-Gyu, Kyung-Won, Influence of cutting parameters on surface characteristics of cut section in cutting of Inconel 718 sheet using CW Nd:YAG laser, Non ferrous Material society,china,19, 2009, 32-39

32. Dubey A K., Yadava V., Simultaneous optimization of multiple quality characteristics in laser beam cutting using Taguchi method. International Journal of Precision Engg. and Mfg. 8, 2007, 10–5

33. Dubey A.K, Yadava Vinod, Optimization of kerf quality during pulsed laser cutting of aluminium alloy sheet, 204, 2008, 412-418

34. Dubey Avanish, Vinod Yadava, Multi-objective optimisation of laser beam cutting process, Optics & Laser Technology, 40, 2008, 562–570

35. Dubey Avanish, Vinod Yadava, Multi-objective optimization of Nd:YAG laser cutting of nickel-based superalloy sheet using orthogonal array with principal component analysis, Optics and Lasers in Engineering,46 , 2008, 124–132

36. Dubey Avanish, Vinod Yadava, Optimization of kerf quality during pulsed laser cutting of aluminium alloy sheet, journal of materials processing technology, 204, 2008, 412–418

37. Eltawahni H.A., Olabi A.G., K.Y. Benyounis, Effect of process parameters and optimization of CO_2 laser cutting of ultra high-performance polyethylene, Materials and Design ,31 , 2010, 4029–4038

38. Eltawahni H.A., Olabi A.G., Benyounis K.Y., Investigating the CO_2 laser cutting parameters of MDF wood composite material Optics & Laser Technology ,43 , 2011, 648–659

39. Eltawahni H.A., M. Hagino , K.Y.Benyounis, T.Inoue , Olabi A.G., Effect of CO_2 laser cutting process parameters on edge quality and operating cost of AISI316L, Optics & Laser Technology ,44 , 2012, 1068–1082

40. Ferreira S.L., Bruns R.E., Ferreira H.S., et al., Box–Behnken design: an alternative for the optimization of analytical methods. Anal. Chim. Acta, 597, 2007, 179–186.

41. Ghany K. A., Newishy M., Cutting of 1.2mm thick austenitic stainless steel sheet using pulsed and CW Nd:YAG laser. Journal of Materials Processing Technology, 168, 2005: 438–447

42. Ghosal A., Manna A., Response surface method based optimization of ytterbium fiber laser parameter during machining of Al/Al_2O_3-MMC.Opt Lasers Eng 46, 2012, 67–76.

43. Giovanni Tani, Luca Tomesani, Giampaolo Campana, Alessandro Fortunato, Quality factors assessed by analytical modelling in laser cutting ,Thin Solid Films, 453, 2004, 486–491

44. Golnabi M. Bahar, Investigation of optimum condition in oxygen gas-assisted laser cutting, Optics & Laser Technology, 41, 2009, 454–460

45. Grabowski A, Jozef S, Marian N. Laser cutting of AlSi alloy/SiCp composite: modelling of the cut kerf geometry, In proceeding of SPIE, Laser Tech 659, 2007. doi: 10.1117/12.726548

46. Grabowski A, Nowak M, Sleziona J., Laser beam interactions with metal matrix AlSi alloy/SiCp composites. J Achiev Mater Manuf Eng 31, 2008, 233-240

47. Grabowski A., Nowak M., Sleziona J., Laser beam interactions with metal matrix AlSi alloy/SiCp composites, journal of Achievements in Materials and Manufacturing Engineering, 31, 2008, 233-239

48. Gunaraj V., Murugan N., Application of response surface methodologies for predicting weld base quality in submerged arc welding of pipes, Journal of Materials Processing Technology, 88, 1999, 266–275

49. Hanadi G. Salem, Mohy S. Mansour, Yehya Badr, Wafaa A. Abbas, CW Nd:YAG laser cutting of ultra low carbon steel thin sheets using O_2 assist gas journal of materials processing technology ,196 , 2008, 64–72

50. Ilio A., Tagliaferri V., Veniali F., Machining parameters and cut quality in laser cutting of aramid fibre reinforced plastics. Materials and Manufacturing processes, 5, 1990, 591-608

51. Jackson M. J., Atomic scale machining of surfaces, Proceedings of 5th international Surface Engineering Congress, 15-17, 2006, USA

52. Jackson M.J., Micro fabrication and Nano Manufacturing, 2006, 1-388, Taylor and Francis, London

53. Jackson M.J., G.M. Robinsona, M.D.H. Gillb, W. O Neill, The effect of nozzle design on laser micro-machining of M2 tool steels ,Journal of Materials Processing Technology, 160, 2005,198–212

54. Jebbari Neila, Jebari M.M., Faycal Saadallah, Annie T.S., Thermal affected zone obtained in machining steel XC42 by high-power continuous CO_2 laser ,Optics & Laser Technology,40 , 2008, 864–873

55. John C. Ion, Laser Processing of Engineering materials, ISBN 07506 6079, 347-365

56. Joshi S.S, Das S., Modeling of spark erosion rate in micro wire-EDM, International Journal of Advanced Manufacturing Technology, 48, 2010, 581-596.

57. Jun Hu, Zhang Zhuoxian, Luo Jingwen, Sheng X., Simulation and experiment on standoff distance affecting gas flow in laser cutting, Applied Mathematical Modelling, 35, 2011, 895–902

58. Kang Bongchul, GunWoo Kim, MinyangYang, Sung-Hak Cho, Jong-K weon Park, A study on the effect of ultrasonic vibration in nanosecond laser machining,50, 2012, 1817-1822

59. Kheloufi Karim, Amara E.H., Numerical investigation of the effect of some parameters on temperature field and kerf width in laser cutting process, Physics Procedia , 39, 2012, 872 – 880

60. Koji Hirano, Remy Fabbro, Experimental investigation of hydrodynamics of melt layer during laser cutting of steel, Physics Procedia, 12, 2011, 555–564

61. Kovalev O.B. , Yudin P.V., Zaitsev A.V., Modeling of flow separation of assist gas as applied to laser cutting of thick sheet metal, Applied Mathematical Modelling,33 , 2009, 3730–3745

62. Kwak J.S., Application of Taguchi and response surface methodologies for geometric error in surface grinding process, International Journal of Machine Tools Manufacturing, 45, 2005, 327–334.

63. Lamikiz A., Lacalle N., Sanchez A, et al., CO_2 laser cutting of advanced high strength steels. App Surf Sci, 242, 2005, 362–368.

64. Lau S, Yue M, Lee C, et al.., Un-conventional machining of composite materials. J of Mater Proc Tech, 48, 1995, 199–205.

65. Lee Mein Wee, Lin Li, An analytical model for striation formation in laser cutting, Applied Surface Science, 247 , 2005, 277–284

66. Liming Liu, Meili Zhu, Desheng Xu, et al.., Study of the interfacial reaction of SiC-Al in 6061Al reinforced with SiC whisker at laser beam. Composite interfaces, 9, 2002, 135-142

67. Lin Li, Sobih M., Crouse P.L., Striation-free Laser Cutting of Mild Steel Sheets, Annals of the CIRP, 56, 2007, 193-196

68. Lum K.C.P., Ng S.L., Black I., CO_2 laser cutting of MDF, Determination of process parameter settings, Optics & Laser Technology, 32 , 2000, 67-76

69. Lung Kwang Pan, Wang Che Chung, Wei Shien Long, Hai Feng Sher, Optimizing multiple quality characteristics via Taguchi method-based Grey analysis, Journal of Materials Processing Technology,182, 2007,107–116

70. Yu M., Three-Dimensional Finite Element Modelling of Laser Cutting, Journal of Materials Processing Teclnology, 63, 1997, 637-639

71. Man H.C., Duan J., Yue T.M., Dynamic characteristics of gas jets from subsonic and supersonic nozzles for high pressure gas laser cutting, Optics & Laser Technology ,30 , 1998, 497-509

72. Mazahery A., Alizadeh M., Study of tribological and mechanical properties of A356-nano SiC composites, Transactions of the Indian Institute of Metals, 65, 2012, 393-398

73. Mazahery A., Shabani O., Development of the principle of simulated natural evolution in searching for a more superior solution: Proper selection of processing parameters in AMCs, Powder Tech, 245, 2013, 146-155.

74. Mazahery A., Shabani M.O., Assistance of novel artificial intelligence in optimization of aluminum matrix nanocomposite by genetic algorithm, Metallurgical and Materials Transactions A: Physical Metallurgy and Materials Science. 43, 2012, 5279-5285

75. Meung Jung Kim, Transient evaporative laser-cutting with boundary element Method, Applied Mathematical Modelling, 25, 2000, 25-39

76. Meung Jung Kim, 3D finite element analysis of evaporative laser cutting, Applied Mathematical Modelling,29, 2005, 938–954

77. Ming-Fei Chen, Yu-SenHo, Wen-Tse Hsiao, et al., Optimized laser cutting on light guide plates using grey relational analysis, Optics and Lasers in Engineering,49, 2011, 222–228

78. Ming-Jong Tsai, Chen-Hao Li, Cheng-Che Chen, Optimal laser-cutting parameters for QFN packages by utilizing artificial neural networks and genetic algorithm, journal of materials processing technology, 208, 2008, 270–283

79. Ming-Jong Tsai, Chen-Hao Li, The use of grey relational analysis is to determine laser cutting parameters for QFN packages with multiple performance characteristics, Optics & Laser Technology, 41, 2009, 914–921

80. Miracle B. Metal matrix composites from science to technological significance. Composites Science and Technology, 65, 2005, 2526-2540.

81. Montgomery D.C, Design and Analysis of Experiments, 4th ed., 2002, Wiley, New York.

82. Muhammad N., Whitehead D., Boor A., Li L., Comparison of dry and wet fiber laser profile cutting of thin 316L stainless steel tubes for medical device applications. Journal of Materials Processing Technology, 210, 2010, 2261–2267.

83. Muller F., Monaghan J., Non-conventional machining of particle reinforced metal matrix composites. Journal of Materials Processing and Technology, 118, 2001, 278-285

84. Myers R.H., Montgomery D.C., Response Surface Methodology: process and product optimization using designed experiments, John Wiley & Sons, 2002, New York.

85. Nowak A., Grabowski J., Optical and conductive properties of AlSi-alloy/SiCp composites: application in modelling CO2 laser processing of composites, Optics and Lasers in Engineering, 43, 2005, 233-246.

86. Nyon K., Nyeoh C., Mokhtar M., et al., Finite element analysis of laser inert gas cutting on Inconel 718. J Adv Manuf Tech, 60, 2012, 995–1007.

87. Olsen Flemming, Bagger Claus, pulsed mode laser cutting of sheets for tailored blanks, Journal of Material Processing Tech.,115, 2001, 131-135

88. Ozden Sedat, Ekici Recep, Nair Fehmi, Investigation of impact behaviour of aluminium based SiC particle reinforced metal–matrix composites. Composites: Part A, 38, 2007, 484–494.

89. Pandey A.K, Dubey A. Kumar, Fuzzy expert system for prediction of kerf qualities in pulsed laser cutting of titanium alloy sheet. Machining Science and Technology, 17, 2013, 545-574

90. Pandey Arun, Avanish Kumar Dubey, Simultaneous optimization of multiple quality characteristics in laser cutting of titanium alloy sheet, Optics & Laser Technology, 44, 2012, 1858–1865

91. Pandey Arun, Avanish Kumar Dubey, Taguchi based fuzzy logic optimization of multiple quality characteristics in laser cutting of Duralumin sheet, Optics and Lasers in Engineering, 50, 2012, 328–335

92. Paul S. Sheng, Joshi V. S., Analysis of heat-affected zone formation for laser cutting of stainless steel, Journal of Materials Processing Technology,53 , 1995, 879-892

93. Pecas P., Henriques E.A., Influence of silicon powder nixed dielectric on conventional discharge machining, International Journal of Machine Tools and Manufacture, 43, 2003, 1465-1471.

94. Pfeifer Ronny, Dirk Herzog, Michael Hustedt, Stephan Barcikowski, Pulsed Nd:YAG laser cutting of NiTi shape memory alloys—Influence of process parameters, Journal of Materials Processing Technology, 210, 2010, 1918–1925

95. Poprawe R., Konig W., Modeling, monitoring and control in high quality laser cutting. Manuf Technol, 50, 2001, 137–140.

96. Powell S.O., Al-Mashikhi, Kaplan A.F.H., Voisey K.T., Fiber laser cutting of thin section mild steel An explanation of the striation free effect Optics and Lasers in Engineering, 49 , 2011, 1069–1075

97. Pramanik A., Littlefair Guy, Machining of Titanium Alloy (Ti-6Al-4V)-Theory to Application, Machining Science and Technology, 19, 2015, DOI: 10.1080/10910344.2014. 991031

98. Quintero J. Pou, Fernandez J.L., et al., Optimization of an off-axis nozzle for assist gas injection in laser fusion cutting, Optics and Lasers in Engineering ,44 , 2006, 1158–1171

99. Quinteroa, Riveiroa A., Lusquinosa F., Comesanaa R., Poua J., CO_2 laser cutting of phenolic resin boards, Journal of Materials Processing Technology, 211, 2011, 1710–1718

100. Raghavendra Rao, Vinod Yadava, Multi-objective optimization of Nd:YAG laser cutting of thin super alloy sheet using grey relational analysis with entropy measurement, Optics & Laser Technology,41 , 2009, 922–930

101. Rajaram N, Ahmad J., Cheraghi S., CO_2 laser cut quality of 4130 steel. J Mach Tools Manuf, 43, 2003, 351–358.

102. Rao R., Yadava V., Multi-objective optimization of Nd:YAG laser cutting of thin super alloy sheet using grey relation a analysis with entropy measurement. Optics and Laser Technology, 41, 2009, 922–30.

103. Rao Tirumala, Kaula Rakesh, Tiwarib Pragya, et al.., Inert gas cutting of titanium sheet with pulsed mode CO_2 laser. Opt Lasers in Engg; 43, 2005, 1330–1348.

104. Riveiro A., Quintero F., Lusquinos F., Comesana R, Pou J. Influence of assist gas nature on the surfaces obtained by laser cutting of Al–Cu alloys. Surface Coat Tech, 205, 2010, 1878–1885

105. Riveiro A., Quintero F., Lusquinos F., et al.., Study of melt flow dynamics and influence on quality for CO_2 laser fusion cutting. J Phys D Appl Phys, 44, 2011, 1-12

106. Riveiro A., Quintero F., Lusquinos F., et al.., Parametric investigation of CO_2 laser cutting of 2024-T3 alloy. Journal of Materials Processing Technology, 210, 2010, 1138–1152

107. Riveiro F., Quintero F., Lusquinos, et al.., Effects of processing parameters on laser cutting of aluminium–copper alloys using off-axial supersonic nozzles, Applied Surface Science, 257, 2011, 5393–5397

108. Riveiro F., Quintero F., Lusquinos R., et al.., Parametric investigation of CO_2 laser cutting of 2024-T3 alloy, Journal of Materials Processing Technology, 210, 2010, 1138–1152

109. Riveiroa F., Quinteroa F., Lusquinosa R., et al.., The Role of the Assist Gas Nature in Laser Cutting of Aluminum Alloys, Physics Procedia,12 , 2011, 548–554

110. Rosso M., Ceramic and metal matrix composites: route and properties. Journal of Materials Processing Technology, 175, 2006, 364-375.

111. Basavarajappa S., Chandramohan G., et al., Application of Taguchi Technique to Study Dry-sliding Wear Behaviour of Metal Matrix Composites, Materials and Design, 28, 2007, 1393-1398.

112. Sangwan K.S., Saxena S., et al., Optimization of machining parameters to minimize surface roughness using integrated ANN-GA approach, Procedia CIRP, 29, 2015, 305-310

113. Salman Nisar, Sheikh M.A., Lin Li, et al., The effect of material thickness,laser power and cutting speed on cut path deviation in high-power diode laser chip-free cutting of glass, Optics & Laser Technology,42 , 2010, 1022–1031

114. Schuocker D., Muller P., Dynamic effects in laser cutting and formation of periodic striations. Proceedings of SPIE, 801, 1987, 258–264.

115. Scintilla D., Tricarico L., Experimental investigation on fiber and CO_2 inert gas fusion cutting of AZ31 magnesium alloy sheets, Opt Laser Tech, 46, 2013, 42-52.

116. Scintilla L.D, Tricarico L., Mahrle A., et al., A comparative study on fusion cutting with disk and CO_2 lasers, in ICALEO2010 Proceedings of the 29th International Congress on Applications of Lasers& Electro-Optics, Anaheim,CA,USA, 249–258.

117. Scintilla L.D., Tricarico L., Mahrle A., Wetzig A., Beyer E., Primary losses in disk and CO_2 laser beam inert gas fusion cutting. Journal Materials Processing Technology, 211, 2011, 2050 - 2061.

118. Scintilla L.D., Tricarico L., Experimental investigation on fiber and CO_2 inert gas fusion cutting of AZ31 magnesium alloy sheets, Optics & Laser Technology, 19, 2012, 1000-1016

119. Shabani Ostad, Mazahery A., Fabrication of AMCs by spray forming: Setting of cognition and social parameters to accelerate the convergence in optimization of spray forming process, Ceram Int, 39, 2013, 5271-527.

120. Shahrizal H., Performance evaluation of nitrogen gas-assisted laser cutting on 316 austenitic stainless steel plate, M.E thesis, Lappeenranta University of Technology, Finland, 2010

121. Shang-Liang Chen, The effects of gas composition on the CO_2 laser cutting of mild steel, Journal of Materials Processing Technology,73 ,1998, 147–159

122. Shang-Liang, The effects of high-pressure assistant-gas flow on high-power CO_2 laser cutting Chen, Journal of Materials Processing Technology, 88, 1999, 57–66

123. Shanjin L., Yang W., An investigation of pulsed laser cutting of titanium alloy sheet. Opt Lasers Eng, 44, 2006, 1067–1077.

124. Sharma A., Yadava V., Modelling and optimization of cut quality during pulsed Nd:YAG laser cutting of thin Al-alloy sheet for curved profile. Optics and Lasers in Engineering, 51, 2013, 77-88

125. Sharma A., Arora N., Mishra B. K., Mathematical model of bead profile in high deposition welds, Journal of Materials Processing Technology, 220, 2015, 65-75

126. Sharma A., Vinod Y., Optimization of cut quality characteristics during Nd:YAG laser straight cutting of Ni-based superalloy thin sheet using grey relational analysis with entropy measurement. Mater Manuf Processes, 26, 2011, 1522–1529

127. Sharma A., Yadava V., Rao R., Optimization of kerf quality characteristics during Nd:YAG laser cutting of nickel based super alloy sheet for straight and curved cut profiles. Opt Lasers Eng, 48, 2010, 915–925.

128. Sharma A., Yadava V., Modelling and optimization of cut quality during pulsed Nd:YAG laser cutting of thin Al-alloy sheet for curved profile. Opt Lasers Eng, 51, 2013, 77-88.

129. Sharma A., Yadava V., Rao R., Optimization of kerf quality characteristics during Nd:YAG laser cutting of nickel based super alloy sheet for straight and curved cut profiles. Optics and Lasers in Engineering, 48, 2010, 915–925

130. Sharma Amit, Vinod Yadava, Modelling and optimization of cut quality during pulsed Nd:YAG laser cutting of thin Al-alloy sheet for straight profile, Optics & Laser Technology ,44 , 2012, 159–168

131. Sharma Amit, Vinod Yadava, Raghavendra Rao, Optimization of kerf quality characteristics during Nd:YAG laser cutting of nickel based super alloy sheet for straight and curved cut profiles, Optics and Lasers in Engineering, 48 , 2010, 915–925

132. Sharma P., Dubey A., Pandey A., Numerical Study of Temperature and Stress Fields in Laser Cutting of Aluminium Alloy Sheet. Procedia Mater Sci, 5, 2014, 1887–1896

133. Sharma P., Dubey A., Pandey A., Numerical study of temperature and stress fields in laser cutting of aluminium alloy sheet, Procedia Mat Sc 2014; 5:1887-1896.

134. Singh Ramesh, Alberts Matthew, Shreyes Melkote, Characterization and prediction of the heat-affected zone in a laser-assisted mechanical micromachining process. J Mach Tools Manuf, 48, 2008, 994–1004.

135. Sirahbizu L., Mahapatra M. Mohan, et al., Influence of Reinforcement Type on Microstructure, Hardness, and Tensile Properties of an Aluminum Alloy Metal Matrix Composite. Journal of Minerals and Materials Characterization and Engineerin, 1, 2013, 124-130

136. Souza A.S., Dos S., Walter N.L., et al., Application of Box–Behnken design in the optimization of an on-line pre-concentration system using knotted reactor for cadmium determination by flame atomic absorption spectrometry. Spectrochimica Acta Part-B, 609, 2005, 737–742.

137. Srivatsan T. S., Al-Hajri M., Smith C., Petraroli M., The tensile response and fracture behavior of 2009 aluminium alloy metal matrix composite. Mater Sci Eng, 346, 2003, 91–100.

138. Stournaras A., Stavropoulos P., Salonitis K., et al., An investigation of quality in CO_2 laser cutting of aluminium. J Mfg Sc Tech, 2, 2009, 61–69.

139. Stournaras P., Stavropoulos K., Salonitis G., An investigation of quality in CO_2 laser cutting of aluminum, CIRP Journal of Manufacturing Science and Technology,12 , 2009, 61–69

140. Thawari J.K., Sarin Sundar, Sundararajan G., Joshi S.V., Influence of process parameters during pulsed Nd:YAG laser cutting of nickel-base super alloys, Journal of Materials Processing Technology ,170 , 2005, 229–239

141. Tirumala Rao, Kaula Rakesh, Tiwari Pragya, Nath A.K., Inert gas cutting of titanium sheet with pulsed mode CO_2 laser, Optics and Lasers in Engineering, 43, 2005, 1330–1348

142. Tod Gilbert, Vladimir D. Krstic, Gene Zak, Machining of aluminium nitride with ultra-violet and near-infrared Nd:YAG lasers, Journal of Materials Processing Technology,189 , 2007, 409–417

143. Tofigh A., Shabani O., Efficient optimum solution for high strength Al alloys matrix composites, Ceramics Int. 39, 2013:7483-7490.

144. Tsai C.H, Liou C.S., Fracture mechanism of laser cutting with controlled fracture. Journal of Manufacturing Science and Engineering, Trans ASME, 125, 2003, 519–528

145. Venkata B., Ganguly I., Srinivasarao G., Machinability of Aluminum Metal Matrix Composite Reinforced with In-Situ Ceramic Composite Developed from Mines Waste Colliery Shale. Mat Manuf Proc, 28, 2013, 1082-1089.

146. Wang J., Wong W.C.K., CO_2 laser cutting of metallic coated sheet steels, Journal of Materials Processing Technology, 95, 1999, 164-168

147. Wang X., Kang R., Xu W., Guo D., Direct laser fabrication of aluminum-alloy slot antenna array, First international symposium on systems and control in aerospace and astronautics, IEEE Cat. No. 06EX1168C, 2006, 50

148. Yan B., Tsai H., Chung, Huang Yuan, et al., Examination of wire electrical discharge machining of Al_2O_3p/6061Al composites, J Mach Tools Manuf, 45, 2005, 251–259.

149. Yan Y., Ji L, Bao Y., Jiang Y., An experimental and numerical study on laser percussion drilling of thick-section alumina. J Mater Proc Tech, 212, 2012, 1257– 1270

150. Yang Jihong, Shoujin Sun, Milan Brandt, et al., Experimental investigation and 3D finite element prediction of the heat affected zone during laser assisted machining of Ti6Al4V alloy. J Mat Proc Tech 2010; 210:2215–2222.

151. Yang Li, Shengsun Hu, Junqi Shen, Bao Hu, Dissimilar Welding of H62 Brass-316L Stainless Steel Using Continuous-Wave Nd:YAG Laser. Materials and Manufacturing Processes, 29, 2014, 916-921

152. Yigezu B.S., Mahapatra M. M., Jha K.P., Influence of Reinforcement Type on Microstructure, Hardness, and Tensile Properties of an Aluminum Alloy Metal Matrix Composite. J Min Mater Charact Eng, 1, 2013, 124-130

153. Yilbas B., Laser cutting of thick sheet metals: Effects of cutting parameters on kerf size variations, J Mat Proc Tech, 201, 2008, 285–290

154. Yilbas B. S., Akhtar S. S., et al., Laser Cutting of Triangular Geometry into Alumina Tiles: Morphological Changes and Thermal Stress Analysis. Machining Science and Technology, 18, 2014, 424-447

155. Yilbas B.S., C. Karatas, Uslan I., et al., Wedge cutting of mild steel by CO_2 laser and cut-quality assessment in relation to normal cutting, Optics and Lasers in Engineering, 46, 2008, 777– 784

156. Yilbas B.S., Arif A.F.M., Laser cutting of steel and thermal stress development, Optics & Laser Technology, 43, 2011, 830–837

157. Yilbas B.S., A.F.M. Arif, Abdul B.J., Laser cutting of sharp edge Thermal stress analysis, Optics and Lasers in Engineering, 48, 2010, 10–19

158. Yilbas B.S., Laser cutting of thick sheet metals: Effects of cutting parameters on kerf size variations, journal of materials processing technology, 201, 2008, 285–290

159. Yilbas B.S., Laser cutting quality assessment and thermal efficiency analysis, Journal of Materials Processing Technology, 155, 2004, 2106–2115

160. Yilbas S., Khan S., Raza K., et al., Laser cutting of 7050 Al alloy reinforced with Al_2O_3 and B_4C composites. J Adv Mfg Tech, 50, 2010, 185–193.

161. Yinzhou Yan, Lingfei Ji, Yong Bao, Yijian Jiang, An experimental and numerical study on laser percussion drilling of thick-section alumina, Journal of Materials Processing Technology, 212, 2012, 1257– 1270

162. Yue T.M., Lau W.S., Pulsed Nd-YAG laser cutting of Al-Li/SiC metal matrix composites, Mater Manuf Processes, 11, 1996, 17-29

APPENDICES

Nomenclature

SEM: scanning electron microscope

EDS: energy-dispersive X-ray spectroscopy

HAZ: heat affected zone (μm)

K_d : kerf deviation (mm)

K_w : kerf width (mm)

MMC: Metal matrix composite

t : specimen thickness (mm)

S.A : striation angle (degree, α_s)

X_1 : cutting speed (mm/min)

K_t: kerf taper (degree)

MRR: material removal rate

R_z : surface roughness

D_t : dross height (mm)

X_2 : laser power (Watt)

X_3: standoff distance (mm)

X_4 : nozzle diameter (mm)

X_5 : gas pressure (bar)

X_6 : ZrO_2 particles (%wt)

X_7 : arc radius (mm)

ZrO_2 : zirconium oxide (%wt)

E.L: energy losses(watt)

SiC: silicon carbide (%wt)

Al_2O_3 : aluminium oxide(%wt)

Table 1 Experimental and RSM predicted results and prediction error

	Experimental results		**RSM Model Predictions**		**Predicted Percentage Error(%)**	
Exp no.	Surface roughness	Kerf Deviation	Surface roughness	Kerf Deviation	Surface roughness	Kerf Deviation
1	1.23	0.0021	1.20	0.002	2.4	4.8
2	1.45	0.0180	1.394	0.017	4.1	5.6
3	1.25	0.0114	1.210	0.011	3.2	3.5
4	1.26	0.0148	1.214	0.014	2.9	5.4
5	0.92	0.024	0.885	0.023	3.9	4.2
6	1.26	0.032	1.21	0.031	4.0	3.1

Table 2 Analysis of variance for surface roughness

Source	SS	DOF	MS	F-Value	P >F	Remarks
Model	22.26	15	1.48	23.88	< 0.0001	Significant
Cutting Speed	5.02	1	5.02	80.81	< 0.0001	Significant
Laser Power	1.29	1	1.29	20.87	< 0.0001	Significant
Stand-off Distance	0.27	1	0.27	4.46	0.0401	Significant
Nozzle Diameter	0.02	1	0.02	0.33	0.5639	Not-significant
Gas Pressure	0.98	1	0.98	15.76	0.0002	Significant
Reinforced Particles	0.84	1	0.84	13.51	0.0006	Significant
Arc Radius	7.63	1	7.63	122.8	< 0.0001	Significant
(Cutting Speed)^2	1.95	1	1.95	31.45	< 0.0001	Significant
(Arc Radius)^2	1.33	1	1.33	21.45	< 0.0001	Significant
(Cutting Speed × Nozzle Diameter)	0.32	1	0.32	5.277	0.0262	Significant
(Cutting Speed × Gas Pressure)	1.17	1	1.17	18.95	< 0.0001	Significant
(Cutting Speed × Reinforced Particles)	0.55	1	0.55	8.95	0.0044	Significant
(Cutting Speed × Arc Radius)	0.30	1	0.30	4.95	0.0309	Significant
(Stand-off Distance × Gas Pressure)	0.32	1	0.32	5.21	0.0271	Significant
(Reinforced Particles × Arc Radius)	0.46	1	0.46	7.49	0.0088	Significant

R-Squared = 0.8862

Table 3 Analysis of variance for kerf deviation

Source	SS	DOF	MS	F-Value	P >F	Remarks
Model	0.0976	15	0.00651	17.486	< 0.0001	Significant
Cutting Speed	0.0305	1	0.03053	82.006	< 0.0001	Significant
Laser Power	0.0069	1	0.00693	18.630	< 0.0001	Significant
Stand-off Distance	0.0054	1	0.00543	14.585	0.0004	Significant
Nozzle Diameter	0.0002	1	0.00021	0.0071	0.9329	Not-Significant
Gas Pressure	0.0059	1	0.00592	15.906	0.0002	Significant
Reinforced Particles	0.0037	1	0.00372	10.005	0.0028	Significant
Arc Radius	0.0078	1	0.00788	21.177	< 0.0001	Significant
(Cutting Speed)^2	0.0087	1	0.00872	23.433	< 0.0001	Significant
(Laser Power)^2	0.0074	1	0.00745	20.034	< 0.0001	Significant
(Nozzle Diameter)^2	0.0078	1	0.00786	21.137	< 0.0001	Significant
(Reinforced Particles)^2	0.0031	1	0.00319	8.5935	0.0052	Significant
(Arc Radius)^2	0.0065	1	0.00655	17.608	0.0001	Significant
(Cutting Speed × L.Power)	0.0063	1	0.00632	16.997	0.0002	Significant
(Cutting Speed × Arc Radius)	0.0050	1	0.00505	13.564	0.0006	Significant
(Gas Pressure × R. Particles)	0.0025	1	0.00255	6.8658	0.0119	Significant

R-Squared = 0.901

Table 4 Process parameters combinations for high value of desirability

	Factors						Predicted Resposes			
E.No.	X_1	X_2	X_3	X_4	X_5	X_6	X_7	R_z	K_d	Desirabilty
	mm/min	watt	mm	mm	bar	%	mm	µm	mm	
1	2990.85	1827.72	1.96	1.49	13.95	11.42	58.87	1.093	0.001	1.00
2	2760.04	1741.41	2.00	1.52	13.99	11.45	55.80	1.202	0.002	1.00
3	2962.56	1973.58	1.97	1.57	13.93	11.69	53.34	1.116	0.008	1.00
4	2943.09	1978.94	1.99	1.51	13.99	9.64	57.31	0.898	0.011	1.00
5	3000.00	2040.05	1.00	1.70	12.14	10.00	60.00	0.897	0.010	0.90
6	2769.30	2103.90	1.99	1.68	14.00	13.23	54.48	1.210	0.021	0.98
7	3000.00	1894.55	1.99	1.40	14.00	17.13	56.19	1.394	0.017	0.96
8	3000.00	1500.56	2.00	1.66	14.00	15.53	60.00	1.632	0.015	0.94
9	2570.67	2042.22	1.00	1.84	10.10	0.18	55.27	1.210	0.011	0.93
10	2307.23	1892.05	1.00	1.82	10.20	0.00	57.98	1.210	0.011	0.93
11	2236.05	2048.52	1.00	1.75	10.00	0.00	56.18	1.183	0.012	0.93
12	2562.29	1943.48	1.00	1.77	10.81	0.00	52.72	1.204	0.011	0.92
13	2699.40	2127.57	1.00	1.82	10.00	0.00	54.00	1.214	0.014	0.92
14	2803.71	1814.85	1.00	1.81	11.34	0.01	60.00	1.168	0.011	0.92
15	2759.82	1801.53	1.00	1.87	11.29	0.00	53.88	1.210	0.017	0.92
16	2233.83	2191.32	1.00	1.70	10.00	0.00	53.28	1.172	0.020	0.92
17	2473.85	2027.69	1.00	1.84	10.91	0.00	51.48	1.210	0.025	0.92
18	2852.32	1887.68	1.00	1.76	12.14	0.00	59.55	0.885	0.023	0.91
19	2999.99	2110.12	1.38	1.64	13.64	11.16	57.97	1.213	0.036	0.91
20	2999.99	1685.95	1.21	1.67	13.98	3.89	53.42	0.894	0.020	0.91
21	3000.00	1659.12	1.07	1.65	14.00	0.11	53.87	0.653	0.034	0.90
22	2534.28	2215.75	1.00	1.53	10.00	0.00	59.73	0.969	0.024	0.89
23	2560.15	2426.67	1.00	1.73	10.00	0.00	60.00	1.150	0.048	0.88
24	2959.53	1500.00	1.06	1.91	14.00	0.00	50.55	0.965	0.059	0.88
25	2999.96	1786.08	1.00	1.49	14.00	9.82	50.24	1.210	0.031	0.86